



The  
University  
Of  
Sheffield.

**Investigating variability in the diet, distribution and demographics of  
Barents Sea cod, 1991-2017: A combined statistical modelling approach**

**Joseph Louis Molloy**

A thesis submitted in partial fulfilment of the requirements for the degree of  
Doctor of Philosophy

The University of Sheffield  
Faculty of Social Sciences  
Department of Geography

December 2021

## Abstract

Rising global ocean temperatures are changing marine ecosystems globally. Over the past decade, temperatures in the Barents Sea have been at a historic high due to the increasing temperature of Atlantic water and a decrease in sea ice volume. Studies investigating the effects of temperature variability on the Barents Sea ecosystem have highlighted the complexity and difficulty of predicting how future change may affect the species and communities here. Environmental variability has ramifications for every aspect of the ecosystem, but one particularly complex relationship is between the environment and trophic dynamics. As environmental changes may affect species within a community in different ways and to different extents, predicting how the whole system may be affected can be challenging. This thesis seeks to quantify some aspects of the relationship between environmental variability and trophic dynamics in the Barents Sea by applying a novel statistical modelling approach to a spatio-temporal diet database for Barents Sea cod, a top predator. We examine spatio-temporal patterns in diet, distribution and demographics for cod and several key prey species. We utilise a species distribution model, Maxent, and a nonlinear system identification model, NARMAX, to synthesise existing data and identify the factors driving spatio-temporal change in these aspects of the ecosystem. We found a trend of distribution spreading into the northern Barents Sea following increasing water temperatures. We found further evidence for the borealization of the arctic environment in the Barents Sea, with *Boreogadus saida*, a landmark arctic species, increasing in significance as a prey item with consumption rising as *Mallotus villosus* and *Pandalus borealis* consumption falls. We found that higher order biotic effects were more informative in our models than direct measurements of climate, and some of the measures we attempted to predict could not be adequately explained by either the biotic or abiotic data that were used.

## Acknowledgements

I would like to thank my supervisors: Prof Grant Bigg, Dr Hua-Liang Wei and Dr Geir Ottersen, for their guidance, support, enthusiasm, and especially for their patience. The long road to this thesis would not have been travelled without their excellent supervision paving the way.

I am inexpressibly grateful to my fiancée Bethan, who has selflessly supported me at any cost, and without whom I would not have had the conviction to overcome the many obstacles we have faced over these past four years. I would also like to thank my family and friends who have offered words of encouragement, practical support and much-needed respite from work over these past years, and I am grateful to be blessed with so many of these wonderful people that I cannot name them all here. However, I would like to specifically thank those friends who have walked this road alongside me. To Sean, Josephine and Florentine, though we arrive separately, we set out together, and I will never forget the shared camaraderie of our time together in Sheffield as new PhD students.

Finally, this thesis is dedicated to my mum Elaine and dad Joseph, who told me that I could do anything I set my mind to, and taught me by example to never, ever, give up.

## Declaration

*I, the author, confirm that the Thesis is my own work. I am aware of the University's Guidance on the Use of Unfair Means ([www.sheffield.ac.uk/ssid/unfair-means](http://www.sheffield.ac.uk/ssid/unfair-means)). This work has not previously been presented for an award at this, or any other, university.*

# Table of Contents

Acknowledgements	4
Declaration	5
Table of Contents	6
List of Tables	10
List of Figures	12
Chapter 1 - Introduction	18
1.1. Research Context, Aims and Null Hypotheses	18
1.2. Thesis Structure	20
1.3. Cod: DIet and food web dyNAMics (CoDINA)	21
1.4. Scientific Background	22
1.4.1 The Barents Sea	22
1.4.1.1. Physical characteristics of the Barents Sea	22
1.4.1.2. Barents Sea Climate and Ecosystem	24
1.4.2. The significance of Atlantic cod, <i>Gadus morhua</i>	26
1.4.2.1. An overview of <i>Gadus morhua</i>	26
1.4.2.2. Barents Sea cod	28
1.4.3 Trophic dynamics	29
1.5 Study Novelty	32
Chapter 2. Analysis of cod diet and demographics from the IMR-PINRO stomach database	33
2.1. Metadata and sampling distribution	33
2.2. Characteristics of the Barents Sea cod population	37
2.2.1. Population size structure	37
2.2.1.1. Temporal patterns in size structure	39
2.2.1.2. Spatial patterns in size structure	40
2.2.2. Population age structure	42
2.2.2.1. Temporal patterns in age structure	43
2.2.2.2. Spatial patterns in age structure	44
2.2.3. Summary	46
2.3. Analysis of diet in Barents Sea cod	47
2.3.1 Temporal patterns in diet	49
2.3.2. Spatial patterns in diet	53
2.3.3. Ontogenetic patterns in diet	57
2.3.3.1. Body length and size group classification	57
2.3.3.2. Ontogenetic prey categories and diversity	59

2.3.3.3. Ontogenetic patterns in diet over time	63
2.3.3.4. Ontogenetic diet in space	65
2.3.4. Summary	67
2.4. Conclusions	68
Chapter 3 - Testing the effect of data structure and hyperparameter settings on the performance of Maxent for modelling the distribution of cod	70
3.1. Introduction	70
3.2. Methodology	72
3.2.1. Species records	72
3.2.2. Background point selection	73
3.2.3. Environmental Layers	74
3.2.4. Model parameter setting with ENMEval	79
3.2.5. Model Evaluation	80
3.2.6. Prey availability layer	82
3.2.7. Size stratified models	83
3.2.8. Temporal sensitivity	84
3.3. Results	85
3.3.1. Maxent model for Atlantic cod	85
3.3.1.1. Model Evaluation	85
3.3.1.2. Model Structure	85
3.3.1.3. Projection	89
3.3.2. Maxent model for Atlantic cod with a prey availability layer	91
3.3.2.1. Prey availability layer	91
3.3.2.2. Model Evaluation	92
3.3.2.3. Model Structure	92
3.3.3. Size Stratified Maxent Models for Atlantic cod	100
3.3.3.1. Model Structure	101
3.3.3.2. Projected distribution	102
3.3.4. Time stratified Maxent Models for Atlantic cod	104
3.3.4.1. Annual, Five-Year and Ten-Year Model Structure	106
3.3.4.2. Seasonal Model Structure	109
3.3.4.3. Model Projections	111
3.4. Discussion	112
3.5. Conclusions	114
Chapter 4 - The changing distribution of cod and critical prey species in the Barents Sea	115
4.1. Introduction	115
4.2. Methodology	116
4.2.1. Seasonal Maxent model design	116
4.2.1.1. Environmental Layers	116
4.2.1.2. Occurrence records and background points	118

4.2.1.3. Parameter setting and validation	119
4.2.1.4. Producing binary suitability maps by thresholding Maxent predictions	119
4.2.2. Average Maxent model design for missing data	120
4.2.3. Calculation of distribution and overlap area	121
4.3. Results	122
4.3.1. Model Performance	123
4.3.1. Temporal Variability of Predicted Distributions	125
4.3.1.1. <i>Gadus morhua</i> (S)	125
4.3.1.2. <i>Gadus morhua</i> (M)	127
4.3.1.3. <i>Gadus morhua</i> (L)	129
4.3.1.4. <i>Mallotus villosus</i>	131
4.3.1.5. <i>Melanogrammus aeglefinus</i>	133
4.3.1.6. <i>Pandalus borealis</i>	135
4.3.1.7. <i>Boreogadus saida</i>	137
4.3.2. Spatial overlap between predator-prey groups	139
4.3.2.1 <i>Gadus morhua</i> (S) and prey species	139
4.3.2.2 <i>Gadus morhua</i> 20 - 100 cm	141
4.3.2.3 <i>Gadus morhua</i> > 100 cm	142
4.3.2.4. <i>Gadus morhua</i> size group overlap	144
4.3.3. Model Structures	145
4.3.3.1. Seasonal Models	145
4.3.3.2. Average Models	148
4.4. Discussion	150
Chapter 5 - Modelling the variability of diet, population demographics and size structure over time	152
5.1. Introduction	152
5.1.1. System Identification	153
5.1.2. NARMAX	155
5.2. Methodology	157
5.2.1. Hyperparameters	158
5.2.2. Performance measures	161
5.2.3. Model Validation	161
5.3 Results	162
5.3.1 Prey Consumption by Weight	162
5.3.1.1. <i>Mallotus villosus</i>	163
5.3.1.2. <i>Melanogrammus aeglefinus</i>	165
5.3.1.3. <i>Pandalus borealis</i>	167
5.3.1.4. <i>Boreogadus saida</i>	170
5.3.1.5. <i>Gadus morhua</i>	172
5.3.2 Barents Sea cod population measures	174
5.3.2.1. <i>Gadus morhua</i> Biomass	174

5.3.2.2. <i>Gadus morhua</i> Spawning Biomass	176
5.3.2.3. <i>Gadus morhua</i> Recruitment	178
5.3.3 Barents Sea cod Size Structure	180
5.3.3.1. Fraction of <i>Gadus morhua</i> Population <20cm in length [ <i>Gadus morhua</i> (S)]	180
5.3.3.2. Fraction of <i>Gadus morhua</i> population between 20cm and 100cm in length [ <i>Gadus morhua</i> (M)]	182
5.3.3.3 Fraction of <i>Gadus morhua</i> population > 100cm in length [ <i>Gadus morhua</i> (L)]	184
5.4 Discussion	186
Chapter 6 - Discussion	189
6.1. Spatio-temporal and ontogenetic patterns in the diet of Barents Sea cod	190
6.2. Temporal variability in the distribution and overlap of Barents Sea cod and critical prey species	192
6.3. Drivers of variability in the diet, demographics and size structure of Barents Sea cod from 1991-2017	194
Chapter 7 - Conclusions	197
7.1. Limitations of this study	197
7.2. Further work	200
Bibliography	202
Appendices	211
Appendix A - IMR-PINRO metadata and sampling locations	211
A.1. Table of variables recorded in the IMR-PINRO database	211
A.2. IMR-PINRO Sampling Locations per Year.	213
Appendix B - Prey species maxent prediction maps used in the creation of the prey availability layer	214
Appendix C - Model permutation importance tables for temporal sensitivity testing	222
C.1. Annual, Five and Ten-year model variable permutation importance	222
C.2. Annual models variable permutation importance	224
C.3. Five-year period model variable permutation importance	226
C.4. Ten-year period model variable permutation importance	228
C.5. Summer model variable permutation importance	229
C.6. Winter model variable permutation importance	231
Appendix D - Seasonal prediction maps and binary maps for each species group modelled in Chapter 4.	233
Appendix E - NARMAX input data table	261

## List of Tables

Table	Page
Table 3.1. A description of each environmental layer that is included in the initial model building process.	76
Table 3.2. A description of each environmental layer that is included in the model building process for summer and winter models.	78
Table 3.3. AUC for each size group model with and without an included prey layer	100
Table 4.1. Environmental layer schematic for seasonal Maxent models (Continued on next page)	117
Table 5.1. List of NARMAX hyperparameters tested ranges and a description of each.	158
Table 5.2 NARMAX model performance measures for MV_PFRAC	164
Table 5.3. NARMAX model structure for MV_PFRAC (Variable Explanations in Appendix E)	164
Table 5.4 NARMAX model performance measures for MA_PFRAC	166
Table 5.5 NARMAX model structure for MA_PFRAC (Variable Explanations in Appendix E)	166
Table 5.6 NARMAX model performance measures for PB_PFRAC	168
Table 5.7 NARMAX model structure for PB_PFRAC (Variable Explanations in Appendix E)	169
Table 5.8 NARMAX model performance measures for BS_PFRAC	171
Table 5.9 NARMAX model structure for BS_PFRAC (Variable Explanations in Appendix E)	171
Table 5.10 NARMAX model performance measures for GM_PFRAC	173
Table 5.11 NARMAX model structure for GM_PFRAC(Variable Explanations in Appendix E)	173
Table 5.12 NARMAX model performance measures for TOTALBIO	175
Table 5.13 NARMAX model structure for GM_PFRAC (Variable Explanations in Appendix E)	175
Table 5.14 NARMAX model performance measure for TOTS BIO	177

Table 5.15 NARMAX model structure for TOTSBIO (Variable Explanations in Appendix E)	<i>177</i>
Table 5.16 NARMAX model performance measures for RECRUITS	<i>179</i>
Table 5.17 NARMAX model structure for RECRUITS (Variable Explanations in Appendix E)	<i>179</i>
Table 5.18 NARMAX model performance measures for SMALLFRAC	<i>181</i>
Table 5.19 NARMAX model structure for SMALLFRAC (Variable Explanations in Appendix E)	<i>181</i>
Table 5.20 NARMAX model performance measures for MEDFRAC	<i>183</i>
Table 5.21 NARMAX model structure for MEDFRAC (Variable Explanations in Appendix E)	<i>183</i>
Table 5.22 NARMAX model performance measures for LARGEFRAC	<i>185</i>
Table 5.23 NARMAX model structure for LARGEFRAC (Variable Explanations in Appendix E)	<i>185</i>

## List of Figures

Figure	Page
Figure 1.1. Map of the Barents Sea showing bottom topography and currents adapted from (Johannesen et al., 2012b)	23
Figure 1.2. Long-term mean water temperature in the Barents Sea as of August-October 2008. The delineation between Atlantic (>3C), Mixed (0-3C) and the Arctic (< 0C) water is visible.	24
Figure 1.3. A photograph of an adult <i>Gadus morhua</i> .	26
Figure 1.4. The distribution of <i>Gadus morhua</i> and spawning sites across the North Atlantic	27
Figure 1.5. A simplified Barents Sea food web	29
Figure 2.1. Counts of unique cod individuals sampled each year of the IMR-PINRO stomach survey.	35
Figure 2.2. Counts of total samples for each month in the study period. Darker shades of blue indicate a higher number of samples. Counts have been binned into five categories for the sake of visual contrast.	36
Figure 2.3. BS cod body length distribution.	37
Figure 2.4 Distribution of BS cod body weight.	38
Figure 2.5. Relative abundance of each 10cm length class of cod. Each stack represents the relative proportion of each length group in the population for each year in the study period.	40
Figure 2.6. Left: hex map of BS cod body length difference from the sample mean. Samples from red shaded hexes are smaller than the sample mean, while blue shaded hexes are larger than the sample mean. Right: Map of the number of cod sampled within each hex. There were 24,028 trawls across all stations in the study period.	41
Figure 2.7. Distribution of BS cod age	43
Figure 2.8. The relative proportion of BS cod age deciles across the study period as a fraction of total samples.	44
Figure 2.9. Top: Map of mean age within each hex. Sampled individuals tend to be older in the northern region of the Barents Sea and the southwest. Bottom: The map of when researchers first sampled each area shows the survey area's expansion into the northeast Barents Sea.	45
Figure 2.10. Total counts for each prey category	48

Figure 2.11. Fraction of total diet by weight for each prey category.	48
Figure 2.12. Fraction of total diet by weight for each year, each sub chart represents a different prey category.	50
Figure 2.13. Fraction of total diet by weight for each month, each sub chart presents a different prey category. The background is shaded to represent each meteorological season. spring - Green, summer - Pink, autumn - Yellow, winter - Blue.	51
Figure 2.14. Fraction of weight contributed by the category with the most significant contribution in each year or 'top' prey category. Each category is identified with a unique colour. The dotted line is a fitted LOESS function which suggests that the fraction of diet accounted for by the top prey category varies over time.	52
Figure 2.15. Top prey category by dietary weight and number of samples in a 2°x1° grid across the study domain.	54
Figure 2.16. The number of unique species identified in diet within each grid cell.	55
Figure 2.17. cod sampled per cell vs Unique prey identified per cell. Points are from data, and the line of best fit was produced using LOESS smoothing.	56
Figure 2.18. The relationship between cod length and prey length. The maximum prey length increases with cod length.	58
Figure 2.19 Dendrogram of length clusters identified by diet.	59
Figure 2.20. Diet fraction by weight for each prey category within each size group.	60
Figure 2.21 Diet fraction by weight for each prey category within each size group. This plot shows the same information as Figure 2.20 but allows an intuitive view of how diet makeup varies between groups.	61
Figure 2.22. Shannon Diversity Index for each cod size group [<20cm (S), 20-100cm (M) and >100cm (L)] in each year	62
Figure 2.23. Top prey categories by the fraction of total prey weight consumed by each cod size group in each year of the study. A LOESS function highlights trends in the dominance of the top prey category in the diet.	64
Figure 2.24. Top prey category in each cell of a 2° x 1° grid across the study area, separated by size group. A top prey category contributed the largest fraction of weight to diet within that cell and size group. The right column shows the number of individual prey items identified within the cod of each size group sampled within each cell. Cells with fewer than five samples were omitted.	66
Figure 3.1. An example of checkerboard2 partitioning. The space is split into checkerboards at two spatial scales, resulting in four groups. Colored circles represent grouped presence records.	80

Figure 3.2. Variable Contribution Percentages for Maxent model. Species: <i>Gadus morhua</i> , Model Structure: LQH 3. Data period: 1991-2017.	86
Figure 3.3. Permutation Importance Percentages for Maxent model. Species: <i>Gadus morhua</i> , Model Structure: LQH 3. Data period: 1991-2017. These results suggest that mean annual bottom temperature is the most important predictor.	87
Figure 3.4. Maxent response curves for each variable in the final model. Each curve shows the relationship between the variable value and the predicted value of suitability in a cell.	88
Figure 3.5. Predicted suitability of each cell as an environment for Atlantic cod. Higher values represent a more suitable environment based upon the Maxent model formulation.	90
Figure 3.6. The prey_layer was created from modelling the distribution of 13 key prey species with Maxent. Each cell is a count of how many species were predicted to be above a threshold of environmental suitability there.	92
Figure 3.7. Percent Contribution of variables in model	94
Figure 3.8. Permutation importance of variables in model	95
Figure 3.9. Response curves for each variable in model	96
Figure 3.10. Maxent model with prey availability map projection	97
Figure 3.11. Differences between base and prey model projections	99
Figure 3.12. Permutation importance of each variable across size structure groups with and without a prey availability layer	101
Figure 3.13. Maxent models for each size group with and without a prey layer map projections	102
Figure 3.14. Boxplots of Test AUC values for each time period length group	104
Figure 3.15. Mean P.I. % with 95% confidence intervals for Annual, Five-year and Ten-year model variables. The number of models containing each variable is labelled at $y = 0$ for each variable.	106
Figure 3.16. Seasonal model variable P.I. distributions. Top - summer, Bottom - winter.	109
Figure 3.17. Mean and standard deviation suitability scores per cell for each temporal group.	111
Figure 4.1. Overview of where ‘Average Model Projections’ were used in lieu of temporally specific models. The number of occurrence records available within each period is labelled.	120
Figure 4.2. Distribution of test AUC’s for summer and winter models for all species. Boxes show median, upper quartile and lower quartile of data. Whiskers show the maximum and minimum of the data, while outliers are shown as ‘X’s and are not	123

included in the median/quartile calculations but are shown independently.	
Figure 4.3. Mean cloglog, Standard Deviation cloglog and Earliest Suitable Year maps for <i>Gadus morhua</i> (S) in summer and winter.	125
Figure 4.4. Distribution area (km <sup>2</sup> ) for <i>Gadus morhua</i> (S) in summer and winter.	126
Figure 4.5. Mean cloglog, Standard Deviation cloglog and Earliest Suitable Year maps for <i>Gadus morhua</i> (M) in summer and winter.	127
Figure 4.6. Distribution area (km <sup>2</sup> ) for <i>Gadus morhua</i> (M) in summer and winter.	128
Figure 4.7. Mean cloglog, Standard Deviation cloglog and Earliest Suitable Year maps for <i>Gadus morhua</i> (L) in summer and winter.	129
Figure 4.8. Distribution area (km <sup>2</sup> ) for <i>Gadus morhua</i> (L) in summer and winter.	130
Figure 4.9. Mean cloglog, Standard Deviation cloglog and Earliest Suitable Year maps for <i>Mallotus villosus</i> in summer and winter.	131
Figure 4.10. Distribution area (km <sup>2</sup> ) for <i>Mallotus villosus</i> in summer and winter.	132
Figure 4.11. Mean cloglog, Standard Deviation cloglog and Earliest Suitable Year maps for <i>Melanogrammus aeglefinus</i> in summer and winter.	133
Figure 4.12. Distribution area (km <sup>2</sup> ) for <i>Melanogrammus aeglefinus</i> in summer and winter.	134
Figure 4.13. Mean cloglog, Standard Deviation cloglog and Earliest Suitable Year maps for <i>Pandalus borealis</i> in summer and winter.	135
Figure 4.14. Distribution area (km <sup>2</sup> ) for <i>Pandalus borealis</i> in summer and winter.	136
Figure 4.15. Mean cloglog, Standard Deviation cloglog and Earliest Suitable Year maps for <i>Boreogadus saida</i> in summer and winter.	137
Figure 4.16. Distribution area (km <sup>2</sup> ) for <i>Boreogadus saida</i> in summer and winter.	138
Figure 4.17. Area of Overlap (km <sup>2</sup> ) between <i>Gadus morhua</i> (S) and prey groups in summer and winter	139
Figure 4.18. Area of Overlap (km <sup>2</sup> ) between <i>Gadus morhua</i> (M) and prey groups in summer and winter.	141
Figure 4.19. Area of Overlap (km <sup>2</sup> ) between <i>Gadus morhua</i> (L) and prey groups in summer and winter.	142
Figure 4.20. Area of Overlap (km <sup>2</sup> ) between <i>Gadus morhua</i> (S), <i>Gadus morhua</i> (M) and <i>Gadus morhua</i> (L) in summer and winter.	144
Figure 4.21. Mean, standard deviation in P.I. and number of models included in for each variable separated by species group, summer.	145

Figure 4.22. Mean, standard deviation in P.I. and number of models included in for each variable separated by species group, winter.	147
Figure 4.23. Mean P.I. for each variable in the Average models separated by species group, summer.	148
Figure 4.24. Mean P.I. for each variable in the Average models separated by species group, winter.	149
Figure 5.1. Structure of the simulation problem	153
Figure 5.2. Structure of the System Identification Problem	154
Figure 5.3. Schematic representation of NARMAX dictionary of terms for a model with a maximum lag of 1, minimum input data delay of 1 and an autoregressive term and two input variables. The maximum degree of the model is 2, allowing for nonlinear second order model terms.	156
Figure 5.4. Schematic representation of the nested structure is used to identify the optimal combination of hyperparameters in the final NARMAX model. The NARMAX model is nested within a brute force search of the hyperparameter space. This process is repeated for every target variable, so hyperparameter structure varies between experiments.	160
Figure 5.5 NARMAX fit versus fraction of cod diet accounted for by <i>Mallotus villosus</i> . Blue: Observed data, Green: NARMAX fit to training data, Thick Red: NARMAX fit to test data. Thin Red: Difference between Observed and fitted lines.	163
Figure 5.6 NARMAX fit versus fraction of cod diet accounted for by <i>Melanogrammus aeglefinus</i> . Blue: Observed data, Green: NARMAX fit to training data, Thick-Red: NARMAX fit to test data, Thin-Red: Difference between Observed and NARMAX fit.	165
Figure 5.7 NARMAX fit versus fraction of cod diet accounted for by <i>Pandalus borealis</i> . Blue: Observed data, Green: NARMAX fit to training data, Thick-Red: NARMAX fit to test data, Thin-Red: Difference between Observed and NARMAX fit.	167
Figure 5.8. NARMAX fit versus fraction of cod diet accounted for by <i>Boreogadus saida</i> . Blue: Observed data, Green: NARMAX fit to training data, Thick-Red: NARMAX fit to test data, Thin-Red: Difference between Observed and NARMAX fit.	170
Figure 5.9. NARMAX fit versus fraction of cod diet accounted for by <i>Gadus morhua</i> . Blue: Observed data, Green: NARMAX fit to training data, Thick-Red: NARMAX fit to test data, Thin-Red: Difference between Observed and NARMAX fit.	172
Figure 5.10 NARMAX fit versus total mature biomass of <i>Gadus morhua</i> . Blue: Observed data, Green: NARMAX fit to training data, Thick-Red: NARMAX fit to test data, Thin-Red: Difference between Observed and NARMAX fit.	174
Figure 5.11 NARMAX fit versus total spawning biomass of <i>Gadus morhua</i> . Blue: Observed data, Green: NARMAX fit to training data, Thick-Red: NARMAX fit to test data, Thin-Red: Difference between Observed and NARMAX fit.	176

Figure 5.12 NARMAX fit versus recruitment of <i>Gadus morhua</i> . Blue: Observed data, Green: NARMAX fit to training data, Thick-Red: NARMAX fit to test data, Thin-Red: Difference between Observed and NARMAX fit.	178
Figure 5.13 NARMAX fit versus fraction of sampled <i>Gadus morhua</i> population in IMR-PINRO database <20cm in length. Blue: Observed data, Green: NARMAX fit to training data, Thick-Red: NARMAX fit to test data, Thin-Red: Difference between Observed and NARMAX fit.	180
Figure 5.14 NARMAX fit versus fraction of sampled <i>Gadus morhua</i> population in IMR-PINRO database >20cm, <100cm in length. Blue: Observed data, Green: NARMAX fit to training data, Thick-Red: NARMAX fit to test data, Thin-Red: Difference between Observed and NARMAX fit.	182
Figure 5.15 NARMAX fit versus fraction of sampled <i>Gadus morhua</i> population in IMR-PINRO database >100cm in length. Blue: Observed data, Green: NARMAX fit to training data, Thick-Red: NARMAX fit to test data, Thin-Red: Difference between Observed and NARMAX fit.	184

# Chapter 1 - Introduction

## 1.1. Research Context, Aims and Null Hypotheses

Global ocean warming is causing unprecedented changes in the physical conditions of marine ecosystems worldwide (Cheung et al., 2013; Johnson and Lyman, 2020). These changes are profoundly felt in the arctic and subarctic seas, where sea ice is on a trend towards thinning and retreating earlier in the year (Francis and Hunter, 2006; Holland et al., 2006) and an increase in warm water transported into the region from the Atlantic ocean is driving water temperatures higher and fundamentally changing the basis of arctic and subarctic marine ecosystems (Årthun et al., 2012; Barton et al., 2018; Boitsov et al., 2012; Dalpadado et al., 2012). The consequences of this warming are extensive and multilayered, as there are macroscale changes in the distribution, growth and feeding behaviour of fish assemblages (Dalpadado et al., 2014; Eriksen et al., 2017; Gjørseter and Loeng, 1987; Johannesen et al., 2012a, 2012b). These behavioural changes have non-trivial ramifications for ecosystem management and fisheries planning due to the interactions between species in the same food web (Bogstad et al., 2000; Casini et al., 2009; Eriksen et al., 2021a). Understanding the consequences of environmental change on the food web of subarctic ecosystems becomes an important goal for marine policymakers, and the expectation of continued environmental variability and change has resulted in uncertainty about how ecosystems will respond. (ICES, 2017; Olsen et al., 2007).

The Barents Sea is a subarctic sea with a highly productive ecosystem and several commercially important fish species. Foremost amongst them is *Gadus morhua*, Atlantic cod. The Barents Sea cod stock is the largest globally, following extensive stock collapses in the East Atlantic in the late 20th century. Barents Sea cod is a top predator in the ecosystem (Bogstad et al., 2000; Holt et al., 2019) with a diverse diet across its varied life history, predated on a wide range of benthos and fish, including cannibalism between larger and smaller individuals of its species. Trophic dynamics are built on a foundation determined by the characteristics of the physical environment: temperature, light, salinity, oxygen content etc. (Kortsch et al., 2015). These factors determine the health of marine populations, how large individuals grow, the rate of mortality, abundance, distribution and more. First-order environmental effects have far-reaching consequences for the trophic interactions between species in the region. These changes, and the resulting feedback effects on the demographics of involved species populations, are difficult to predict. Long term environmental

change in the Barents Sea is already ongoing, and the consequences of further change must be understood to prevent catastrophic mismanagement of ecological resources.

Extensive surveys of the Barents Sea ecosystem and, in particular, the state of the Barents Sea cod stock provide a vast source of quantitative and qualitative data about the region's trophic dynamics, which have yet to be fully explored. Statistical analysis of existing data can give us insight into the historical state of the cod population, including measures of the health and size of the stock, its trophic interactions with other species and internal demographic measures such as size structure. These are difficult properties to estimate and predict from mechanistic or theoretical frameworks alone. Using statistical modelling techniques, we can gain new insights into factors that drive patterns that we observe in historical data and attempt to quantify the relationship between crucial ecosystem parameters. The IMR-PINRO cod stomach database (Dolgov et al., 2007; Holt et al., 2019; Mehl and Yaragina, 1992) provides a rich and underexplored source of data on the diet and demographics of Barents Sea cod.

This thesis seeks to quantify the effects of environmental variability on Barents Sea cod's diet, demographics, and distribution using a novel combined statistical modelling approach. Three research aims constitute a holistic investigation into the relationship of diet, distribution, and demography.

Aim 1 - To identify the spatio-temporal and ontogenetic dimensions of variability in the diet of Barents Sea cod.

- Objective 1.1. Analyse the spatio-temporal patterns in Barents Sea cod diet from the IMR-PINRO stomach database
- Objective 1.2. Analyse the spatio-temporal population demographic patterns in Barents Sea cod from the IMR-PINRO stomach database
- Objective 1.3. Analyse the ontogenetic dimension of Barents Sea cod diet from the IMR-PINRO stomach database and identify diet-based size groups

Aim 2 - To model the distribution of Barents Sea cod and key prey species over time during the recent past to reveal changes in distribution driven by environmental change.

- Objective 2.1. Test the validity of applying the Maxent species distribution model to Barents Sea cod and evaluate the utility of possible methodological improvements
- Objective 2.2. Model the distribution of Barents Sea cod and key prey species at the highest possible temporal resolution using an optimised Maxent modelling approach
- Objective 2.3. Measure the spatio-temporal variability in the spatial overlap between species groups

Aim 3 - To model key ecological measures of the Barents Sea cod stock and quantify the system of factors that drive variability, incorporating new information about temporal variability in predator-prey spatial overlap.

- Objective 3.1. Model critical measures of population demographics using a NARMAX system identification approach
- Objective 3.2. Model key measures of cod diet using a NARMAX system identification approach
- Objective 3.3. Model key measures of cod size structure using a NARMAX system identification approach

## 1.2. Thesis Structure

Chapter 2 explores a database of cod stomach contents collected since 1984 in the Barents Sea. We use data analysis techniques to investigate the spatio-temporal patterns in cod diet and population demographics (Objectives 1.1, 1.2.). We consider the ontogenetic dimension of diet and use hierarchical clustering to stratify the cod population into three size groups based on the novelty of their diet composition (Objective 1.3.). The results of our analysis are used to direct the modelling process in Chapters 3, 4 and 5.

Chapter 3 presents a methodological assessment of the species distribution model Maxent as applied to Barents Sea cod (Objective 2.1.). We investigate the potential of the model to predict distribution

successfully and explore a range of methodological improvements to improve our confidence in model validity. We investigate the impact of changing the time scale of the input data and establish the highest suitable temporal resolution for mapping species distributions.

In Chapter 4, we apply the methodology optimised in Chapter 3 to produce Maxent models at a seasonal scale for each of the size classes of *Gadus morhua* determined from Chapter 2, *Mallotus villosus*, *Melanogrammus aeglefinus*, *Pandalus borealis* and *Boreogadus saida* in each year from 1991-2017 (Objective 2.2.). We examine the long-term distribution changes for each group and discuss the factors responsible for distribution and what is driving change. We then examine the spatial overlap between various predator-prey pairings (Objective 2.3.).

In Chapter 5, we investigate time-series measures of key ecological variables. We apply a NARMAX system identification model to fit polynomial models to a range of measures from population dynamics (Objective 3.1), size structure (Objective 3.2.) and diet (Objective 3.3.). We incorporate a wide range of plausible inputs, including new variables derived from our Maxent modelling in Chapter 4 to represent the spatial overlap between species. We discuss what the resulting model structures tell us about the system under study and the relationship between spatial overlap and key ecological measures.

In Chapters 6 and 7, we present a discussion of the results of our investigation, synthesising our data analysis and modelling into a cohesive whole. We evaluate our success in achieving the aims and objectives set out in Section 1.4, and we present our overall conclusions. Finally, we discuss the limitations of our study and what could be done to improve it, and we suggest some avenues for further work.

### 1.3. Cod: DIet and food web dyNAMics (CoDINA)

This PhD candidacy was carried out as part of a collaboration between the University of Sheffield (UK), CEFAS (UK), the Institute of Marine Research (IMR, Norway) and PINRO (Russia). The CoDINA project aimed to improve our understanding of pelagic sub-arctic marine ecosystems through an ensemble data analysis and modelling approach on existing diet and hydrographic data. The modelling methodologies used in this thesis, Maxent and NARMAX, were the University of Sheffield's contribution to the ensemble. Though the aims of this thesis are in line with the

objectives of the CoDINA project, they constitute an independent, holistic investigation of the diet and demographics of Barents Sea cod.

## 1.4. Scientific Background

### 1.4.1 The Barents Sea

#### 1.4.1.1. Physical characteristics of the Barents Sea

The Barents Sea is a subarctic shelf sea located off the northern coast of Norway and Russia. It is outlined by a 500m depth contour to the west and north, separating it from the Norwegian sea and the Arctic. In the east, the archipelago of Novaya Zemlya marks its eastern boundary adjacent to the Kara Sea. The Barents Sea covers approximately 1.6 million kilometres squared and is relatively shallow, with an average depth of 230 metres distributed over a rough topography of small basins separated by shallow ridges. There are several deep troughs running from the central Barents Sea to the northern and western shelf breaks, which allow for the influx of relatively warm Atlantic water to pass through and into the Arctic basin. The influence of the Atlantic water is significant for many aspects of the physical and ecological properties of the Barents Sea (Dalpadado et al., 2012; Loeng, 1991), and as a result, it is sensitive to large scale atmospheric effects, e.g. the North Atlantic Oscillation (Ottersen et al., 2001). Figure 1.1 shows the Barents Sea's location, topography, and major currents.

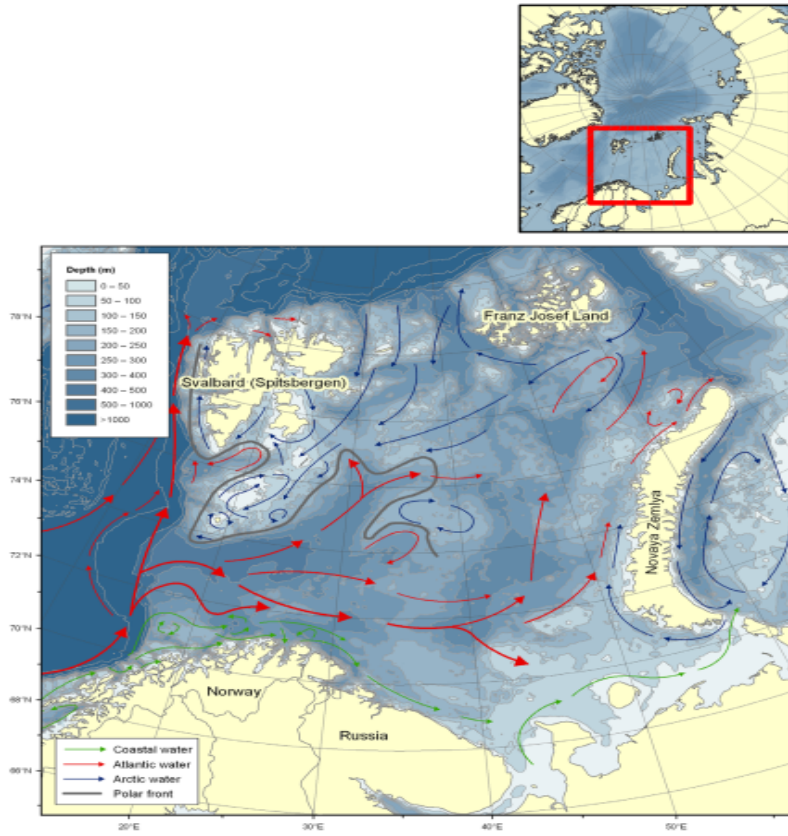


Figure 1.1. Map of the Barents Sea showing bottom topography and currents adapted from (Johannesen et al., 2012b)

#### 1.4.1.2. Barents Sea Climate and Ecosystem

The climate of the Barents Sea is dominated by the interaction between relatively warm ( $> 3\text{C}$ ) Atlantic water flowing in from the southwest and colder ( $< 0\text{C}$ ) Arctic water in the north. The two water bodies maintain separation, with a barrier of Mixed water between them. The extent of these water masses is visible in Figure 1.2. These water mass boundaries create distinct environmental subregions with profound implications for the Barents Sea ecosystem.

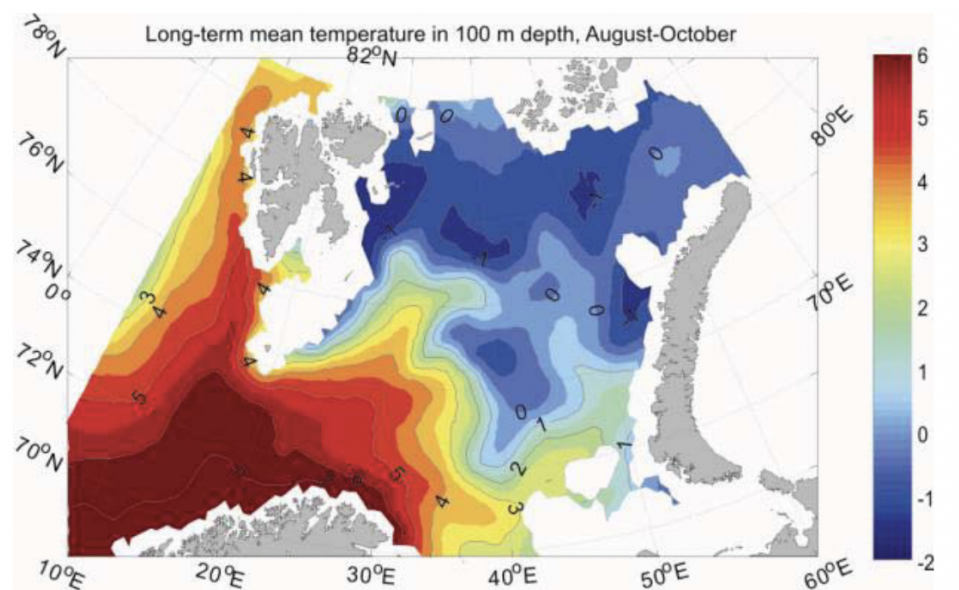


Figure 1.2. Long-term mean water temperature in the Barents Sea as of August-October 2008. The delineation between Atlantic ( $> 3\text{C}$ ), Mixed ( $0-3\text{C}$ ) and the Arctic ( $< 0\text{C}$ ) water is visible. (Aanes et al., 2009)

The oceanographic environment is primarily determined by the properties of the Atlantic water flowing into the Barents Sea (Jakobsen and Ozhigin, 2011), which varies due to larger Atlantic circulation patterns and environmental variability (Skagseth et al., 2008). Temperatures are also affected to a lesser extent by surface-air exchange (Sandø et al., 2010) and solar radiation. The Barents Sea has been warming in recent decades due to increased heat flux from the Atlantic water since the 1970s (Årthun and Schrum, 2010; Eriksen et al., 2017; Kohnemann et al., 2017), which has reduced sea-ice cover during the winter (Smedsrud et al., 2013), increased net primary production (Arrigo et al., 2008; Sakshaug, 2004) and provided better feeding conditions for species such as capelin and cod (Dalpadado et al., 2014, 2012). The environment changes significantly by season, with most sea ice melting entirely during the summer (Smedsrud et al., 2013). The mixing of Atlantic and Arctic water creates a productive environment supporting a robust marine ecosystem.

The assemblages of the Barents Sea are broadly grouped into boreal, semi-boreal and arctic species, depending on their distribution due to environmental preference. (Aanes et al., 2009).

A detailed description of the Barents Sea ecosystem can be found in many existing resources, e.g. Jakobsen and Ozhigin (2011), but a brief overview of the major components are provided here. High levels of primary production provide the foundation for the rich Barents Sea ecosystem (Sakshaug, 2004). Phytoplankton blooms occur seasonally in the southern Barents Sea and following sea ice retreat in the summer (Hodal and Kristiansen, 2008; Signorini and McClain, 2009). The abundant and diverse phytoplankton are consumed by herbivorous macrozooplankton, such as Euphausiids (Krill), which are themselves key prey species for larger fish species such as *Mallotus villosus* (Capelin) and *Boreogadus saida* (Polar cod) as well as a range of juveniles from the wide range of piscine species in the ecosystem. (Dalpadado et al., 2020)

Zoogeographical groupings of fish species in the Barents Sea were organised by Andriyashev and Chernova (1995), into seven groups: Arctic; Mainly arctic; Arctic-boreal; Mainly boreal; Boreal; South boreal and Widely distributed. These groups are broad definitions of the environments exploited by fish in the Barents Sea. Generally, the water mass, water depth and sediment type are the essential factors for defining the habitat of any given species. Ten fish species accounted for over 90% of the total number of specimens caught during the 2007 Barents Sea ecosystem survey (Stiansen et al., 2009), though around 100 or more fish species are generally identified during routine ecosystem surveys in a given year. Some of these species inhabit the Barents Sea exclusively. Others spawn elsewhere before migrating to the Barents Sea to feed, while others temporarily migrate through or into the Barents Sea. In this thesis, we are interested in the role of a commercially important species, *Gadus morhua*, in the Barents Sea ecosystem, particularly how it relates to the Barents Sea food web. The following section provides an overview of the species, specifically the Barents Sea stock.

## 1.4.2. The significance of Atlantic cod, *Gadus morhua*

### 1.4.2.1. An overview of *Gadus morhua*



Figure 1.3. A photograph of an adult *Gadus morhua*. Credit: FAO website (“FAO Fisheries & Aquaculture - Cultured Aquatic Species Information Programme - *Gadus morhua* (Linnaeus, 1758),” n.d.)

This section details the key characteristics of *Gadus morhua* physiology and ecology. A comprehensive resource detailing the bio-ecology of Atlantic cod can be found in Rose (2018).

*Gadus morhua* (Atlantic cod) are a widespread, piscivorous, demersal fish species, pictured in Figure 1.3. They have a maximum lifespan of around twelve years and develop from eggs to fry, then juveniles, reaching maturity from between two to eight years of age depending on their location. *Gadus morhua* moves through life stages with distinct ecological roles as they mature. As eggs and larvae, they are distributed throughout the spawning region by ocean currents and consume mainly zooplankton, such as *Calanus finmarchicus* (Endo et al., 2022), while being preyed upon by larger species. Conditions during the larval stage have profound impacts for a particular year class of the population, as the availability of food (or lack thereof) during the fixed spawning period determines the speed of growth and survival rates, often studied as the ‘match/mismatch’ hypothesis (Endo et al., 2022). As juveniles, they are pelagic, spending most of their time in the water column preying on a range of non-piscine species. The age of maturity varies between stocks, but maturity refers to the age at which the individual has reached sexual maturity and is capable of reproduction. At this stage, *Gadus morhua* is demersal and highly mobile within its environment and is a voracious predator.

Mature *Gadus morhua* can grow up to lengths of 150cm and weigh up to 90kg (Wilmot, n.d.), and a mature female cod can lay millions of eggs each year. Despite vast numbers of fertilised eggs being released yearly, only a fraction survive long enough to develop into juveniles. This reproductive strategy is very effective, resulting in large historic stocks with enormous biomass. Unfortunately, the reputation for the species as abundant, combined with other desirable qualities, led to mismanagement of cod fisheries across the Atlantic (Milich, 1999; Walters and Maguire, 1996).

As the name suggests, Atlantic cod are distributed across seas in the North Atlantic, as shown in Figure 1.4.

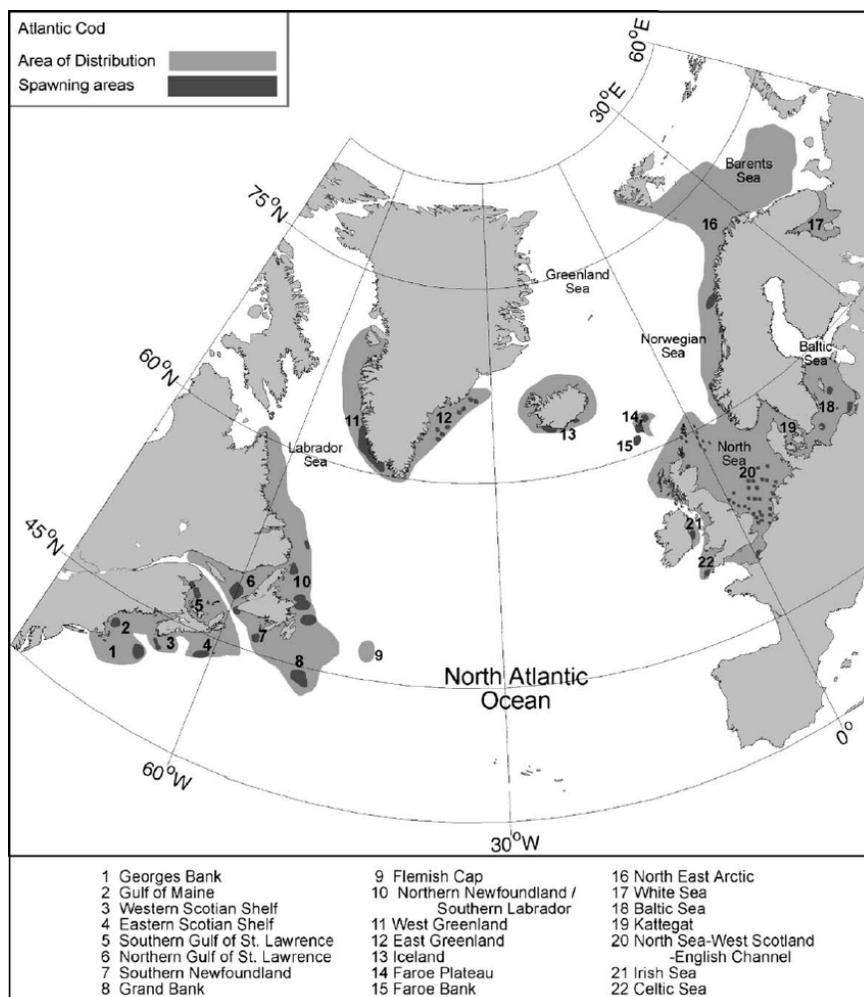


Figure 1.4. The distribution of *Gadus morhua* and spawning sites across the North Atlantic. Source: (Drinkwater, 2005).

*Gadus morhua* is a valuable commercially fished species due to its taste, abundance and historical consumption (Kurlansky, 1997). In the 20th century, overexploitation of cod fisheries led to stock collapses in the West Atlantic. (Milich, 1999; Walters and Maguire, 1996). The overexploitation was due to a combination of more efficient fishing techniques, complex socio-economic factors, and a belief that cod was so abundant that it could sustain higher yields. Unfortunately, once the signs of overexploitation were apparent, it was too late to prevent further collapse. In the Labrador sea and off the coast of Newfoundland, the cod stock lost up to 95% of its biomass in the 1990s (Milich, 1999).

Today, Atlantic cod is still a vital fished resource, with hundreds of thousands of tonnes extracted from east Atlantic fisheries each year, e.g. (ICES, 2017). While the west Atlantic fisheries have struggled to recover from the collapse, the east Atlantic fisheries now contain the largest stocks of Atlantic cod globally, with the largest stock by far being Barents Sea cod.

#### 1.4.2.2. Barents Sea cod

Barents Sea cod is also known as Arctic-Norwegian cod or Northeast arctic cod. However, all names refer to *Gadus morhua* occupying the Barents Sea, from the Norwegian coast near Lofoten to the coast of Svalbard and the arctic, and from west to east at the border of the Norwegian Sea to the archipelago of Novaya Zemlya. Cod spawn along the Norwegian coast, migrating during the winter-spring season to do so (Opdal et al., 2008; Ottersen et al., 2014).

The Barents Sea cod stock is currently the largest in the world, the stock is stable, and the fishery has been declared sustainable since 2010 (ICES, 2017). Cod abundance in the region has been at its highest levels since the early 20th century. Although the factors that have led to such a strong recovery are not entirely understood, it is generally considered to have been encouraged by a warming climate that has bolstered primary production, causing an increase in food availability across the ecosystem as well as increasing growth rates (Kjesbu et al., 2014; Ottersen et al., 2010) and extending the suitable range of the species further to the north (Ingvaldsen et al., 2017).

Barents Sea cod are a top predator (Bogstad et al., 2000; Link et al., 2009). Juvenile cod feed primarily on crustaceans and other benthic species, while mature cod feed primarily on a range of pelagic species, including capelin, shrimp and through cannibalism of smaller cod. Due to their position in the food web, cod is an influential species, and variations in their abundance and distribution can directly impact the welfare of key prey species. This unique position makes cod a valuable indicator species for the overall state of the Barents Sea ecosystem. Food web dynamics are

complicated; they are influenced by an array of factors, including climate variation in the short and long term; population dynamics within individual species and between multiple species; variability in fishing mortality affecting each fished species uniquely (Jennings and Kaiser, 1998) and changing spatial overlap between predator and prey species (Fall, 2019). Figure 1.5 shows a simplified Barents Sea food web, focused on the trophic position of cod relative to some key species.

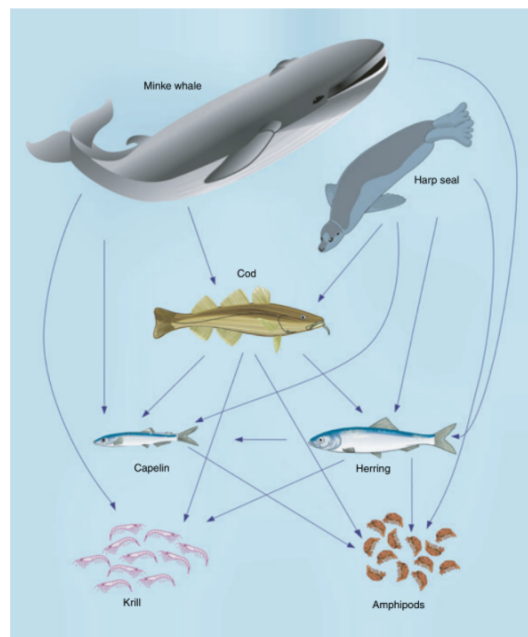


Figure 1.5 - A simplified Barents Sea food web (Link et al. 2009)

### 1.4.3 Trophic dynamics

Trophic or food web dynamics is the primary energy transfer process between different trophic levels within an ecosystem (Lindeman, 1942). The trophic level of a species is relative to the other species in its food web and is distinguished by the direction of predation between species groups. The primary producers at the lowest trophic level create energy through photosynthesis. In the Barents Sea, this is the phytoplankton. At the highest trophic level are the apex predators, with no other species who predate upon them systematically within their local food web. *Gadus morhua* is one such apex predator within the marine food web, though minke whales, harp seals and seabirds are occasional cod consumers.

All the species within the ecosystem are intrinsically linked to one another through the food web. The abundance of a species is strongly linked to the mortality rate due to predation of species of higher trophic levels and the availability of sufficient food in lower trophic levels. Therefore, there are many factors driving trophic dynamics and the broader ecosystem. Environmental variability has a direct impact on growth rate (Boeuf and Payan, 2001; Brander, 1995), fecundity (Hansen et al., 2001; Kjesbu et al., 1998), mortality (Ciannelli et al., 2007) and more on an individual species level. This has the secondary effect of changing the distribution of species within an ecosystem, e.g. (Albouy et al., 2014; Franklin and Miller, 2010), altering the potential for interactions between co-occurring species. Further effects of climate variability on trophic dynamics include altered foraging conditions such as less or more available light or suspended particulates (Puvanendran and Brown, 2002, 1998).

Understanding these complicated dynamics is difficult but essential for ecosystem management (Wassmann et al., 2006). It is important to understand where a fished species stands in the food web before catch targets are set, if a targeted fish species is a major prey item for another species, or is the major predator of a species of a lower trophic level, those species will inadvertently be impacted by a reduction of the targeted species population, and this may lead to damaging trophic cascades (Casini et al., 2009, 2008; Frank et al., 2005). There have been many studies concerning Barents Sea food web dynamics, e.g. (Bogstad et al., 2000; Hjermann et al., 2007; Hop and Gjørseter, 2013; Link et al., 2009; Wassmann et al., 2006) and how climate variability affects the ecosystem (Dalpadado et al., 2014, 2012; Kortsch et al., 2015). Further, the role of cod has been investigated (Ingvaldsen et al., 2017; Renaud et al., 2012). Despite this, there is still significant uncertainty in how the Barents Sea ecosystem will respond to future climate change, and there is still great interest in furthering our understanding of dynamics from a fisheries and management perspective.

There are two broad approaches to modelling trophic dynamics, mechanistically or empirically, though there is a wide overlap between the two. Mechanistic models of trophic dynamics simulate aspects of the system, investigate how changes to the simulated system affect it, and validate those results with observations (Boit et al., 2012; Cohen et al., 1990; Williams and Martinez, 2000). Mechanistic models represent trophic dynamics as an interconnected web of interactions between species and examine aspects such as connectedness (Paine, 1980) and robustness to perturbation (Dunne et al., 2004). Mechanistic models are helpful and provide an interpretable insight into the effects of changes in the food web, but they face challenges when the theoretical model of the

system may not match up with observations (Link, 2002). Conversely, empirical or statistical models explore trophic dynamics by analysing quantitative or qualitative data from the ecosystem that captures predator-prey interactions. One such source of data in marine environments is the stomach contents of predatory species (Hall et al., 1995). Stomach content data provide direct evidence of trophic interaction between two species within a short period before sampling and provides a wealth of information about the feeding habits of the sampled species, not only which species are interacting, but also in aggregate allows relationships in body size to be measured (Cohen et al., 1993; Emmerson and Raffaelli, 2004; Yodzis and Innes, 1992).

Principally, predator-prey interactions in marine ecosystems are driven by a few factors: opportunity of interaction, suitability of relative body-size between predator and prey, the relative fitness of both and the satiety of the predator (Ballard, 2011; Embling et al., 2012). These factors are driven by the physical environment, population dependent effects and human interference. However, each external pressure varies depending on the specific species, location, etc., resulting in a highly complex system that does not operate in the same way across ecosystems. The opportunity for predation can be considered at different scales, from fine-scale individual ambush-escape studies to large scale studies of environmental overlap at a regional or global scale. It is this latter spatial scale that we will examine in this thesis.

At a regional scale, both species must share physical space for predator-prey interactions between a particular species pair. The broadest requirement for this to happen is that a particular location must have environmental conditions suitable for both species, i.e., they have an overlapping environmental niche (Colwell and Futuyma, 1971; Eriksen et al., 2021b). In the marine environment, factors such as the temperature, salinity, oxygenation, and depth drive species distribution within an ecosystem (Andrews et al., 2020; Franklin and Miller, 2010). Further, there are two categories of ecological niches - the fundamental and realised niche (Colwell and Rangel, 2009). The fundamental niche of a species describes all locations within an ecosystem where environmental conditions are suitable for the species to live (Kearney and Porter, 2004). The realised niche is where the species actually live and is a subset of locations within the fundamental niche (Colwell and Rangel, 2009). Factors that limit the realised niche are dispersal, the ability for a species to reach a location from their existing habitat, and biotic variables, such as the availability of sufficient food resources or the avoidance of predators (Franklin and Miller, 2010; Soberon and Nakamura, 2009).

## 1.5 Study Novelty

There are four novel contributions to the field emerging from this thesis. Firstly, we mapped the distribution of *Gadus morhua* and several important species in the Barents Sea with an SDM for the first time, showing how distribution has changed since 1991 as a result of warming water. Secondly, we successfully applied the NARMAX system identification model to a new domain, demonstrating the power of the method for future studies. Thirdly, we combined Maxent and NARMAX for the first time and demonstrated that the information provided by Maxent output improved NARMAX model performance on this system. Finally, we produced new evidence for the borealization of the Barents Sea ecosystem and our results suggest that arctic species such as *Boreogadus saida* are going to play an increasingly important role in the trophic dynamics of Barents Sea cod.

## Chapter 2. Analysis of cod diet and demographics from the IMR-PINRO stomach database

This chapter explores the primary data source supporting this thesis, the IMR-PINRO cod stomach database. This database contains an enormous amount of information about the Barents Sea cod stock and its diet, collected since 1984 and across almost the total span of the region. There are countless ways to interrogate this data and uncover the complex patterns within. Here we provide one such analysis, examining both diet patterns and those measurements taken from the cod population, which are most relevant to our interest in trophic dynamics.

This chapter is organised into three sections. Section 2.1 is a short description of the IMR-PINRO database metadata and the sampling structure in space and time. Section 2.2 outlines the patterns found in the ontogenetic structure of the cod population, which are most relevant to our diet investigation. The size and age structures of the population are explored in both space and time. We raise questions about the causal factors of variability within size structure and the interrelation of size structure and diet. In Section 2.3, we explore the patterns in cod diet within the database. We examine diet overall and how it varies in space, time and on the size of individual cod. We identify complex spatial, temporal and ontogenetic patterns in the diet of Barents Sea cod and consider how we can use our combined modelling approach to explain some of this variation, providing insights essential for the modelling work in Chapter 3 and beyond.

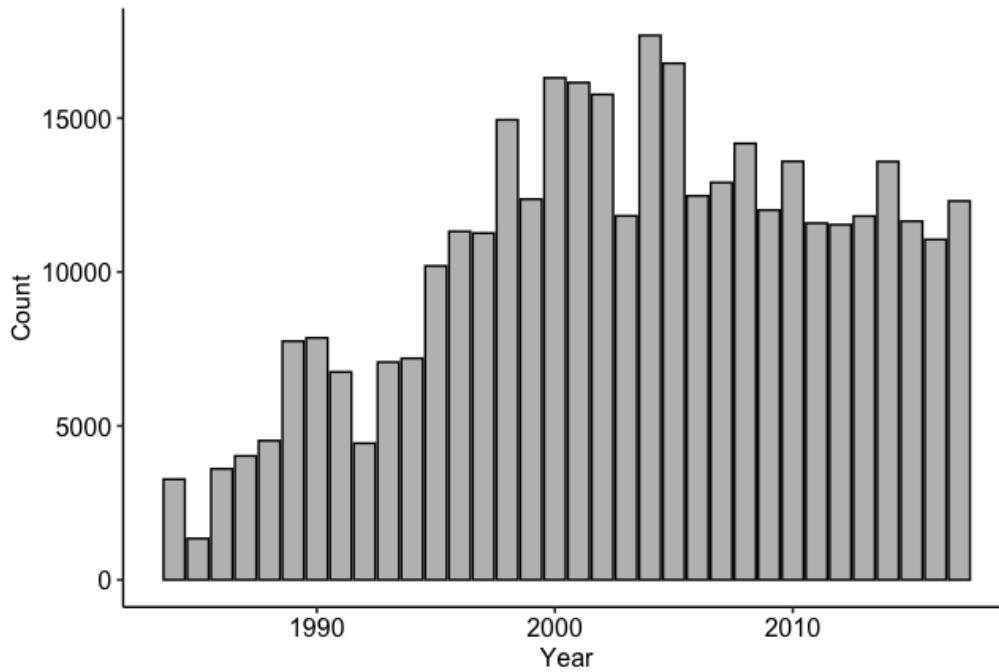
### 2.1. Metadata and sampling distribution

The Norwegian-Russian cod stomach database is a spatiotemporally detailed record of cod stomach samples collected in the Barents Sea between 1984 and the present by a joint team of researchers from the Institute of Marine Research (IMR) in Norway and the Knipovich Polar Research Institute of Marine Fisheries and Oceanography (PINRO) in Russia. The context and background of this study have been discussed in several existing publications, e.g. (Dolgov et al., 2007; Jakobsen and Ozhigin, 2011; Mehl and Yaragina, 1992), among others.

The data used in this thesis is curated by researchers at IMR and contains records collected from 1984 until 2017. The data is stored as a comma-separated values file (.csv) with 576,340 rows (observations) and 41 columns (measures). A table describing each variable recorded in the database can be found in Appendix A.1.

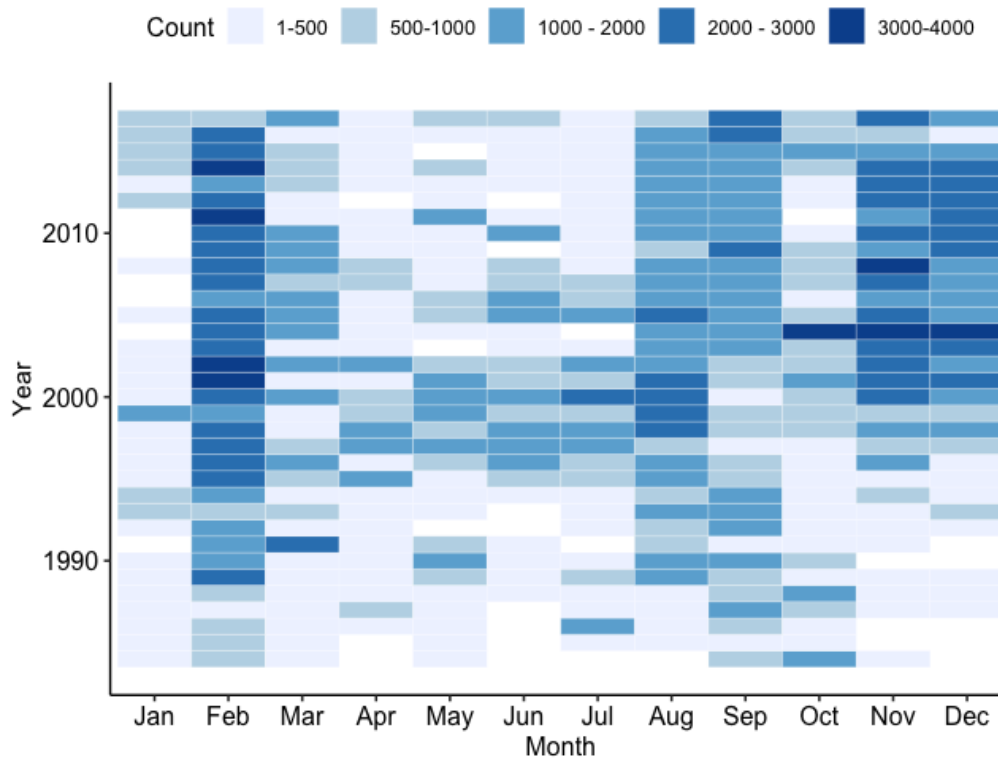
Stomach samples are collected by bottom and pelagic trawls at fixed stations and times across the Barents Sea; sampling methodology is described by (Mehl and Yaragina, 1992). The number of stations in each field season were not consistent, and the position of these stations has changed over time. In general, this has been due to the expansion of stations, but there have been several years with missing stations, particularly from the Russian cruises. The number and location of sampling stations followed the distribution of cod found during a particular season; the surveys extended to additional stations if cod were found at previous stations until no cod were found at the most recent station. The ability of cruises to sample every planned station was sometimes limited by weather and sea-ice. See Appendix A.2 for maps of sample stations for each dataset year.

Figure 2.1 shows the number of unique cod stomachs sampled each year. The range of sampling counts is between its lowest of 1,342 in 1985 and 17,686 in 2004. The mean number of samples is 10,622. This consistently large sample gives us a good source of annual data with no gaps since the surveys began.



*Figure 2.1. Counts of unique cod individuals sampled each year of the IMR-PINRO stomach survey.*

Figure 2.2 shows the temporal sampling pattern at a monthly scale, where the intensity of colour represents the number of samples collected in each month of the study period. This shows the seasonal pattern of sampling and how the sample collection structure has changed over time. The number of samples has increased in recent years, and more of those have been collected during the winter than previously. Across the study period, there are only 34 out of 408 months for which we have no data.



*Figure 2.2. Counts of total samples for each month in the study period. Darker shades of blue indicate a higher number of samples. Counts have been binned into five categories for the sake of visual contrast.*

The spatiotemporal comprehensiveness of this dataset provides an unprecedented window into the diet of Barents Sea cod, and by extension, the trophic dynamics of the Barents Sea ecosystem. By examining the measurements taken of individual cod and the contents of their stomachs in the context of the place and time researchers collected them, we can identify patterns at a very high resolution. In the next section, we investigate the population demographics of Barents Sea cod through the lenses of body length, body weight and age structure. We summarise the population structure, then delve deeper into the structural change in space and time.

## 2.2. Characteristics of the Barents Sea cod population

### 2.2.1. Population size structure

For each cod sampled, researchers recorded the body length (cm) and weight (kg), a total of 363,942 samples. Figure 2.3 shows the distribution of body length for the sampled cod. We can see that the data are normally distributed with a right skew caused by some long outliers. Most of the cod sampled are between 10 and 100cm. The mean body length is 54.32cm. Note that the methodology for sampling requires researchers on sampling vessels to attempt to sample up to 10 individuals per 10cm size group, per station (Mehl and Yaragina, 1992). This method is likely to affect the size distribution by more accurately measuring the prevalence of individuals from the least populous size classes (very small or large) compared to the proportion of the population accounted for by individuals in the most prevalent size classes, as a greater number of those individuals would not be recorded. This means we should be careful when interpreting the summary statistics for the distribution of sizes, but relative changes in the observance of outliers are likely to be real.

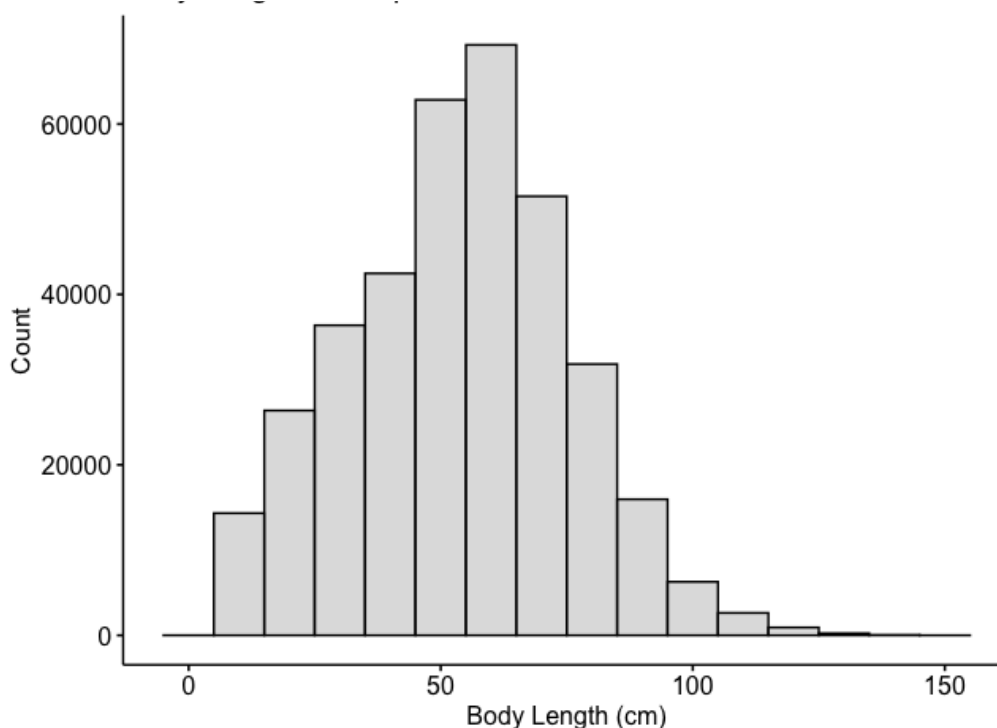
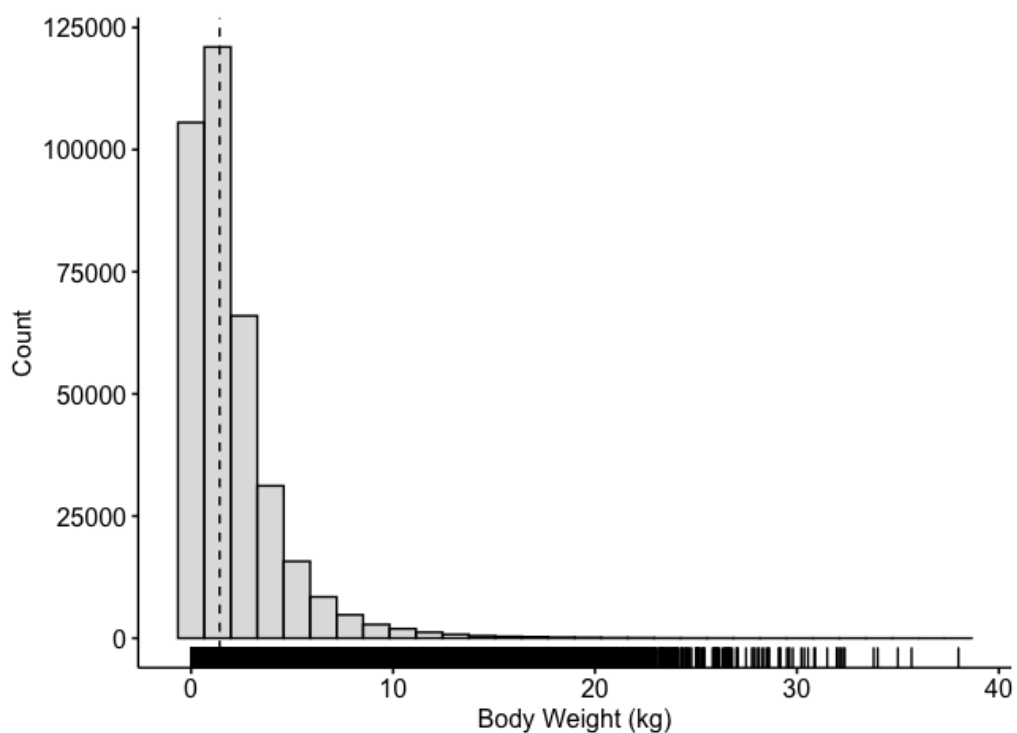


Figure 2.3. BS cod body length distribution.

We can look at body weight distribution in the same way. Figure 2.4 shows this distribution, which has a very long tail into larger weights. The median value of weight is 1.46kg, highlighted by the dotted vertical line. The mean is 2.05kg, influenced by the few very heavy outliers that have been sampled. The same caveats based on sampling methodology described for Figure 2.3 also apply here.



*Figure 2.4 Distribution of BS cod body weight.*

Size structure is an important quality to measure in the population to understand diet. Cod generally consumes prey that falls within a particular ratio of relative body length, which varies between immature and mature individuals (Holt et al., 2019). This means that there is an ontogenetic dimension to diet, which will manifest on a broad scale in the size structure of the population. The data tells us that the size structure of the population varies in time and space, patterns which we will now examine in detail.

### 2.2.1.1. Temporal patterns in size structure

We split the sampled population into 10cm length groups and calculated the fraction of the population accounted for by each group within each annual period from 1984-2017. Figure 2.5 presents this data, with each stacked bar representing a normalised fraction of the population which falls within each 10cm length group from each year. The groups are presented in order of increasing length from bottom to top, from the 0-10cm juveniles to the huge 100cm+ group. We can see the apparent interannual variability in size distribution if we follow any particular group through the years. This figure also indicates that individuals within the population are growing. The proportion of the population longer than 70cm has increased since the study began. There are some potential confounding factors which may affect the observed size structure of the population related to the sampling methodology. First, most of the individuals sampled were captured with bottom trawls which have been shown to find different outcomes than acoustic surveys for population assessment due to the difficulties of catchability for particularly small cod, who can slip through nets, and particularly large cod who are capable of avoiding trawls. Catchability increases with increasing population density in the survey area (Engas and Godø, 1986; Godø et al., 1999).

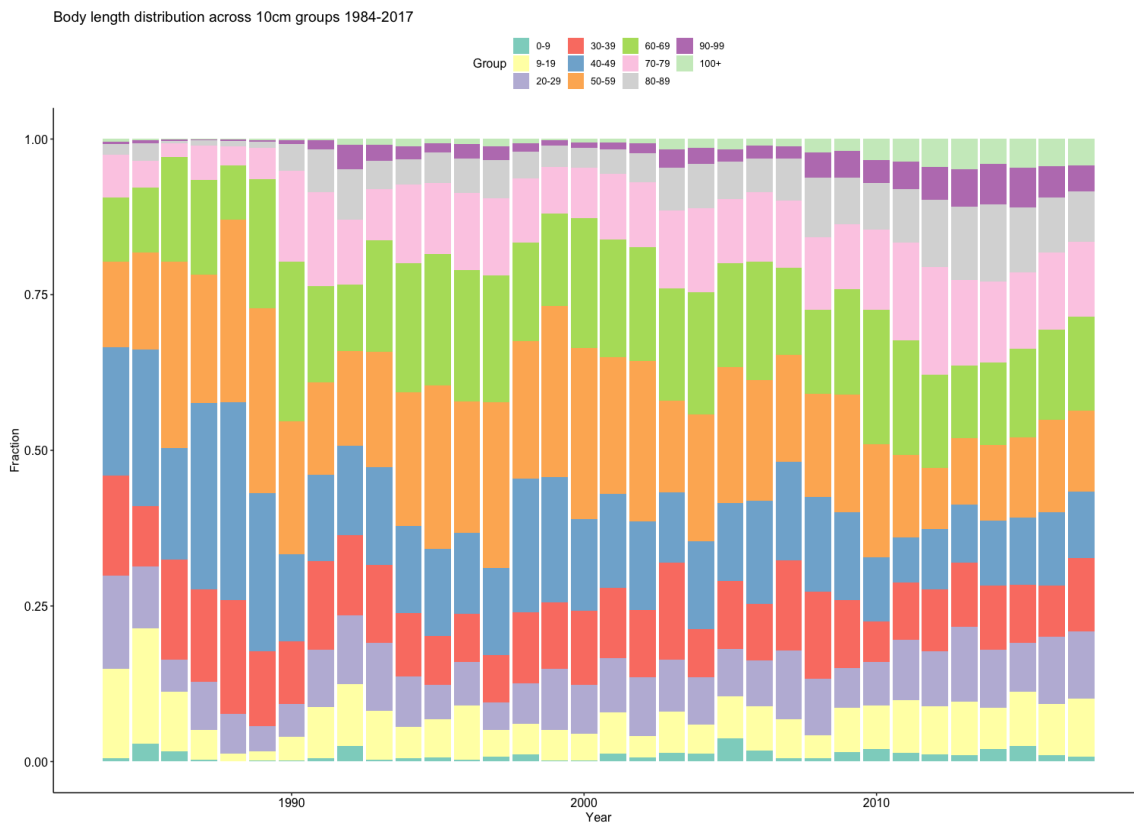


Figure 2.5. Relative abundance of each 10cm length class of cod. Each stack represents the relative proportion of each length group in the population for each year in the study period.

#### 2.2.1.2. Spatial patterns in size structure

Figure 2.6 presents a hex map of the Barents Sea, highlighting how cod sampled from different areas in the region vary in length. The value used to shade each hex is calculated by first taking the mean length of every sample collected within its spatial bounds, then subtracting the mean body length of the sampled population (54.32cm). This highlights regions where the average length of cod sampled deviates from the overall mean. Hexes shaded in red represent areas where the sampled cod are smaller than average, while cod from areas shaded in blue are larger than average. There appears to be a significant spatial variation in the length of samples, with cod from sites in the northeast tending to be larger than average while those around the north coast of Svalbard and in the central-eastern Barents Sea being smaller. Note that this visualisation does not account for the sampling density, also shown in Figure 2.6, and some of these hexes, especially those furthest north, are calculated from tiny sample sizes. Hexes in the most consistently sampled south and the central Barents Sea region are less divergent than hexes in other regions, likely reflecting some sampling bias.

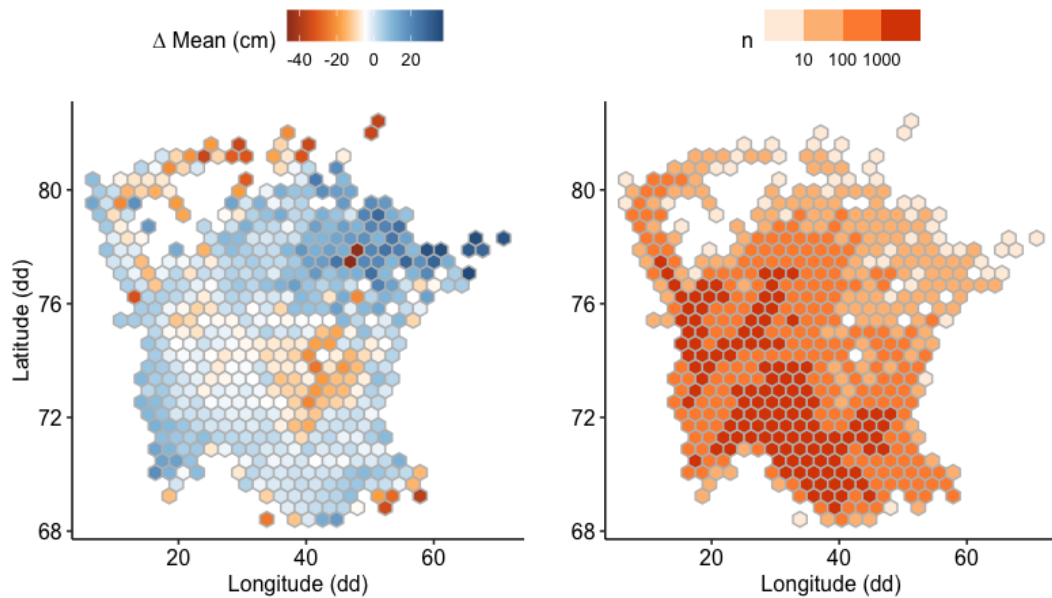


Figure 2.6. Left: hex map of BS cod body length difference from the sample mean. Samples from red shaded hexes are smaller than the sample mean, while blue shaded hexes are larger than the sample mean. Right: Map of the number of cod sampled within each hex. There are 24,028 trawls across all stations in the study period.

We now have some understanding of the size structure of the Barents Sea cod stock. Nothing in this analysis is surprising, but it provides a starting point for a deeper analysis. When we look at how size structure changes over time, we see interannual variability and the emergence of some longer-term growth in the abundance of larger individuals. External factors drive these patterns: the conditions of the physical environment, responses to population density dynamics and the impact of human interference in the form of fishing, to name a few. Quantifying these relationships is difficult, but we can do so using statistical modelling with this large amount of data. We explore this further in Chapter 5.

The spatial size structure is interesting too: it suggests that a long-term spatial heterogeneity exists in the distribution of Barents Sea cod of varying sizes. This species is long-lived, with different environmental tolerances and preferences being observed at various stages of maturity. Some of these factors are well understood from a physiological perspective. One of the most important

environmental factors which affect Barents Sea cod is the temperature of the water. Larger animals are generally distributed in colder regions than smaller animals, a generalisation known as Bergmann's Rule (Blackburn et al., 1999). However, Barents Sea cod are broadly distributed in the region, and the extent to which temperature limits the species within the core of their range is not quantified. The species is also highly mobile and migratory, so it is not evident that we should see such well defined spatial patterns in data collected over 30 years. We might suggest that underlying factors affect the long-term distribution of individuals within the population, stratified by size. Are some subregions of the Barents Sea more suitable for smaller or larger individuals? We will investigate this question further in Chapter 3 and Chapter 4.

### 2.2.2. Population age structure

Age is estimated by counting the number of rings in an individual's otolith, a calcium carbonate structure that grows in the ear canal (Jakobsen and Ozhigin, 2011; Mehl and Yaragina, 1992; Vitale et al., 2019). Age is strongly related to individual size, maturity (Kotenev et al., 2009) and spawning behaviour (Hutchings and Myers, 2011; Marshall et al., 2011) and, by extension, a range of other metrics including mortality and feeding habits.

Figure 2.7 shows that the age of the population follows an approximately normal distribution with a right skew. The mean age is five years, and the oldest individual recorded is 20 years old. The upper tail is so long because the natural lifespan of Atlantic cod is much longer than ten years. Still, fishing mortality is very high in the Barents Sea cod stock, a heavily exploited fishery. Fishing disproportionately targets larger, and therefore generally older individuals. This means that the population is younger than if the stock were untouched by anthropogenic factors.

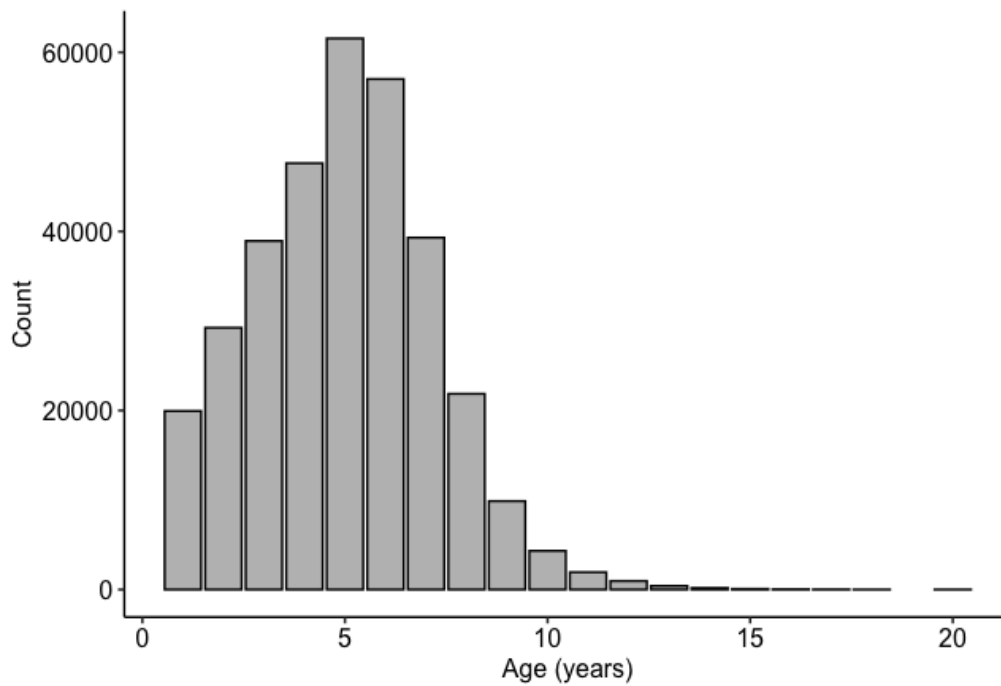


Figure 2.7. Distribution of BS cod age

#### 2.2.2.1. Temporal patterns in age structure

To examine how the age structure has changed, we apply a similar method of cutting the population into ten groups stratified by age. We again examine the proportion of the population accounted for by each age group. This analysis can be seen in Figure 2.8. Consider that the distribution may be skewed as a result of sampling methodology, where up to 10 individuals per 10cm size group were sampled and their otoliths taken.

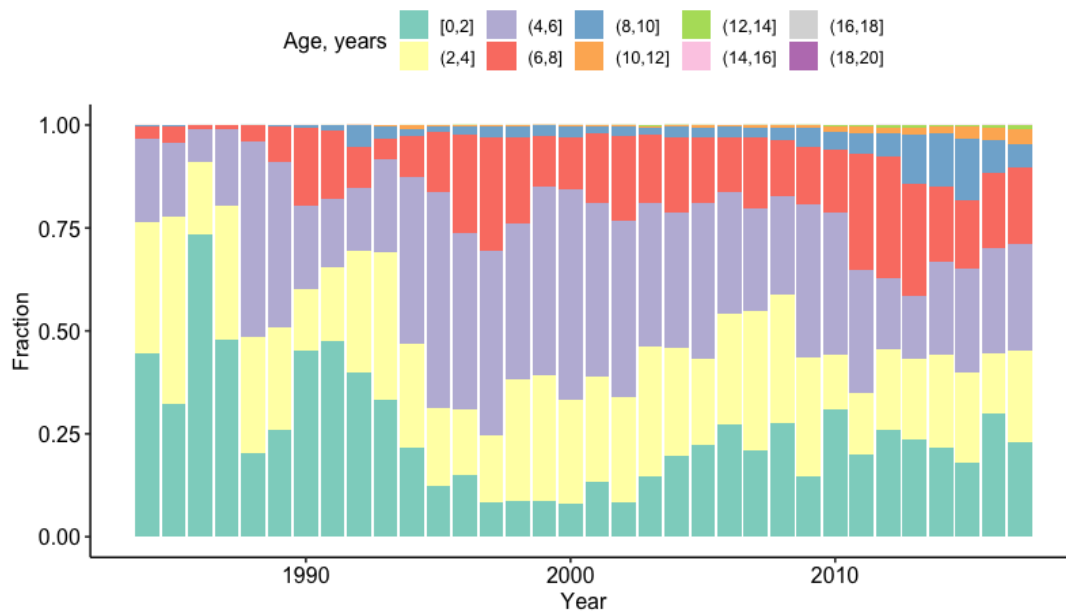


Figure 2.8. The relative proportion of BS cod age deciles across the study period as a fraction of total samples.

We see that the pattern in age structure over time is closely related to the pattern found in body length over time. There has been an increase in the fraction of the population within the older age groups in recent years, particularly in the 2010s. In particular, notice how the proportion of 8 years or older individuals is much larger after 2012. Those older than ten years appear to be steadily increasing in number. Though these are still a small fraction of the population, this growth pattern has ramifications for the short and long term. Seeing the increase in the proportion of older individuals is interesting. Unlike growth, which can be accelerated or slowed depending on environmental conditions, age can only be progressed by avoiding mortality. The increase in particularly old individuals within the sample population may be due to the expansion of the study area into more northern regions of the Barents Sea, where the average age and size of individuals sampled tends to be older and larger than the rest of the sampled population. It could also be possible that this pattern is accurate and that mortality rates for larger individuals have been lower in the 2010s than in previous decades.

#### 2.2.2.2. Spatial patterns in age structure

When we examine the spatial distribution of ages in Figure 2.9, we see that the average age of individuals sampled across the study region seems to vary. Two areas stand out: the northeast and the southwest. In the northeast Barents Sea, it appears that there is a pattern of individuals who are much

older than the population average, over about 7.5 years, within a larger region where individuals are generally older than 5. Compared to the south, the central and north-west area surrounding Svalbard, these regions have a distinct definition. However, when we look at the bottom map in Figure 2.9, we see the disparity when each part of the Barents Sea has been sampled. This north-eastern area has only been sampled in the latter half of the study period, generally after 2000, with some of the most extreme north-east data being collected only after 2010. It is unclear how much this age distribution pattern in the northeast is due to natural spatial diversity, recency bias, or low sample sizes. It could also be a result of lower fishing pressure due to sea ice, allowing individuals residing in the area to live longer, or be an effect of seasonal migration amongst the largest fish.

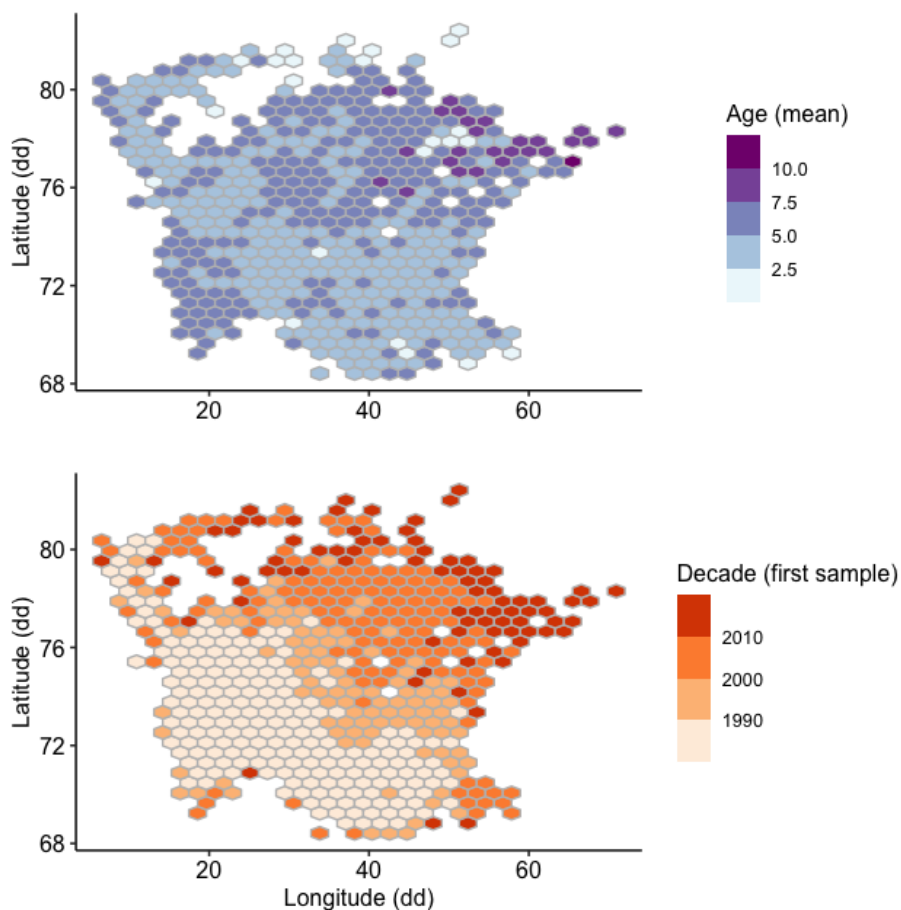


Figure 2.9. Top: Map of mean age within each hex. Sampled individuals tend to be older in the northern region of the Barents Sea and the southwest. Bottom: The map of when researchers first sampled each area shows the survey area's expansion into the northeast Barents Sea.

Putting this aside for the moment, we have a more concrete understanding of the other interesting contrast: the southwest. This region has been sampled since the study began, has a large sample size (Figure 2.15) and appears to identify a contiguous area where the average age of sampled cod is five characterised years or higher, compared to the bulk of the other high and consistently sampled regions where the average age tends to fall below five years. One potential explanation for this pattern is that the southwest Barents Sea, close to the Norwegian coast, is a spawning site for cod. The actual spawning site is further south than the survey area covers, but we could be seeing the effect of repeat migration by mature, fecund cod through this area.

### 2.2.3. Summary

In this section, we have explored the Spatio-temporal patterns in the size and age structure of the Barents Sea cod stock. We have found that these population characteristics are dynamic; both age and size structure vary at annual scales. In both, we are seeing an increase in the fraction of the population accounted for by larger, older individuals. We have found some spatial heterogeneity in the distribution of individuals by size and age. Still, the degree of confidence we can have in these patterns at the northern extremes of the survey area is limited due to small sample sizes and a possible recency bias.

In Chapter 3 and Chapter 4, we will incorporate information about the size structure of the population when building Maxent distribution models and investigating the spatial overlap between cod and its prey. Chapter 5 will re-examine some cod population characteristics and quantify the relationships between the population, its prey consumption, and external factors. We will now explore the diet data, following a similar method of checking the overall patterns, the Spatio-temporal dimension, and the ontogenetic aspects.

### 2.3. Analysis of diet in Barents Sea cod

Cod is a top predator in the Barents Sea and has a diverse diet. Although a few species account for a significant fraction of consumption, over five hundred unique prey species have been identified in the IMR-PINRO database. Here, we use the prey categories defined by (Holt et al. 2019) to group less abundant species and share similar physiological characteristics or taxonomic groups.

Seventeen prey categories encapsulate the many species which are recorded in the database. The total number of prey items recorded for each category is shown in Figure 2.10. 'Other food' is the most frequent category recorded, contrasted with 'Other fish', the 'Other food' category includes a wide range of non-piscine organisms, mostly small in size. 'Shrimp', 'Other fish', 'Capelin' and 'Euphausiids' make up large numbers of the total count, with all other categories appearing to be much less frequent. We can look at this another way by examining the contribution of each category by the weight of prey consumed.

Figure 2.11 shows the same categories, with each bar measuring the fraction of total diet weight that each category contributes. Here we see that capelin provides almost 30% of the total diet by weight, significantly more than the next prey group, 'Other food'. From this perspective, the importance of shrimp is much lower, while both cod (cannibalism) and haddock each appear to be much more critical. BS cod are opportunistic predators; though they seem to rely on a few prey groups for the bulk of their diet, the importance of the smaller groups becomes more apparent when we examine the spatio-temporal context that these records are found in.

For the rest of this analysis, we will be focusing on the fraction of diet contributed by each prey category. This way of interpreting the data is more valuable than strict frequency because it accounts for the size difference between species in each group. A certain amount of energy is transferred from prey to predator, and one large prey item may contain the same energy as multiple smaller prey.

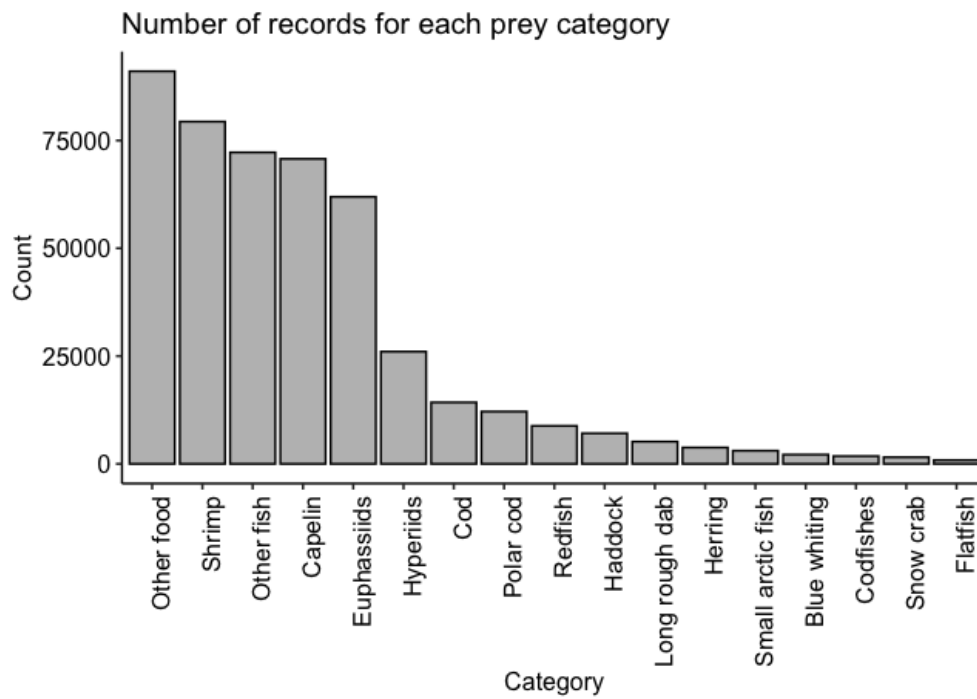


Figure 2.10. Total counts for each prey category

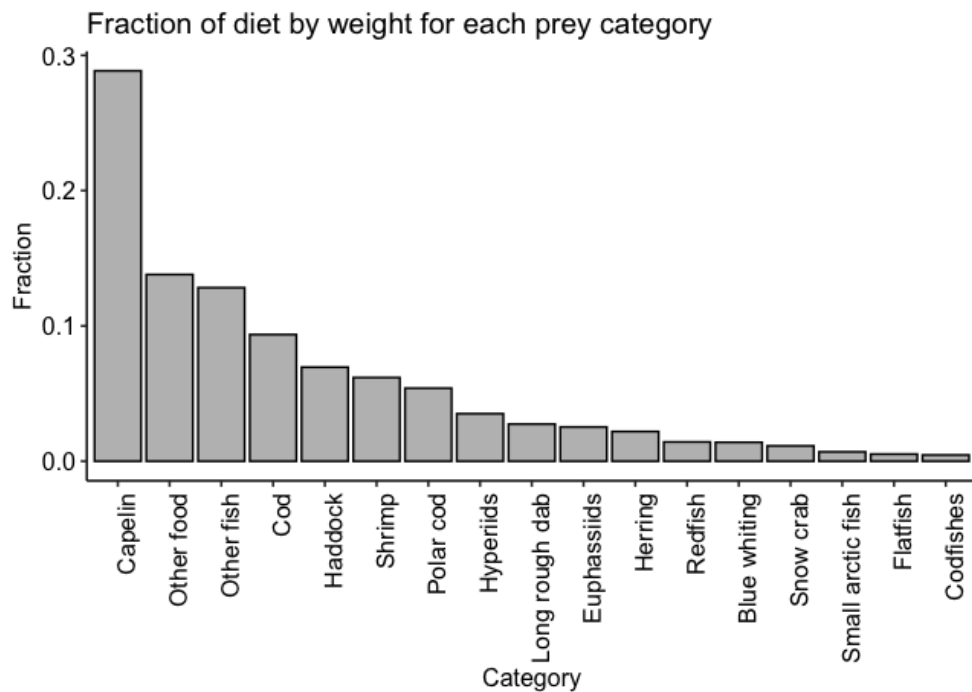


Figure 2.11. Fraction of total diet by weight for each prey category.

### 2.3.1 Temporal patterns in diet

We will now consider how diet has changed over time. Figure 2.12 shows the annual prey contribution to diet as a fraction of total weight consumed in that year. Each chart represents a different prey category. This way of viewing the data shows us which groups generally contribute a significant fraction of total consumed weight and the considerable variability within groups across the study period. Capelin is the most important prey item, and we see that sudden, intermittent collapses characterise the consumption pattern. We know that these events are driven by a collapse in the capelin stock, and when there are not enough capelin available, other prey groups must fill the void (Gjørseter et al., 2009; Holt et al., 2019; Hop and Gjørseter, 2013). When capelin consumption fell dramatically in 1986, we saw a sharp rise in the consumption of hyperiids and a slight increase in cod (cannibalism). Then in the early 1990s, there was a second crash in capelin consumption, but now we see a correspondingly large spike in cannibalism. The dietary response of BS cod to a capelin collapse is complex. There is no clear replacement species or apparent order of preference appearing, which can be discerned from examining consumption patterns alone. We also note that cannibalism increases slightly over time, matching observations of growth in the population structure, and larger individuals are more likely to engage in cannibalistic feeding behaviour. There are other long term dietary changes such as the decreased importance of redfish after the year 2000 and the emergence of snow crab (*Chionoecetes opilio*) in the diet at around the same time. Snow crab is an invasive species that researchers first observed in the Barents Sea in 1996 (Huse and Bakketeig, 2018). We see that it appears to be growing in importance as a prey item, possibly due to the settlement and growth of snow crab as a source population (Agnalt et al., 2011; Alvsvåg et al., 2009).

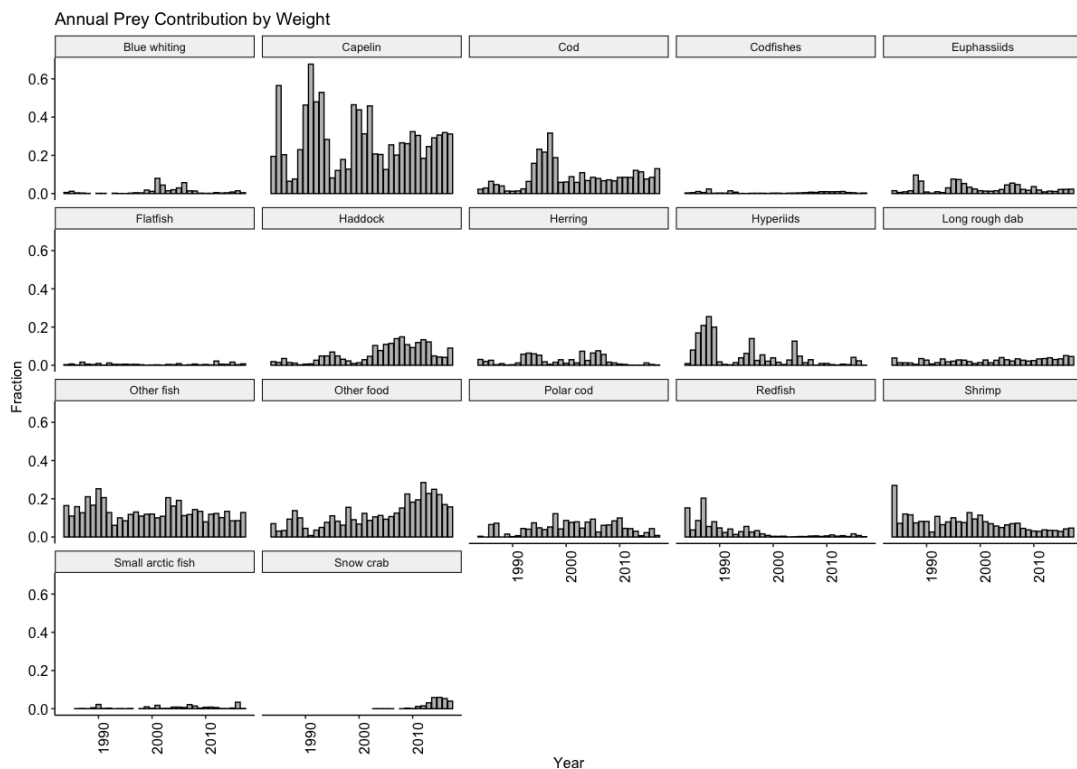


Figure 2.12. Fraction of total diet by weight for each year, each sub chart represents a different prey category.

There is also a significant variation on a seasonal scale. This perspective is presented in Figure 2.13, which shows the diet by weight contributed by each prey category for each month, totalled across the study period. Again, each chart represents a different category, and the background is coloured to demarcate the meteorological seasons that each month falls into. We see the dominance of capelin again, but now we can also see that there is a strong seasonal element: capelin dominates diet in the late winter and early spring but is less prevalent in the summer and autumn. This is likely due to the seasonal migration of cod and the seasonality of spatial overlap between cod and capelin (Fall et al., 2018; Holt et al., 2019; Ottersen, 1998). This seasonality extends to practically all groups that significantly contribute to the diet. During the summer, it seems that cod (cannibalism), euphausiids and shrimp have relative increases in importance and then in autumn, we see a period of high polar cod consumption.

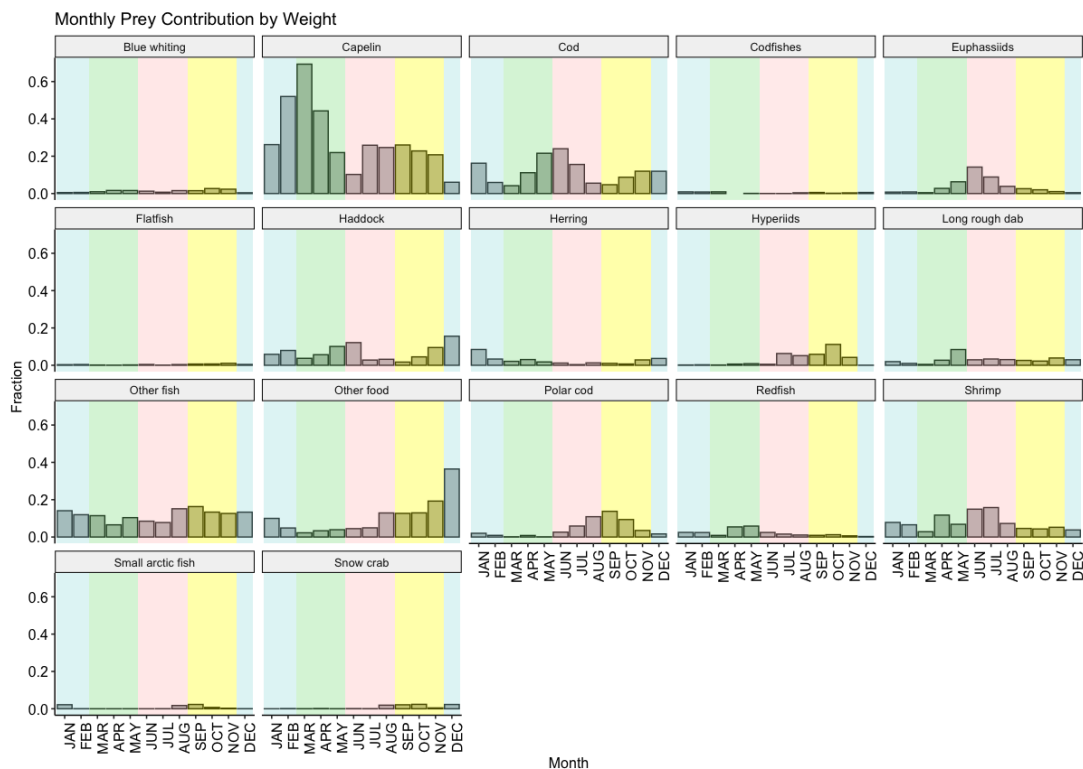


Figure 2.13. Fraction of total diet by weight for each month, each sub chart presents a different prey category. The background is shaded to represent each meteorological season. Spring - Green, summer - Pink, Autumn - Yellow, winter - Blue.

Another interesting perspective on diet is to examine ‘prey switching events’, or sudden changes in the primary prey category. We can see from Figure 2.12 that there are clear patterns of rising and falling within categories across multiple years. Figure 2.14 shows the proportion of diet by weight contributed by the top category for each year in the dataset. Each unique category that was ever a top contributor is presented in a different colour. We see that only six categories have ever been the top contributor to diet by weight in any given year. Out of 33 total years, capelin was the top prey category in 25. Cod (cannibalism) was the top prey category in 4 years, then hyperliids for two years, then shrimp, other food and other fish for one year each. We see that prey switching events in practice mark periods where capelin consumption has significantly fallen for any reason.

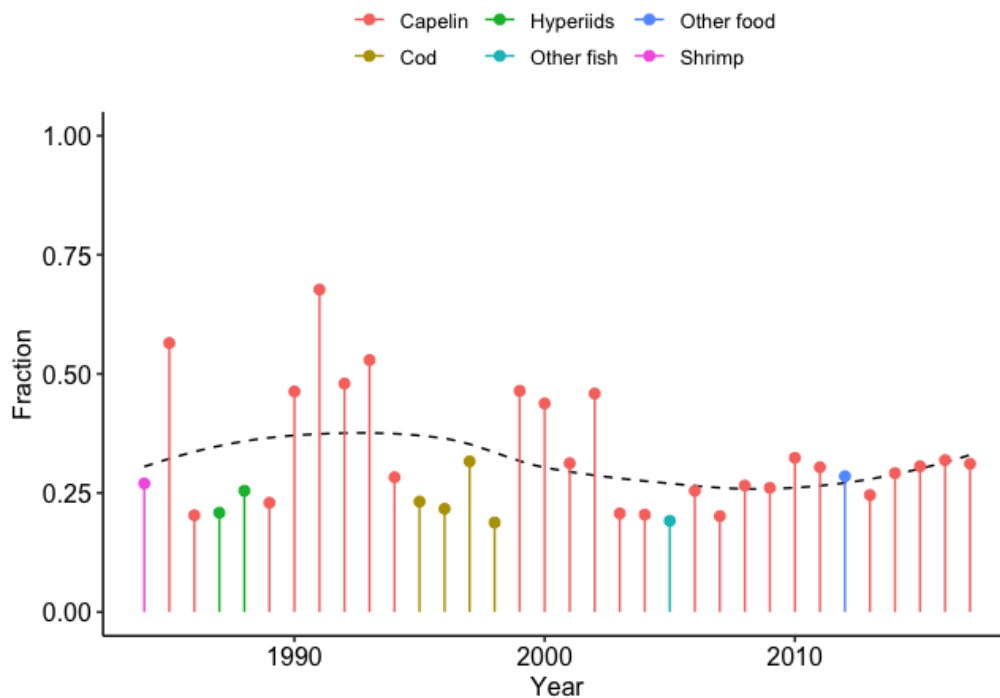


Figure 2.14. Fraction of weight contributed by the category with the most significant contribution in each year or 'top' prey category. Each category is identified with a unique colour. The dotted line is a fitted LOESS function which suggests that the fraction of diet accounted for by the top prey category varies over time.

Another interesting pattern in the annual top prey category measurement is that it reveals that the fraction of diet accounted for by the top prey category is variable and seems to oscillate over scales of several years. When the fractional dietary weight supplied by the top category is lower, the stock must be feeding on other species to make up the deficit, but not on any one group so exclusively that it becomes the top contributor by weight. In effect, the oscillations of dietary weight provided by the top prey category reveal something about diet diversity within that period.

### 2.3.2. Spatial patterns in diet

Spatial variation in diet is due to the relative potential for interactions between cod and any particular species. On a broad scale, this means that there must be some overlap in the distribution of predator and prey. On a finer scale, it includes added complexities such as the relative body sizes of the individuals present or the ability for cod to successfully hunt a particular species, which could be modified by the physical environment, e.g. light availability, water quality or the specifics of bathymetry.

To examine patterns in spatial distribution, we aggregated the individual prey data into a  $2^\circ \times 1^\circ$  grid in space. This resolution was chosen as a trade-off between precision and availability of sufficient data in more sparsely sampled areas of the Barents Sea. We then identify the top prey category by weight within each cell. Figure 2.15 shows a map of the Barents Sea with this grid overlaid; then another grid shows the number of prey samples collected within each cell. Due to the large spread of sample counts across cells, the counts have been binned into a rough order of magnitude, highlighting the extreme values.

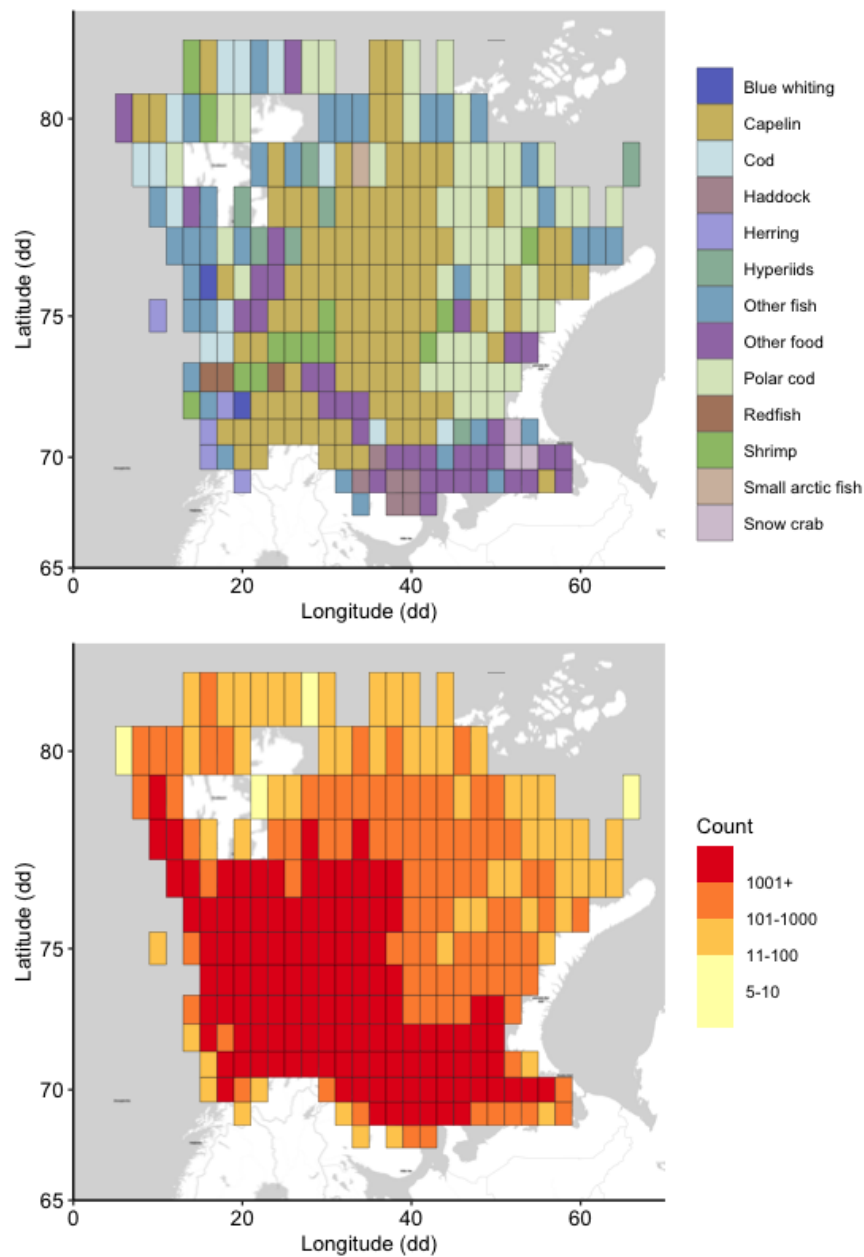


Figure 2.15. Top prey category by dietary weight and number of samples in a 2°x1° grid across the study domain.

Overall, we can see that diet is heterogeneous in space. Of the 17 prey categories, 13 are the most significant contributor to diet in at least one cell. Capelin dominates spatially, particularly in the central and southwest Barents Sea. Surprisingly, the second most widely significant category is polar cod, the top contributor to diet in a large swathe of the northeast Barents Sea, even though it is not a significant source of overall dietary weight (Fig 2.11). This interesting perspective would be missed

if we only considered diet as a regional aggregate. While summarising the overall dynamics is insufficient for capturing the full complexity, we can see that there is a robust spatial pattern in diet which has consequences for how we approach predicting changes in the trophic system under future environmental variability and that we must consider the full range of species that are potential prey for cod to be important, not just those that contribute the most dietary weight.

We can also consider the diet diversity in space by counting the number of unique prey species identified from individuals within each grid cell. Figure 2.16 shows this data. There is a strong correlation between the number of unique species identified and the sampling intensity, examining three ways of measuring intensity yields pearson's correlations of  $\sim 0.83$  with the number of individual cod sampled,  $\sim 0.85$  with the number of times a cell has been trawled and  $\sim 0.88$  with the number of individual prey items sampled. Figure 2.17 presents the relationship between the number of cod sampled in a given cell and the number of unique prey species identified. There is a rapid increase in the number of unique prey items identified as small sample sizes increase, with the growth levelling off with increasing sample size, with more variability.

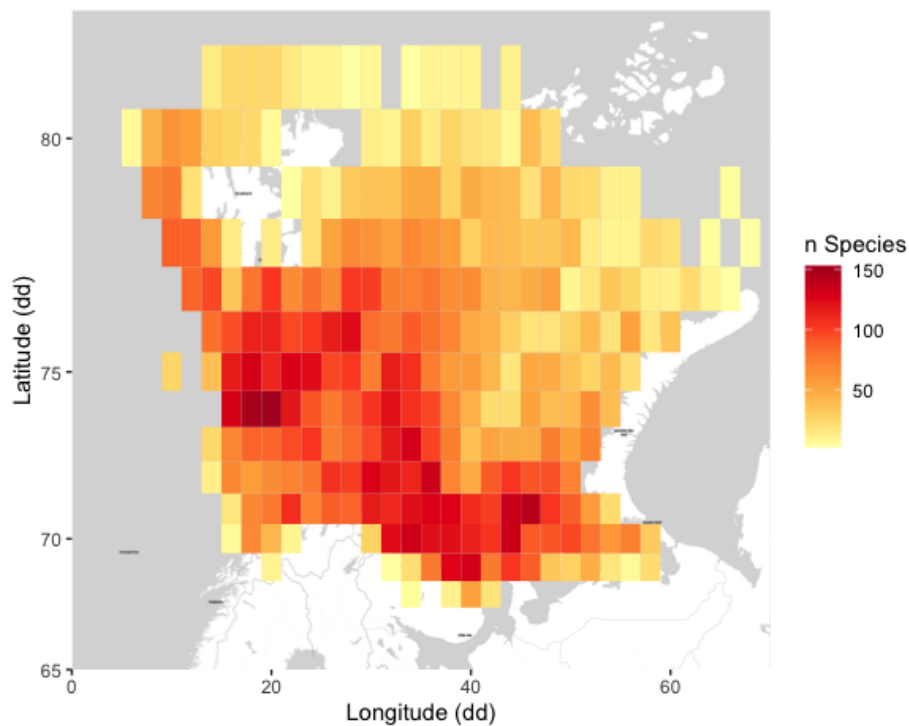


Figure 2.16. The number of unique species identified in diet within each grid cell.

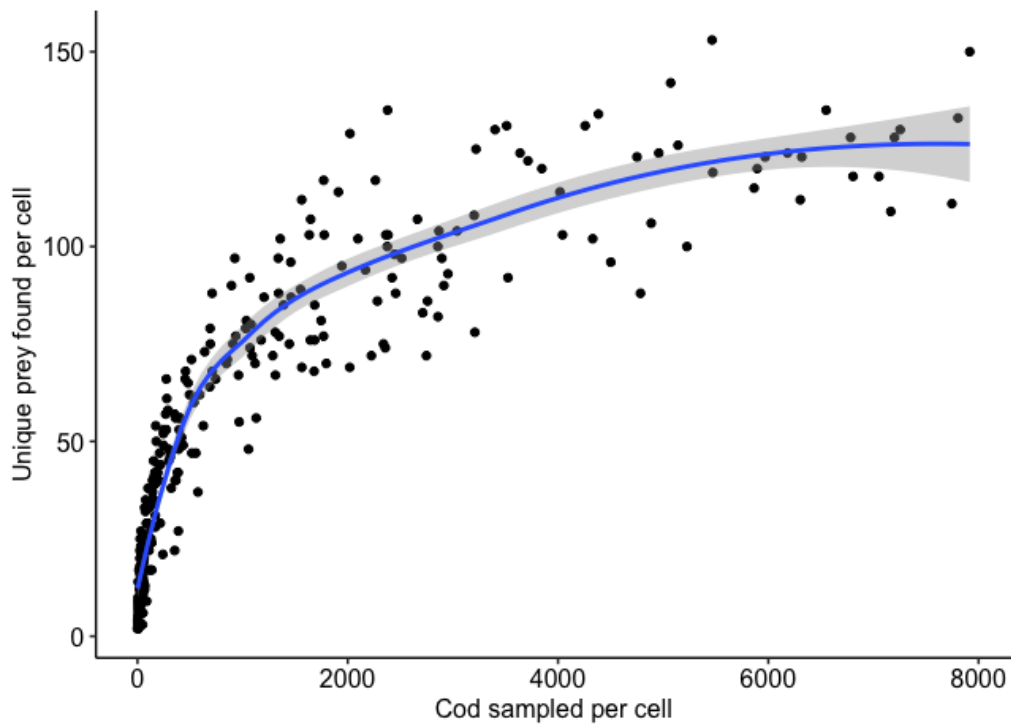


Figure 2.17. *cod sampled per cell vs Unique prey identified per cell. Points are from data, and the line of best fit was produced using LOESS smoothing.*

This suggests that there may be a minimum sample size needed to assess spatial diversity properly. The spatial extent of the survey has been expanded since it began, resulting in a disparity of records between the northernmost subareas and the rest of the Barents Sea. Further, this analysis does not take into account the temporal dimension of the samples, as such diversity within cells is counted as a cumulative tally since the study began and does not indicate that that diversity exists within a given year, or at the current time, as the distribution of prey is not static. Controlling for time and space is difficult, as the sample size is already so small in some regions that segregating the data further is not feasible.

We conclude that there is spatial variation in diet and that it is complex and challenging to capture directly even with considerable sample size and long study period. The data we have reveals long term spatial variation in the top prey category by weight, suggesting that some prey groups are more critical than others in particular locations, even when those categories do not rate highly as important in the overall diet from all samples. As a specific example, polar cod appears to be a top prey item in the north and the eastern Barents Sea but is not a leading contributor to overall diet weight. What causes this spatial variability is not entirely clear. Still, the answer is likely to be found in the

physical environmental conditions that determine species niche overlap and, therefore, the opportunity for contact and relative population densities, which results in variable predation rates between prey groups. This thesis will investigate the relationship between distribution overlap and predation rate within cod-prey pairings using Maxent in Chapter 4.

Now that we have considered the temporal and spatial dimensions of diet, we summarise the ontogenetic or size-based trends in the data. Cod is a long-lived species that can grow to over 150cm in length, and juveniles may be anywhere from 0-30cm. With growth comes a change in behaviour, environmental tolerance and feeding preferences. This means that treating diet as an amalgamation of all cod sizes may miss essential dynamics, so we also consider ontogenetic diet trends' spatial and temporal cross-section.

### 2.3.3. Ontogenetic patterns in diet

#### 2.3.3.1. Body length and size group classification

There is a strong link between cod body length and the body length of prey items, as shown in Figure 2.18. The maximum prey length increases as cod length increases, though there seems to be no particular minimum prey length in cod shorter than around 80cm. Further analysis by (Holt et al. 2019) shows that small cod choose prey up to 33% of their body length, while larger cod choose prey with a body length up to 50% of their own.

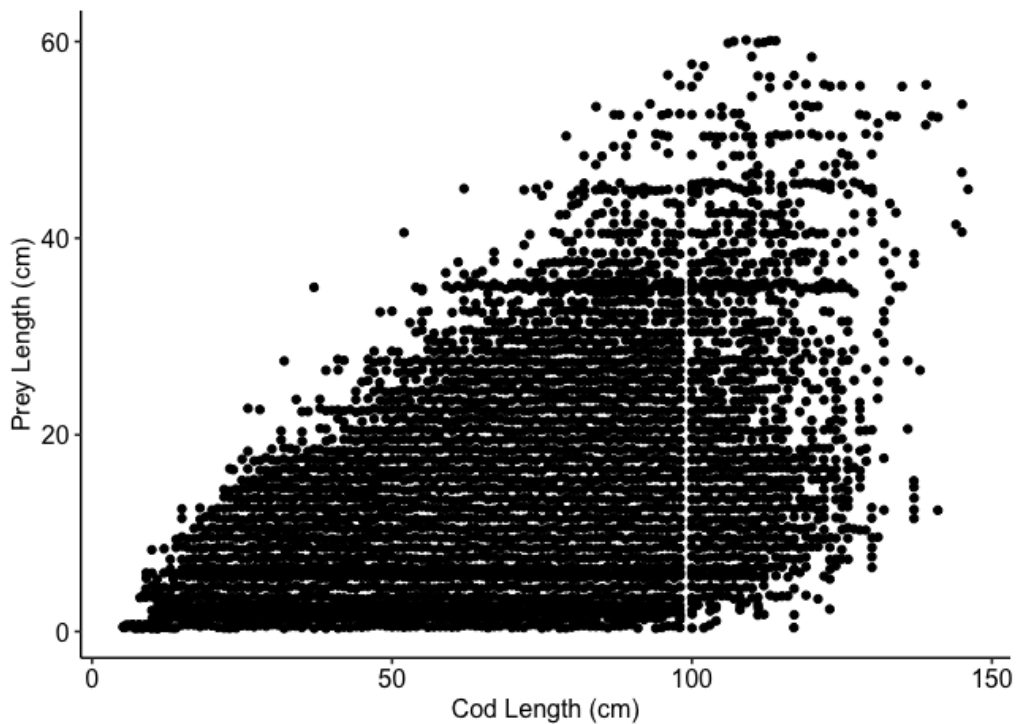


*Figure 2.18. The relationship between cod length and prey length. The maximum prey length increases with cod length.*

Studying the ontogenetic dimension of diet requires categorising the population into discrete groups for analysis based on size or age. There are many ways that size classes are distinguished. This study used a hierarchical clustering algorithm (Johnson, 1967; Suzuki and Shimodaira, 2006) to identify unique diet profiles across 10cm size classes. We discovered three clusters with unique diet profiles: <20cm, 20-100cm and >100cm. Figure 2.19 presents these clusters as a dendrogram, with each stem representing a size group and a bounding box identifying each cluster. The red numbers indicate the level of confidence in each cluster after bootstrapping. Each of these identified clusters is significant at  $P < 0.05$ . The disjoint in the point cloud at around 97cm is an artefact of the data.

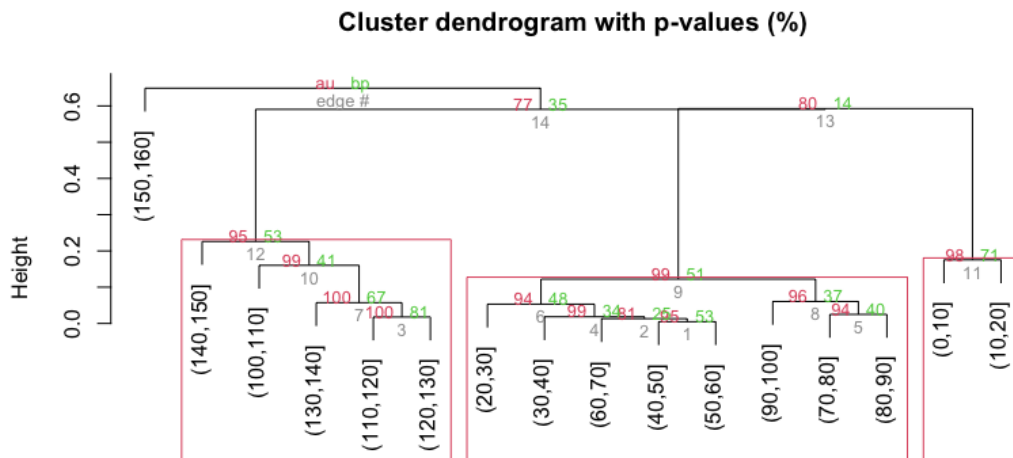


Figure 2.19 Dendrogram of length clusters identified by diet.

### 2.3.3.2. Ontogenetic prey categories and diversity

Now we examine the specific differences in diet that we can detect between these clusters. Figure 2.20 and Figure 2.21 present a series of plots showing the fraction of diet by weight that each prey category contributes to each clustered size group's overall diet. Blue whiting, codfishes, redfish and small arctic fish remain small contributors to diet across groups with slight variation. In the small group, consumption is higher among euphausiids, other food, shrimp and hyperiids than the other size groups. Medium group cod have a diet which favours capelin and polar cod, while large group consumption of cod (cannibalism), haddock, long rough dab, herring and snow crab is higher than the other groups. This evident variation in diet between size groups reveals the ontogenetic dimension of diet. This is an important consideration for this thesis, as the response to exogenous factors such as environmental variability, prey population abundance and structure and others, is likely to be different across cod sizes, resulting in a non-uniform effect on the overall diet of the population.



Figure 2.20. Diet fraction by weight for each prey category within each size group.

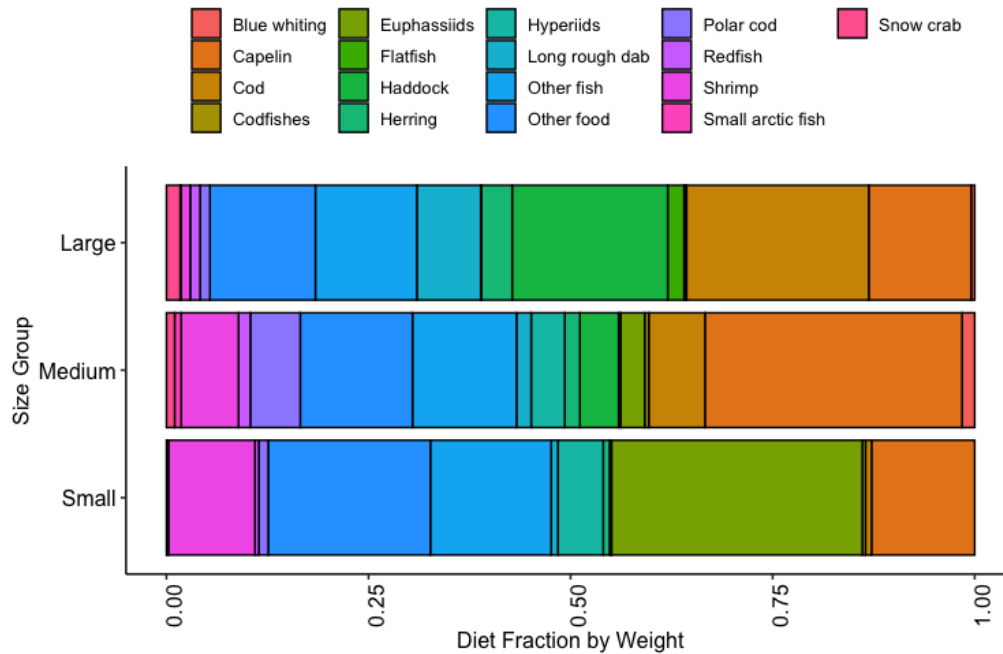


Figure 2.21 Diet fraction by weight for each prey category within each size group. This plot shows the same information as Figure 2.20 but allows an intuitive view of how diet makeup varies between groups.

Prey diversity varies between size groups. We calculated the Shannon diversity index for each size group annually from 1991-2017, plotted in Figure 2.22. The Shannon diversity index is a standard tool for measuring the diversity of a population (Shannon, 1948), it is calculated as:

$$H' = - \sum_{i=1}^S p_i \ln p_i$$

Where  $H$  is the Shannon diversity index,  $S$  is the number of species in the sample and  $p_i$  is the proportion of the sample made up of species  $i$ . In this case, each sample was a count of the species consumed by a particular cod size group within a given year.

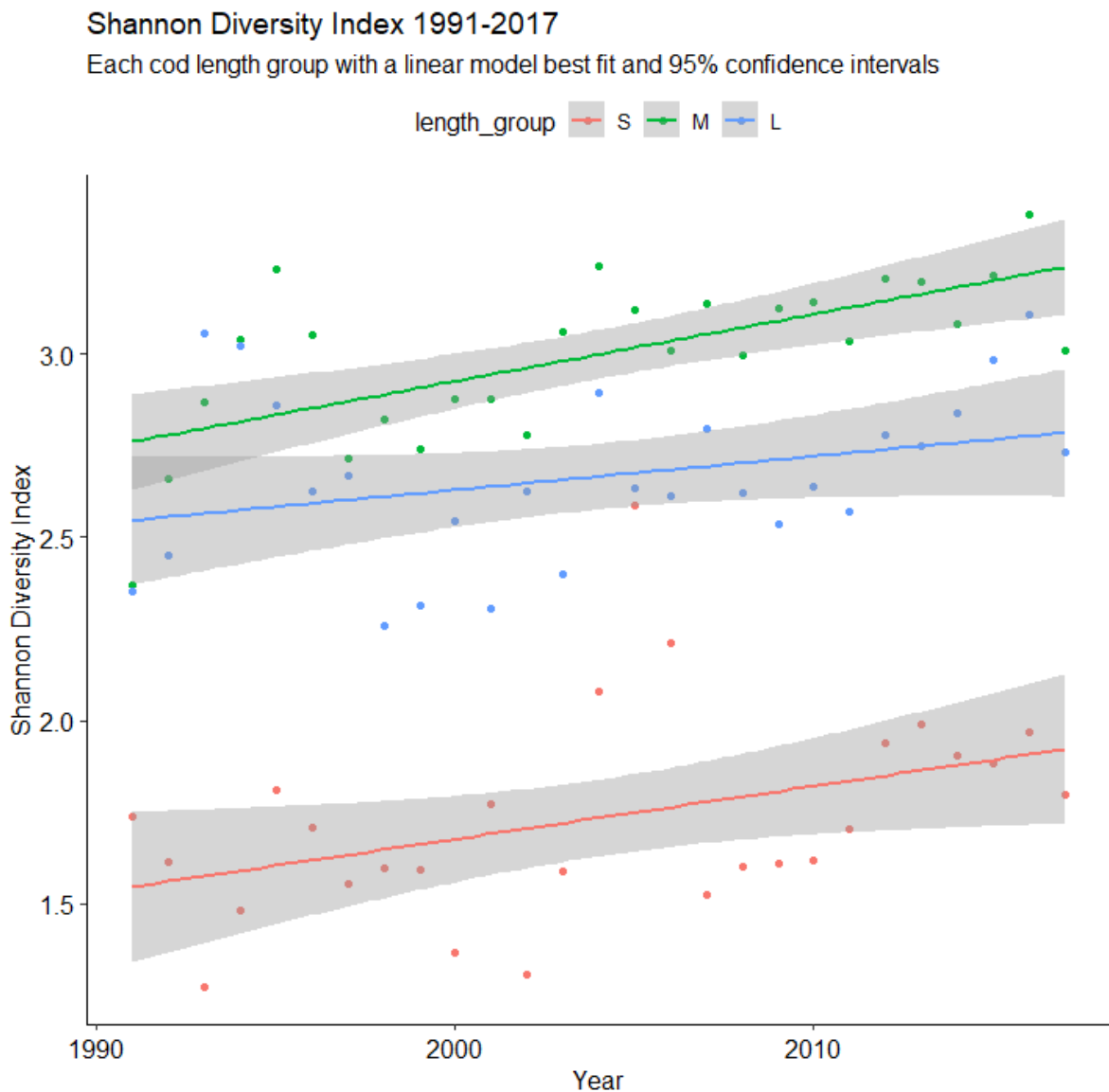


Figure 2.22. Shannon Diversity Index for each cod size group [ $<20\text{cm}$  (S),  $20\text{-}100\text{cm}$  (M) and  $>100\text{cm}$  (L)] in each year

Pearson's correlation coefficients were calculated for each size group. The small group has a correlation coefficient of  $\sim 0.4$ , with a p-value of 0.04. The medium group has a correlation coefficient of  $\sim 0.66$  and a p-value of 0.0002. The large group had a correlation coefficient of  $\sim 0.3$ , with a p-value of 0.11. Based on these results, there is a statistically significant positive correlation for diet diversity in small and medium cod size groups, but not within the large cod group.

### 2.3.3.3. Ontogenetic patterns in diet over time

A few prey categories dominate consumption by weight within groups. Figure 2.23 shows the top prey category by dietary weight fraction within each size group and year. The top prey category for the small group is usually euphausiids, occasionally shrimp or other food. In the medium group, capelin is consistently the top prey group. Only two periods had any category contributing more to diet for over a year in a row: 1987-1988 with Hyperiid and 1997-1999 when cod (cannibalism) was the dominant group. The large group has the most diverse top prey group list, with eight categories dominating for at least one year. Cod (cannibalism) is the most frequent top prey group, followed by haddock. The black dotted lines show a fitted linear model (Fraction ~ Year) for each size group. These trends tell us about the diversity of diet over time. As the fraction of diet accounted for by the top category decreases, there must be an increase in consumption among groups whose individual contribution is still lower than the top group. We see that the small group has maintained a similar level across the period, with a very slight increasing trend. The medium group shows a weak trend of decreasing weight fraction contributed by the top prey category. However, there is significant volatility in individual years before 2010; the last seven years are much steadier. In the large cod group, we see the most significant downward trend. The top prey groups are contributing much less towards total diet now than they were over the first few decades of the study. This indicates an increase in dietary diversity among the largest individuals in the population.

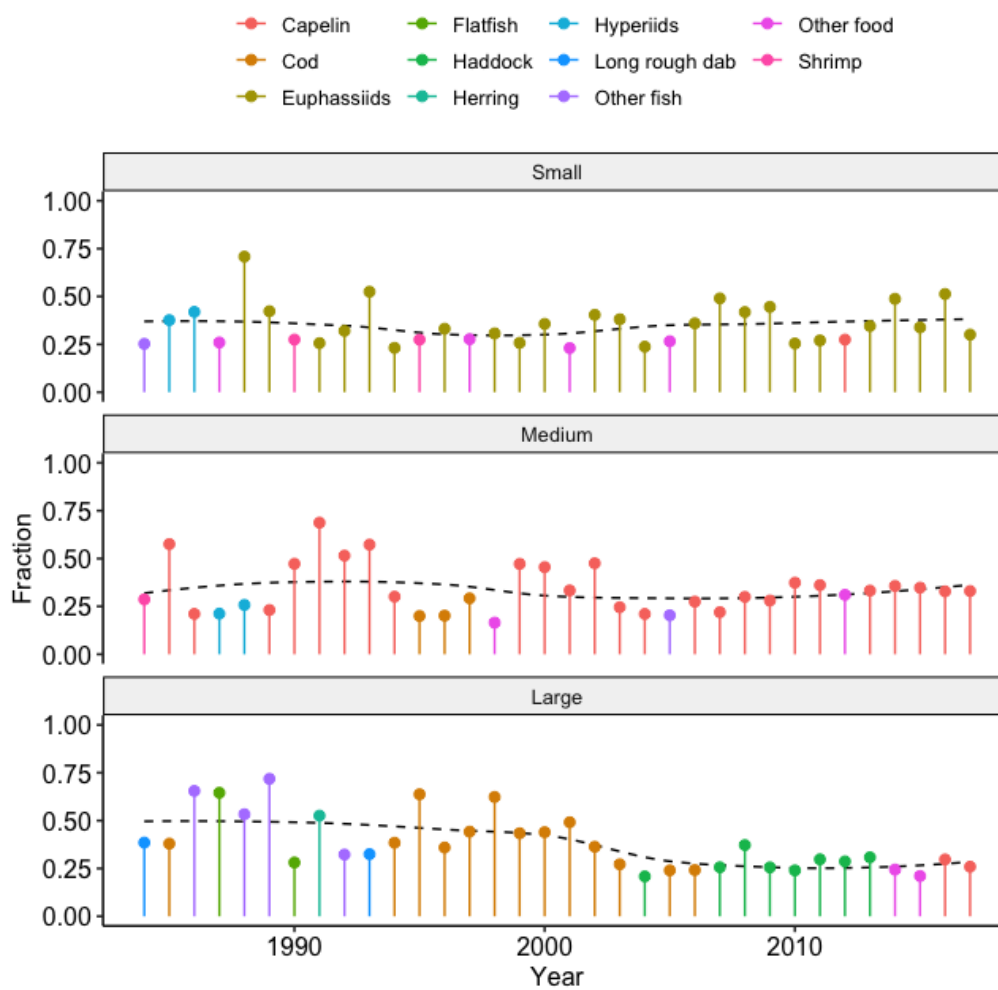


Figure 2.23. Top prey categories by the fraction of total prey weight consumed by each cod size group in each year of the study. A LOESS function highlights trends in the dominance of the top prey category in the diet.

#### 2.3.3.4. Ontogenetic diet in space

We can examine the spatial aspect of ontogenetic diet through the top prey category by weight in small sections of the study area, the same method we used for the complete population data. Here, we calculated the fraction of diet contributed by each category of prey item for each size class of cod in a  $2^{\circ} \times 1^{\circ}$  grid. Figure 2.24 shows the top prey category within each cell in the study area where there are samples. This way, all 17 prey categories are the most consumed in at least one cell when we view the data. At a glance, the heterogeneity of diet becomes apparent. Three categories dominate the spatial pattern in the small group: Euphausiids, Other food, and capelin. There appears to be an East-West divide in diet, with Euphausiids in the east, Other food in the west and capelin in the centre. The physical environment in the east and the west Barents Sea is quite different. Water in the southwest is warmer Atlantic water, and the water in the northeast is colder Arctic water, which is a likely factor in determining the available prey species. Cod is a generalist, and even small cod are found in the northern Barents Sea, so spatial differences in diet are likely due to the underlying distribution of prey species and relative availability for cod to feed.

We see a similar spatial divide in diet within the Medium Group. Though now capelin is highly dominant, there is a region in the northeast where herring is generally the top category by weight. Considering the range of prey categories contributing more to diet than capelin in specific areas is essential as spatial changes in trophic dynamics are likely to be heterogeneous when compelled by changes in the physical environment such as warming or anthropogenic activity such as fishing or construction. The large group shows the highest spatial diversity in diet, with no one category dominating. Capelin and Snow Crabs are the top categories in two small contiguous regions in the north-centre and southeast, but otherwise, there are no apparent patterns. The sample size in this group is the smallest of the three, and many of the cells outside of the southern Barents Sea have fewer than ten samples, so we must acknowledge that there is a higher chance that this pattern is an artefact of a small sample size. Figure 2.24 also shows the distribution of cod sampled within each size group. There are significantly more individuals in the 20-100cm (Medium) group, but a good sample size for the Small and Large groups was distributed widely throughout the study region.

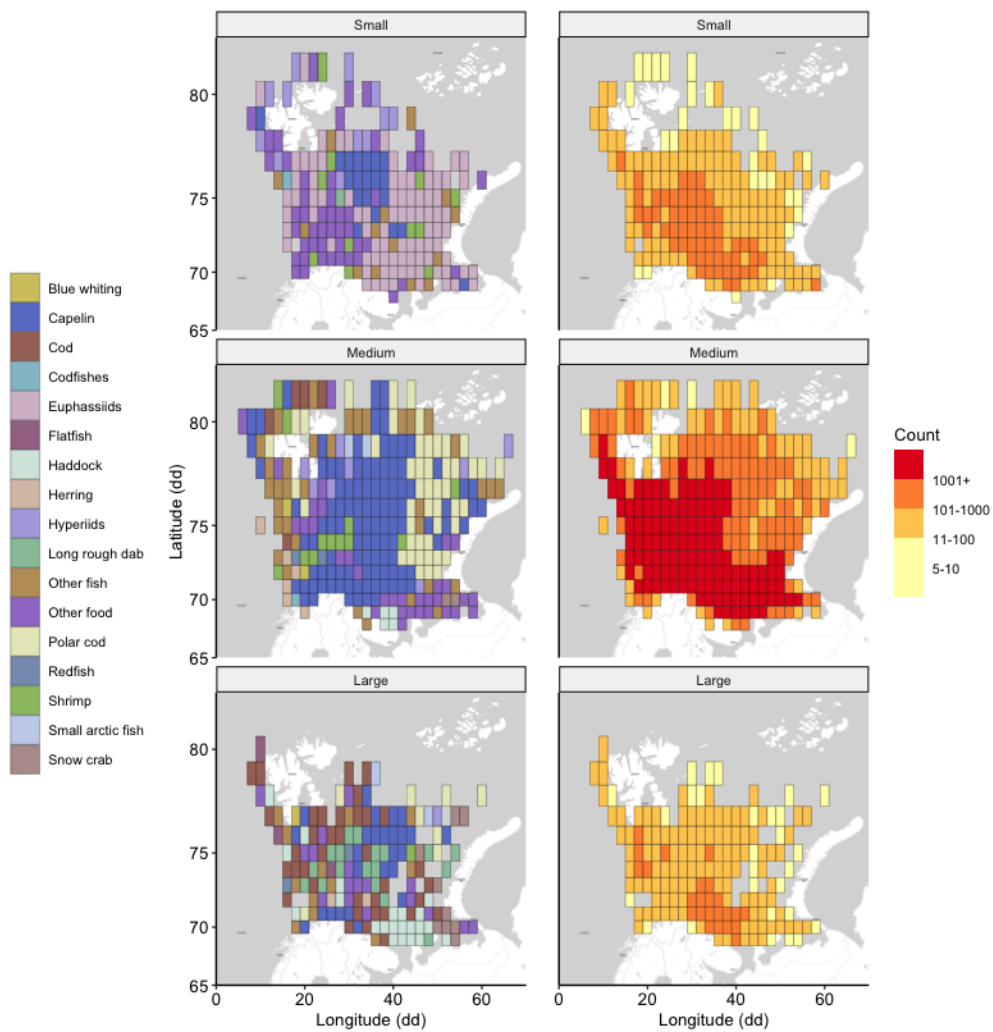


Figure 2.24. Top prey category in each cell of a  $2^\circ \times 1^\circ$  grid across the study area, separated by size group. A top prey category contributed the largest fraction of weight to diet within that cell and size group. The right column shows the number of individual prey items identified within the cod of each size group sampled within each cell. Cells with fewer than five samples were omitted.

### 2.3.4. Summary

In this section, we have investigated the ontogenetic patterns in cod diet. Our hierarchical clustering into three groups is only one plausible way to split the population into length groups. The strength of our method is that it separates the population into groups with distinct prey selection profiles based on the structure of the data and not externally motivated by prior knowledge. This should provide a parsimonious structure to our analysis and provide a solid foundation for using size stratified subpopulations in this thesis.

We have found that the diet of Barents Sea cod is ontogenetically heterogeneous and within size groups varies in space and time. We have shown that prey diversity varies between groups, with the small and large groups having less diverse diets than the medium group. Still, prey diversity is not static, as the large group displays a trend of decreasing dietary weight contribution from the top prey category, indicating an increase in diversity over time.

Another dimension of prey selection, which we do not examine in this thesis, is prey quality and optimal foraging theory. Each prospective prey item offers a different energy density, so consuming a high energy prey such as capelin may be highly rewarding but difficult, and may result in high energy expenditure (Pyke et al., 1977; Townsend and Winfield, 1985). An individual cod may instead choose to consume several lower quality prey items which are easier to catch. There are many factors which affect the foraging behaviour of cod, for example, the relative density of available prey items (Jónsdóttir, 2017) or conditions of the environment such as light availability (Johannesen et al., 2012; Puvanendran and Brown, 2002).

## 2.4. Conclusions

This chapter presents the IMR-PINRO database and explores the distribution of samples in space and time. The survey has good coverage of the study domain and is consistent throughout the study period. Though the geographical coverage of the survey has spread further into the north over time, it is important to note that due to the high latitude, the visualisations in this chapter do not accurately represent the area covered by the survey, with any cells or hexes shown to represent areas in the far north Barents Sea, in reality, representing much smaller areas than those in the south. The reason for the extent of the survey is also holistic, not arbitrary, following the expectation of cod presence at high latitude stations. We then analysed patterns in cod size structure and cod age structure. We found that both size and age structure vary in time and space and that there is a pattern of growth over time and that individuals appear to be larger and older in the north of the Barents Sea. We identify the potential limitations of interpreting the data in these regions but suggest that the broad patterns found are in line with independent studies, which also show an increase in the number of large cod and the spread of the population further into the northernmost Barents Sea.

We then explored the diet of Barents Sea cod over the study period, identifying top prey groups and examining the Spatio-temporal variability in diet. We found variability in the most important prey group in diet over seasonal and annual scales and in the meaningful diversity in diet. Our analysis shows that although capelin dominates diet, it is not always the top prey item at certain times or locations within the Barents Sea. Polar cod, in particular, may only contribute a small fraction of total dietary weight but is a top prey item in most of the more recently sampled north-east Barents Sea. We have established the connection between the size structure of the population and diet by examining the relationship between cod-prey body length and clustering of diet in size stratified cod subgroups. We found that small (<20cm) and large cod (>100cm) have diets that are distinct from the rest of the population. These differences are marked by lower diversity and different top prey categories. Small cod mainly feed on benthic prey groups, while large cod feed primarily via cannibalism or large piscine groups like haddock.

We use this information to direct our modelling in the rest of this thesis. This data does not tell us why these patterns exist, but there are ways that we can use it to try and answer these questions. In Chapters 3 and 4, we build and apply a species distribution model (Maxent) to predict the distribution of Barents Sea cod, the small and large cluster groups and several important prey

species. We try to see how the overlap between these predator-prey pair groups has changed over time and quantify the connection between geographic niche overlap to consumption.

Chapter 5 models the temporal trends in diet and population characteristics using a system identification approach (NARMAX). We attempt to quantify the external factors that drive population demographics, size structure and diet changes over time and how those metrics might depend upon each other.

## Chapter 3 - Testing the effect of data structure and hyperparameter settings on the performance of Maxent for modelling the distribution of cod

### 3.1. Introduction

There are a variety of methods for predicting the distribution of species in geographic space. Species distribution modelling (SDM), alternatively called environmental niche modelling (ENM) or climate envelope modelling, is a popular approach. These names all describe a class of correlative models that fit the distribution of a species to a mathematical description of its environment (Franklin and Miller, 2010). This study utilises Maxent (Philips et al., 2006), a popular model, to investigate the distribution of Northeast Arctic cod (*Gadus morhua*) and key prey species within the Barents Sea. Maxent is named for its approach, maximum entropy, which essentially is a way to approximate an unknown probability distribution (Jaynes, 1957). The maximum entropy principle states that the best way to approximate an unknown probability distribution is to ensure that while any known constraints on the distribution are satisfied, the approximate distribution should have maximum entropy. This is effectively saying that our best approximation of the distribution shouldn't make any choices or assumptions about it beyond what we are sure about from the constraints, in this context, our constraints are the environmental profiles of locations containing samples of the target species versus the environmental profile of the study background. Philips et al. 2006 explains the mathematics in the following way. If we allow our domain to be a set of pixels  $X$ , where each pixel is a point ( $x$ ) and each point has a non-negative probability, the sum of probabilities across all points summing to 1, we can denote the entropy of our approximate distribution  $H(\pi)$  as:

$$H(\pi) = - \sum_{x \in X} \pi(x) \ln \pi(x)$$

Maxent uses a machine learning approach to identify the distribution of  $\pi$ , given any constraints, which maximises  $H(\pi)$ . The implementation of this machine learning approach can be found in e.g. Philips et al. (2006) and Elith et al. (2011).

Maxent is a presence-only model; it only requires positive observations and no information about species absence. This is useful for marine studies where absences are challenging to identify and validate. Maxent has been shown to produce more accurate predictions across a wide range of applications than other methods, is computationally inexpensive and requires a small minimum number of occurrence records to build models with good performance (Elith et al., 2011; Robinson et al., 2017; Wisz et al., 2008). Maxent allows a user to make predictive maps of distributions and quantifies each environmental feature's contribution to the model, which tells us which regions are suitable for the species and why they are suitable. This, in turn, provides new ecological insight into the species under study.

This chapter describes the design of a Maxent model that is optimised explicitly for *Gadus morhua* and that takes advantage of a novel source of occurrence data. First, a Northeast Arctic (NEA) cod model is built, which follows a standard methodology that uses all the available occurrence data and physical environmental layers. This model is designed within a quality control framework to produce the most accurate, robust and ecologically valid results possible.

We demonstrate the impact of building distribution models using a finer temporal resolution. The primary benefit of using time-sensitive data is that the environmental layers used and aggregate estimates of actual conditions should be closer to the natural conditions that existed at record collection. Environmental layers created from average climate values across long periods do not capture the dynamic nature of those variables. This is a critical issue in the Barents Sea, where sea temperatures have risen significantly over the past few decades (Chapter 1). We attempt to identify the highest possible temporal resolution, which is limited by the availability of data and ecological considerations. This investigation is essential and provides the rationale for further experiments in this study investigating the potential for change in NEA cod distribution across the study period.

We demonstrate improved modelling performance when separating NEA cod into three classes: Small cod <20cm, Mature cod 20-100cm and Large cod >100cm. These size groups are identified with hierarchical clustering analysis of diet as having unique diet profiles and are in broad agreement with pre-existing methods of stratifying the cod population by size. The ecological rationale for this process is that cod are long-lived species with a marked behavioural difference throughout their life history. Larger cod are more robust to environmental extremes than smaller cod and occupy a different position in the food web. Smaller cod feed primarily on small benthic species, whilst

mature cod feed primarily on capelin and other fish. The largest cod category is primarily cannibalistic, likely due to a lack of sufficiently large non-cod prey. We expected that modelling these size groups separately would better interpret the underlying ecology and improve predictive power.

We explore the inclusion of biotic factors as predictors in a Maxent model for NEA cod. Following the method Gerghel et al. (2018) described, we produce a prey availability layer that describes the relative diversity of prey items within each grid cell. Information about the physical environment alone may be insufficient for building a suitable SDM for cod in the Barents Sea, and we hope that the inclusion of biotic interaction data will yield new insight and improve model performance. We produce Maxent models for many key prey species following the good practices discussed in this chapter and utilise a prediction threshold to translate raw Maxent output into binary grids, one for each prey species. The sum of these grids constitutes the measurement of prey availability.

Occurrence data for these models is collected from existing biodiversity databases such as Fishbase and GBIF, and proxy occurrences are extracted from the IMR-PINRO cod diet database. We discuss the impact of prey availability on the prediction and interpretation of Maxent models for NEA cod.

Finally, we compare these potential improvements and judge which may be useful and compatible with one another. The inclusion of prey availability limits temporal resolution due to the lack of available time-sensitive data. cod size classes may be used in all cases. Temporal resolution can be variable dependent upon the needs of any particular experiment, between a theoretical maximum and minimum range dependent upon data availability and ecological rationale. The summary of these findings is used to inform model building in the next chapter, where Maxent is applied to both Northeast Arctic cod and critical prey species to investigate how the distribution of these species has changed over time, and the relationship between niche overlap and predation is explored.

## 3.2. Methodology

### 3.2.1. Species records

Maxent takes two input variables. The first is a list of spatially explicit species occurrence records. These are usually latitude-longitude pairs within a specified coordinate reference system. Each record should represent a precise and independent observation of the target taxon, and the set of records should ideally represent the full range of the species within the target domain in both

geographic and environmental space. The highest quality of occurrence records comes from well-designed surveys targeting the species' full local range and consistent sampling effort.

These records are used to train and test the Maxent Model. The environment at these locations is assumed to be suitable for the species, and Maxent assigns a value to each grid cell, calculated by how similar the environmental conditions are to those found at known presence locations. If the occurrence records are spatially or environmentally biased, imprecise or based on misidentified taxa, the resulting Maxent model will be less useful.

To reduce spatial bias and correlation, we apply a thinning method to reduce the number of occurrences to 100 representative points. This number was chosen as a compromise between identifying the full range of environmental conditions that are suitable for cod while avoiding spatial autocorrelation. Maxent has been shown to perform well with sample sizes as small as ten records, but this is more appropriate for rare species with a low environmental tolerance (Hernandez et al., 2006; McPherson et al., 2004; Stockwell and Peterson, 2002; Wisz et al., 2008). Thinning points was achieved by first taking an initial occurrence record, randomly selected from the ~21,000 unique occurrences and adding it to a new set of "thinned" records. Next, the point which is maximally distant from the initial point is selected and added to the set. Programmatically, new points are selected in this way until the target number of records have been met (Aiello-Lammens et al., 2015)

Distance is defined as the cartesian distance between two points. This could be in either geographic space, where distance is defined in metres, or in N-dimensional environmental space, where distance measures environmental dissimilarity. The choice of whether thinning should be done in geographic or environmental space depends on the particular study. Here we build models using both geographically and environmentally thinned occurrence records to compare the effectiveness of both methods.

### 3.2.2. Background point selection

Maxent is a presence-only model, which means it does not explicitly utilise records of species absence. Instead, Maxent attempts to identify the novelty of the environmental profile of occurrence sites when compared to the environmental profile of the entire study area. To do this, typically, a large number (10,000) of random points are selected from the region to represent the overall

environmental conditions, which are called background points and sometimes referred to as pseudo-absences (Elith et al., 2011; Merow et al., 2013; Philips et al., 2006).

This study used the standard approach of 10,000 randomly sampled points from the study environment, with one added restriction. The range of background selection was limited to any area in the study region which is within a reasonable range of dispersion from the sampled region. In practice, this meant that occurrence records were selected from the full range of the Barents Sea, but not from the Kara Sea, as the archipelago of Novaya Zemlya acts as a dispersal barrier between the two seas.

There is an ongoing debate surrounding background point selection methods (Jarnevich et al., 2017; Lobo and Tognelli, 2011; Phillips et al., 2009; Senay et al., 2013). The general agreement is that there is no perfect solution and the best approach depends on the particular details of any given study. There is some good news that Maxent is the least sensitive to background point selection methods compared to other species distribution models. In comparison to our chosen approach, we extensively tested a novel background point selection method proposed by Senay et al. (2013) but ultimately rejected it because it produced models that were less accurate and less interpretable than those built with our chosen protocol.

### 3.2.3. Environmental Layers

Predictor variable layers are produced from spatially explicit data about the study environment. Variables are selected from those qualities which are considered to be ecologically significant to the target species. Because each layer is a static uniform grid, sometimes several layers may be used to represent one variable. For example, when including relevant temperature measures, it may be necessary to include an average annual temperature and average seasonal temperatures to capture the most relevant aspect of temperature that constrains distribution.

In this study, an initial 18 environmental layers were produced. These layers are time-averaged rasters that capture the dynamics of critical physical environmental variables: sea surface temperature, sea bottom temperature, sea surface salinity, fractional ice coverage and sea ice thickness. Two static layers are also included, representing the bathymetry of the Barents Sea and the

distance of each grid cell to the nearest shoreline. Layers for temperature, salinity and sea ice measures are produced from the CMEMS ARC MFC ocean reanalysis (Traon et al., 2017; Xie et al., 2017). Bathymetry and distance layers are produced from the IBCAO arctic bathymetry atlas (Jakobsson et al., 2012). Table 3.1 shows a list of the environmental rasters which are included in the initial model building process. Rasters are projected as latitude-longitude grids with a resolution of 0.1 degrees. Raster resolution is limited by the lowest resolution of all used data.

Table 3.1. A description of each environmental layer that is included in the initial model building process.

Var no.	Var name	Description	Unit	Source
1	temp_max	Mean surface temperature, the warmest month	°C	CMEMS ARC MFC
2	temp_min	Mean surface temperature, the coldest month	°C	CMEMS ARC MFC
3	temp_mean	Mean surface temperature, annual	°C	CMEMS ARC MFC
4	btemp_max	Mean bottom temperature, the warmest month	°C	CMEMS ARC MFC
5	btemp_min	Mean bottom temperature, the coldest month	°C	CMEMS ARC MFC
6	btemp_mean	Mean bottom temperature, annual	°C	CMEMS ARC MFC
7	sal_max	Max salinity per cell, annual	PSU	CMEMS ARC MFC
8	sal_min	Min salinity per cell, annual	PSU	CMEMS ARC MFC
9	sal_mean	Mean salinity per cell, annual	PSU	CMEMS ARC MFC
10	hice_max	Max sea ice thickness, annual	cm	CMEMS ARC MFC
11	hice_min	Min sea ice thickness, annual	cm	CMEMS ARC MFC
12	hice_mean	Mean sea ice thickness, annual	cm	CMEMS ARC MFC
13	fice_max	Max sea ice fraction (cell coverage), annual	/	CMEMS ARC MFC
14	fice_min	Min sea ice fraction (cell coverage), annual	/	CMEMS ARC MFC
15	fice_mean	Mean sea ice fraction (cell coverage), annual	/	CMEMS ARC MFC
16	bathymetry	Mean seafloor depth per cell	m	IBCAO
17	distance	Distance from land	m	IBCAO

Co-linear layers do not affect Maxent model performance. However, they profoundly affect the ecological interpretation of the model, mainly when using a model to project onto a different geographic or temporal domain where the correlations between variables are not the same. This study removes co-linear variables, leaving only the most significant variables from within each correlated group as determined by jackknife testing within Maxent. This method yields more straightforward and more transferable models to other periods or spatial extents (Dormann et al., 2013; Feng et al., 2019).

Alternatively, for the seasonal models explored in Section 3.3.4. Layers were created for specific summer/winter months from the same reanalysis layers. This was done to improve model interpretability.

Table 3.2. A description of each environmental layer that is included in the model building process for summer and winter models.

Var no.	summer Layers	winter Layers	Unit	Source
1	BTemp.Aug	BTemp.Dec	°C	CMEMS ARC MFC
2	BTemp.Jul	BTemp.Feb	°C	CMEMS ARC MFC
3	BTemp.Jun	BTemp.Jan	°C	CMEMS ARC MFC
4	FIce.Aug	FIce.Dec	/	CMEMS ARC MFC
5	FIce.Jul	FIce.Feb	/	CMEMS ARC MFC
6	FIce.Jun	FIce.Jan	/	CMEMS ARC MFC
7	HIce.Aug	HIce.Dec	cm	CMEMS ARC MFC
8	HIce.Jul	HIce.Feb	cm	CMEMS ARC MFC
9	HIce.Jun	HIce.Jan	cm	CMEMS ARC MFC
10	Sal.Aug	Sal.Dec	PSU	CMEMS ARC MFC
11	Sal.Jul	Sal.Feb	PSU	CMEMS ARC MFC
12	Sal.Jun	Sal.Jan	PSU	CMEMS ARC MFC
13	SST.Aug	SST.Dec	°C	CMEMS ARC MFC
14	SST.Jul	SST.Feb	°C	CMEMS ARC MFC
15	SST.Jun	SST.Jan	°C	CMEMS ARC MFC
16	Bathymetry		m	IBCAO
17	Distance		m	IBCAO

### 3.2.4. Model parameter setting with ENMEval

Maxent handles the model building process automatically once provided with the occurrence records and environmental data, but a wide range of parameters can be set that profoundly alter the structure of the model produced. The authors of Maxent have selected default parameters which they suggest are suitable for most applications, though others have shown that there are many cases where this is not true (Merow et al., 2013).

The ENMEval R package (Muscarella et al., 2014a) provides a suite of tools to determine the optimal parameter settings. ENMEval builds several Maxent models with different parameter settings, specifically different values for the regularisation parameter, where higher numbers represent a model which penalises complexity more severely and for the categories of allowable feature types. A wide range of evaluation metrics are calculated and summarised for the user, allowing for the best parameter set to be chosen for the study's goals.

Maxent builds model features as one of five types: Linear, Quadratic, Hinge, Product and Threshold (Philips et al., 2006; Phillips and Dudík, 2008), which is shortened in this discussion as LQHPT. These categories determine the form that model functions can take when relating multiple predictor layers. The more feature types that are used, the more complex the Maxent model may become. This can be useful when trying to maximise raw model accuracy but may produce models which overfit the training data or are difficult to interpret ecologically.

In this study, ENMEval was used to produce each combination of the following parameter settings: One of six allowable feature type groups (L, LQ, H, LQH, LQHP and LQHPT) and a regularization multiplier value between 0.5 and 4 in intervals of 0.5 (0.5, 1.0, 1.5, 2.0, 2.5, 3.0, 3.5, 4.0), a total of 48 unique parameter sets. This range for the regularization multiplier is the default in ENMEval, and is suitable for use in this study as it covers a wide range of values above and below the default Maxent settings. For each parameter set, a series of performance measures are recorded which can be used to support the choice of optimal parameters to use in Maxent, depending on the study goal.

### 3.2.5. Model Evaluation

Records are split into training and test data using the “checkerboard2” method in ENMEval, with 4 folds. This method is likely to reduce spatial correlation between training and test data by aggregating the data at two spatial scales in a checkerboard fashion. Figure 3.1 shows an example of occurrence data being partitioned using the checkerboard2 method from Muscarella (2014). A grid is overlaid on each cell in the environmental raster, and cells are assigned to one of four groups depending on their position relative to the grid.

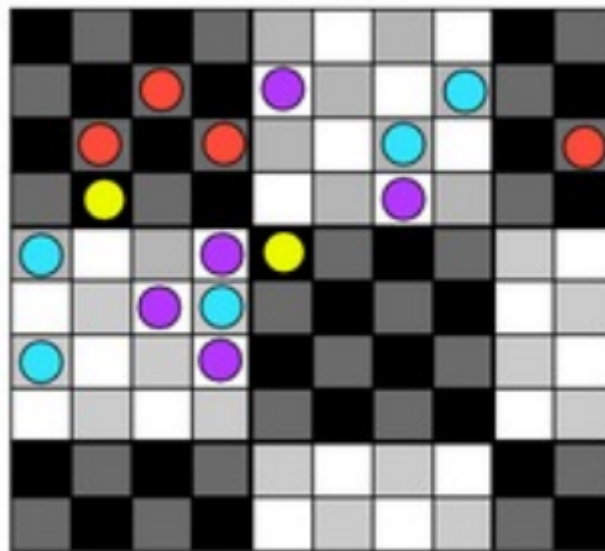


*Figure 3.1. An example of checkerboard2 partitioning. The space is split into checkerboards at two spatial scales, resulting in four groups. Colored circles represent grouped presence records. (Muscarella et al., 2014a)*

For each fold, 75 points are used for training and 25 points are assigned for testing. The method used for partitioning data has an effect on model structure and performance, and using a spatially explicit method of partitioning is a better choice than randomly assigning points to groups in order to avoid bias in the final model.

Once data is partitioned into training and test sets and Maxent has fitted a model to the data, there are many ways to measure its effectiveness. One very popular measure of model performance is to calculate the area under the curve (AUC) of the receiver operating characteristic (ROC). This is a value between 0 and 1 which provides a shorthand description of how often the model successfully

identifies both true positives (sensitivity) and true negatives (specificity). The strength of AUC is that it is easily understandable and provides a way for two models to be compared.

However, one issue which has been raised about AUC is that many methodological choices in the model building process result in an inflated AUC value. For example, choosing a background which is much larger than the span of the area which has been sampled for the target species often results in a model with a high AUC, but which is ecologically questionable (Acevedo et al., 2012; Jarnevič et al., 2017). Additionally, if model complexity is not properly treated, AUC can be high simply due to an overfitted model which has little use in explaining the results ecologically and falls apart when applied to new data. The issues with AUC are not only methodological but ecological. The maximum theoretical value of AUC is 1, but in practice it is  $1 - a/2$ , where  $a$  is the prevalence of the target species with a maximum value of 1 meaning the species is present in every location (Lobo et al., 2008; Raes and Steege, 2007). Therefore, for species with high prevalence, AUC values may be lower than might be expected for a successful model.

In order to avoid over complex models and an inflated AUC value, complexity must be addressed during the model building process. One of the evaluation measures calculated by ENMEval is Akaike's Information Criterion (AIC), which effectively measures the loss of information between model application on training data vs test data. This is a method of measuring over-parameterisation and by selecting the model which minimises AIC, we can choose the simplest of the "true" models (Bozdogan, 1987; Muscarella et al., 2014b). From the full set of models produced by ENMEval using different parameter sets, we select the one which minimises AIC. This selected model is the one which performs most consistently across training and test data, and it is not necessarily the model with the highest test AUC.

### 3.2.6. Prey availability layer

It has been suggested that including biotic factors may improve SDM's for marine species. Interspecies interactions such as predation or competition may be useful predictors of habitat suitability over regional spatial scales (e.g. Atauchi et al., 2018; Gherghel et al., 2018; Trainor et al., 2014; Wisz et al., 2013). cod is a top predator in its environment, so including information about the availability of prey items is likely to be relevant to any model of distribution.

To include this information, some measure of prey availability must be produced as an environmental layer to include in the model. In this study, we adapt the method outlined by Gherghel et al. (2018) to produce a map of relative prey diversity from predicted distributions of prey species.

Occurrence records for these species were extracted from the IMR-PINRO stomach database. Records of each species as identified from cod stomachs were filtered to only include undigested prey; this selection method minimises the error introduced by using stomach records as a proxy for occurrence while also targeting species which are highly prevalent as prey targets. From these filtered records, 15 species were deemed suitable for inclusion because they were identified to the *genus* taxonomic level and at least 30 unique occurrences were recorded.

Maxent models were produced for all 15 species using the same methodology as outlined previously in this section. Geographic projections of habitat suitability were transformed into binary grids of predicted presence or absence by applying a threshold which maximises Specificity + Sensitivity, called the MaxSSS (Liu et al., 2015). The predictive maps and binary grids of each prey model can be found in Appendix B. The sum of these binary grids was calculated and used to produce the prey availability layer which is shown in Figure 3.6 in section 3.3.2.

### 3.2.7. Size stratified models

Atlantic cod is a species which can live for over 13 years and undergoes significant changes in biology and environmental requirements throughout its life history. Juvenile cod are pelagic, while mature cod are demersal, meaning that they prefer different water depths and have different behaviours. One meaningful difference between the life stages of cod is the dietary profile of the species. cod choose prey based on their relative sizes, so juvenile and mature cod have unique diet profiles and interact with the ecosystem in different ways. In this study, we identified three distinct size-groups of Barents Sea cod using hierarchical clustering of diet.

Using the IMR-PINRO stomach content database, the diet contribution by weight was calculated for each of 19 prey groups defined by (Holt et al., 2019) as they were found in different size groups of cod. We stratified the population into 10cm length groups and found their normalised prey consumption percentage for each of these groups. Using these values, we applied a hierarchical clustering algorithm to attempt to identify distinct dietary patterns within groups. This analysis revealed three distinct diet clusters: small cod <20cm in length, mature cod between 20 and 100cm in length and large cod > 100cm in length. Figure 2.19 shows these clusters.

We seek to discover if modelling these groups separately will improve our ability to predict the distribution of cod. The ecological rationale is that, if these different size classes prefer different environments, they may have better defined environmental niches than Barents Sea cod does as a whole. In particular we expect that juvenile cod, which are smaller and less tolerant of extreme temperatures, will have a distribution which is more confidently identified from the available environmental data.

Of interest is whether the models are successful in terms of discrimination, but also as to whether they are significantly different from one other. This is measured using a niche-overlap metric.

### 3.2.8. Temporal sensitivity

The environmental layers used to build species distribution models are static grids, but they represent a dynamic quantity which changes over time. As an aggregation, there is always a chance that the layers used fail to capture important time sensitive information about the study environment. This is particularly problematic when attempting to model the distribution of highly mobile marine species as they may be more able to respond to short term environmental conditions which significantly affect them and are not captured at the resolution of the environmental layers, that is as an averaged value over time. There is a question then of temporal resolution: how much time should be represented by the environmental layers? There are several competing problems with answering this question. In the study by (Fernandez et al., 2017), they found that the selection of temporal scales has a significant effect on model predictions. They suggest that scales as short as daily or weekly yield more accurate results in some cases.

Due to data limitations, the shortest period we are able to study is seasonal, as finer scale models result in occurrence sample sizes below the minimum for Maxent, or no data at all in many cases.

We investigate the effects of changing temporal scales on model accuracy and prediction characteristics by building many models for each of five time period windows: Annual; Five-year; 10-year; Annual-summer and Annual-winter from 1991 and 2017. We compare the summarised results of these models to our base model, which uses data from across the full range. We are interested in any noticeable gains to model performance which may reveal an ideal temporal scale, but also to test if models built using a wide range of temporal resolutions still produce valid predictions. If so, this will allow us to use Maxent to investigate species distributions at a variety of time scales in the next chapter.

### 3.3. Results

#### 3.3.1. Maxent model for *Atlantic cod*

A Maxent model tells us several things about the distribution of our target species. First, we can use the model to generate predictive maps in geographic space which tell us where the environment is suitable for the species. Secondly, by examining the model structure: the parameter settings and individual variable responses, we gain some insight as to *why* the environment is suitable, or why it is not.

##### 3.3.1.1. Model Evaluation

The model performs well on test data, with an average test AUC value of 0.81. This means that approximately 81% of presences and background points are correctly classified in the test data. This is comfortably above the field standard threshold of 0.7 as an indicator of good model performance, and suggests that we have identified a strong pattern.

##### 3.3.1.2. Model Structure

The optimal model structure found using ENMEval was achieved when using three feature classes: Linear, Quadratic and Hinge. Product and Threshold features were not allowed. The regularization multiplier for the optimal model was, at  $\beta = 3$ , higher than the default Maxent settings. Of the 17 candidate environmental predictors, 5 were kept in the final model. These variables: bathymetry; btemp\_mean; distance; salinity\_min and temperature\_min, were the uncorrelated layers which were found to be the most important in jackknife testing.

Maxent measures the impact of each variable on the model in two ways. First, the “percent contribution” measure indicates how much each variable contributed to the final model. This value is heuristically defined, and does not necessarily imply that a variable with a higher contribution is actually more important as the values here depend on which route Maxent takes to build an optimal model. The percent contribution values for this model are shown in Figure 3.2. This shows us that the variable with the highest percent contribution is *distance* with 57.75%, however this does not mean that distance is the most important predictor. While it is useful to know how Maxent has actually built the model which generates our predictions, it is the second measure which is most interesting when interpreting the model

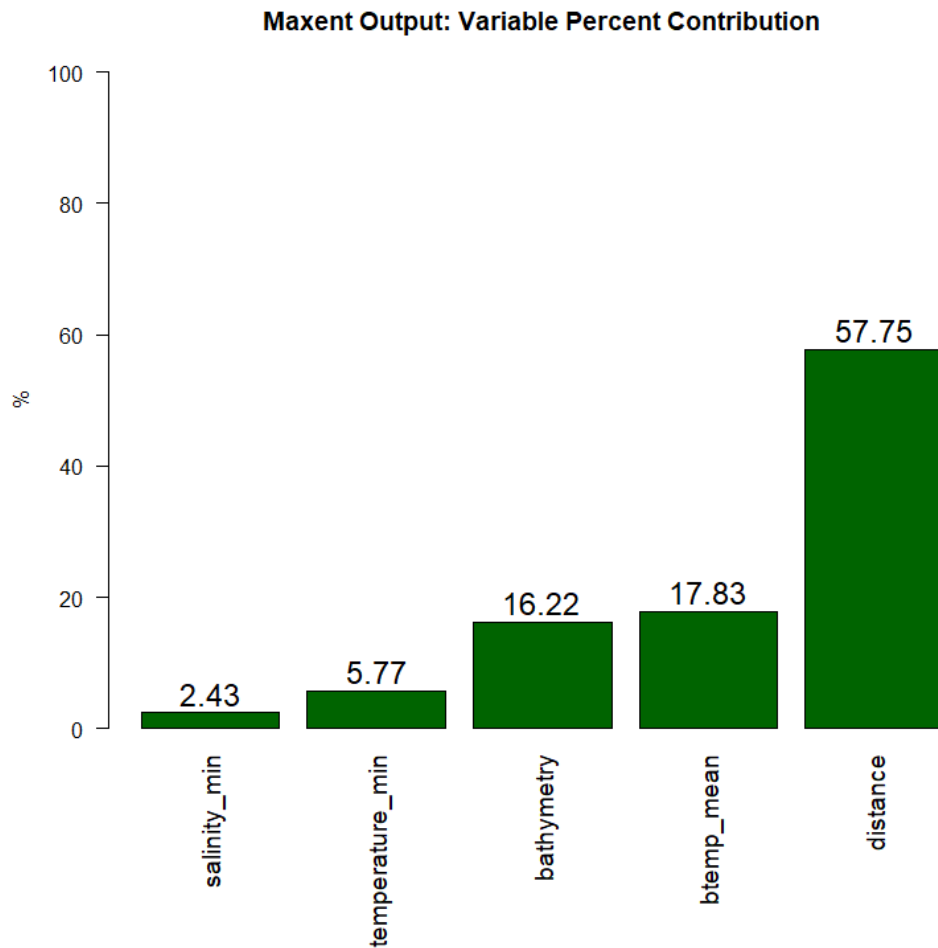


*Figure 3.2. Variable Contribution Percentages for Maxent model. Species: Gadus morhua, Model Structure: LQH 3. Data period: 1991-2017.*

The second measure of variable importance is “permutation importance”. To calculate this value, each variable has its values randomly changed and the resulting drop in training AUC is measured. This shows how sensitive the model is to changes in each predictor, and higher values in this measure do indicate more important variables. Figure 3.3 shows the normalised permutation importance percentages for this Maxent model.

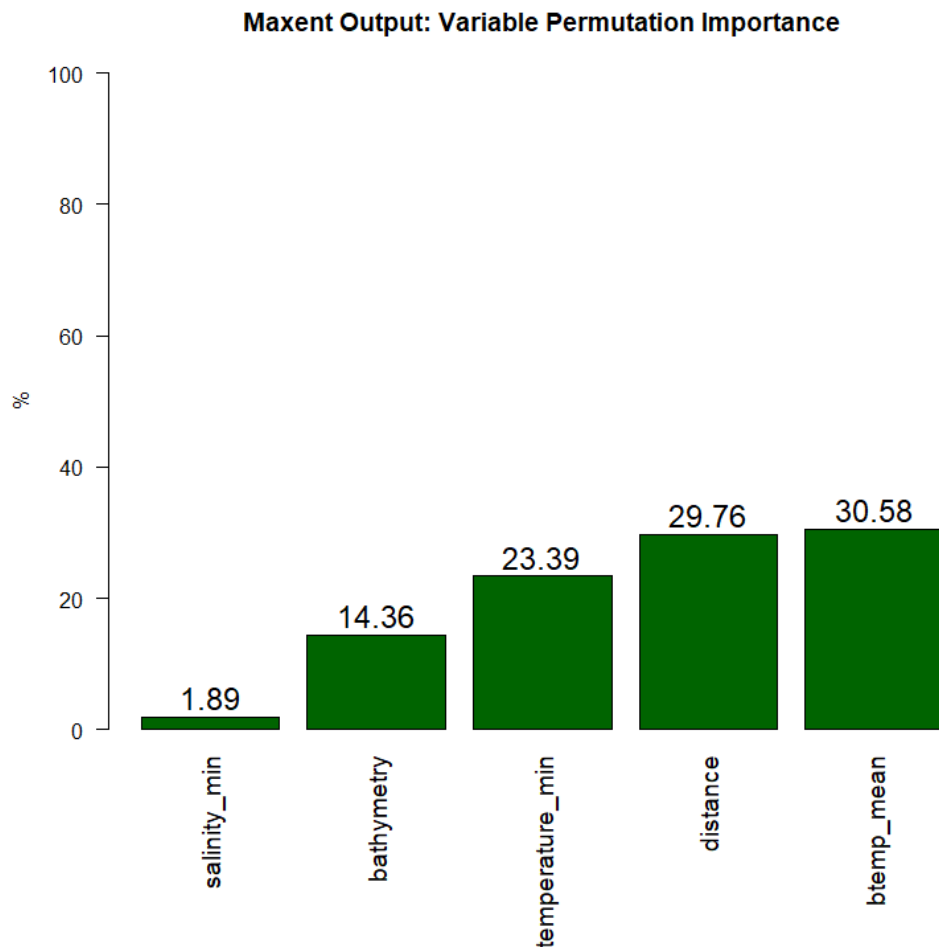


*Figure 3.3. Permutation Importance Percentages for Maxent model. Species: *Gadus morhua*, Model Structure: LQH 3. Data period: 1991-2017. These results suggest that mean annual bottom temperature is the most important predictor.*

We can see that the most important variables appear to be btemp\_mean (Mean annual bottom temperature) and distance (Distance from shore), while salinity\_min (Minimum surface salinity) appears to be the least important. It is interesting to note that each predictor used in the final model appears to be useful.

These results tell us which variables are important to Maxent, but the ecological interpretation of these results must be carefully considered. It is likely, based on expert knowledge of cod ecology, that the variable btemp\_mean is indeed an important primary predictor of habitat suitability. On the other hand, distance from shore is not a dynamic property of the environment and is likely a proxy

for some other unmeasured variables. It is still very useful information, but may indicate a need for further investigation of other environmental properties which could be correlated to distance from shore.

Maxent provides further sensitivity analysis of each variable in the form of response curves. These plots show us the predicted value of a cell, in terms of the probability of the presence of NEA cod, across a range of values for that variable, when all other variables are kept at their median value. This allows us to identify how each variable limits the species niche within the model. The response curves for each variable in this model are shown in Figure 3.4. Each subchart has the predicted Maxent output value on the y axis and the values for each covariate layer in the x axis (e.g. kilometres (km) for distance).

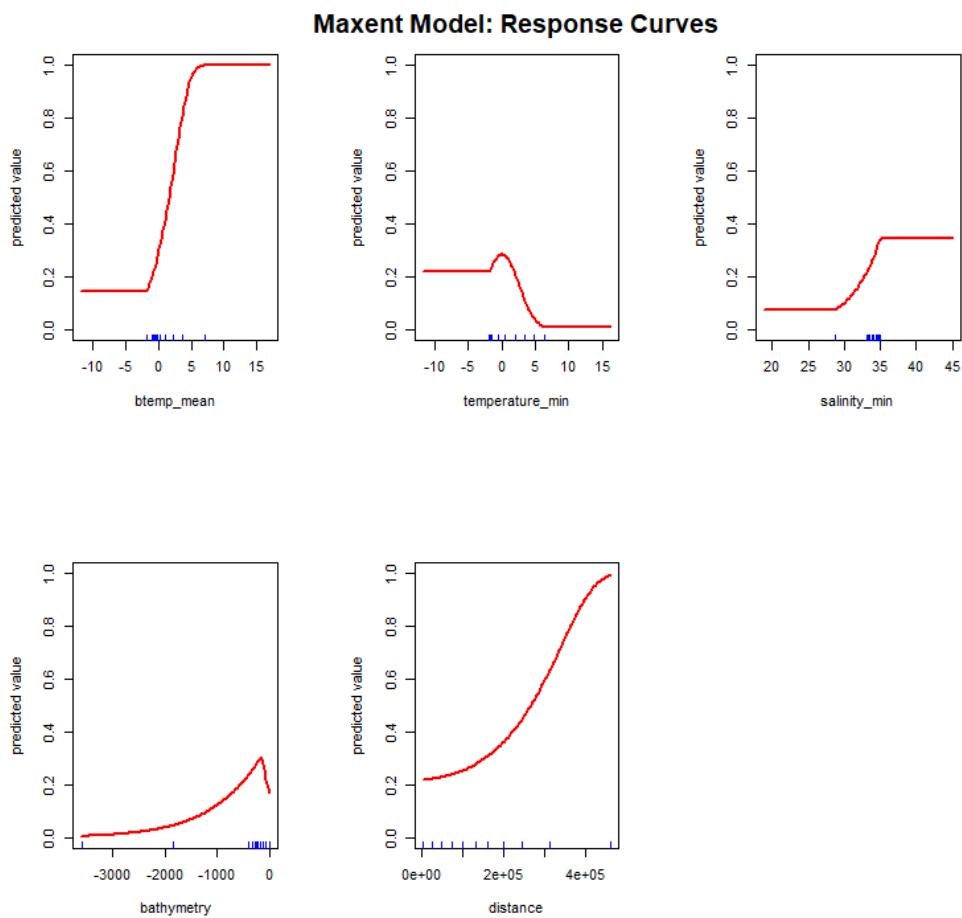


Figure 3.4. Maxent response curves for each variable in the final model. Each curve shows the relationship between the variable value and the predicted value of suitability in a cell.

We can see that each variable has a distinct relationship to the predicted value of a cell. We can immediately see that both `btemp_mean` and `distance` are strongly positively correlated to predicted value, with both variables reaching a predicted value of 1.0 (maximum) with large values. One obvious concern that arises from these curves is that the values are not clamped at the extremes, so if this model were used to predict cod distribution in a region with values outside of these environmental limits, the results may be quite inaccurate. However, for `temperature_min` and bathymetry there are clear “sweet spots”, with predicted values falling on either side.

Overall, these curves seem sensible within the bounds of the study region. Maxent tells us that the most suitable environment for *Gadus morhua* has high average bottom temperature, is far from the shore, has a minimum annual surface temperature of about 0-5 degrees celsius, has a depth of a few hundred metres and about average salinity for the region.

By applying the Maxent model back onto the study area, we can map the predicted environmental suitability for *Gadus morhua*.

### 3.3.1.3. Projection

Figure 3.5 shows the cloglog output map for this Maxent model with the environmental layers that were used to build the model (1991-2017). Each cell of this map represents a normalised measure of environmental suitability between 0 and 1, where higher values represent cells which Maxent estimates to be more suitable for the target species. These maps allow us to visually inspect our predictions.

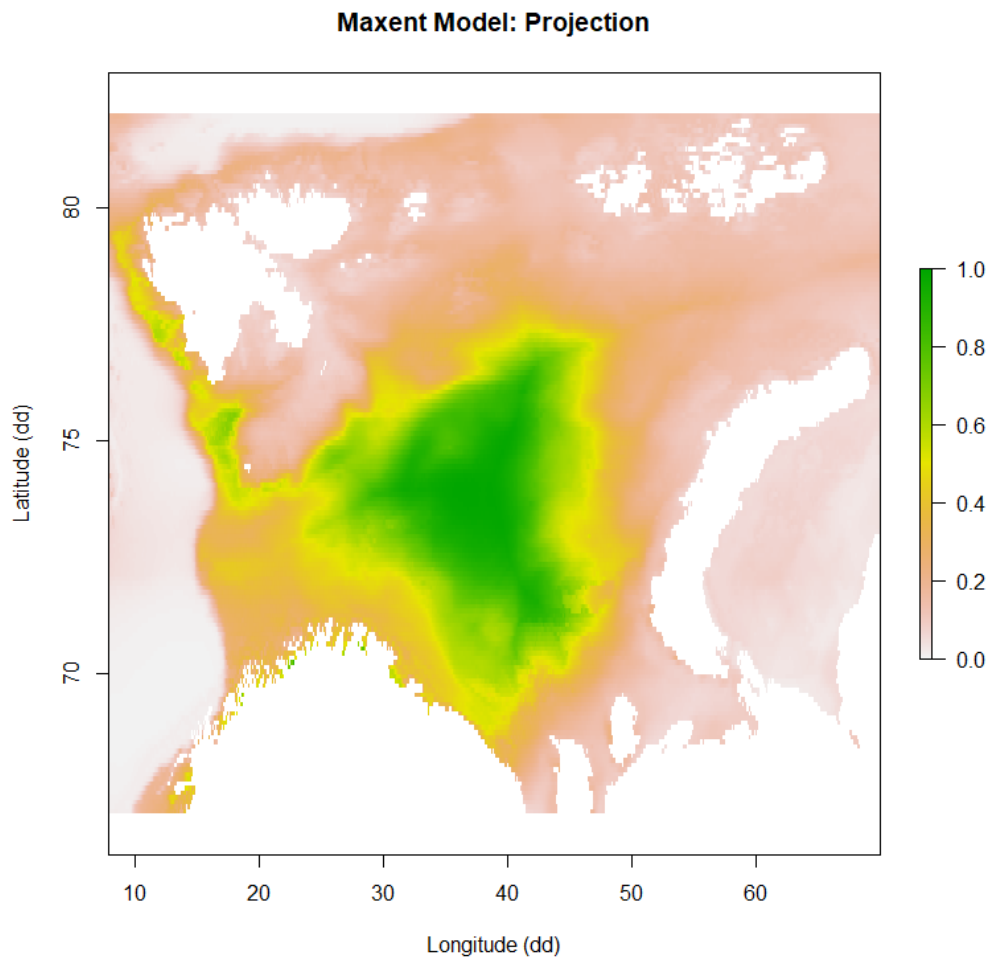


*Figure 3.5. Predicted suitability of each cell as an environment for Atlantic cod. Higher values represent a more suitable environment based upon the Maxent model formulation.*

The shape of the distribution is relatively smooth, and covers most of the central and south-eastern Barents Sea, with a narrow band of suitability along the western edge from the Sea's centre, up to the west of Svalbard. Generally, coastal regions do not appear to have high suitability, and the northern Barents Sea and Kara Sea have very low suitability under this model structure. This result matches our existing knowledge of Barents Sea cod distribution: the species prefers the warmer waters in the south while there are fewer individuals in the north, though there is an ongoing spread of the species in that region due to increasing temperatures (Ingvaldsen et al., 2017; Nakken and Raknes, 1987).

This model uses data from across a long period of time while environmental conditions in the Barents Sea are highly variable. This projection thus represents the distribution of BS cod under long

term environmental averages, resulting in a smoothing where the intricacies of their distribution may not be captured. However, it also means that this projection represents a consistency across the period. The cells which have a high predicted suitability here are likely to have been stable for a long time, and this map represents a core suitable environment within the Barents Sea where average conditions are ideal for cod. Likewise, areas of low suitability likely represent areas where suitability is always poor, or is poor on average. We investigate the impact of the data time period in section 3.3.4.

### 3.3.2. Maxent model for Atlantic cod with a prey availability layer

#### 3.3.2.1. Prey availability layer

We built a prey availability layer by modelling the distribution of 13 key prey species using proxy records from the IMR-PINRO cod diet database. The model predictions for each species were transformed into binary grids of suitable-unsuitable environment cells. These grids were added together on a cell by cell basis to produce a new raster which represents the total number of prey species for which the environment is suitable in each cell. Each cell in the grid has a value between 0 and 13. The individual model predictions and binary grids are included in chapter appendix A. We produced the prey layer based upon the availability of sufficient records for Maxent to create reasonable models, rather than using raw measures of abundance from the data as there were insufficient samples.

The new layer, *prey\_layer* is shown in Figure 3.6. We can see that the region of highest prey diversity is in the south-western and central Barents Sea and along the border with the Norwegian Sea to the west of Svalbard. There are similarities between this aggregate distribution of prey items and our base model for Atlantic cod. This follows our understanding that conditions in the southern Barents Sea are generally preferable for most species due to higher temperatures in the Atlantic water body.

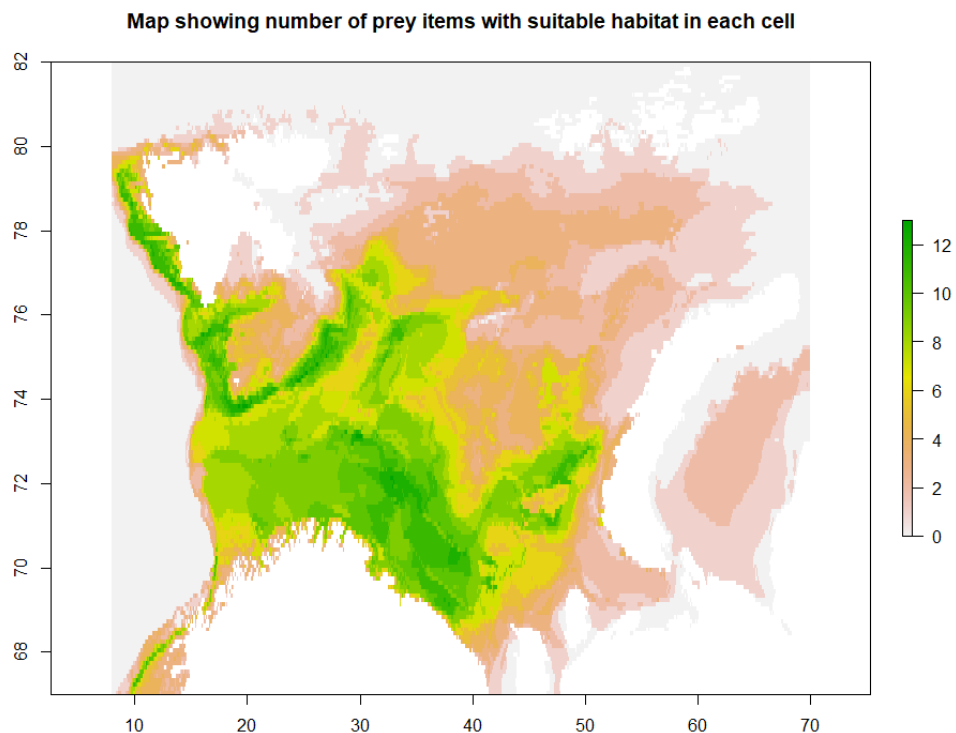


*Figure 3.6. The prey\_layer was created from modelling the distribution of 13 key prey species with Maxent. Each cell is a count of how many species were predicted to be above a threshold of environmental suitability there.*

### 3.3.2.2. Model Evaluation

Compared to the base model, including a prey availability layer has reduced model accuracy significantly. Now, the AUC on test data is only 0.74, lower than the 0.81 achieved by the base model. The result here is still above the threshold for a good model (0.7), but it is not clear that the addition of this prey availability layer has resulted in a better model. Though there is no improvement in model accuracy, there is a notable change in model structure and predicted distribution.

### 3.3.2.3. Model Structure

The optimal model structure found using ENMEval was achieved when using two feature classes: Linear and Quadratic. Product, Threshold and Hinge features were not allowed. The regularization multiplier for the optimal model was at  $\beta = 2$ , higher than the default Maxent settings but lower than in the base model, meaning that this model is likely to be comparatively less generalised. Of the 18

candidate environmental predictors, 6 were kept in the final model. These variables: bathymetry; btemp\_max; distance; salinity\_max and hicc\_mean and prey\_availability were the uncorrelated layers which were found to be the most important in jackknife testing. Only bathymetry and distance are shared between this model and the base model.

In both models, bottom temperature and salinity were included in the final model, while surface temperature has now been dropped and sea ice thickness has been retained. Instead of btemp\_mean from the base model, Maxent has found btemp\_max to be more significant in jackknife testing. Likewise, salinity\_max has been found to be more significant than salinity\_min in this new model structure.

To better understand the underlying structure of this new model, we can examine the variable percent contribution and permutation importances. Figure 3.7 shows the percent contribution of each variable in the model with prey\_availability included.

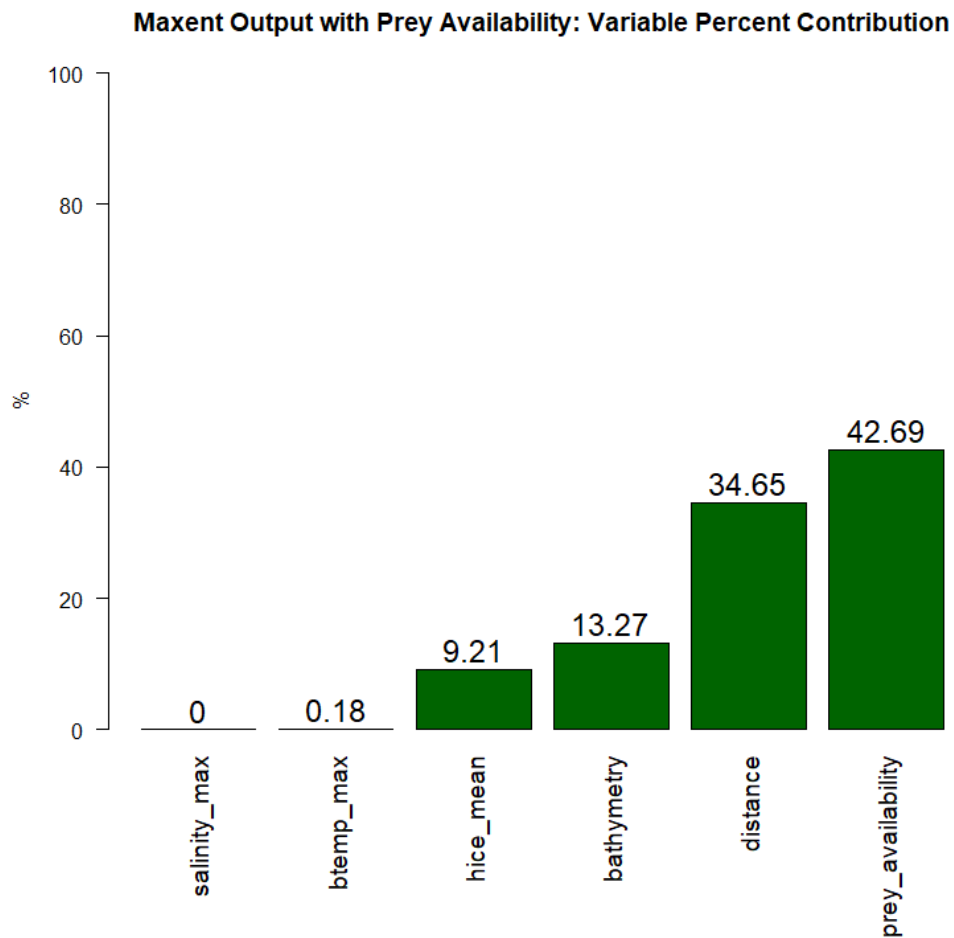


*Figure 3.7. The percent contribution of each variable in the Maxent model. Each value is between 0 and 100.*

This new layer provides a large percentage of model structure, followed by the static environmental variables of distance and bathymetry, with only a small amount provided by the dynamic variables. This is obviously very different to our base model structure, but we must examine permutation importance to get a true measure of the significance of each variable. Figure 3.8 shows these permutation importance values, and it is clear that this model structure is very different from the base model.

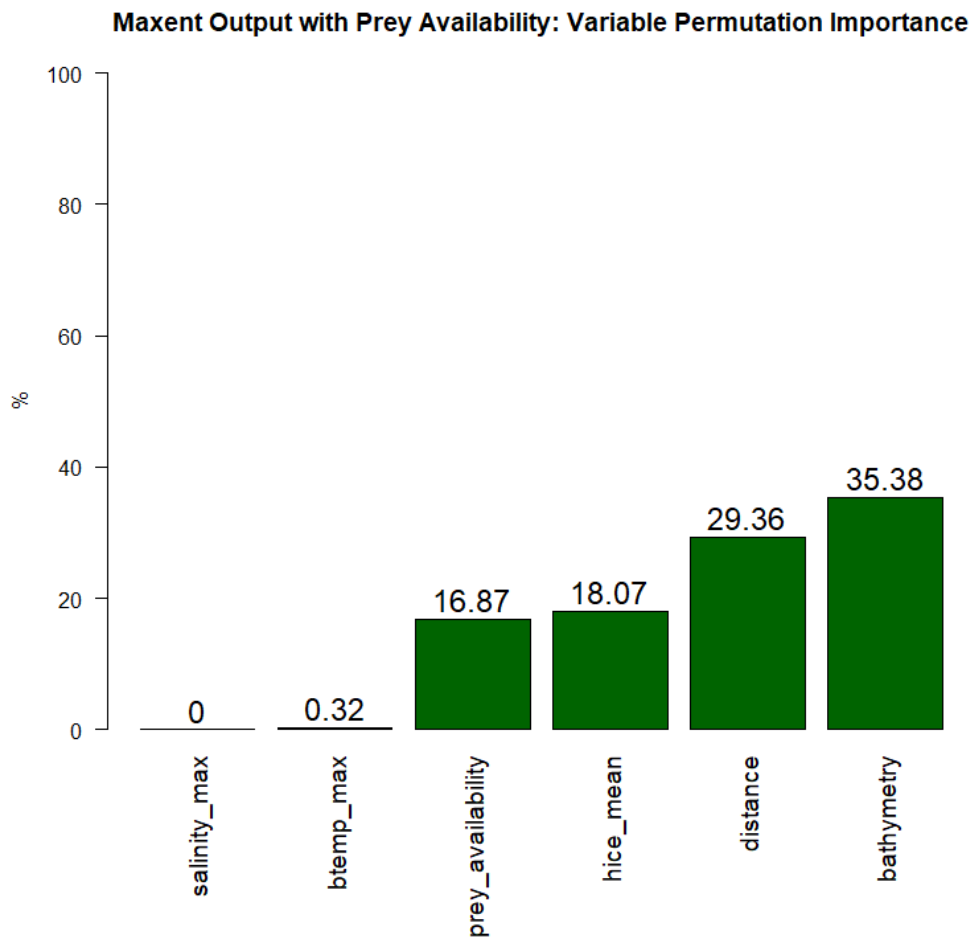
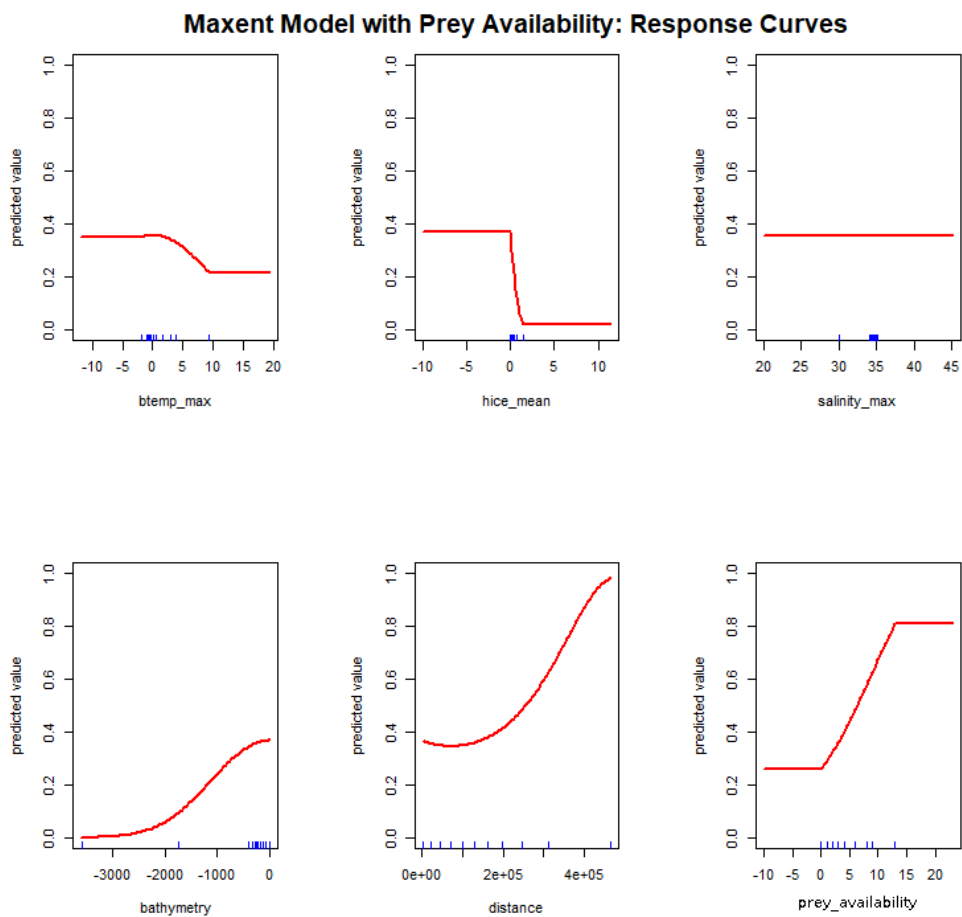


Figure 3.8. The permutation importance of each variable in the model. Each value is between 0 and 100.

Salinity is once again an apparently unimportant variable, an understandable result due to the relative uniformity of salinity values across the background region. A perhaps surprising result is that btemp\_max has a permutation importance of only 0.32%, when compared to the importance of btemp\_mean in the base model (30.58%). While we might consider that to be an inherent difference in the importance of mean vs maximum bottom temperature, due to the way this model was built, Maxent had already identified btemp\_max as having a higher permutation importance than btemp\_mean at an intermediate model building stage. This shows the innate variability in model construction which can be difficult to predict, and suggests that we should interpret these results with caution, particularly when considering the generalisability of the model. Figure 3.9 shows the response curves for each variable. As in Figure 3.4, each subchart shows the predicted Maxent

output on the y axes (no units) and the relevant covariate layer on the x axis.



*Figure 3.9. Response curves for each variable in model*

Salinity\_max has a unimodal response, which we have already seen in the variable importance measures above, it isn't contributing any useful information. The patterns in the other variables are different than in the base model, partly because different measures have been selected but also due to the different model hyperparameters which have been identified by ENMEval. There are two variables which are unique to this model: hicc\_mean and prey\_availability. Sensibly, hicc\_mean shows a maximum value at about 0, or no ice, and decreases rapidly with ice thickness. The curve misleadingly suggests values below 0, but a negative thickness measure would never be found. This is unlikely to cause any issues with using this model on another set of test data, unless there were

errors in the new environmental layers provided. Finally, the response curve for prey\_availability shows an increasing suitability with increasing prey availability. This seems like a sensible relationship. It is possible that the presence of a wide range of edible species for cod is an additional positive environmental factor. However, it is also possible that the observed relationship here is due to a strong correlation between the environmental niche of cod, and the environmental niche in aggregate of other species in the environment. Figure 3.10 shows the environmental suitability prediction for this Maxent model with the same environmental layers used for model building.

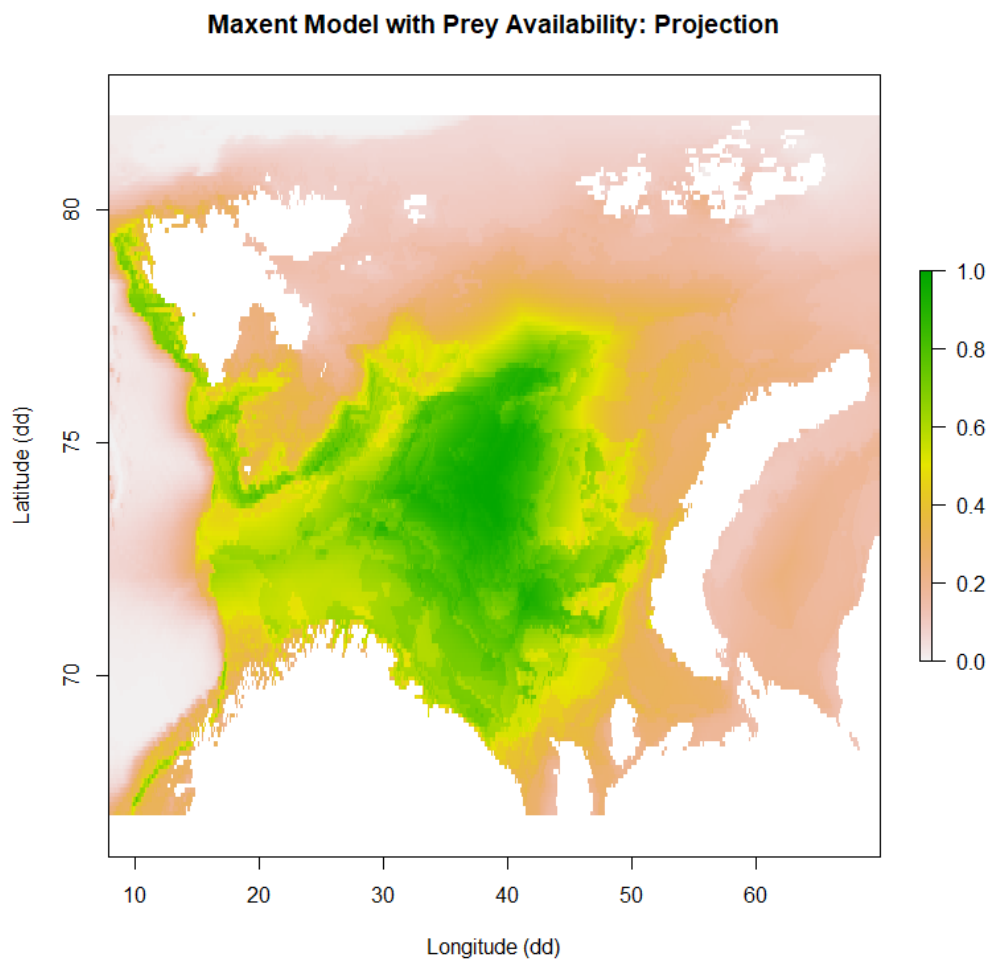


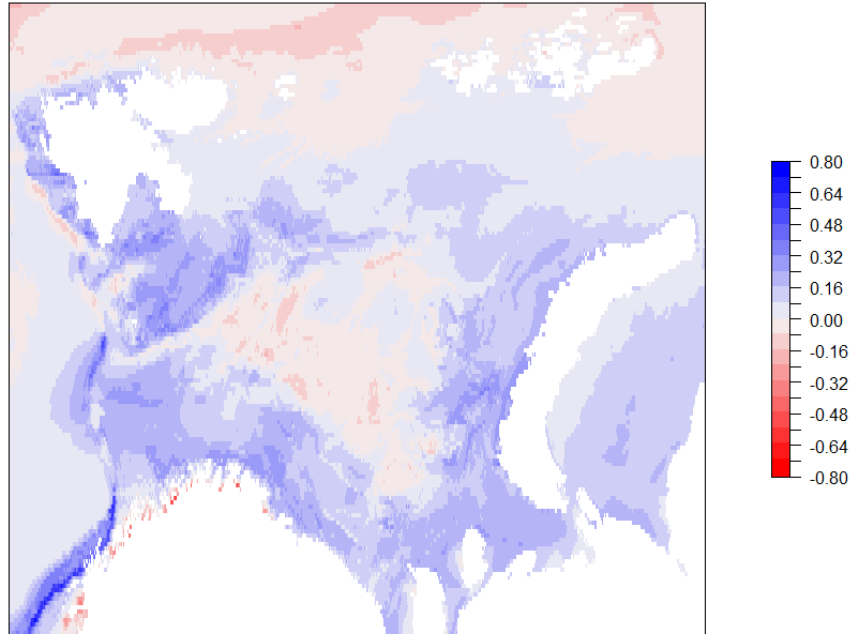
Figure 3.10. *Maxent model with prey availability map projection*

Here, we see a very large region of the Barents Sea has been identified as having a suitable environment for BS cod. Only the areas in the north of the sea have been predicted with low suitability. Compared to the base model (Figure 3.5), including the prey layer appears to have

expanded the number of suitable cells, particularly in the south west but also further to the north. There is also more texture to the suitable areas than in Figure 3.5, and less of a smooth transition from high to low suitability, likely due to the limited range of prey availability values which cause a stepped response in the prediction.

Ecologically, that including a measure of prey availability has expanded the suitable habitat for cod under this model makes some sense. We understand that the environment in the Barents Sea is broadly very good for cod, and that they are highly prevalent and widespread. This map seems to indicate that when we consider the availability of food, cod may be inclined to utilise less ideal physical environments, expanding their range beyond what our base model suggests. We must note that the formal performance of this model, as measured by the AUC, is slightly worse than our model without a prey layer, but we can't say to what extent this is based on a failure of the model to capture patterns or simply due to the reality that the species has a high prevalence and there is not a high environmental contrast between areas where the species inhabits and where it does not within the study domain.

Both models have an AUC high enough for consideration and both suggest a broadly similar pattern to cod distribution throughout the Barents Sea. The choice of whether or not to include a prey layer in future models must be informed by the specific question that the model is being employed to answer, and whether there are sufficient data available. Figure 3.11 highlights the differences between the model projection with the prey layer included compared with the base model projection. Positive values mean that the model built with a prey layer predicted a higher value than the base model while negative values mean that it predicted a lower value than the base model.

**Change between base model and prey model projections**

*Figure 3.11. Differences between base and prey model projections*

### 3.3.3. Size Stratified Maxent Models for Atlantic cod

Here we present six size stratified models for *Gadus morhua*. For each size group: Small (<20cm), Medium (20-100cm) and Large (>100cm) we present two models, one without prey availability and one with prey availability.

*Table 3.3. AUC for each size group model with and without an included prey layer*

Group	AUC
Gadus morhua (S)	0.830
Gadus morhua (S) /w Prey Layer	0.834
Gadus morhua (M)	0.804
Gadus morhua (M) /w Prey Layer	0.813
Gadus morhua (L)	0.847
Gadus morhua (L) /w Prey Layer	0.840

Model test AUC scores are listed in Table 3.3. We found no significant difference in model predictive performance between groups with prey layer information and those without. Model performance was also similar for size groups. All models performed well (AUC > 0.8).

## 3.3.3.1. Model Structure

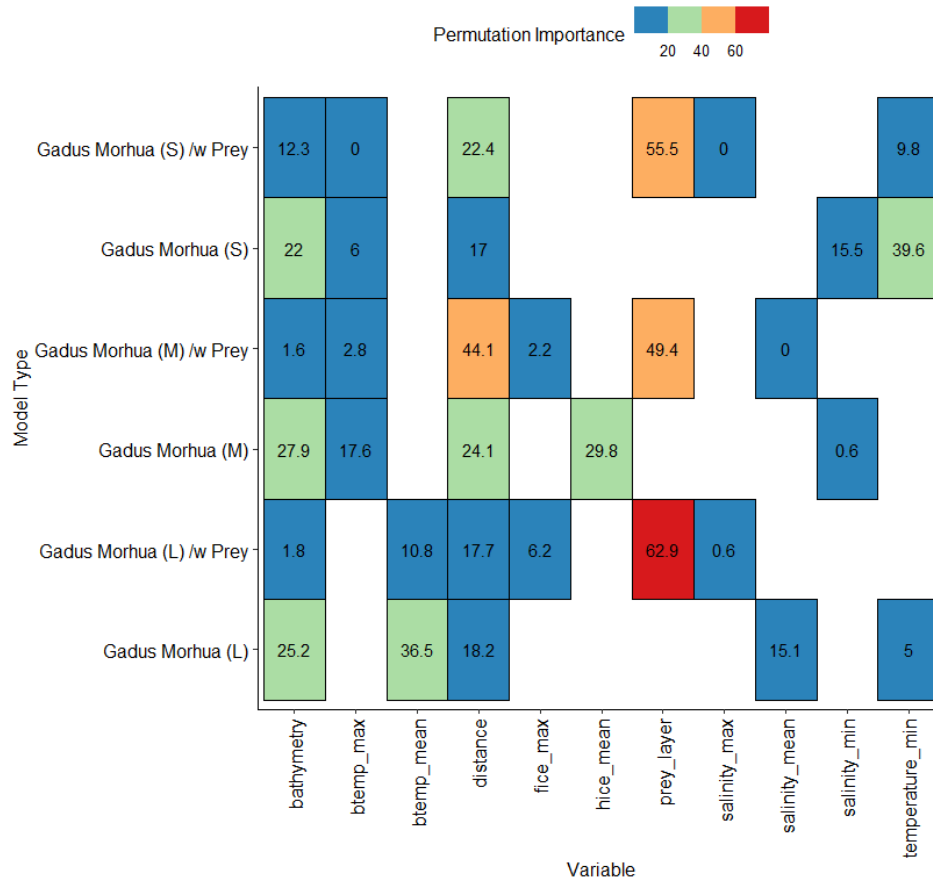
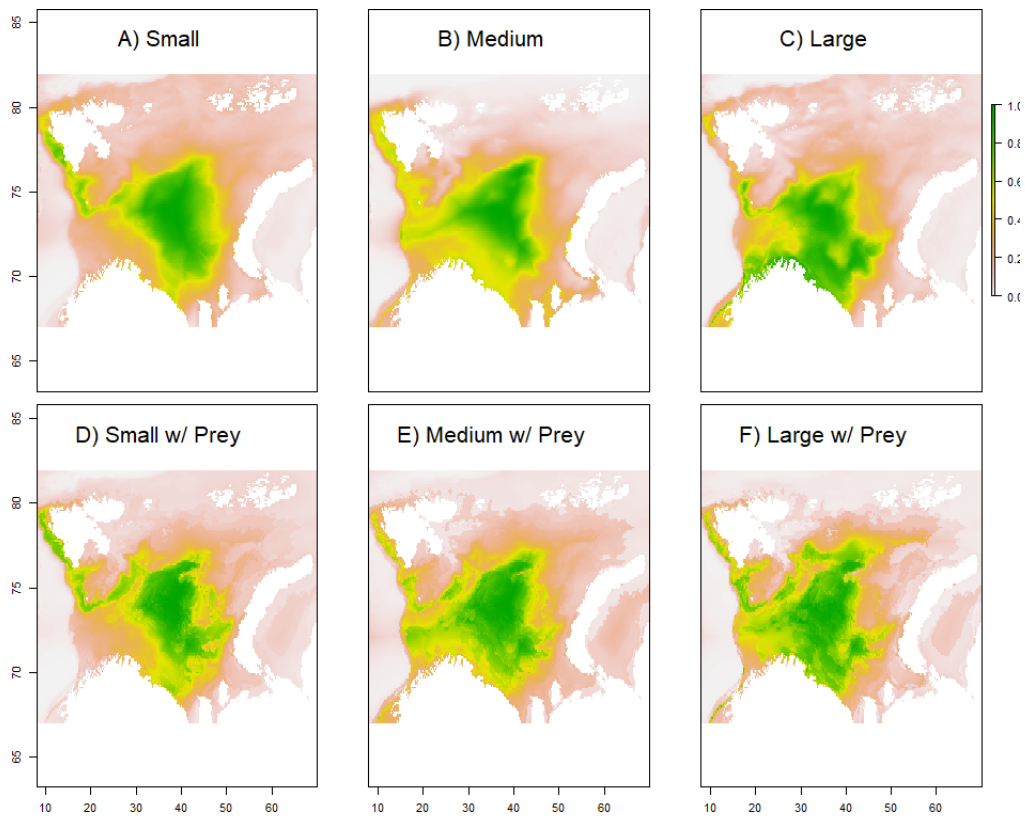


Figure 3.12. Permutation importance of each variable across size structure groups with and without a prey availability layer

The permutation importance of each variable included in the size class models both with and without a prey availability layer is shown in Figure 3.12. We see that when we include the prey layer, it is the most informative layer in each model, with a P.I of 55.5%, 49.4% and 62.9% for small, medium and large cod respectively.

For the models not including a prey layer, we observe a different hierarchy of variable importance between size groups. For *Gadus morhua* (S), we see that *temperature\_min* has the highest P.I, followed by *bathymetry*. For *Gadus morhua* (M) the most informative layers are close in P.I: *hicc\_mean*, *distance* and *bathymetry*. Finally, the model for *Gadus morhua* (L) was most informed by *btemp\_mean* and *bathymetry*.

## 3.3.3.2. Projected distribution



*Figure 3.13. Maxent models for each size group with and without a prey layer map projections*

Figure 3.13 above shows the projections generated by each Maxent model in this group. The top row shows each size class without the prey layer, while the bottom row shows each group with the prey layer included. We can see that there are notable differences in the predicted suitability of the environment between size groups, as well as between the base and prey layer models.

Broadly, there appears to be some core agreement between models that the central and southern regions of the Barents Sea are generally suitable environments. There are some interesting and significant differences in the exact extents and shapes of these predicted suitability maps, and we can see that the Large group models are quite different from the other two groups, as well as the base

model predictions. When there is no prey layer used, the Large cod model suggests that there is a high suitability along the Norwegian coastline, a feature which we do not see in the other size groups. Then, in the Large model with a prey layer, we lose the area of suitability along the coast but there is a significant spread into the northern parts of the Barents Sea, where the water is colder. This map seems to conform to our understanding of the situation in the Barents Sea, where larger individuals are better able to withstand the more challenging conditions in the northern areas while smaller individuals are more frequently found in the warmer southern waters.

At this stage it is perhaps most important to acknowledge simply that a difference in projected suitability between groups does exist. The results from this modelling process are ecologically sensible - Atlantic cod is a highly mobile species which is widely distributed in the Barents Sea, has a life history which includes a movement from a pelagic to demersal species and the environmental conditions to which they are best suited do change as they grow.

Here we have shown that there is value in further investigation of these size groups as distinct populations and by doing so we may capture more ecologically realistic patterns in species distribution and provide a new window through which to examine changes in the Barents Sea ecosystem.

### 3.3.4. Time stratified Maxent Models for *Atlantic cod*

We investigated how Maxent models for Atlantic cod were affected by the time sensitivity of the input data. We built 67 maxent models using input data from different subsets of the full environmental data period (1991-2017). These were each continuous 1 (26 models), 5 (23 models) and 10 (18 models) year periods. Figure 3.14 compares the model performance results between groups. This way of viewing the outcomes allows us to examine the relationship between data period length and model performance.

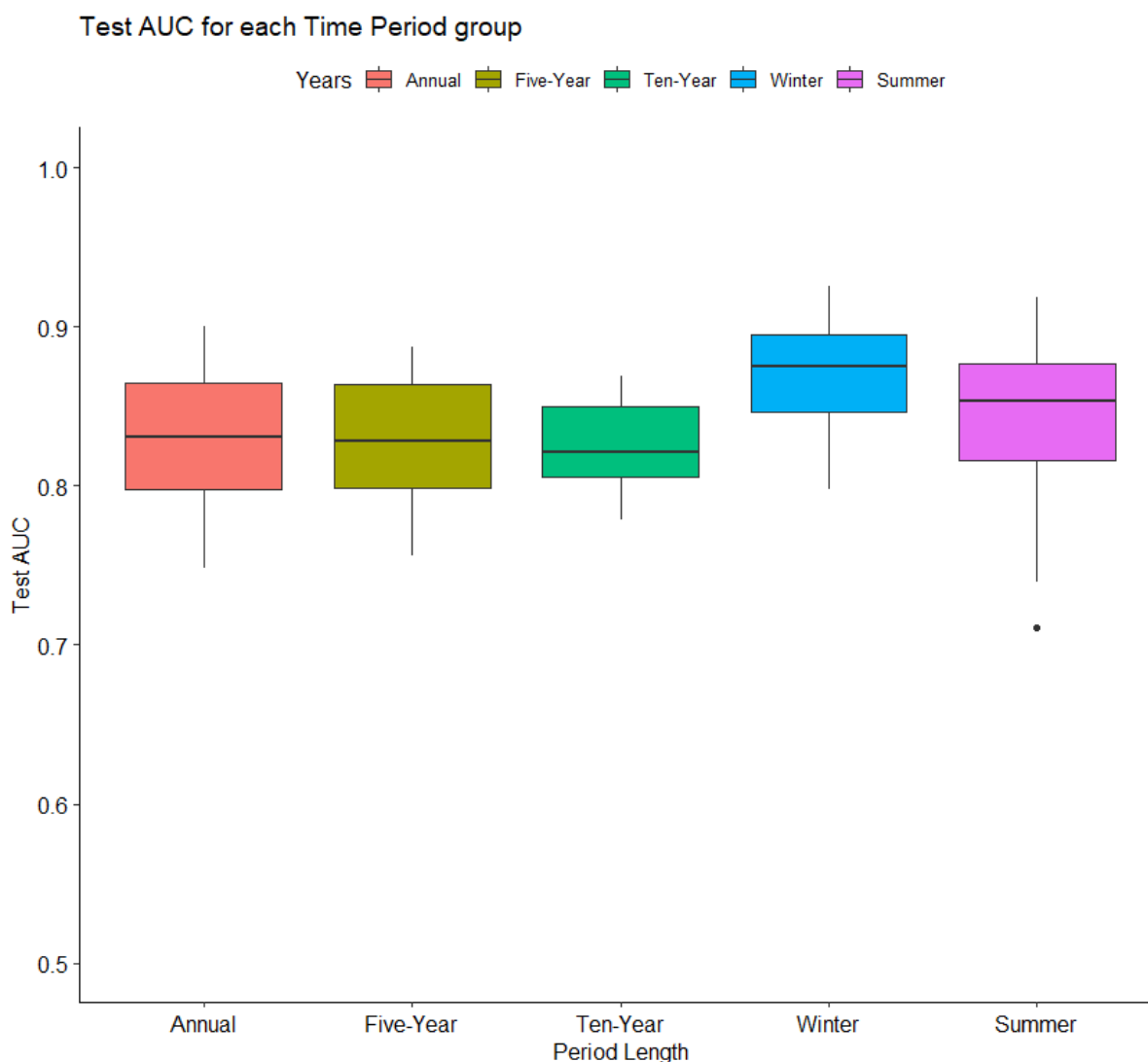


Figure 3.14. Boxplots of Test AUC values for each time period length group

We see a difference in the distribution of test AUC values between the time period groups, with the winter models in particular having a significantly higher average test AUC than the other groups. One way ANOVA testing results in a P-Value of 0.0007 ( $P < 0.05$ ), indicating a significant difference between one or more group means. Additional testing with Tukey's range test shows that the winter group AUC mean is significantly different from the annual, five-year and ten-year period groups AUC mean at the  $P < 0.05$  level ( $P = 0.004$ ,  $P = 0.003$ ,  $P = 0.004$  respectively). There is no statistically significant difference between the summer groups mean AUC and any other group, and there is no difference between the annual, five-year and ten year group mean AUC.

In absolute terms, none of the models in any group achieved a test AUC value below 0.7, suggesting that a model of sufficient accuracy can be built at any of the period lengths that we investigated. This is particularly interesting for the annual and seasonal model groups, where the effects of environmental volatility are more likely to be captured and we might expect to see outliers which cause a significant drop in model performance. Only one statistical outlier is present in the data, the model for 2015-summer, which had a test AUC of 0.711.

When we examine the model structure we see a very clear difference in the patterns that Maxent is identifying in the environmental data. Tables summarising the permutation importance of each variable within each group can be found in Appendix C.

3.3.4.1. Annual, Five-Year and Ten-Year Model Structure

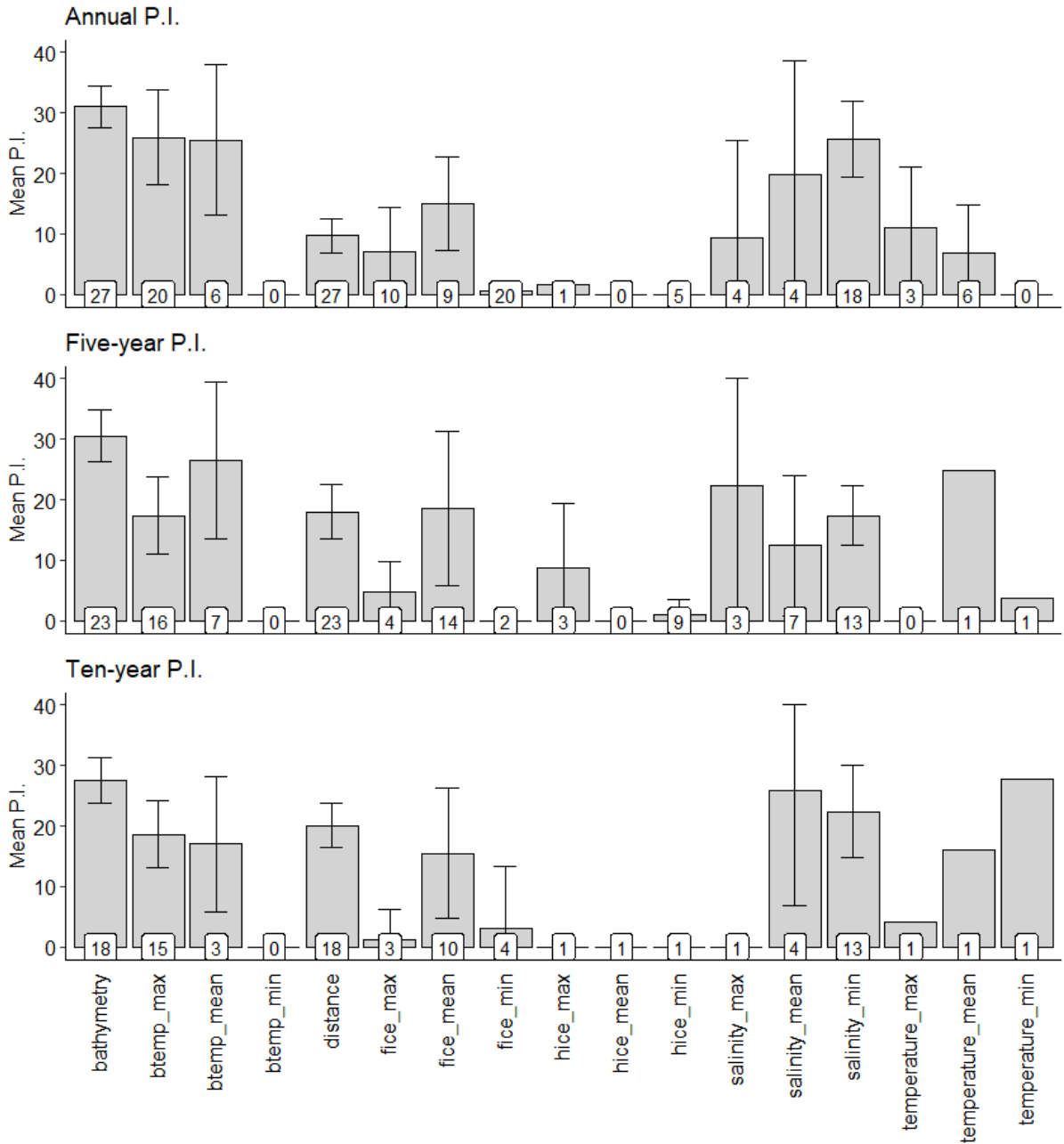


Figure 3.15. Mean P.I. % with 95% confidence intervals for Annual, Five-year and Ten-year model variables. The number of models containing each variable is labelled at y = 0 for each variable.

With all groups combined in Figure 3.15, we see a distribution of which variables are included in the final models and how important each of these variables are. The static variables *bathymetry* and *distance* are used in every model, because they are not co-linear with any other variable. The average P.I. of *bathymetry* is 30% and 15% for *distance*, with standard deviations of 9% and 10% respectively. These are high levels of variability, and we see that there are significant differences in importance between time groups. Across all three periods *bathymetry* maintains an average of between 27-31% average P.I., while *distance* increases its average P.I. from 8% in the 1 year group to 18% in 5 years and 20% in 10 years. This suggests that distance from shore is much more important when the data is aggregated over a longer time period, while seafloor depth maintains its importance even at a 1 year period. The reasons for this disparity are unclear. Both variables are likely representing the effect of other, unmeasured variables as there is no direct requirement between the physiological needs of Barents Sea cod and how deep the water is, or how far from shore they may be. Whatever dynamics are captured by these variables, it seems that *bathymetry* is a useful indicator of presence under all time scenarios while *distance* is less useful over short periods. It seems plausible that, over long periods of aggregated environmental data, the most suitable conditions in the environment relate to distance from shore in some meaningful but indirect way.

From the set of co-linear variables which represent temperature we see some variation in selection. Across models Maxent selects *btemp\_max* for inclusion in 51 models, with an average P.I. of 21.1% and a standard deviation of 13.8%. The second most selected variable, *btemp\_mean* is chosen in only 16 models with an average P.I. of 24.3% and a standard deviation of 11.9%. Maxent never selected *btemp\_min* for inclusion. Of the variables representing surface temperature, only 14 models included any one of them. Overall, maximum bottom temperature seems to be the most important quality of its variable type. Average P.I. for *btemp\_max* is highest in the 1 year group and lowest in the 5 year group.

The next most widely used variable is *salinity\_min* in 44 out of 67 models, with an average P.I. of 22.2%. In 15 models, *salinity\_mean* was selected instead with an average P.I. of 18.0%. There is no obvious pattern across time period groups. Of the ice cover and thickness variables, only one was found to have a high average P.I., *fice\_mean* (33 models) with 16.6% however the standard deviation was 17%, and this extreme variability is present in all time groups.

The variability measured for each layer tells us that although it is useful to recognise broad patterns in model structure associated with time period groups, each model is quite unique and sometimes an

unexpected variable is found to be essential. It is difficult to identify a strong pattern which differentiates the structures of models built using different data periods, but the increasing importance of *distance* as period length increases suggests that it is representing another environmental quality which is being lost as the layers are produced from longer-term averages, and in the annual period group whatever information *distance* offers is being better represented by the dynamic environmental variables.

3.3.4.2. Seasonal Model Structure

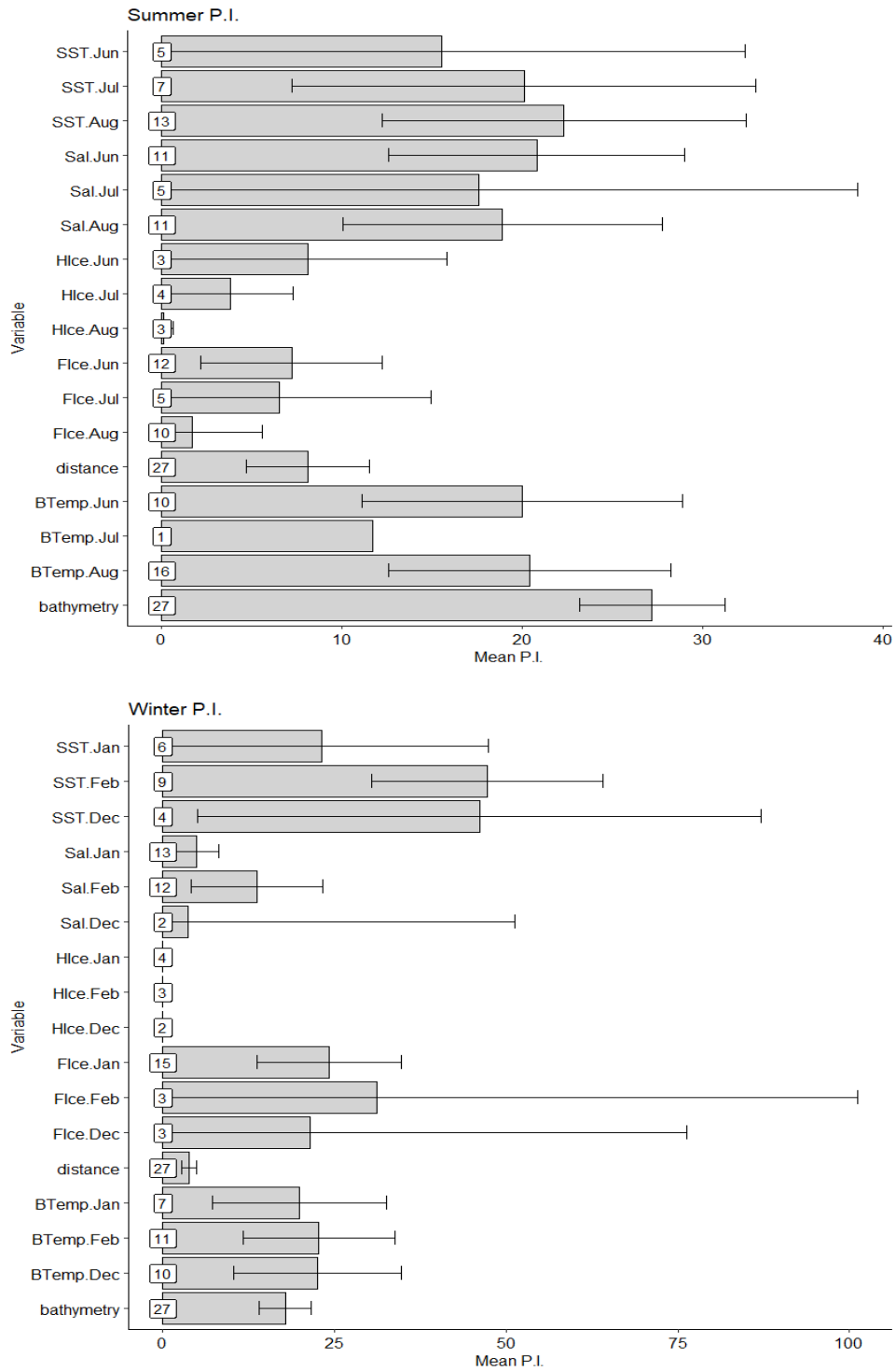


Figure 3.16. Seasonal model variable P.I. distributions. Top - summer, Bottom - winter.

For the seasonal models shown in Figure 3.16, *bathymetry* and *distance* were again used in every model. *Bathymetry* has a mean P.I. of 27.2% and 17.8% in summer and winter respectively, with a standard deviation of 10.2% and 9.5%. *Distance* has a mean P.I. of 20.1% and 8.1% with a standard deviation of 7.4% and 8.7% in summer and winter. Both static variables have a higher P.I. during summer than winter. SST variables had high variability in P.I. across summer and winter, with the summer layers reporting: SST.Jun ( $15.5 \pm 13.6\%$ ), SST.Jul ( $20.1 \pm 13.9\%$ ) and SST.Aug ( $22.3 \pm 16.7\%$ ) compared to the equivalent winter layers: SST.Dec ( $46.1 \pm 25.8\%$ ), SST.Jan ( $23.2 \pm 23.1\%$ ) and SST.Feb ( $47.2 \pm 21.9\%$ ).

In the summer models, the most frequent variable is BTemp.Aug in 16 models. All 27 models contain at least one bottom temperature variable, with only 1 model using BTemp.Jul. The mean P.I. for bottom temperature variables are between  $11.7\% \pm 0\%$  (Jul),  $20.0 \pm 12.4\%$  (Jun) and  $20.4 \pm 14.7\%$  (Aug) .

In the winter models, the most frequent variable is FIce.Jan in 15 models, with a mean and standard deviation P.I. of  $24.2 \pm 19\%$ . As in summer, all models contain at least one bottom temperature variable. Across all variables, permutation importance is lower on average for the winter models than the summer models. Sea surface temperature variables have the highest P.I. overall, specifically SST.Dec and SST.Feb, but as discussed both layers also have very high variability.

## 3.3.4.3. Model Projections

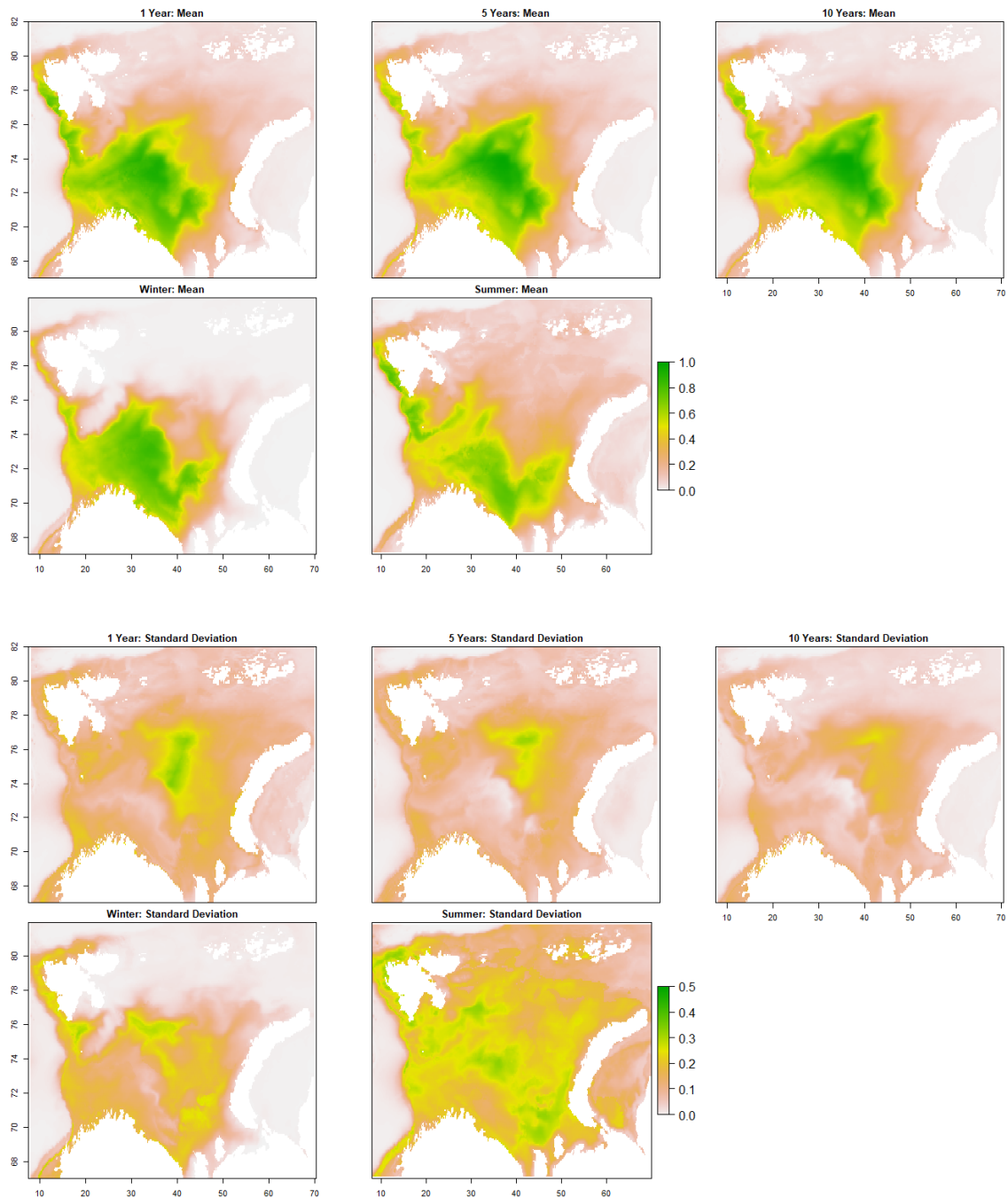


Figure 3.17. Mean and standard deviation suitability scores per cell for each temporal group.

The mean and standard deviation cell values for each temporal group are shown in Figure 3.17. From this figure, we can see that changing the temporal window has a profound effect on the

predicted cell suitabilities. The annual, five and ten-year groups produce a similar overall distribution. The winter group produces an overall distribution which is confined to the southern Barents Sea, though the core area of suitability is similar to those for the annual, five and ten-year models. The summer model group is the most divergent from the others, with a core area split into two groups, one in the southern Barents Sea and the other to the south of the Svalbard archipelago. When we examine the standard deviation of cell values, we see decreasing variability as the period length increases. The seasonal models are the most variable, with the winter group showing a frontier of high variability in the centre-north Barents Sea and the summer group showing high variability across the study region.

### 3.4. Discussion

We have successfully modelled the distribution of *Gadus morhua* in the Barents Sea. Though SDM's have been applied to other migratory marine species (Bigg, 2014; Bigg et al., 2008), the temporal and ontogenetic dimension of this study is novel. We applied best practices from the literature to improve model performance and validity to varying degrees of success. The importance of choosing temporally sensitive data has been raised (Fernandez et al., 2017; Mannocci et al., 2017), and we found that our model performance was not significantly affected by changing temporal period, except for seasonal winter models which reported a statistically significant increase in model AUC. In the study by Fernandez et al., their temporal window was much shorter than even our seasonal scale, over hours. With the data available to us, we could not achieve these short timescales for comparison.

When we included a covariate layer representing prey availability following the example of (Gherghel et al., 2018), we found no increase in model performance. The layer was a composite of Maxent prediction maps for key prey species; it is possible that other methods of including prey availability might have been useful. We did not have enough data to include covariate layers representing the absolute abundance of specific species or even groups, due to the discontinuous nature of the sampling stations. Future work could consider alternative methods of generating prey availability covariate layers, such as applying, for example a spatial zero-inflated Poisson model (Lyashevskaya et al., 2016) to create continuous abundance maps, but such a study is beyond the scope of this thesis. Our final models were built using only physical environmental layers, though existing studies have shown that biotic interactions are important to capture in SDM's (Araújo and Luoto,

2007; Wisz et al., 2013). Future work could explore a much broader range of potential biotic covariates to help improve model performance.

Our modelling of distinct cod size groups as individual species in Maxent is a novel application of the tool as we have applied it. Though previous studies have used environmental niche models to examine differences in ontogenetic distribution (e.g. Druon et al., 2016; Galaiduk et al., 2017), none have done so in this manner for *Gadus morhua* in the Barents Sea. We found both significant differences in model performance and structure for each size class, particularly when comparing large cod (>100cm) to the other two groups. This matches existing studies on the life histories, distribution and behaviour of the species (e.g. Ingvaldsen et al., 2017; Nakken and Raknes, 1987; Ottersen et al., 2014). We propose that this method could be usefully applied to any species with distinct life stages with different environmental tolerances and preferences in order to more accurately capture variation in distribution.

### 3.5. Conclusions

In this chapter, we have presented a robust framework for producing Maxent models which are capable of predicting the distribution of *Gadus morhua* in the Barents Sea while addressing issues of overfitting and model complexity. We have shown that the addition of a relevant biotic interaction layer does not result in higher overall model accuracy but that it does change the model structure and projected distribution. We have identified a significant difference in the suitable habitat for large cod when compared to the rest of the population and provided rationale for the further treatment of these size-stratified cod groups as having distinct distributions in the Barents Sea. Finally, we have thoroughly investigated the sensitivity of our models to the temporal range of the input data and shown that valid models appear to be produced at a range of time scales.

These investigations provide a basis for the application of Maxent as a tool in examining the spatio-temporal patterns in the Barents Sea food web. In the following chapter, we use Maxent to examine how the distributions of Atlantic cod and several important prey species have changed over time, and we attempt to identify any relationships between the spatial-temporal synchronicity of these species with their relationship as predator and prey. With Maxent, we can examine these relationships at a range of timescales and identify broad and fine scale evolutions of the Barents Sea ecosystem, the trophic dynamics beneath, and attempt to predict how future climate changes will drive this evolution.

## Chapter 4 - The changing distribution of cod and critical prey species in the Barents Sea

### 4.1. Introduction

In Chapter 3, we presented a thorough methodological investigation of using Maxent to model the distribution of Barents Sea cod. We demonstrated that valid models can be built for different size classes of cod, producing significantly different distribution predictions. We investigated the effects of changing the input data period on model performance and changing various parameters. This chapter applies the Maxent modelling framework to analyse Spatio-temporal patterns in the distribution of Barents Sea cod and several key prey species.

We selected four prey species to include in this analysis: *Mallotus villosus* (capelin), *Boreogadus saida* (polar cod), *Pandalus borealis* (shrimp) and *Melanogrammus aeglefinus* (haddock). These species were selected due to their importance as prey species as determined in Chapter 2. Not all important prey species are included here due to a lack of sufficient occurrence records from the IMR-PINRO database for the temporal resolution of this investigation.

Previous studies have identified long term interseasonal variation in the overlap between *Gadus morhua* and *Mallotus villosus* (Fall et al., 2018), *Boreogadus saida* (Renaud et al., 2012), *Melanogrammus aeglefinus* (Dalpadado et al., 2009) and others. These changes in spatial overlap are generally related to changes in temperature, population density, relative population abundance and the availability of suitable prey. Species distribution models such as Maxent have been successfully used to model the distribution of marine species (Robinson et al., 2017), where domain specific issues such as the temporal sensitivity of occurrence records for migratory species have been addressed (Fernandez et al., 2017).

There are two aims to this chapter. The first aim is to measure how the distribution of each species group has changed over the study period. We will measure these changes in distribution by examining the predictive maps produced by Maxent for each modelling period and comparing all the models within a species group. We seek to uncover the Spatio-temporal patterns in distribution by

examining which areas of the Barents Sea may be considered ‘core’ habitat and which sites are varyingly suitable. We expect to see variability in the specific shape of suitable habitat for each species and possibly a range expansion across the study period due to increasing water temperatures.

The second aim is to examine the temporal pattern of spatial overlap between the target species groups. We will measure the overlap of distribution between various groups over time to establish the growth or diminishment of areas in the Barents Sea where environmental conditions create suitable habitats for predator-prey interactions to occur. We expect to see a complex relationship between time and overlap for various predator-prey combinations as each species responds to environmental variability differently. We might expect an overall increase in the overlap between cod and prey species over time due to the spread of suitable conditions for cod, but this might not hold if conditions which benefit cod are detrimental to a particular prey species.

## 4.2. Methodology

### 4.2.1. Seasonal Maxent model design

#### 4.2.1.1. Environmental Layers

For each of the seven species groups targeted, two models were trained for each year between 1991-2017 using environmental layers representing the summer or winter months respectively (see also Section 3.3.4). Each layer is constructed using data which is specific to the year being modelled, so each year/season has a unique set of environmental layers. The schematic for environmental layers used in each season is presented in Table 4.1. The species groups modelled are : *Gadus morhua* < 20cm [*Gadus morhua* (S)], *Gadus morhua* 20 - 100cm [*Gadus morhua* (M)], *Gadus morhua* > 100cm [*Gadus morhua* (L)], *Mallotus villosus*, *Boreogadus saida*, *Melanogrammus aeglefinus* and *Pandalus borealis*.

Table 4.1. Environmental layer schematic for seasonal Maxent models (Continued on next page)

	Summer	Winter
Layer 1	Surface Temperature (June) SST.Jun	Surface Temperature (December) SST.Dec
Layer 2	Surface Temperature (July) SST.Jul	Surface Temperature (January) SST.Jan
Layer 3	Surface Temperature (August) SST.Aug	Surface Temperature (February) SST.Feb
Layer 4	Bottom Temperature (June) BTemp.Jun	Bottom Temperature (December) BTemp.Dec
Layer 5	Bottom Temperature (July) BTemp.Jul	Bottom Temperature (January) BTemp.Jan
Layer 6	Bottom Temperature (August) BTemp.Aug	Bottom Temperature (February) BTemp.Feb
Layer 7	Salinity (June) Sal.Jun	Salinity (December) Sal.Dec
Layer 8	Salinity (July) Sal.Jul	Salinity (January) Sal.Jan
Layer 9	Salinity (August) Sal.Aug	Salinity (February) Sal.Feb
Layer 10	Sea Ice Cover (June) FIce.Jun	Sea Ice Cover (December) FIce.Dec
Layer 11	Sea Ice Cover (July) FIce.Jul	Sea Ice Cover (January) FIce.Jan
Layer 12	Sea Ice Cover (August) FIce.Aug	Sea Ice Cover (February) FIce.Feb

		Fice.Feb
Layer 13	Sea Ice Thickness (June) HIce.Jun	Sea Ice Thickness (December) HIce.Dec
Layer 14	Sea Ice Thickness (July) HIce.Jul	Sea Ice Thickness (January) HIce.Jan
Layer 15	Sea Ice Thickness (August) HIce.Aug	Sea Ice Thickness (February) HIce.Feb
Layer 16	Average water column depth within cell bathymetry	
Layer 17	Distance to shore distance	

Specific environmental layer sets were created by subsetting the CMEMS ARC MFC reanalysis product (Traon et al., 2017) to the relevant year/months for each model.

#### 4.2.1.2. Occurrence records and background points

Occurrence records for small, medium and large cod groups are extracted from the IMR-PINRO cod diet database. The occurrences are filtered by year, season and length. The occurrences for prey species are also extracted from the IMR-PINRO cod diet database. These records are filtered by year and season and by the degree of digestion. Only records within the least digested classification are included to limit displacement effects after consumption on positional accuracy. We assessed each period for the number of available occurrences. In general, where the number of available occurrences is between 15 and 100, those occurrences are used directly to build the model. If more than 100 occurrences are available, the thinning procedure outlined in section 3.2.1 is applied to reduce the number of occurrences to 100. If fewer than fifteen occurrences are available, then no model is built directly. Instead, an average model for that species is applied to that period's environmental layers, and the existing occurrences are used as an additional test set for validation. If there are no occurrences available at all, an average model is used without further validation. The methodology used for producing these Average models is presented in Section 4.2.2.

For each model, 10,000 background points were selected from non-presence locales within the main body of the Barents Sea following the standard methodology described in Section 3.2.2.

#### 4.2.1.3. Parameter setting and validation

Optimal parameter sets for each model were identified using the method outlined in Section 3.2.4 using the ENMEval R package (Muscarella et al., 2014). Model validation followed the same procedure outlined in Section 3.2.5, using checkerboard style splits on training-test points.

#### 4.2.1.4. Producing binary suitability maps by thresholding Maxent predictions

We apply a thresholding rule to Maxent prediction maps to produce binary grids of environmental suitability prediction. This assigns each cell within the modelled domain a value of either 1 (suitable) or 0 (unsuitable) based on a fixed threshold over the Maxent cloglog output map; this threshold is specific to each particular model and is determined by Maxent. We select a threshold value which maximises the sum of specificity and sensitivity of the resulting map, which is a standard threshold used in existing studies (Liu et al., 2015). These binary maps are used to measure the overlap area between two species during a particular temporal period.

### 4.2.2. Average Maxent model design for missing data

In some cases, insufficient occurrence record samples were available to produce a model using annual-seasonal specific data. In those cases, to avoid missing data, we used a Maxent model trained on a larger, non-temporally specific dataset for each species to project onto the annual-seasonal environmental layers of the period of insufficient data. Figure 4.1 highlights which periods have predicted maps generated from the projection of an average model.

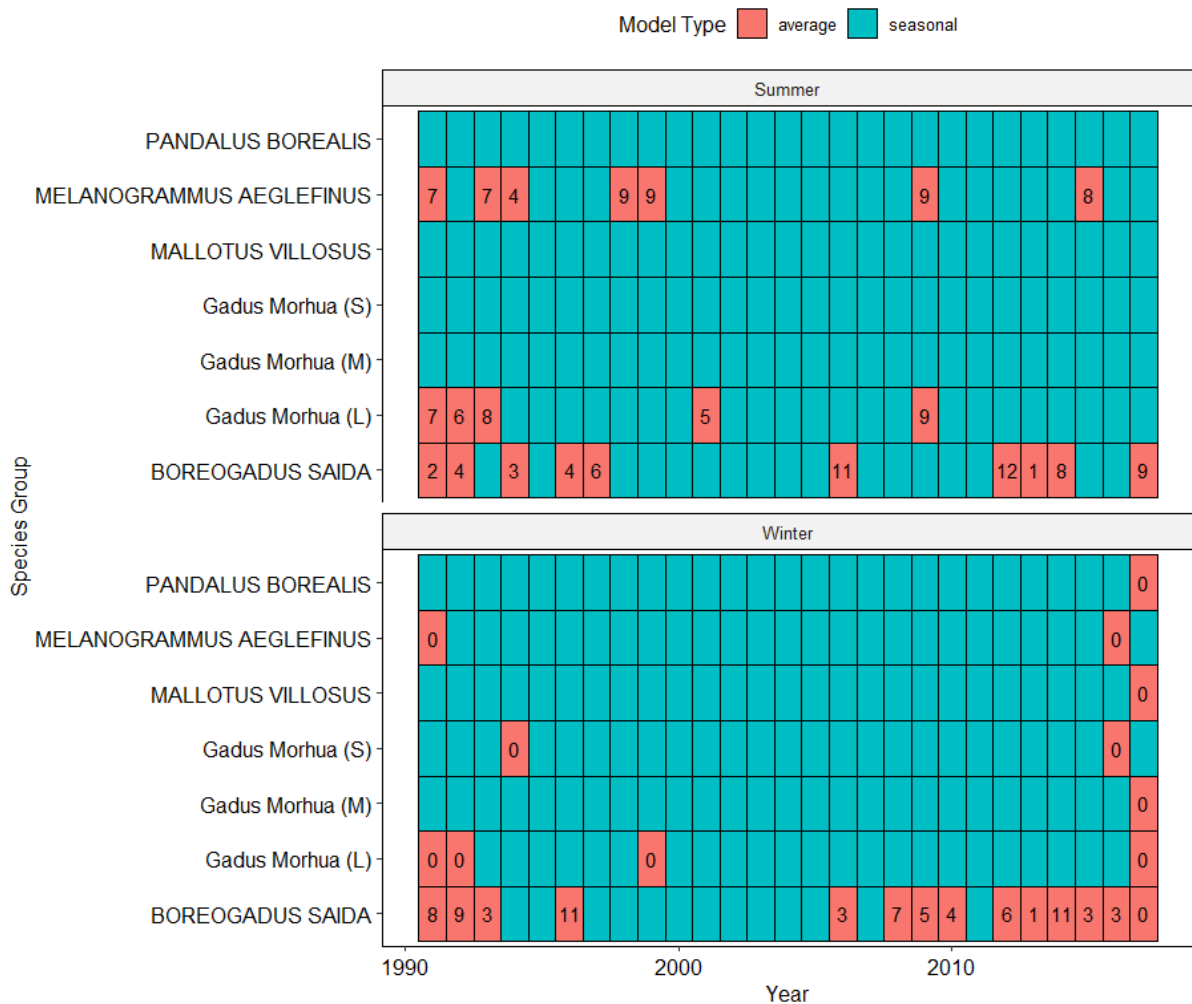


Figure 4.1. Overview of where ‘Average Model Projections’ were used in lieu of temporally specific models. The number of occurrence records available within each period is labeled.

There were 22 summer/species periods and 25 winter/species periods where an average model projection was used to produce maps of distribution due to insufficient occurrence records. Of these,

all summer/species periods had at least one occurrence record while 12 of the 25 winter/species periods had no occurrence records available at all.

Fourteen average models, seven summer and seven winter for each species group, were created using the methodology outlined in Chapter 3 and in Section 4.2.1. Occurrence records were selected from the entirety of the study period (1991-2017) in summer and winter, where there were more than 100 occurrences, these were thinned to 100 using the method outlined in Section 3.2.1.

Environmental layers were produced following the schematic in Table 4.1, but rather than each layer representing one month, they were calculated as the mean of each month across the study period.

Model parameters and evaluation were carried out in the same manner as described in Section 4.2.1.3.

### 4.2.3. Calculation of distribution and overlap area

Distribution and overlap area are calculated from the thresholded Maxent cloglog output maps.

Distribution is calculated as the sum of the area of all suitable cells in each map, calculated using the `raster::area()` function in R. Overlap between a pair of species groups is calculated using the same method, but co-occurrence of suitable cells within a period are calculated as an interim step and then area is calculated as the sum of the area covered by co-occurring suitable cells.

Cells at higher latitudes are smaller than those at lower latitudes and this is taken into account, even though the maps presented in this chapter are shown in a non-projected latitude-longitude grid. The `raster::area()` function calculates each cell as a rectangle, so at very high latitudes it becomes less accurate, though not enough to significantly affect our results.

### 4.3. Results

In this section we present the results from the Maxent modelling of *Gadus morhua* and critical prey groups in the Barents Sea in the summer and winter seasons from 1991-2017. In subsection 4.3.1, we summarise model performance across groups and seasons. In subsection 4.3.2, we present a summary of the spatial predictions generated by Maxent for each group, focussing on temporal/seasonal variability in distribution. In subsection 4.3.3, we examine the spatial overlap between *Gadus morhua* and the modelled prey groups and the seasonal and interannual change in overlap area. Finally, in subsection 4.3.4, we examine the overall pattern in model structure by group and environmental layer to reveal the most important factors driving these distributions.

## 4.3.1. Model Performance

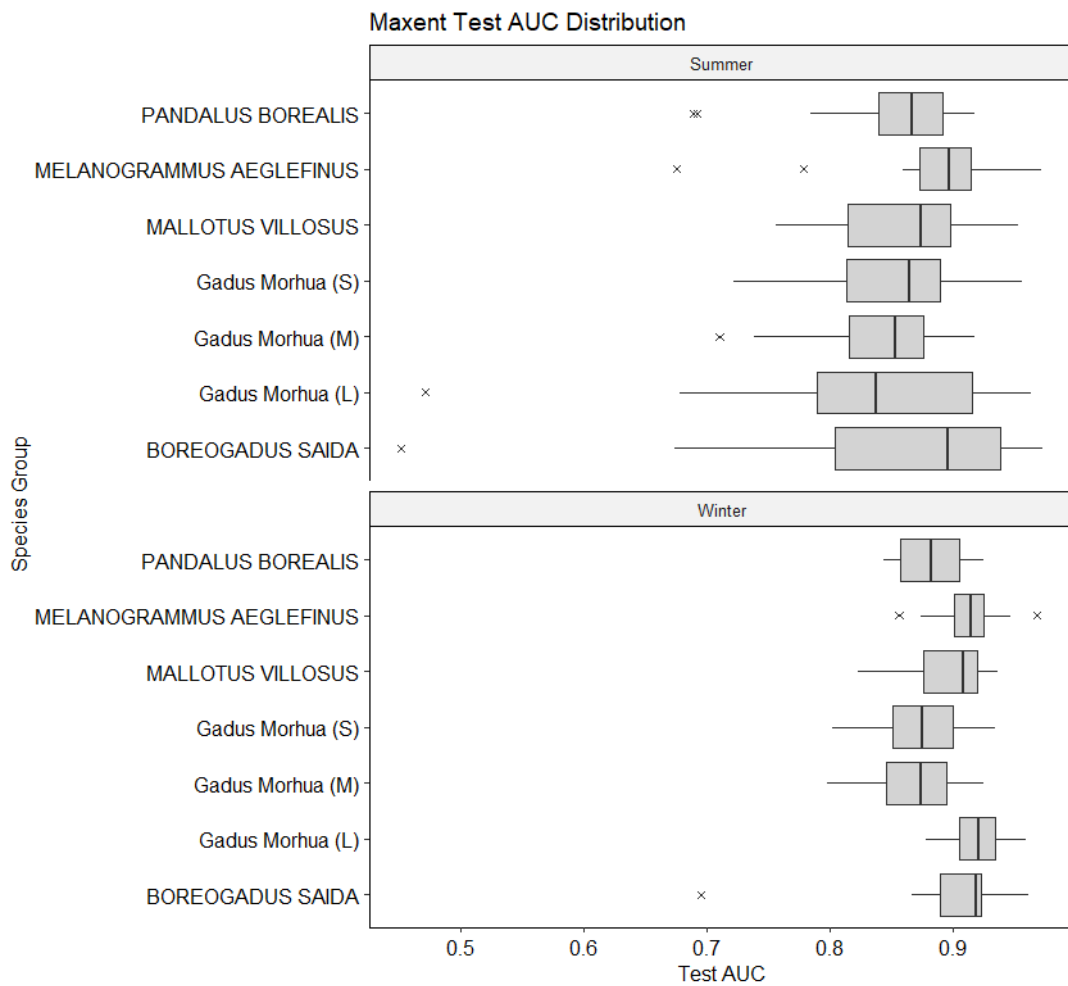


Figure 4.2. Distribution of test AUC's for summer and winter models for all species. Boxes show median, upper quartile and lower quartile of data. Whiskers show the maximum and minimum of the data, while outliers are shown as 'X's and are not included in the median/quartile calculations but are shown independently.

Figure 4.2 shows the distribution of test AUC values among all models for each species group, separated by season. Overall performance for all groups in summer and winter was good, with almost all models achieving a test AUC of over 0.7, and the lowest in-group average AUC being

above 0.8. There is a disparity between summer and winter model performance, with winter models generally performing better than the equivalent summer model. Also, summer models show a significantly higher variability in performance within groups, and several summer models achieved test AUC values lower than 0.7, with two summer models (*Boreogadus saida* and *Gadus morhua* (*L*)) resulting in a test AUC below 0.5.

### 4.3.1. Temporal Variability of Predicted Distributions

#### 4.3.1.1. *Gadus morhua* (S)

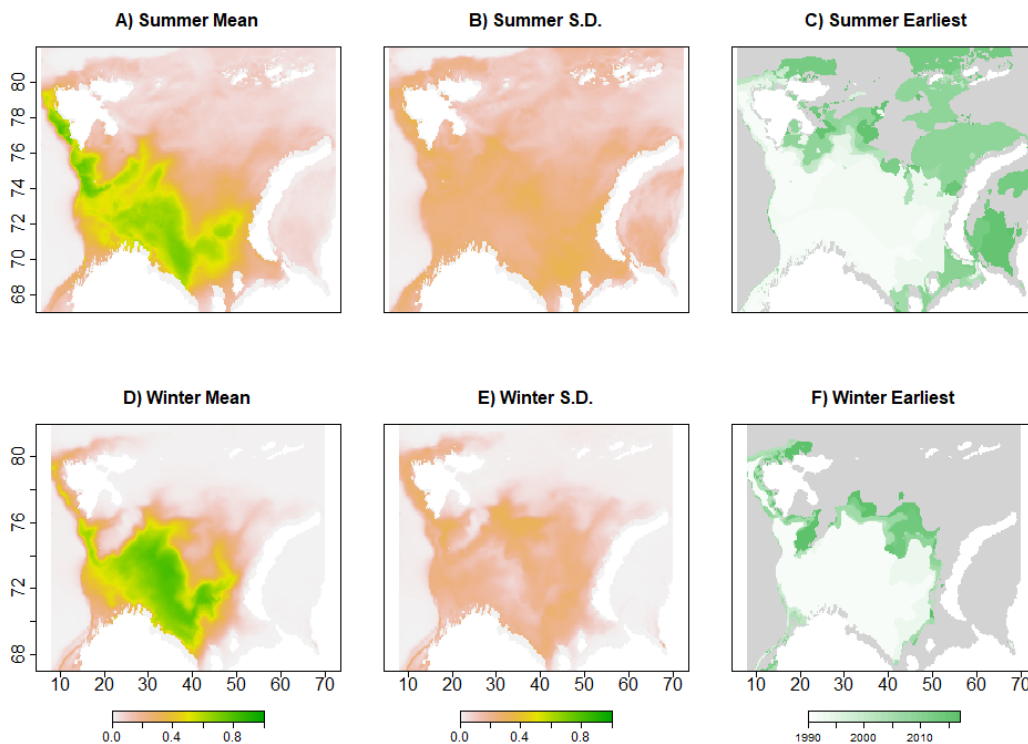


Figure 4.3. Mean cloglog, Standard Deviation cloglog and Earliest Suitable Year maps for *Gadus morhua* (S) in summer and winter.

We observe significant differences in the mean distribution of *Gadus morhua* (S) in summer and winter, shown in Figure 4.3.A) and 4.3.D). The core distribution area during the winter is better defined than during the summer, centered in the south-central region of the Barents Sea with a stark divide in predicted suitability between the core area and the northern regions. The distribution of *Gadus morhua* (S) during the summer is broader, with a smaller core area with lower overall mean suitability, but with some higher predicted suitability across the whole region. We can also see in Figures 4.3.B) and 4.3.E) that the cloglog values are generally more variable in the summer models than the winter, though there is an area of relatively high variability during winter to the east of the southern tip of the Svalbard archipelago.

The temporal variability in overall distribution is captured in Figures 4.3.C) and 4.3.F), which shows the earliest model which found each cell to be suitable. From these figures, we can see a clear pattern of northward and eastward expansion of distribution in the latter years of the study. This expansion is present in the summer and winter models, and is larger during the summer but still significant during the winter.

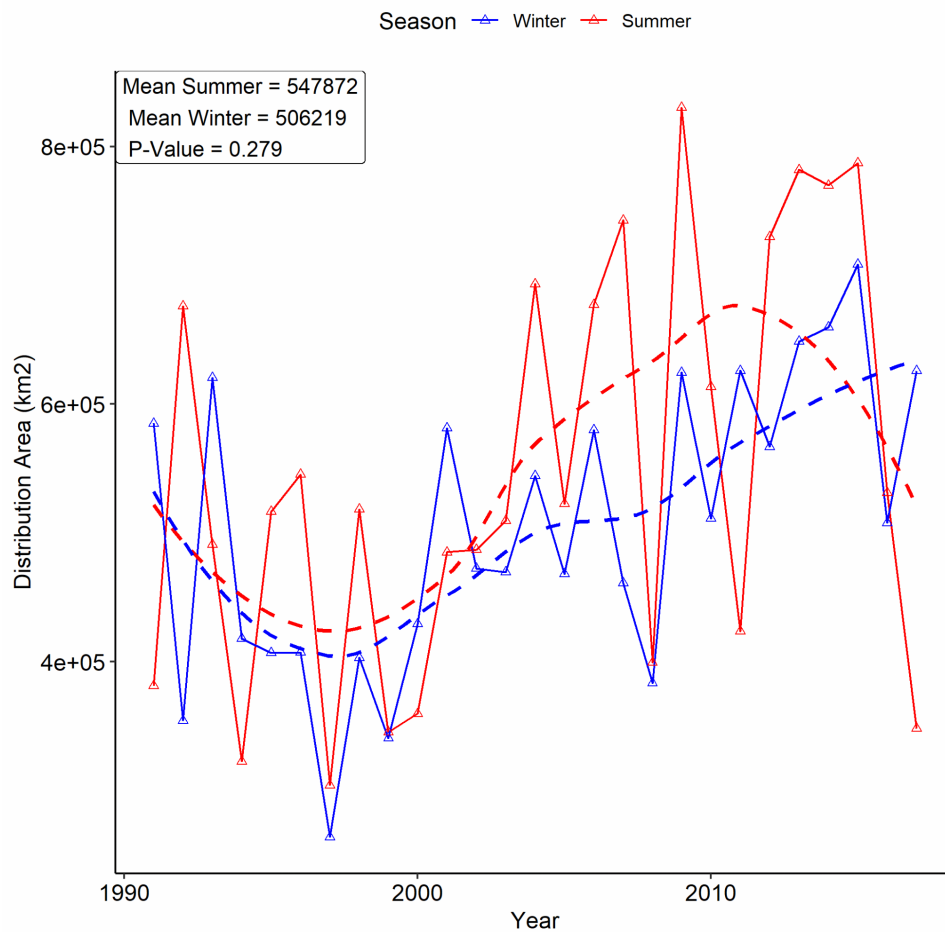


Figure 4.4. Distribution area (km<sup>2</sup>) for *Gadus morhua* (S) in summer and winter.

When we examine the total distribution area of *Gadus morhua* (S) in the summer and winter, shown in Figure 4.4, we see a trend of increasing area in both seasons. There is no significant difference between the distribution area in summer or winter overall, but there is strong interannual variability in both. The moving average (loess) function shows a dip in area during the late 1990's followed by a pattern of growth from around 1998 to the 2010s. A sharp decrease in predicted distribution area

during the summer of 2016 and 2017 may show the beginning of a reverse in this trend, but it may also be in line with earlier variability.

#### 4.3.1.2. *Gadus morhua* (M)

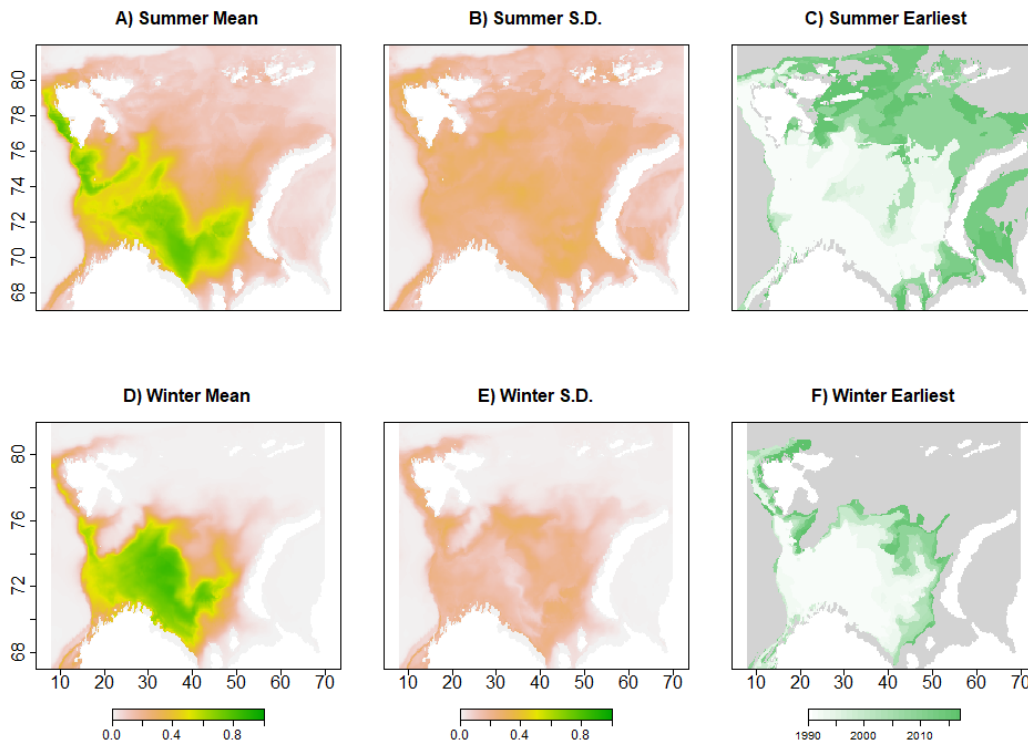


Figure 4.5. Mean cloglog, Standard Deviation cloglog and Earliest Suitable Year maps for *Gadus morhua* (M) in summer and winter.

We observe significant differences between the mean summer and winter distributions of *Gadus morhua* (M). The differences observed in Figures 4.5.A) and 4.5.D) are broadly the same as those in Figures 4.3.A) and 4.3.D), as the model predictions for *Gadus morhua* (M) and *Gadus morhua* (S) appear to be similar.

However, when we examine the earliest suitable year maps in Figures 4.5.C) and 4.5.F) we see a slightly different pattern of distribution expansion in the latter years of the study. Overall, there is an

expansion of distribution to the north and east in both summer and winter, and it is greater during the summer. However, when compared to *Gadus morhua* (S), the expansion is more pronounced in *Gadus morhua* (M). During the summer, the expansion includes almost the entirety of the northern Barents Sea, and during the winter the expansion is comparatively broader than we observed for *Gadus morhua* (S), particularly along the north-east and eastern fronts.

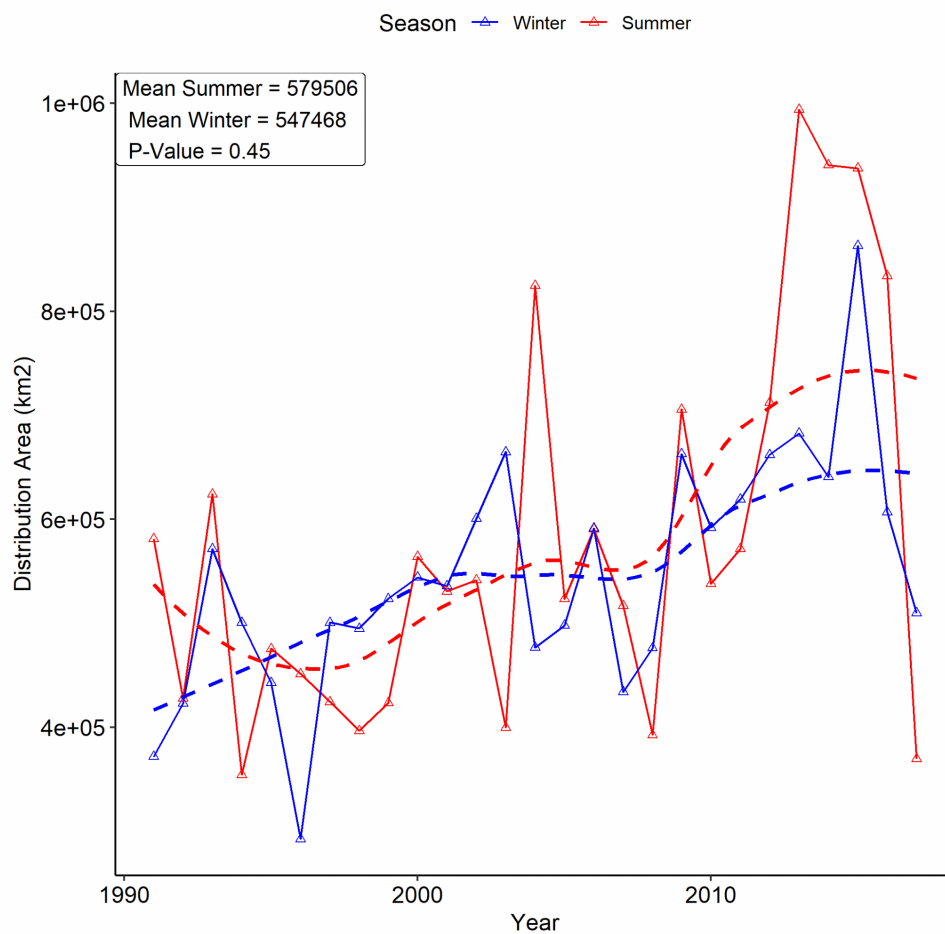


Figure 4.6. Distribution area (km<sup>2</sup>) for *Gadus morhua* (M) in summer and winter.

The total distribution area in summer and winter for *Gadus morhua* (M) shown in Figure 4.6 follows a similar pattern to that which we observed in Figure 4.4 for *Gadus morhua* (S). There is no statistically significant difference in the summer and winter distribution area overall, but both seasons show a trend of increasing distribution area over time. Note that in absolute terms, the

distribution area of *Gadus morhua* (*M*) tends to be greater than *Gadus morhua* (*S*), by about 3000-4000 km<sup>2</sup> on average across seasons.

#### 4.3.1.3. *Gadus morhua* (*L*)

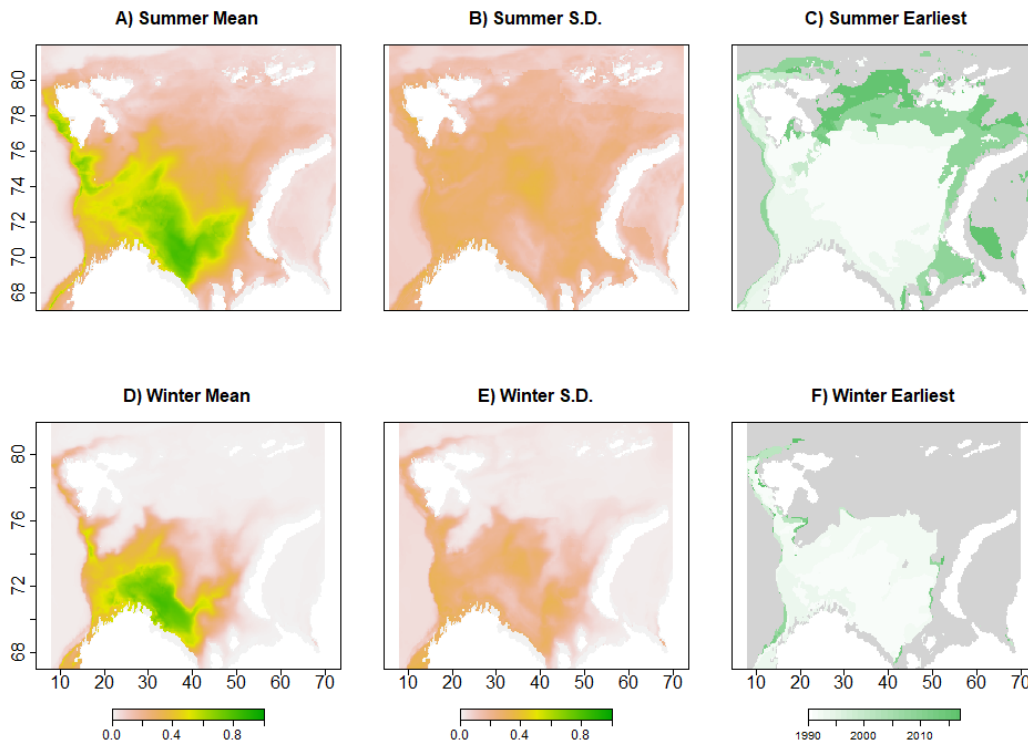


Figure 4.7. Mean cloglog, Standard Deviation cloglog and Earliest Suitable Year maps for *Gadus morhua* (*L*) in summer and winter.

There is a significant difference between the mean cloglog maps for summer and winter in *Gadus morhua* (*L*) as shown in Figures 4.7.A) and 4.7.D). Like in the previous cod groups, the winter distribution is aggregated in a smaller area than the summer distribution, but here the core area during winter is smaller than observed in the other groups, and located in the southern Barents Sea. When compared to the other groups, *Gadus morhua* (*L*) appears to have higher variability over time within its core area in its winter distribution, as shown in Figure 4.7.E).

The maps of earliest suitable year in Figures 4.7.C) and 4.7.F) diverge from the pattern we observed for *Gadus morhua* (*S*) and *Gadus morhua* (*M*). Like those groups, we do see an expansion north in the latter years of the study during summer, but there is no significant expansion during the winter.

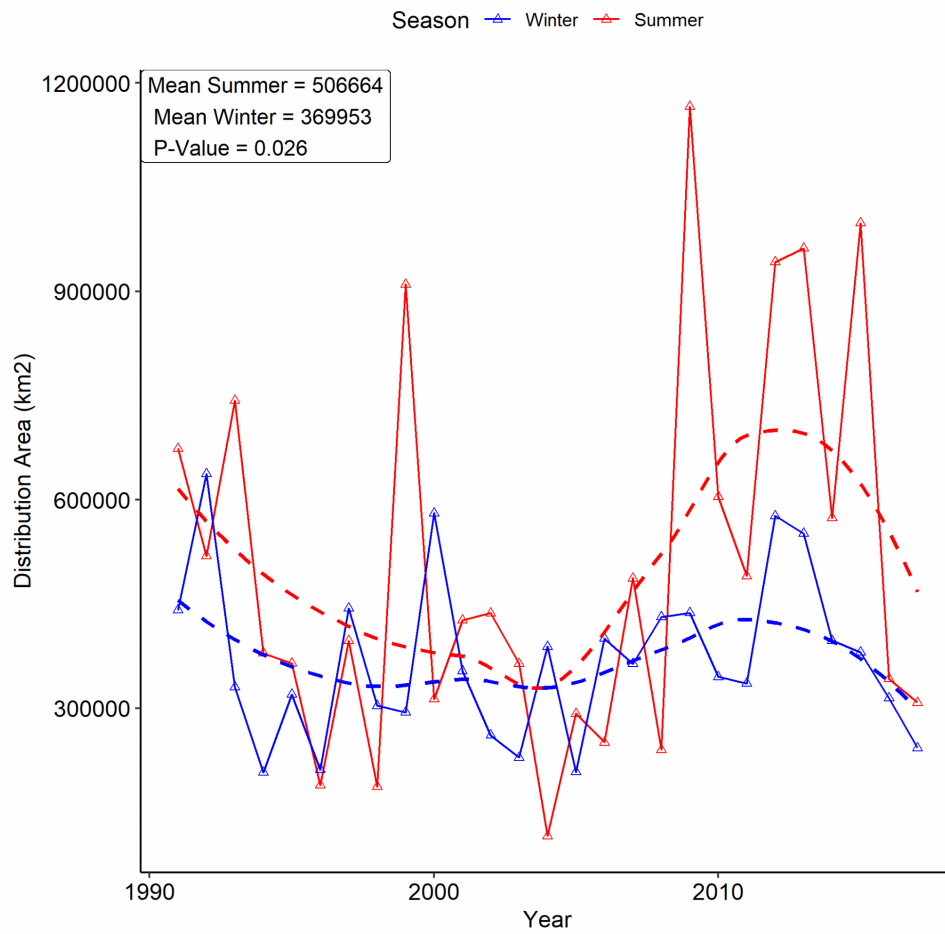


Figure 4.8. Distribution area (km<sup>2</sup>) for *Gadus morhua* (L) in summer and winter.

The total distribution area of *Gadus morhua* (L) in summer and winter is shown in Figure 4.8. There is a statistically significant difference between the summer and winter distribution area for this group ( $P = 0.026$ , significant at the  $P < 0.05$  threshold), with summer distribution area being generally greater than winter distribution area. The trends in the distribution area differ from what we observed in the other *Gadus morhua* groups. Rather than a combined growth, we instead see a significant rise in summer distribution area in the latter years but only a small growth in winter distribution area. Both seasons have a shared minimum distribution area in the early 2000's.

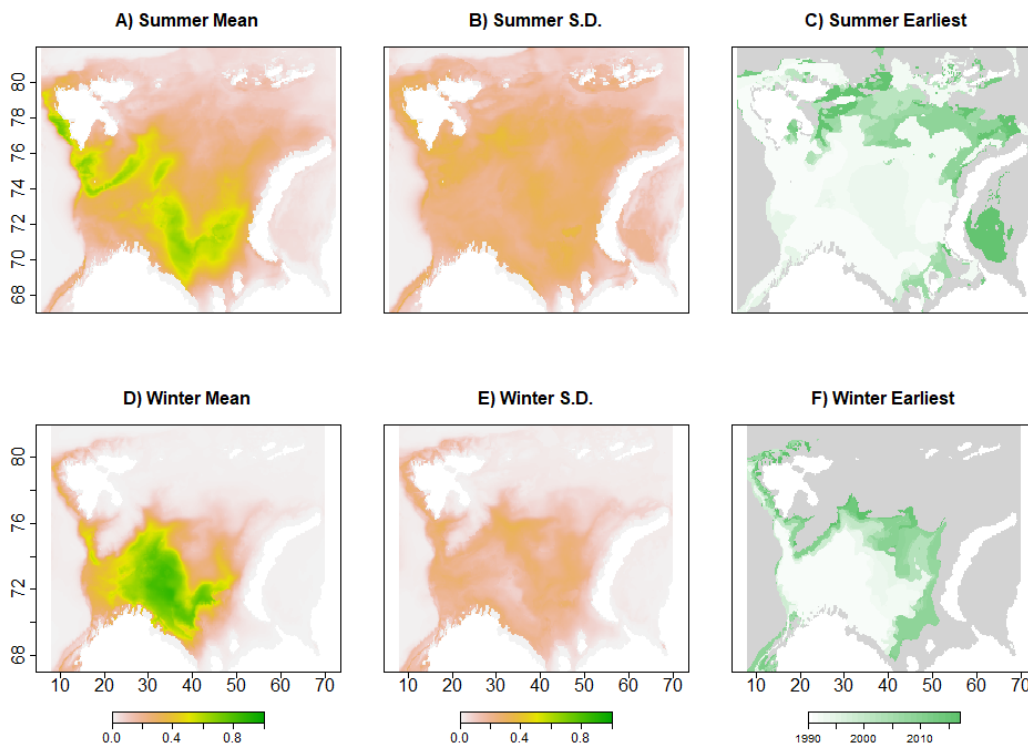
4.3.1.4. *Mallotus villosus*

Figure 4.9. Mean cloglog, Standard Deviation cloglog and Earliest Suitable Year maps for *Mallotus villosus* in summer and winter.

The mean cloglog output maps for *Mallotus villosus* in Figures 4.9.A) and 4.9.D) show significant differences between seasons. The summer mean distribution shows a core area of segments from the south-east Barents Sea to the centre-west near Svalbard and along the west coast of the archipelago. Conversely, the winter mean distribution shows a core area in the south-central region of the Barents Sea as a more or less continuous grouping. In both seasons, we can see similarities to the patterns observed for the *Gadus morhua* group models. The patterns of cloglog standard deviation shown in Figures 4.9.B) and 4.9.E) show a broad space of higher variability during the summer than winter.

The earliest suitable year maps in Figures 4.9.C) and 4.9.F) show an expansion of distribution into the north and east in both summer and winter. This expansion follows a similar pattern to what we observed in *Gadus morhua* (*S*, *M*). In particular, the expansion north during the winter in the latter years of the study period is extensive.

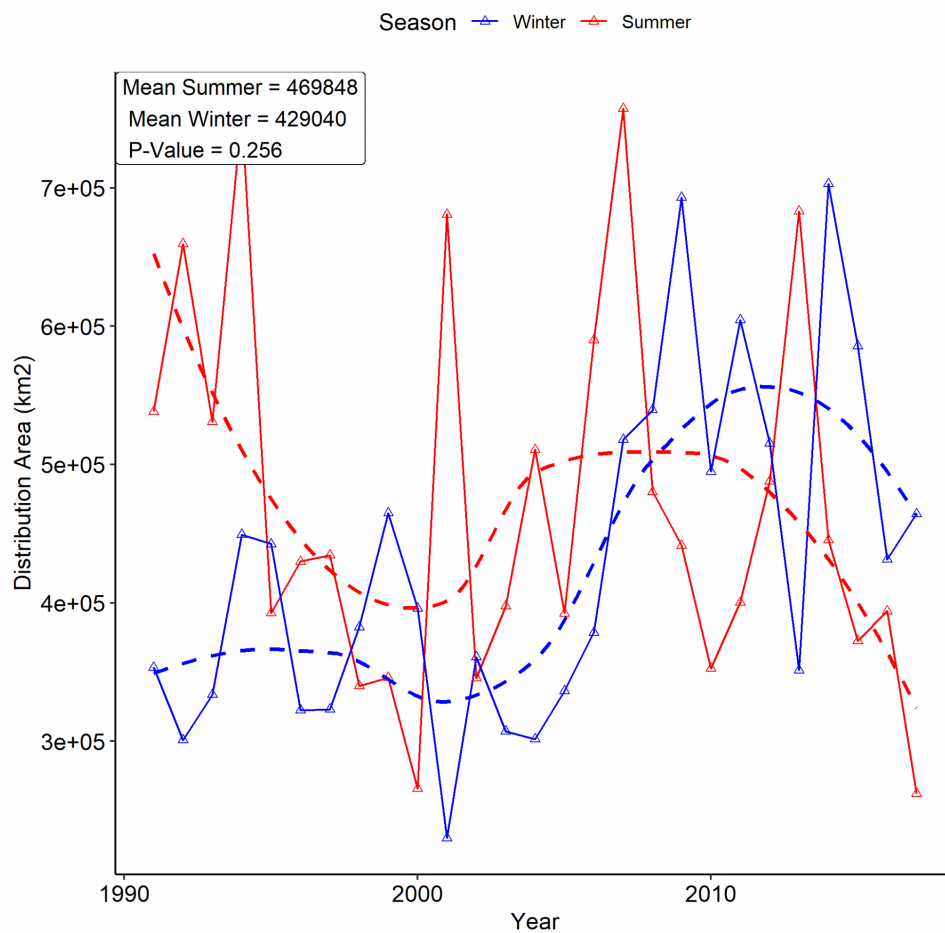


Figure 4.10. Distribution area (km<sup>2</sup>) for *Mallotus villosus* in summer and winter.

The total distribution area for *Mallotus villosus* in the summer and winter is shown in Figure 4.10. There is no statistically significant difference between summer and winter distribution area. We see significant interannual variability in both seasons, and quite different overall trends. During the summer, the distribution area is high at the beginning of the study period, then follows a pattern where there is a single peak followed by several years of relatively low distribution area. The trend during winter is quite different, beginning at a relatively low distribution area in the 1990's, it then rises precipitously from the mid 2000's to a new regime of relatively high distribution area.

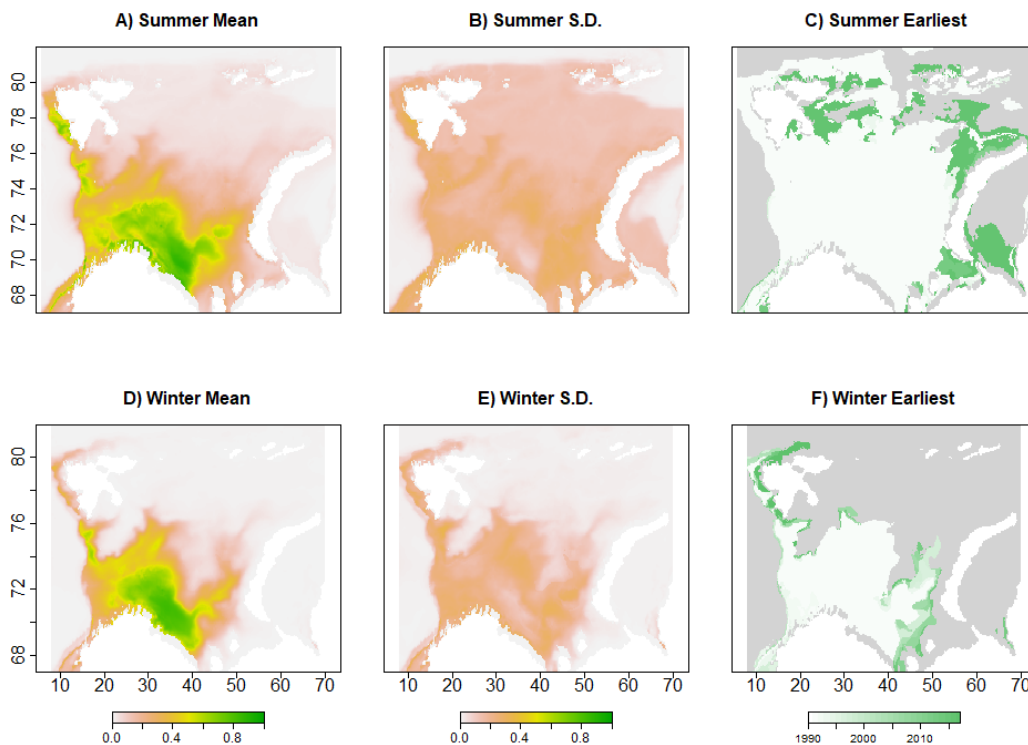
4.3.1.5. *Melanogrammus aeglefinus*

Figure 4.11. Mean cloglog, Standard Deviation cloglog and Earliest Suitable Year maps for *Melanogrammus aeglefinus* in summer and winter.

The mean cloglog maps for *Melanogrammus aeglefinus* in Figures 4.11.A) and 4.11.D) show a broad similarity between summer and winter core distribution areas, compared to earlier results for other species groups. Both seasons have a core area in the south-central Barents Sea, during the summer this area is slightly broader and less constrained. We can see from Figures 4.11.B) and 4.11.E) that the standard deviation maps for *Melanogrammus aeglefinus* show more variability during the summer than winter.

The earliest suitable year maps for *Melanogrammus aeglefinus* shown in Figure 4.11.C) and 4.11.F) follow a familiar pattern, with some expansion further north and eastward during both seasons. However, we can also see that the northern Barents Sea was found to be suitable for *Melanogrammus aeglefinus* during the summer in very early models. Expansion during the winter is

predominantly along the west coast of Novaya Zemlya and around the west coast of the Svalbard archipelago, with little or no expansion into the central north Barents Sea.

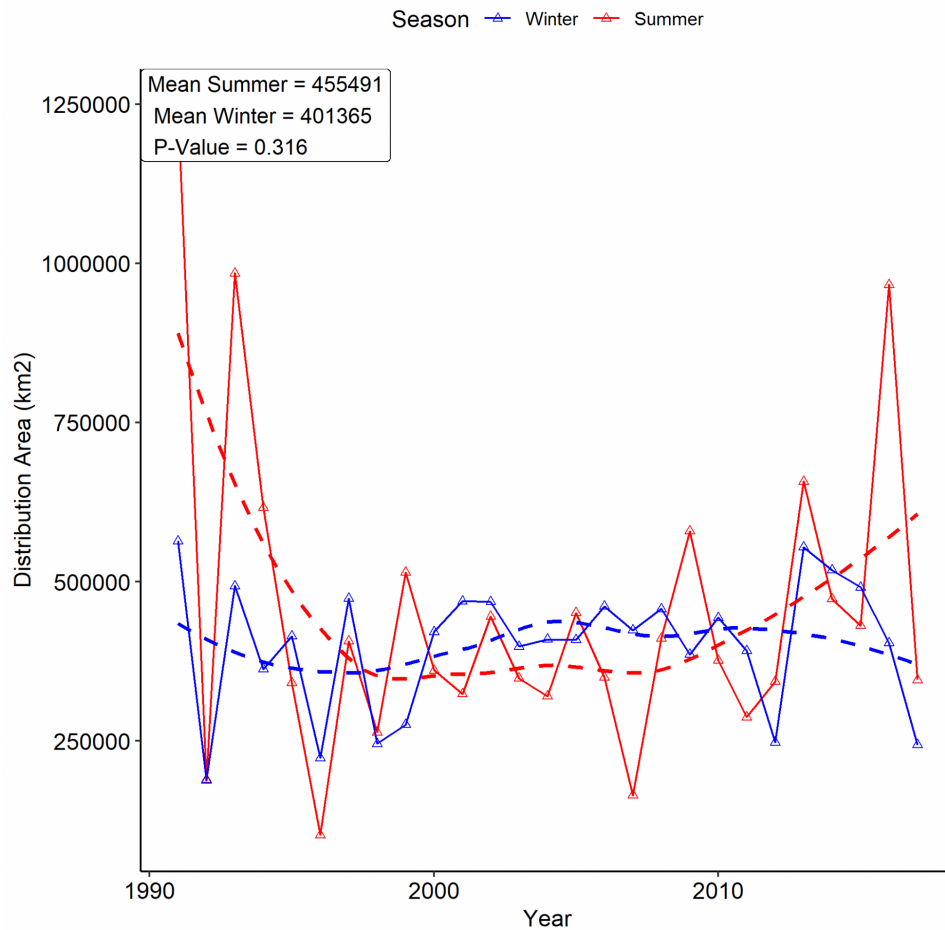


Figure 4.12. Distribution area (km<sup>2</sup>) for *Melanogrammus aeglefinus* in summer and winter.

The total distribution area of *Melanogrammus aeglefinus* in the summer and winter is shown in Figure 4.12. There is no statistically significant difference between the distribution area in summer and winter. The overall trends in summer and winter distribution areas follow different patterns. At the beginning of the study period, summer distribution area was relatively high, it then fell beginning in the late 1990's and stayed low until the late 2000's where we observe a trend of increasing distribution area into the end of the study. Conversely, the winter distribution area remains fairly stable across the study period, though there is significant interannual variability it is generally moving around the mean.

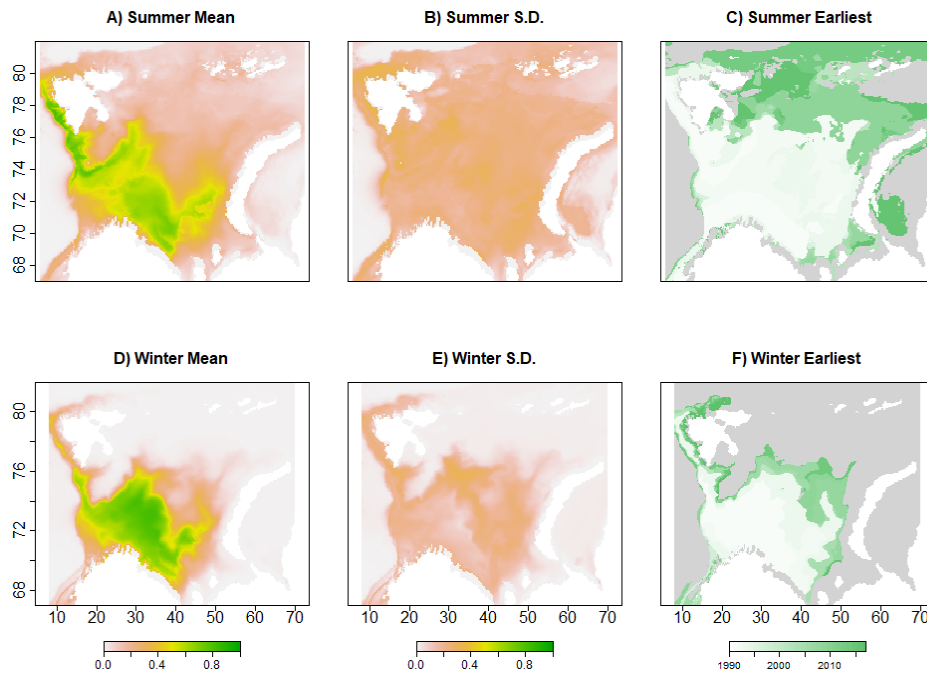
4.3.1.6. *Pandalus borealis*

Figure 4.13. Mean cloglog, Standard Deviation cloglog and Earliest Suitable Year maps for *Pandalus borealis* in summer and winter.

The mean cloglog output maps for *Pandalus borealis* in Figures 4.13.A) and 4.13.D) show an agreement in the broad shape of the core distribution area across seasons, but differ within the core area. The winter distribution is better defined and follows a contiguous area in the south and south-west Barents Sea, while the summer core area is roughly the same shape but with overall lower cloglog values and disconnection between subareas and an extension along the west coast of the Svalbard archipelago. When we examine the maps of standard deviation in cloglog output shown in Figures 4.13.B) and 4.13.E), we see the recurring pattern of greater variability during the summer and variability centred along the northern edge of the core distribution area during the winter.

The earliest suitable year maps shown in Figure 4.13.C) and 4.13.F) follow a pattern that we have observed in many of the modelled groups, with a northward and eastward expansion in the latter years of the study period. This expansion is extensive in both summer and winter.

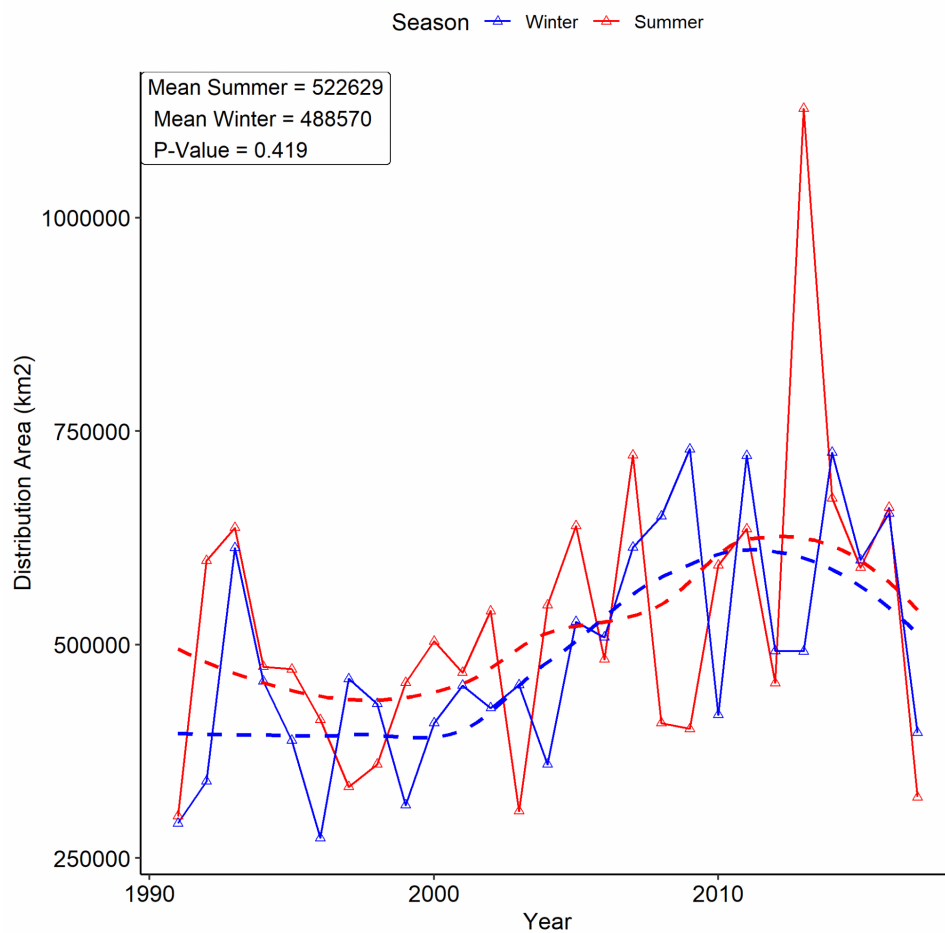


Figure 4.14. Distribution area (km<sup>2</sup>) for *Pandalus borealis* in summer and winter.

The total distribution area of *Pandalus borealis* in summer and winter is shown in Figure 4.14. There is no statistically significant difference between the distribution area in the summer and winter. Both seasons follow a similar overall trend, beginning at a period of relatively low distribution area and increasing from the early 2000s to a new regime of relatively high distribution area by the end of the 2000s, both beginning to decrease again in the late 2010's. There is significant interannual variation in both seasons, but particularly during summer. In particular, the summer distribution area in 2013 is exceptionally high compared to the rest of the period at over one million km<sup>2</sup>.

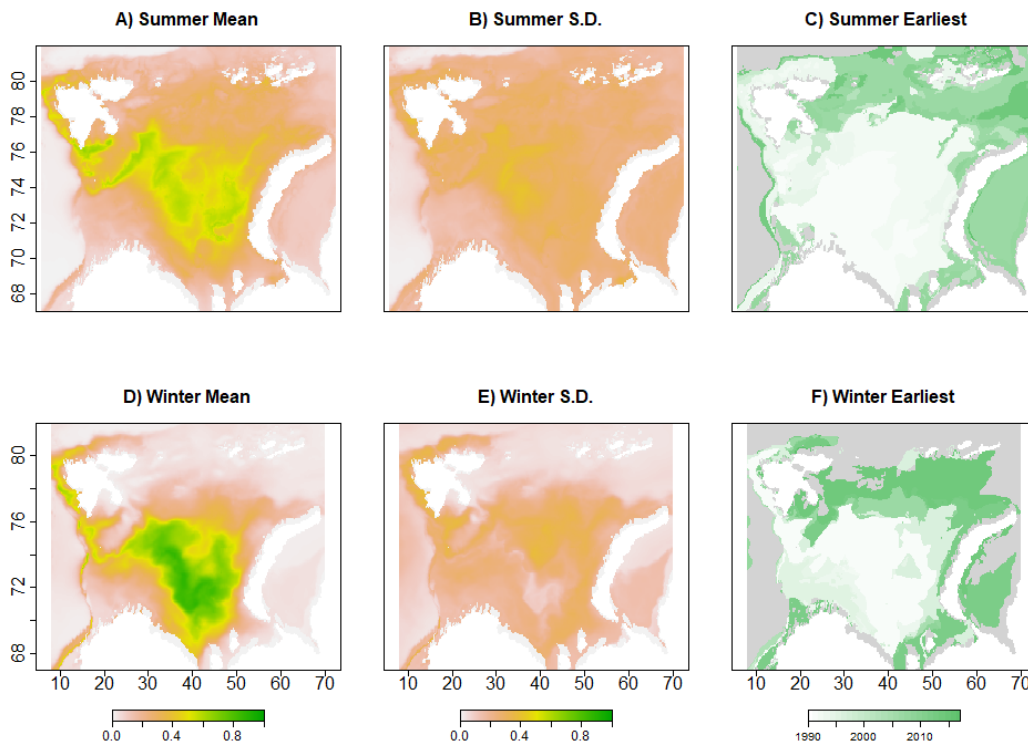
4.3.1.7. *Boreogadus saida*

Figure 4.15. Mean cloglog, Standard Deviation cloglog and Earliest Suitable Year maps for *Boreogadus saida* in summer and winter.

The mean cloglog maps for *Boreogadus saida* in summer and winter in Figures 4.15.A) and 4.15.D) show a significant difference in the core distribution area of the species across seasons. Both seasons show a core distribution area in the central Barents Sea, but the summer distribution is much less constrained than the winter. *Boreogadus saida* is an arctic species, and its distribution is further into the north-central Barents Sea than the other groups modelled. We also see that its winter distribution is broader than we have observed in the other groups. The standard deviation in cloglog maps shown in Figures 4.15.B) and 4.15.E) show significant variability in the central Barents Sea in both summer and winter.

The earliest suitable year maps in Figures 4.15.C) and 4.15.F) show the same pattern we observed in the majority of modelled groups, an expansion into the northern Barents Sea in both seasons in the latter years of the study period. The expansion in both seasons is extensive, reaching latitudes over

80°N during the summer. We also see an expansion into the south-east and south-west during the winter in the later years of the study.

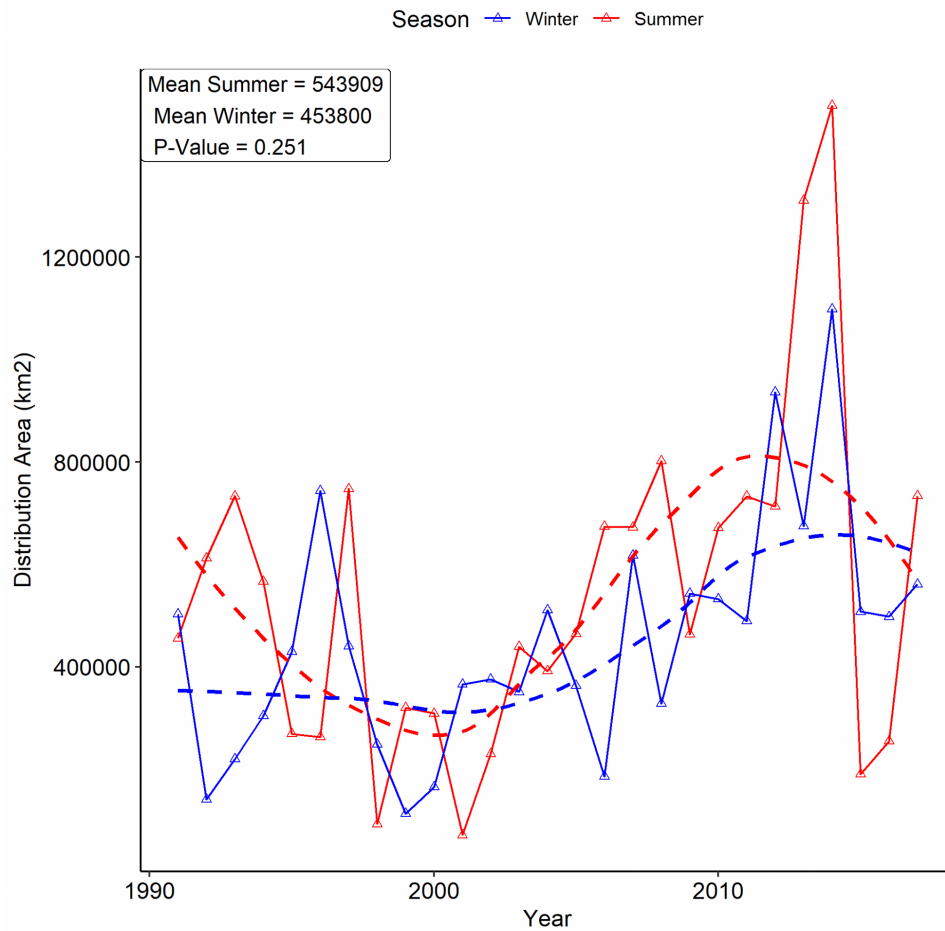


Figure 4.16. Distribution area (km<sup>2</sup>) for *Boreogadus saida* in summer and winter.

The total distribution area for *Boreogadus saida* in summer and winter is shown in Figure 4.16. There is no statistically significant difference in distribution area between seasons. Both seasons follow similar overall trends, beginning with a period of relatively low distribution area until the mid 2000's before rising to a new regime of high distribution area in the mid 2000s to mid 2010s, then falling before the end of the study period. There is high interannual variability, particularly in the summer, with a peak in 2014 of over 1.3 million km<sup>2</sup>, followed by a sheer drop to an area below three hundred thousand km<sup>2</sup> the following year.

### 4.3.2. Spatial overlap between predator-prey groups

In this section we present several time series of overlap areas between predator-prey species pairs. There are four sub-sections, Subsections 4.3.2.1, 4.3.2.2 and 4.3.3.3. present the overlap area for each season/year between *Gadus morhua S*, *Gadus morhua M* and *Gadus morhua L* and each of the four prey groups. Subsection 4.3.2.4 presents the time series of overlap area between the three cod groups.

#### 4.3.2.1 *Gadus morhua* (S) and prey species

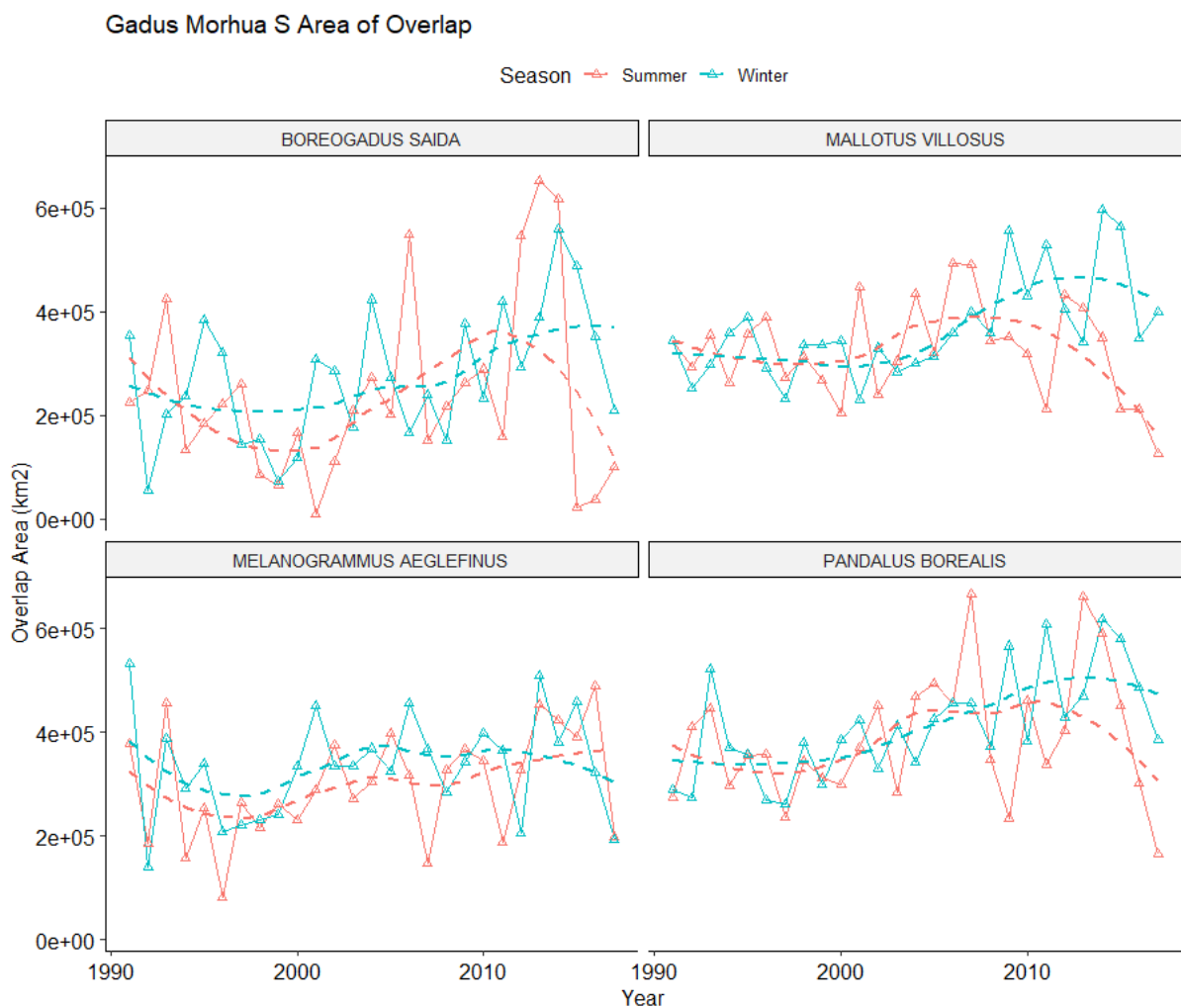


Figure 4.17. Area of Overlap (km<sup>2</sup>) between *Gadus morhua* (S) and prey groups in summer and winter

A time series of spatial overlap between *Gadus morhua* (*S*) and each of *Mallotus villosus*, *Melanogrammus aeglefinus*, *Boreogadus saida* and *Pandalus borealis* are presented in Figure 4.17, with summer and winter results displayed individually.

Overlap area between *Gadus morhua* (*S*) and *Boreogadus saida* is highly inter-annually variable, and there is no statistically significant difference between summer and winter overlap area. There is a periodic fall and rise in summer overlap area over a timescale of several years, a pattern which may also be present during the winter but to a lesser extent. Overlap with *Mallotus villosus* shows a significant divergence between summer and winter in the latter years of the study, with summer overlap area trending down while winter overlap increases compared to earlier years. Overlap with *Melanogrammus aeglefinus* follows a pattern of high interannual variability but shows no significant trends of long term change across the study period. Finally, overlap with *Pandalus borealis* shows some divergence between summer and winter in the latter years of the study period, with summer interannual variability increasing significantly after the year 2000. Overall, the absolute size of the overlap area between *Gadus morhua* (*S*) and each of the prey groups is similar.

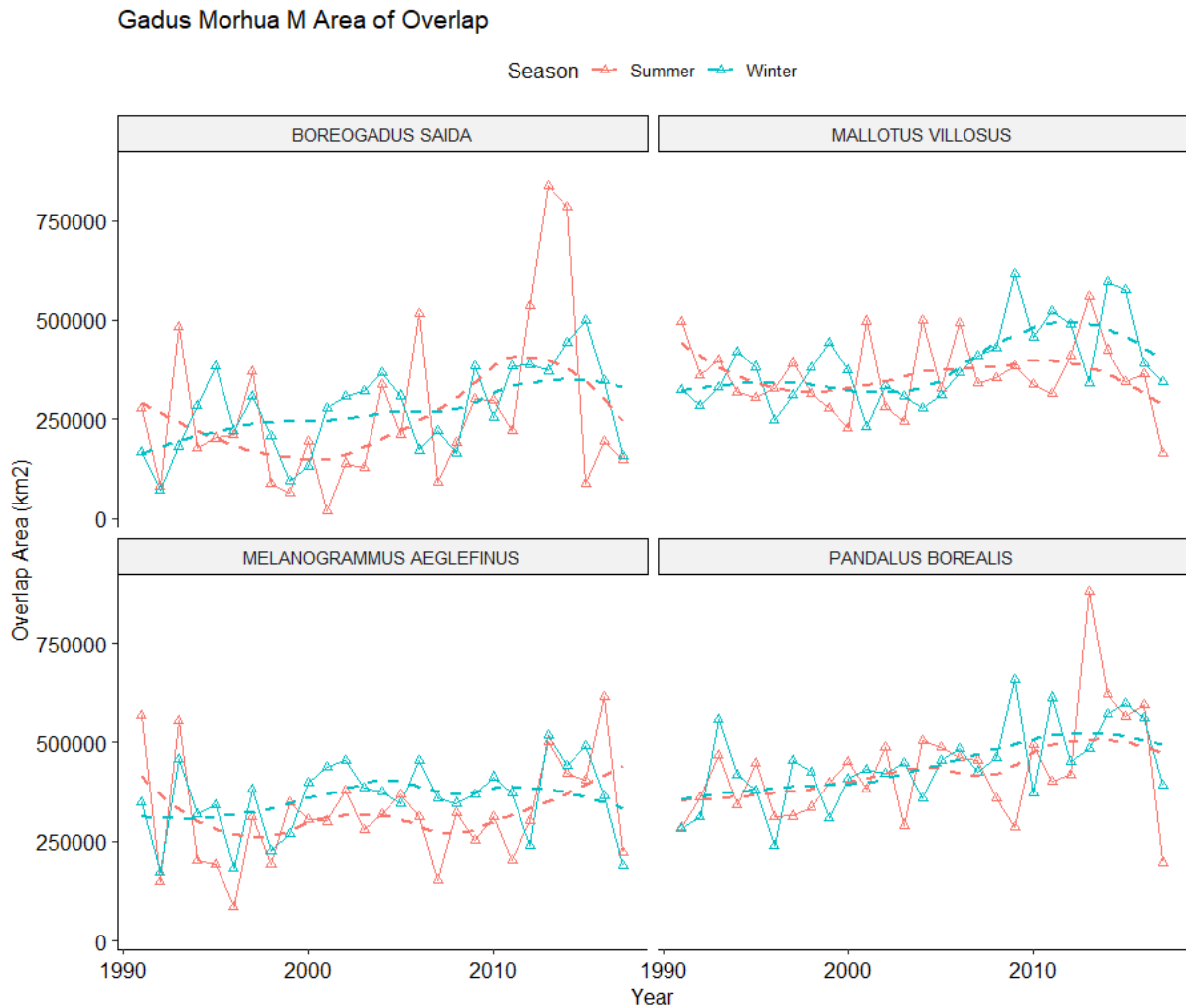
4.3.2.2 *Gadus morhua* 20 - 100 cm

Figure 4.18. Area of Overlap ( $\text{km}^2$ ) between *Gadus morhua* (*M*) and prey groups in summer and winter.

A time series of spatial overlap between *Gadus morhua* (*M*) and each of *Mallotus villosus*, *Melanogrammus aeglefinus*, *Boreogadus saida* and *Pandalus borealis* are presented in Figure 4.18, with summer and winter results displayed individually. Overlap area between *Gadus morhua* (*M*) and each of the prey species follows the same major patterns as we observe for *Gadus morhua* (*S*) in Figure 4.17. Our results in Section 4.3.1.1 and 4.3.1.2 show that there are broad similarities between the distribution of these two groups on an annual scale, so this is an expected outcome. However, the patterns in overlap are not exactly the same. While overlap between *Gadus morhua* (*M*) and both *Boreogadus saida* and *Melanogrammus aeglefinus* follows similar trends as observed for *Gadus morhua* (*S*) and those groups, the absolute overlap area in this case is slightly higher, in the region of

about 10,000 km<sup>2</sup> on average. Conversely, the overlap with *Mallotus Villosus* differs from what we observed in Figure 4.17 in the latter years of the study, in this case we do not find a significant difference between summer and winter overlap areas as there is a much smaller trend of decrease in summer overlap area. Finally, overlap between *Gadus morhua* (*M*) and *Pandalus borealis* follows a consistent trend of increase over the study period, with lower summer interannual variability than we observed in Figure 4.17.

#### 4.3.2.3 *Gadus morhua* > 100 cm

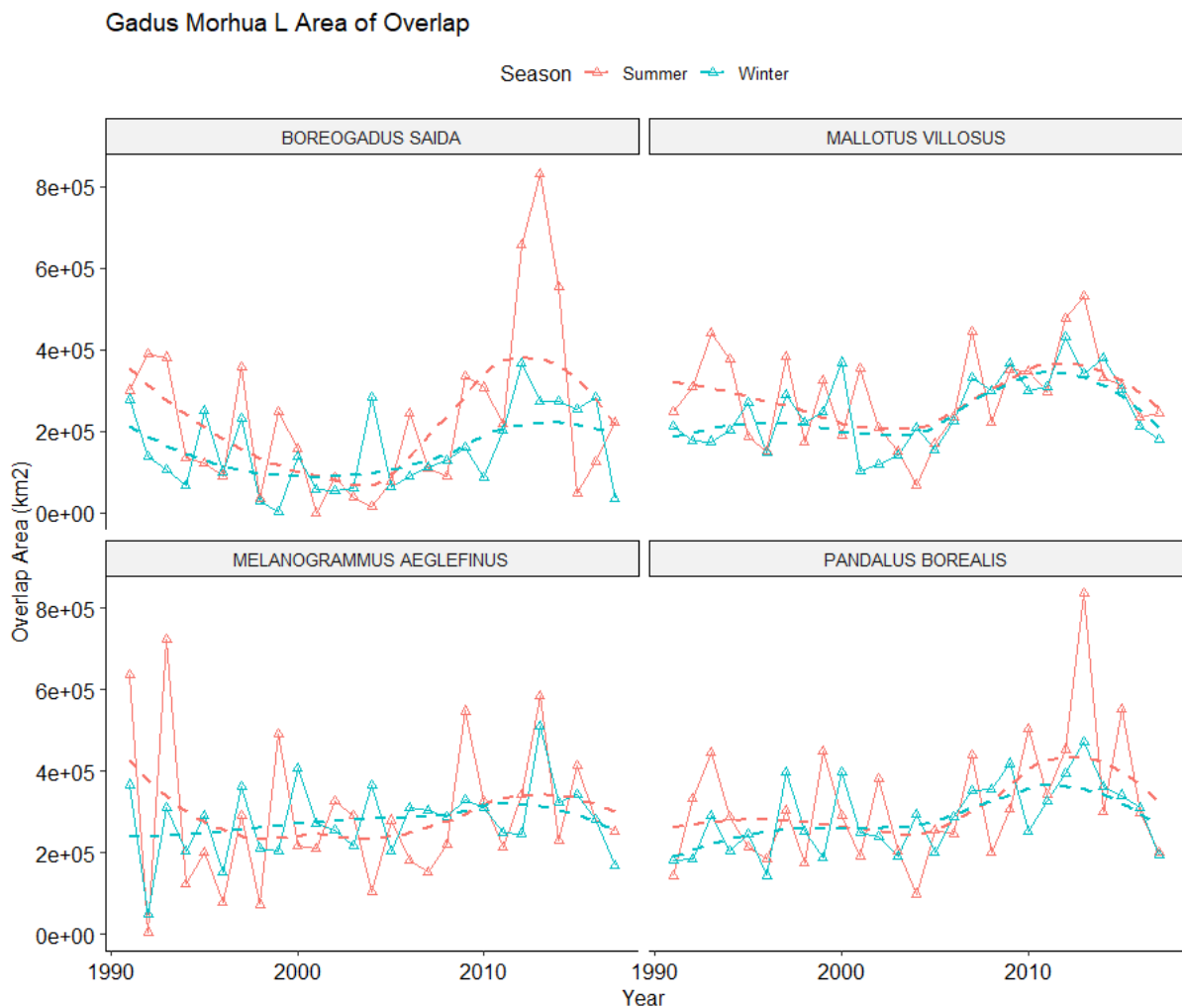


Figure 4.19. Area of Overlap (km<sup>2</sup>) between *Gadus morhua* (*L*) and prey groups in summer and winter.

A time series of spatial overlap between *Gadus morhua* (L) and each of *Mallotus villosus*, *Melanogrammus aeglefinus*, *Boreogadus saida* and *Pandalus borealis* are presented in Figure 4.19, with summer and winter results displayed individually.

Overlap between *Gadus morhua* (L) and each of the prey groups follows a pattern broadly similar to what we have observed in Figures 4.17 and 4.18 for the smaller cod groups. In particular, the overlap between *Gadus morhua* (L) and *Melanogrammus aeglefinus* shows no significant change over the study period in either season. Overlap with the other three groups follow a similar period pattern to one another. Each show a minimum in overlap area in the early-mid 2000's before increasing again to levels at or above those measured during the early years of the study period. There is no significant difference in overall overlap area between seasons in any pairing, however we observe a significant divergence between summer and winter overlap area between *Gadus morhua* (L) and *Boreogadus saida* in the later years of the study period due to a several year long spike in summer overlap area between 2011 and 2013.

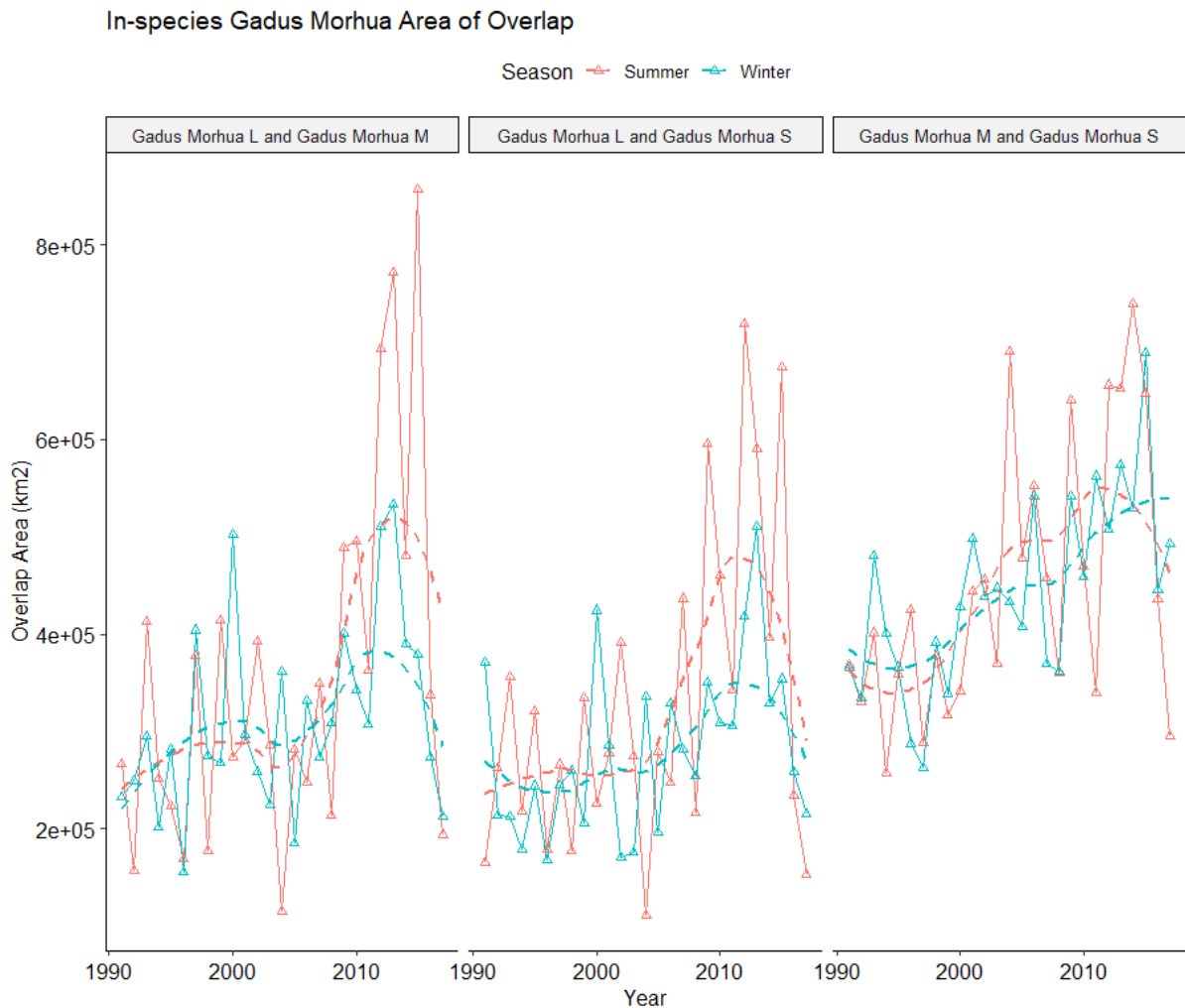
4.3.2.4. *Gadus morhua* size group overlap

Figure 4.20. Area of Overlap ( $\text{km}^2$ ) between *Gadus morhua* (S), *Gadus morhua* (M) and *Gadus morhua* (L) in summer and winter.

A time series of overlap areas between *Gadus morhua* (L, M), *Gadus morhua* (L, S) and *Gadus morhua* (M, S) is shown in Figure 4.20. From this figure we can see that the absolute area of overlap between *Gadus morhua* (M, S) is higher than either share with *Gadus morhua* (L). This is to be expected based on our previous observations about the similarity between the two. However, we also observe a significant trend of a) increase in overlap area between *Gadus morhua* (M,S) over time and b) Increased interannual variability in the summer in the latter years of the study. This increase in interannual variability in overlap area during the summer is also present between *Gadus morhua* (L) and the other size groups. Also as a predictable consequence of our previous observations, the

overlap between *Gadus morhua* (*L*) and the other two size groups follow very similar trends, with no significant difference between seasons until the latter years of the study where there is a sudden increase in summer overlap area.

### 4.3.3. Model Structures

#### 4.3.3.1. Seasonal Models

In this section we present a summary of the model structures for each species group in summer and winter individually. We examine a matrix of a summary of permutation importance for each environmental layer within each species group. We report the mean permutation importance (P.I.) as well as the standard deviation and the number of models each variable was included in within each species group and season. Permutation importance measures the sensitivity of model performance when each variable is randomly permuted while all others remain the same, this tells us which variables are providing the most useful information within all included terms.

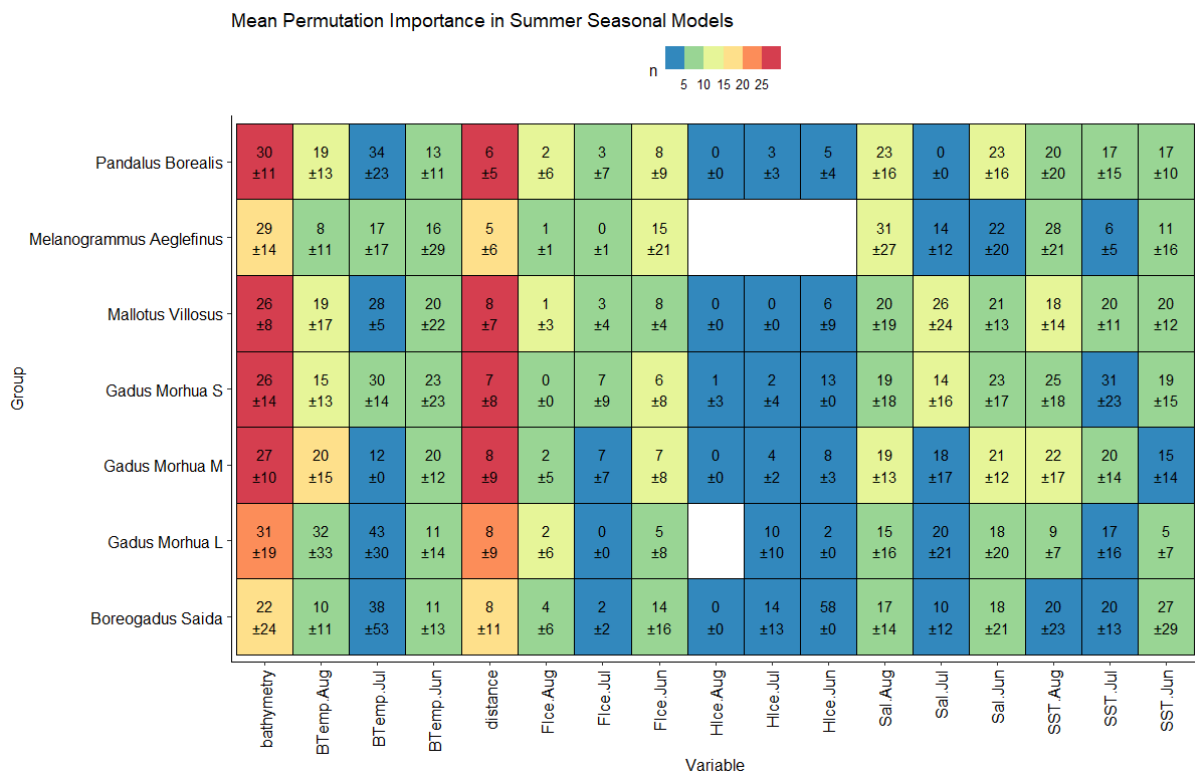


Figure 4.21. Mean, standard deviation in P.I. and number of models included in for each variable separated by species group, summer.

The summary matrix of variable P.I. across species groups during the summer is presented in Figure 4.21. Each tile represents a summary of the P.I. of each variable within all summer models of that species group. The mean P.I. and standard deviation are labelled within each tile, and the fill colour of each tile shows how many times that variable was used within all models in the species group. Blank tiles represent variables which were never included in any model for the species group of the corresponding row. Some variables have a mean and standard deviation in P.I. of zero, but were still included in at least one model.

The most eye-catching feature of this visualization is the fill colour, or the number of times each variable appeared in a model group. Of these most frequent variables, *bathymetry* and *distance* are consistently the most frequently included terms across all species groups. This is due to the fact that they are not highly correlated with any other term, and so always survive the collinearity filtering step. When we examine the actual P.I. values of these layers, we see that *bathymetry* appears to be an informative layer, with mean P.I.'s of around 20-30% for all species groups. By comparison, *distance* is a much less informative layer, with mean P.I.'s of around 5-10% across all groups. To better understand the model structures in practice, it is useful to consider collinear variable groups together: BTemp, FIce/HIce, Sal and SST each contain several layers which are almost always filtered due to high collinearity to one from each group per model.

Viewed this way, we can see that the mean P.I. for variable groups is somewhat consistent across species. At the lowest end, HIce and FIce variables have mean P.I.'s which tend to be below 10%, especially for specific species/layer combinations with a higher  $n$ . In particular, HIce (sea ice thickness) is exceptionally rare as an inclusion, suggesting that it is rarely a more informative layer than FIce (sea ice extent). Next, Sal, SST and BTemp variables compete for the most informative layer categories. The order of highest mean P.I. group varies across species, and there are differences between months within categories. In all variable groups, data for the month of July has a lower frequency of inclusion than either August or June.

For almost every variable/species group combination with sufficient  $n$  for a reasonable measure, there is a high standard deviation in P.I. value. In many cases, the variance of a P.I. measure is greater than the absolute value.

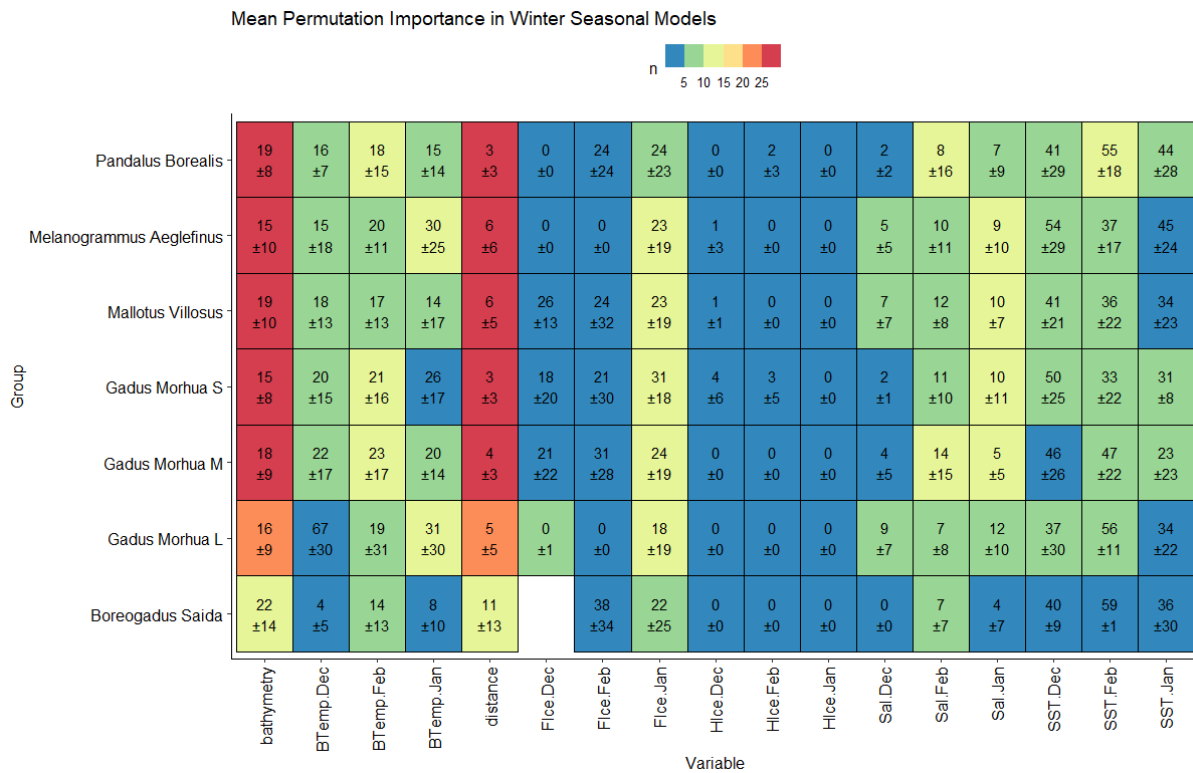


Figure 4.22. Mean, standard deviation in P.I. and number of models included in for each variable separated by species group, winter:

The equivalent P.I. matrix for winter models is shown in Figure 4.22. The relative frequencies of variable groups is similar to what we observed in the structure of summer models, with *bathymetry* and *distance* being included in the majority of models. However, the mean P.I. of these layers is lower than in the summer models, at about 15-20% for *bathymetry* and around 5% for *distance*. The dynamic variable groups show a different structure to what we observed in summer models: rather than being interchangeable depending on species, we see a strong bias towards SST providing the most information across all species. The next most informative group was FIce (sea ice thickness), specifically FIce.Jan, which was significantly more frequent than the other two months of FIce data. Next were the BTemp variables, with the frequency of each month being similar. Finally, the *Sal* variables were the least informative group, and were less informative than the equivalent layers in the summer models.

### 4.3.3.2. Average Models

In this subsection we present the model structures for each of the ‘Average’ species group models used for filling missing data. Each species group has only one model, so labelled P.I. values are exact rather than averages.

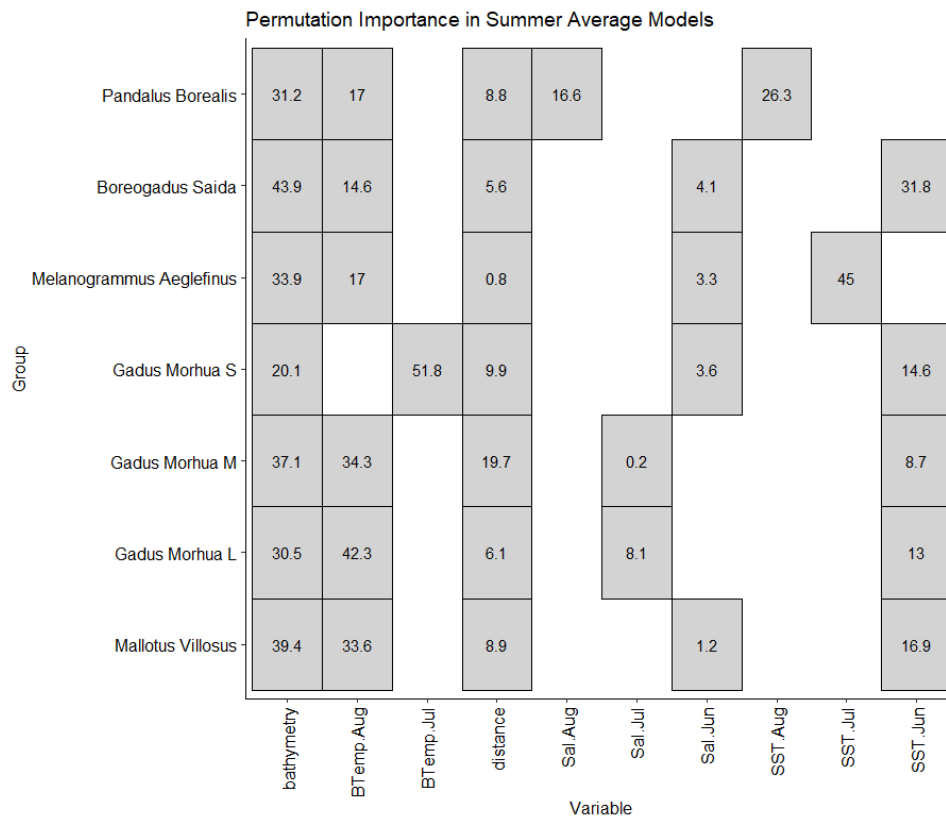


Figure 4.23. Mean P.I. for each variable in the Average models separated by species group, summer.

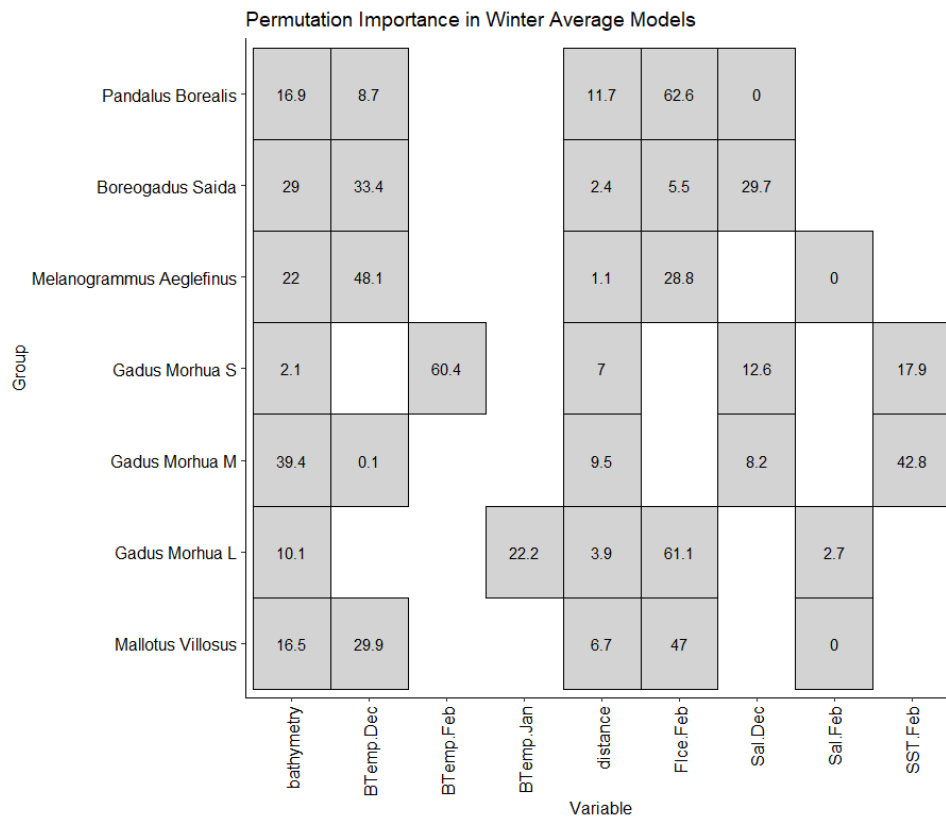


Figure 4.24. Mean P.I. for each variable in the Average models separated by species group, winter.

The Average models have significantly different model structures to the seasonal models across species in summer and winter. Looking at the summer average model structures in Figure 4.23, we see that *bathymetry* has a high P.I. in all models, between 20-45%, which is a higher upper range than we found in the seasonal models. Almost all of the summer models used BTemp.Aug, except for *Gadus morhua* (S) which used BTemp.Jul. No models used BTemp.Jun. BTemp variables had high P.I. values for each cod group and *Mallotus villosus*, but were significantly lower in *Pandalus borealis*, *Boreogadus saida* and *Melanogrammus aeglefinus*. Conversely, we see a reverse of this pattern when we examine the SST variables, where those three species all had significantly higher P.I. associated with SST than the cod groups or *Mallotus villosus*. The *distance* layer was used in all models, with a P.I. around the same as the observed mean across summer seasonal models. No models used any HIce or FIce variable. Salinity variables had very low P.I.'s, except Sal.Aug in the *Pandalus borealis* model (17%).

For the winter average models in Figure 4.24, we observe that *bathymetry* has a higher variability in P.I. than found in the set of winter seasonal models. *Gadus morhua* (S) has a *bathymetry* P.I. of only

2%, while *Gadus morhua* (*M*) has a *bathymetry* P.I. of 40%. BTemp variables have a high P.I. for all species models except *Gadus morhua* (*M*) (0.1%) and *Pandalus borealis* (8%). Of the SST layers, only SST.Feb was included at all, in models for *Gadus morhua* (*S*) (18%) and *Gadus morhua* (*M*) (42%). No HIce variables were included in any model. The only FIce variable included was FIce.Feb, which had the highest P.I. three out of the six models which included it. Only *Gadus morhua* (*S*) and *Gadus morhua* (*M*) did not include FIce.Feb. Salinity layers were included in all models, but had a P.I. of 0 in three of them. The P.I. of the *distance* layer was generally higher in the winter average models than the equivalent seasonal models.

#### 4.4. Discussion

We found that there appears to be a systematic expansion of suitable environments for each modelled species group across seasons over the study period. In the last decade, Maxent modelling of species distributions shows that areas in the north and north-central Barents Sea have become suitable for every modelled species for the first time since 1991. This result agrees with previous studies e.g. (Kortsch et al., 2015; Renaud et al., 2012) In general, although the position of suitable habitat within the Barents Sea is more variable during the summer than winter, the total area of suitable habitat is similar between seasons. We found high interannual variability in total distribution area for every species, with variability being higher during the summer than in the winter. In line with common trends of increasing distribution area for the modelled species, we found a similar pattern of increase in the overlap area of many predator-prey pairings.

Our results suggest that our observed changes in distribution for the seven species groups modelled are a result of increasing temperatures and the reduction of sea ice extent in the northern Barents Sea during the winter. High variability in the permutation importance of each variable within species model groups suggests several possible phenomena. The first could be that changes in surface temperature, bottom temperature and sea ice extent as a result of warming in the Barents Sea are not uniformly imposing or relaxing new environmental bounds in relation to the thermal niche of a species (Righton et al., 2010), so in a given period, distribution may be restrained by surface or deep water conditions, particularly for demersal species. An alternative cause of this variability could be that our models do not capture all of the dynamics which may restrain distribution, this is likely to be a part of the truth as our models contain only broad environmental layers and do not explicitly include biotic interactions which may be highly correlated with changes in bottom or surface temperature and affect distribution to some extent (Gherghel et al., 2018; Wisz et al., 2013b). Our

results support observations from the existing studies. The range expansion of *Gadus morhua* into the northern Barents Sea has been previously observed (Ingvaldsen et al., 2017; Renaud et al., 2012). Our results also support studies suggesting that the spatial overlap between *Gadus morhua* and *Mallotus villosus* has increased in recent years (Fall, 2019; Fall et al., 2018).

This experiment is limited by the availability of high-quality survey data on the species modelled. More accurate information about the prevalence of these species and further empirical surveys of species ranges are needed to contextualise some of our results and improve the underlying data used to generate these model results. If we were to extend this work, it would be helpful to conduct surveys targeting important prey species in the region and cod and establish prevalence estimates. It may also be helpful to experiment with different ways to threshold distribution maps produced by Maxent to see if it impacts the relative breadth of distribution and overlap between seasons and species groups.

We have generated new data on the changing distribution of these critical species in the Barents Sea and examined how their overlapping distributions vary over time. The response to a changing climate is complex but sometimes subtle and difficult to explain without further investigation. However, these results are helpful to us as we consider their implication to the broader field of trophic and population dynamics of Barents Sea cod. In the following chapter, we will use the product of these Maxent models to supply additional information to NARMAX and examine how overlap and consumption relate to one another and other key population and demographic metrics for these species.

# Chapter 5 - Modelling the variability of diet, population demographics and size structure over time

## 5.1. Introduction

Marine ecosystems are incredibly complex, to the extent that it is difficult for us to confidently measure many of the essential components that determine the function of a given system. It is even more difficult then for us to infer knowledge about aspects of the system that we cannot measure at all or make predictions about how an ecosystem will respond to perturbation, such as a changing environment . Nonetheless, our ability to conserve ecosystems and safely exploit marine resources is dependent on our ability to understand how our actions, and other exogenous factors, may affect the system. Failure to do so can have catastrophic consequences for the ecosystem and the human communities which rely on it.

This chapter attempts to quantify the relationship between various components of the Barents Sea marine ecosystem, specifically those related to Barents Sea cod's health and its position in the food web. To do so, we utilise a black-box system identification model called NARMAX (Billings, 2013; Chen and Billings, 1989) to build interpretable models which fit a range of target variables and provide potential insight into the ecological processes underpinning our observations.

Using the results we generated in Chapters 3 and 4, we incorporate temporal measures of predator-prey overlap between cod and several key prey species, combined with a range of relevant time series drawn from ecological and physical measurements of the Barents Sea marine environment. We target a range of variables for modelling, including trophic interactions between cod and critical prey species and the biomass, recruitment and size structure of the BS cod population.

We expect to quantify the factors responsible for driving these critical parameters and for establishing the relationship, if any, between spatial overlap between cod and its prey and temporal trophic dynamics in the Barents Sea.

### 5.1.1. System Identification

A prevalent modelling problem is Simulation: we know the inputs to our system, and we have a model of how the system works. By passing our inputs through our model, we can generate a predictive output. The most straightforward formulation of the simulation problem is demonstrated in Figure 5.1.

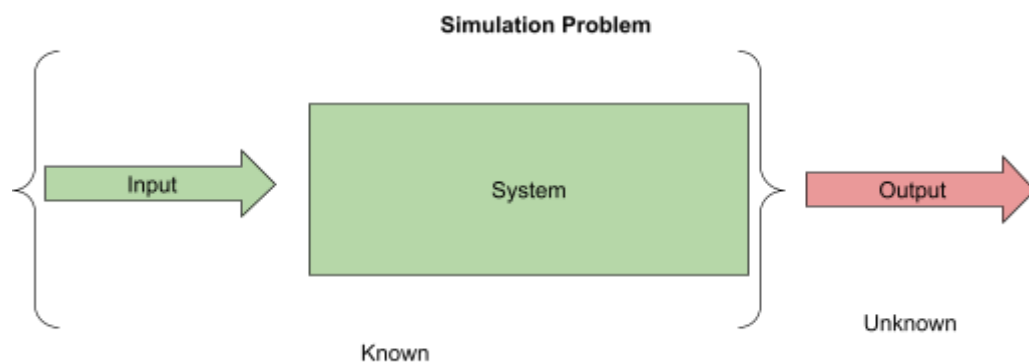


*Figure 5.1. Structure of the simulation problem*

This is a useful framework for simple systems or systems observed in a controlled environment, e.g. the maximum velocity of a ball bearing travelling down slopes of various heights. For systems where the simulation problem is relevant, we have a good idea of the mathematical structure of the system, and we have observations of all the relevant parameters.

This approach fails when we consider systems that are too complicated for us to create prior models for, including most real-world situations. However, we are not entirely incapable of building models for these complex systems, but the problem is different. In this case, when we have observations of the inputs of a system and the system's outputs, and the only thing missing is how our observed inputs and outputs relate, we face a system identification problem. The essential structure of a system identification problem is presented in Figure 5.2.

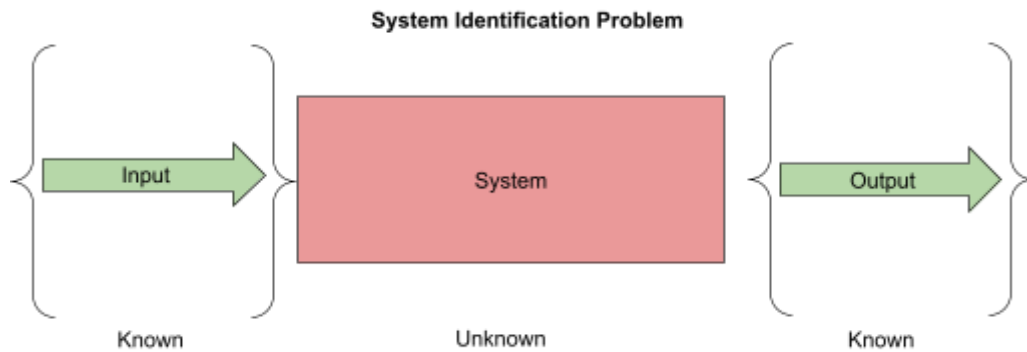


*Figure 5.2. Structure of the System Identification Problem*

This is one way of approaching the core questions of this research: how do our observations about the trophic dynamics of Barents Sea cod relate to each other? We are attempting to identify the mathematical system which connects our observations, and in so doing, gain new insights into the actual interplay of the relevant ecosystem components.

The field of system identification is vast and constantly evolving, and there are countless methods of system identification that could be applied to our study domain. In this study, we utilise an approach called NARMAX (Non-linear **A**uto**R**egressive **M**oving **A**verage model with **e**Xogenous inputs) (Chen and Billings, 1989) to build an interpretable model of the system and identify key factors driving change in the population, demographic and trophic dynamics of Barents Sea cod.

### 5.1.2. NARMAX

There is a lot to say about the NARMAX model, and extended explanations of the foundations, applications and special cases of NARMAX can be found in other texts (e.g. Billings, 2013; Chen and Billings, 1989). To understand the methodology used in this thesis, however, here is an overview of the mathematical foundations of NARMAX and the rationale for applying this model to our research problem.

NARMAX is a comprehensive system identification model which can be applied to model almost any linear or non-linear system in the time or frequency domain. We use NARMAX to model the systems which control our targeted output variables in the time domain. Once we have selected the observational data relevant to our study, NARMAX automatically determines the optimal structure of the model (linear or nonlinear) and identifies which inputs are most significant, systematically eliminating co-linear terms and minimising noise in the prediction by process of feature selection and error reduction. The result is a polynomial function that describes the identified system and analyses model performance on test data.

The mathematical definition of the NARMAX model is:

$$y(t) = F[y(t - 1), y(t - 2), \dots, y(t - n_y), \\ u(t - d), u(t - d - 1), \dots, u(t - n_u), \\ e(t - 1), e(t - 2), \dots, e(t - n_e)] + e(t)$$

Where  $y(t)$  is the system output at time  $t$ , and is a function,  $F$ , of the following components:  $u(t)$  is the system input at time  $t$ , and  $e$  is the system error. The other terms are  $d$ , which is a time delay lag on input terms which is usually  $\geq 1$  (disallowing input terms from the current timestep) and also  $n_y$ ,  $n_u$  and  $n_e$ , which are the maximum time lags for the output, input and error terms respectively.

There are many ways to determine the structure of the function; the algorithm used by our implementation of NARMAX is called ‘Orthogonal Least Squares Estimator and Error Reduction Ratio’. The OLS-ERR algorithm is a way to estimate the structure of a model by identifying the

significant terms which contribute the most information to a model and can provide the final parameter values for the final model. Using OLS-ERR, a sizeable initial parameter space with, for example, many input variables with a high maximum time lag, can be reduced to a much smaller set of orthogonal parameters in the final model, meaning that all of the terms remaining provide unique information and do not correlate with one another. This helps to avoid overfitting and also to improve interpretability.

This is done in several stages. First, a dictionary of all possible model terms is generated from the input data and the set of hyperparameters. A schematic example of a simple NARMAX dictionary is shown in Figure 5.3.

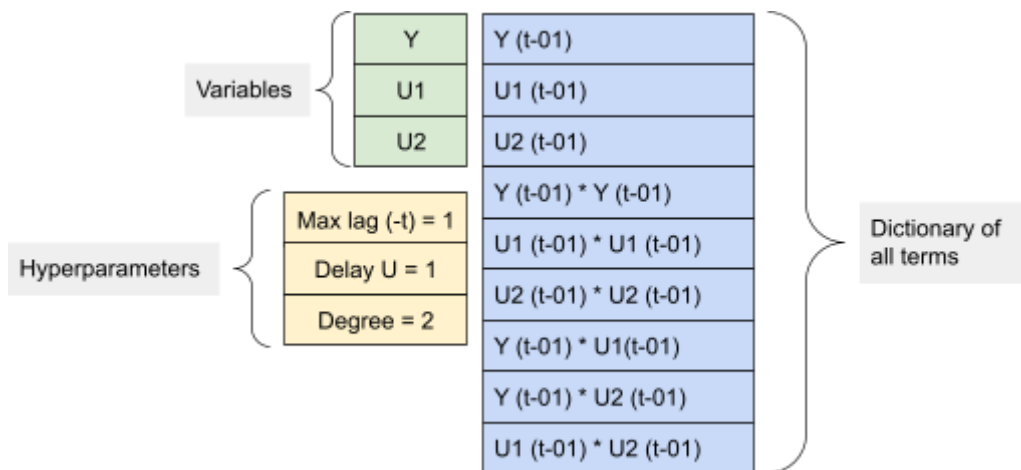


*Figure 5.3. Schematic representation of NARMAX dictionary of terms for a model with a maximum lag of 1, minimum input data delay of 1 and an autoregressive term and two input variables. The maximum degree of the model is 2, allowing for nonlinear second order model terms.*

Next, each possible model term is used to create a single parameter model, and the Error Reduction Ratio, i.e. the amount of error reduced by the addition of that parameter, is calculated. The parameter which reduces the error by the greatest amount is retained in the model, and the process begins again, with a new term added to the existing one. If the addition of the new term reduces the overall error in the model, the term is retained, and this process continues. The number of terms retained in the model can be limited in the hyperparameters, but often the best model has fewer terms than the specified maximum. This is because terms that reduce the error in the model by tiny amounts are not

retained to reduce the risk of overfitting to noise. There is an internal threshold value within NARMAX which rejects terms which have an ERR which is too small (Section 5.2.2.)

The result is a linear-in-the-parameters model formulation where each parameter and coefficient has been identified as the optimal combination to provide the best model fit while minimising the risk of overfitting.

## 5.2. Methodology

We apply the NARMAX model (Chen and Billings, 1989) to a range of study variables, broadly collected into three groups: prey consumption, cod population dynamics and cod population size structure. In total, we modelled 12 variables; the results of each are presented in section 5.3.

Each model consists of three initialisation components: the target variable, input datasets, and a set of hyperparameters determining the search space NARMAX can consider for finding the optimal model. Every variable used, both target variables and input data, represent a time series with one data point per year from 1991-2017. The data is stored as a comma-separated variable (.csv) file, with each column representing a variable and each row representing an observation at each time step.

The input data is normalised in MATLAB prior to the modelling process, using the `normalise()` function, which transforms each variable to have a mean value of 0 and a standard deviation of 1. This eliminates differences in absolute value and unit measurements between input variables while retaining the relationships between them.

The implementation of NARMAX used in this research is maintained by researchers at the University of Sheffield's Department of Automatic Control and Systems Engineering (ACSE). The model is implemented in MATLAB as a function, and the source code is stored in a .p file, an obfuscated code object. Researchers in Sheffield ACSE hold decryption keys for the source code. Access to the source code was not required for this research as no changes to the internal function of the NARMAX model were required, and the implementation is an up to date, efficient one used

actively in many peer reviewed studies e.g. (Gu et al., 2021; Marshall et al., 2016; Wei and Bigg, 2017; Wei et al., 2020).

### 5.2.1. Hyperparameters

Input data and hyperparameters are provided as arguments to the NARMAX function.

Several hyperparameters constrain the model building process and affect overall model performance. In order to identify the optimal set of hyperparameters, we used a brute force search method to try all combinations of hyperparameters within a specific range, which we determined using domain-specific knowledge. The set of hyperparameters that minimised our chosen performance measure (MAPE) were used to train the final model.

The set of hyperparameters and the range of values explored in each are presented in Table 5.1.

*Table 5.1. List of NARMAX hyperparameters tested ranges and a description of each.*

Hyperparameter	Range	Description
nu	1 - 4 Years	The maximum time lag allowed for input variables
ny	0 - 2 Years	The maximum time lag allowed for autoregressive terms (0 means no autoregressive terms)
degree	1 - 3	The highest allowed order for any model term (1st, 2nd or 3rd order polynomials)
delay_u	1 Year	Minimum lag imposed on input data. Set to 1 to restrict model from using input data from current timestep
length_value	3 - 16	The total number of terms allowed in the final model

Limits of hyperparameter values were identified as a combination of knowledge about the study domain to keep model execution time and memory requirements within reasonable bounds. We do

not believe that any of the limitations imposed to restrict the size of the search space were detrimental to the performance or validity of the resulting model, and we investigated a range of limits, discussed below.

It should be noted that the values selected for each hyperparameter refer to a *maximum* allowed value within NARMAX, not a specific requirement for the model structure. For example, when the maximum lag in input terms  $nu$  is set to four years (t-04), the resulting model may not necessarily contain any terms which utilise data from (t-04). We test each value as a maximum because as the total hyperparameter space is explored, there is a potential that unique model structures may be revealed, and the burden of processing time is still small enough to make this approach viable.

The maximum lag in input terms  $nu$  was tested at each value between one year and four years. We did not consider models with no lag in input terms as the validity of such a prediction model would be questionable. This is why we fix the value of the minimum time lag for input data  $delay_u$  as one year. The maximum limit of four years was chosen because, in calibration tests, it was exceedingly rare for NARMAX to use terms up to this value and due to our relatively short time series (27 years), requiring more than four points to be withheld from the beginning of the training data may have unintended consequences on model validity.

The maximum time lag allowed for autoregressive terms  $ny$  was tested at each value between 0 (no autoregressive terms allowed in the model) to two years. Autoregressive terms explicitly include the target variable  $y$  from previous years, which can significantly reduce absolute error if the target variable is not temporally independent, which is usually the case in natural systems. The maximum time lag tested was chosen as two years because, during model calibration, time lags of this value or greater were rare, and the impact of increasing time lag further resulted in an exponential increase in search time.

The maximum value for model *degree* was tested at each value between 1 and 3, including linear first order and nonlinear second and third-order model terms. Increasing maximum degree exponentially increases the size of the model term dictionary and, therefore, the model runtime. Model structures that include fourth-order or higher terms were not allowed due to the infeasibility of exploring such models using the available computing resources. Also, models using parameters of a degree higher than 3 are likely to be challenging to interpret and include terms that could be expressed as lower order. It is unlikely that only very high order model structures can describe truly

essential insights into the system.

Finally, the maximum number of terms allowed in the final model, *length\_value*, was tested at each maximum between 3 and 16 model terms. This range was determined during model calibration tests as regardless of the other settings, models with more than ten terms were rare, but occasionally models with as many as 15 terms were produced. Models with fewer than three terms are highly likely to underfit if the hyperparameters imposed that structure, so we saw no reason to limit the number of terms to 1 or 2. Overall, NARMAX tended to produce models with fewer terms than the allowed maximum.

A visual representation of the hyperparameter optimisation process is shown in Figure 5.4.

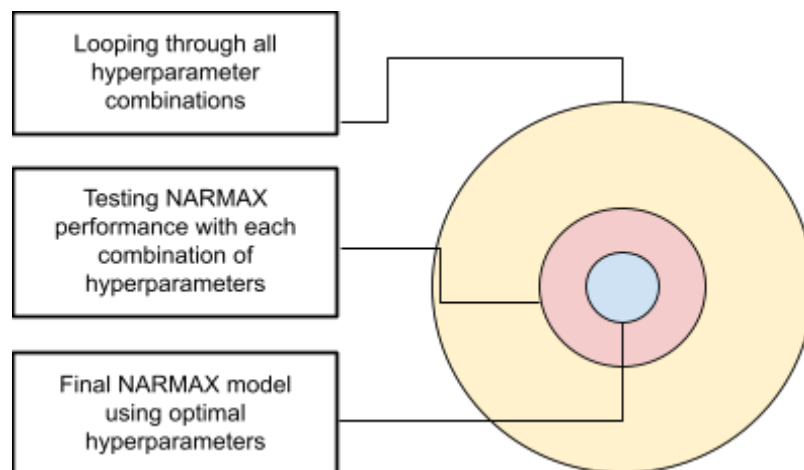


*Figure 5.4. Schematic representation of the nested structure is used to identify the optimal combination of hyperparameters in the final NARMAX model. The NARMAX model is nested within a brute force search of the hyperparameter space. This process is repeated for every target variable, so hyperparameter structure varies between experiments.*

### 5.2.2. Performance measures

We calculate a range of performance measures to compare models during the building process. Within NARMAX, the principal performance measure is Error Reduction Ratio (ERR), which determines how much error is reduced by each subsequent feature added into the model. In the outer loop for finding hyperparameters, we use Mean Absolute Percentage Error (MAPE) calculated on the test data to choose the best model from all candidates.

MAPE has the advantage of being easily interpretable and less sensitive to the small sample size of our test sets. It is a percentage value representing the average error per point as a percentage of the absolute observed value. We also report the Pearson's correlation coefficient (COR), Variance Accounted For (VAF), Normalised Root Mean Square Error (NRMSE) and Mean Absolute Error (MAE) for each model. We select the set of hyperparameters that generate a model with the lowest MAPE on the test points out of all candidate models.

This prioritises performance on test data over training performance in the outer loop. However, the internal NARMAX model building process already builds models that minimise over/underfitting and balance performance on training vs out of sample. Overall, we believe this method of model selection is suitable for our study goals.

### 5.2.3. Model Validation

Each model has a period of 27 years of data, represented by 27 temporally dependent points. This is a short time series, and limits our options for model validation. We split the data into training and test as 24:3, where the first 24 points chronologically were used as training and final 3 points used as test. In practice, the actual size of the training set varied based on the maximum lag of terms in the final model to be  $24 - k$  where  $k$  is the highest value of  $nu$  present in the final model terms. This is because  $k$  points were required to be withheld for initialising each model.

We considered other methods for model validation, including an extensive review of a roll-out nested cross validation approach where the data was subset into a training set of increasing length from 5-24 and used to predict only the next future test point per cycle. This method is used to cross validate time series models where the order of points must be preserved and so normal cross

validation techniques are invalidated. However, we abandoned this method of validation because the models generated were too sensitive to the very small sample sizes. Our full time series of 27 points is at the lower limit of suitability for the NARMAX modelling approach, which is often applied to series with thousands or more points. When compared to a straightforward train/test split approach, the models generated using nested cross validation performed significantly worse on both training and test data with huge swings in performance as the number of samples increased. Ultimately, we believe that our method of validation is appropriate for this study and is the best method available to us given the data.

## 5.3 Results

In this section we present the results of our NARMAX models. This section is split into three subsections, grouping results by variable category. For each target variable we show a figure highlighting the model fit compared to the observed values, with training and test points indicated by colour. We also present two tables: one containing a suite of model performance metrics and the other detailing the structure of the final NARMAX model as a list of parameters, coefficients for each and the ERR accounted for by each. The variables within parameters are named using a short descriptive code within the results tables, and a full description of each variable by name is listed in Appendix E.

### 5.3.1 Prey Consumption by Weight

We fitted NARMAX models to the fraction of annual cod diet by weight accounted for by five prey groups: *Mallotus villosus* (capelin), *Melanogrammus aeglefinus* (haddock), *Pandalus borealis* (shrimp), *Boreogadus saida* (polar cod) and *Gadus morhua* (cannibalism). Overall, model performance on these metrics was uneven. *Melanogrammus aeglefinus* and *Boreogadus saida* in particular were difficult for NARMAX to find well fitting models, and the overall error is much higher than for the other species.

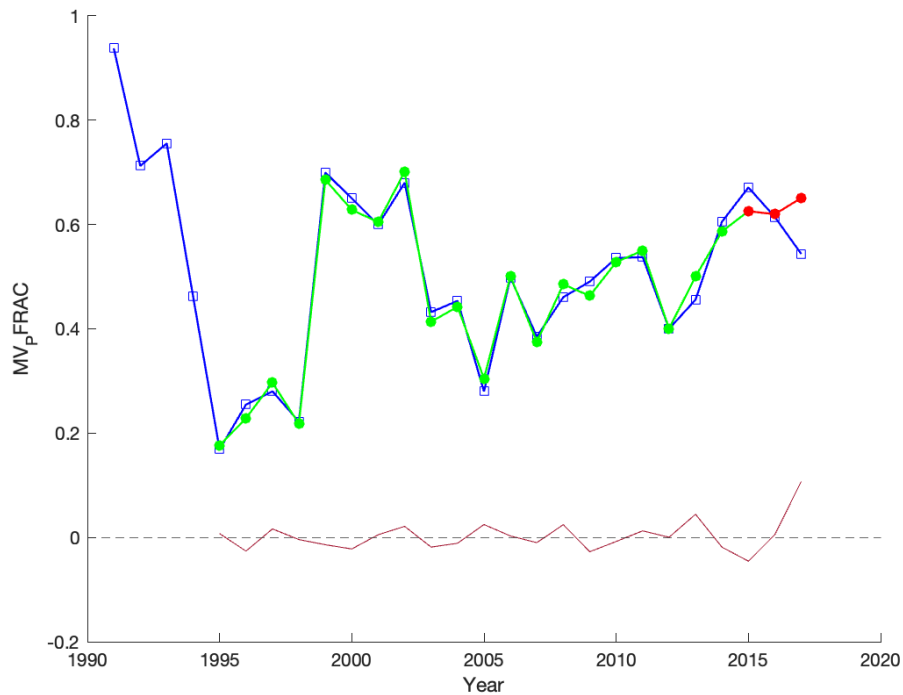
5.3.1.1. *Mallotus villosus*

Figure 5.5 NARMAX fit versus fraction of cod diet accounted for by *Mallotus Villosus*. Blue: Observed data, Green: NARMAX fit to training data, Thick Red: NARMAX fit to test data. Thin Red: Difference between Observed and fitted lines.

The optimal model is of degree 2, with no autoregressive terms and a maximum input lag of 4. Model performance on both training and test data is good, with a MAPE of 3.9% and 9.1% respectively. Further model performance measures are presented in Table 5.2. Visual inspection of model fit in Figure 5.5 demonstrates a very good agreement between observations and model fits during the training period. We see that the model prediction on test data is worse than during training. However, despite the divergence of the model on these points, we still see only small absolute differences between observation and prediction. The model captures even large swings in value, for example between 1998 and 1999.

There are six parameters in the final model, including one constant value of 0.45. The parameters are listed in Table 5.3 in decreasing order of ERR. Five of the six model terms are 2nd order, with no linear terms. The most important term for reducing error is  $TOTSPBIO(t-01) * BS\_PFRAC(t-02)$ , a

term which combines prior spawning biomass with the fraction of *Boreogadus saida* in diet, this term has an ERR of 75.5%. The next most significant nonlinear term, contributing about 3.9% to ERR, is **RECRUITS(t-04) \*GML\_MA\_S\_OV(t-01)** which combines recruitment from four years prior with the spatial overlap between large cod and *Melanogrammus aeglefinus* from the previous year. The remaining nonlinear terms are all combinations of various consumption and spatial overlap terms between cod and different prey groups. Variables chosen represent a range of measures of spatial and trophic domains as well as some key population measures, with some identified terms having long lag times.

Table 5.2 NARMAX model performance measures for MV\_PFRAC

	COR	VAF	NRMSE	MAE	MAPE
Training	0.99197	0.98401	0.12748	0.015979	3.9054
Test	-0.80642	0	0.52865	0.052741	9.1355

Table 5.3. NARMAX model structure for MV\_PFRAC (Variable Explanations in Appendix E)

Parameter	Coefficient	ERR
TOTSPBIO(t-01) *BS_PFRAC(t-02)	-0.089853	75.498
CONST	0.44941	18.1982
RECRUITS(t-04) *GML_MA_S_OV(t-01)	-0.13203	3.87936
MA_PFRAC(t-03) *GMS_BS_S_OV(t-01)	0.065935	1.32977
GM_PFRAC(t-02) *GML_GMS_S_OV(t-02)	0.045403	0.59874
MA_PFRAC(t-04) *GMM_BS_S_OV(t-04)	0.026152	0.337396

### 5.3.1.2. *Melanogrammus aeglefinus*

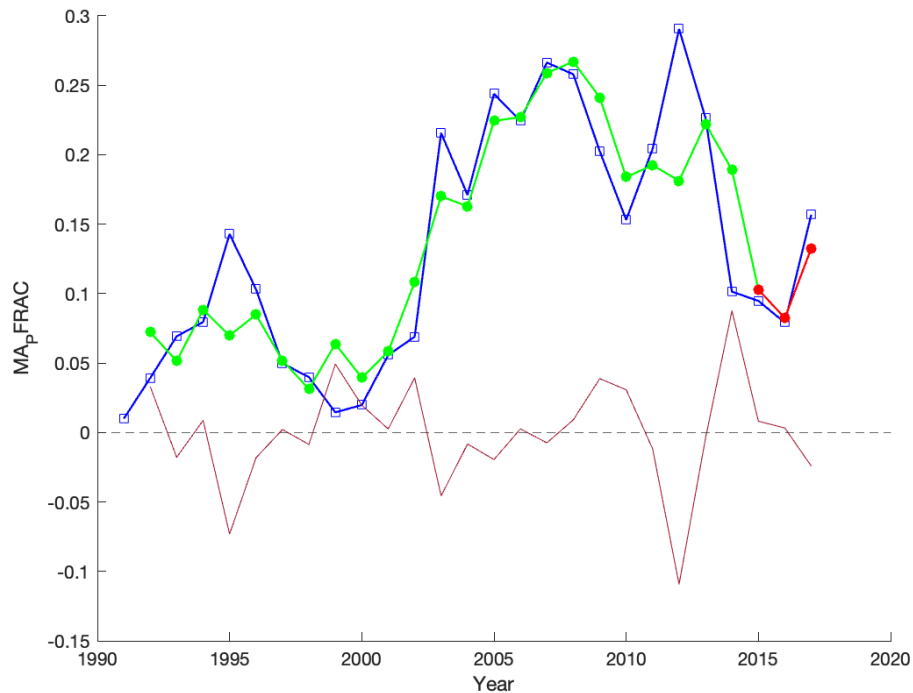


Figure 5.6 NARMAX fit versus fraction of cod diet accounted for by *Melanogrammus aeglefinus*. Blue: Observed data, Green: NARMAX fit to training data, Thick-Red: NARMAX fit to test data, Thin-Red: Difference between Observed and NARMAX fit.

The optimal model for MA\_PFRAC is of degree 1, a linear model, with no autoregressive terms, a maximum lag of 1 year and six parameters. Model fit is shown in Figure 5.6. Model performance is uneven. The model performed well on test data, with a MAPE of 9.4%, but underperformed on training data with a MAPE of 40.3%. Performance measures for this model are listed in Table 5.4. Visual inspection of the model fit shows a general success in fitting the underlying shape of the data, supported by the VAF of 0.79 and 0.82 for training and test points respectively. However, the model generally underperformed at identifying the magnitude of change between points, leading to a higher absolute error. In particular, the peak in the observed consumption of *Melanogrammus aeglefinus* in 2012 was not predicted at all. At some points, the absolute error was greater than the actual observed value. This poor performance may be a result of the small sample size and localised distribution of the species. While this model is not a failure, it is not as successful as the model for MV\_PFRAC previously shown.

The model structure is linear with five variable parameters and one constant, listed in Table 5.5. The constant of 0.14 has the highest ERR at 68.9, with the most significant variable parameter, UNIQUEPREY, having an ERR of only 20.52. The remaining variable parameters have ERR in the range 2.29-0.74. The variables selected for inclusion in the final model are drawn from an interesting combination: UNIQUEPREY is a measure of prey diversity, FBAR is a measure of cod mortality and the remaining variables describe the overlap between cod size groups and prey species, specifically *Boreogadus saida*. The linear structure, few model terms and short time lag combined with the uneven overall model performance may suggest that the data required for a better model fit is not available in this case. The standout result is that UNIQUEPREY(t-01) provides the most information to the MA\_PFRAC model, and there is a positive correlation between the two.

*Table 5.4 NARMAX model performance measures for MA\_PFRAC*

	<b>COR</b>	<b>VAF</b>	<b>NRMSE</b>	<b>MAE</b>	<b>MAPE</b>
Training	0.8895	0.79121	0.513699	0.0281578	40.3731
Test	0.97465	0.820682	0.190938	0.0118535	9.36863

*Table 5.5 NARMAX model structure for MA\_PFRAC (Variable Explanations in Appendix E)*

<b>Parameter</b>	<b>Coefficient</b>	<b>ERR</b>
UNIQUEPREY(t-01)	0.05033	20.5225
<b>constant</b>	0.13625	68.8748
<b>GMM_GMS_S_OV(t-01)</b>	0.029045	2.2896
<b>FBAR(t-01)</b>	-0.035054	0.980002
<b>GMS_BS_S_OV(t-01)</b>	0.015421	0.809816
<b>GML_BS_S_OV(t-01)</b>	0.024385	0.738994

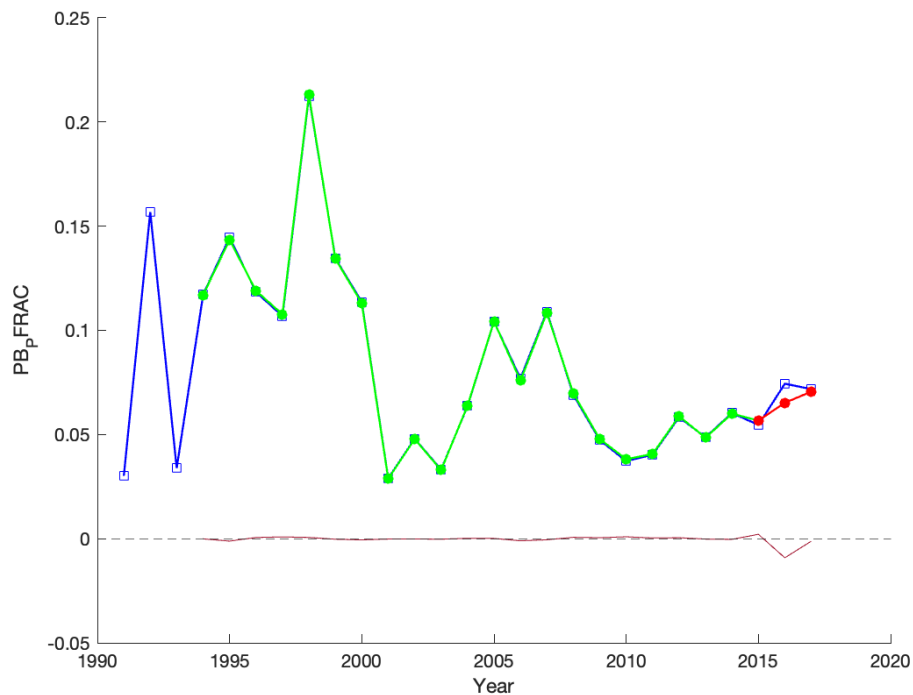
5.3.1.3. *Pandalus borealis*

Figure 5.7 NARMAX fit versus fraction of cod diet accounted for by *Pandalus borealis*. Blue: Observed data, Green: NARMAX fit to training data, Thick-Red: NARMAX fit to test data, Thin-Red: Difference between Observed and NARMAX fit.

The optimal model for PB\_PFRAC is of degree 2, with no autoregressive terms and a maximum lag of 3 years. The model has 11 parameters. Model fit is shown in Figure 5.7. Model performance is excellent, with a MAPE of 0.66% and 6.0% for training and test sets respectively. Performance measures for this model are listed in Table 5.6. Visual inspection of the model fit shows exceptional agreement between the modelled and observed values in the training set and very close agreement within the test set. The model characterises variability in the data exceptionally well, with a training VAF of  $\sim 1$  and a test VAF of 0.71. This marks the best performance for any of the prey consumption variables presented in this subsection.

The model structure is complicated, with eleven 2nd order parameters. These parameters are listed in Table 5.7. The most significant parameter, RECRUITS(t-03)\*BS\_PFRAC(t-01) is a combination of prior cod recruitment and consumption of *Boreogadus saida*, with an ERR of 73.43. The remaining 10 parameters have ERR between 12.30-0.01. The variables included in the final model are drawn

from a range of variable groups. RECRUITS, TOTALBIO and LANDINGS are cod population measures. BS\_PFRAC, GM\_PFRAC, MV\_PFRAC and UNIQUEPREY are diet measures whilst LARGEFRAC and MEDFRAC are population structure measures. Finally, this model uses many overlap measures between cod and prey groups. This model is using a wide range of the available input data, and although it may be difficult to interpret specific model terms, it's clear that the model has identified some key relationships as evidenced by its performance on test data.

*Table 5.6 NARMAX model performance measures for PB\_PFRAC*

	<b>COR</b>	<b>VAF</b>	<b>NRMSE</b>	<b>MAE</b>	<b>MAPE</b>
Training	<b>0.99992</b>	0.99985	0.012455	0.0004719	0.66428
Test	<b>0.87105</b>	0.71026	0.27632	0.0041593	5.9529

Table 5.7 NARMAX model structure for PB\_PFRAC (Variable Explanations in Appendix E)

Parameter	Coefficient	ERR
RECRUITS(t-03) *BS_PFRAC(t-01)	-0.052294	73.4361
GM_PFRAC(t-03) *GML_MA_S_OV(t-02)	-0.028984	12.2968
GML_MV_S_OV(t-01) *GML_MA_S_OV(t-01)	0.073161	6.43946
MV_PFRAC(t-02) *GMM_BS_S_OV(t-01)	-0.024775	4.01137
TOTSPBIO(t-03) *GMS_BS_S_OV(t-01)	-0.019567	2.39996
GMS_BS_S_OV(t-01) *GML_GMM_S_OV(t-01)	0.0080309	0.614998
UNIQUEPREY(t-03) *GMS_BS_S_OV(t-03)	0.0089127	0.379653
LARGEFRAC(t-03) *GML_MA_S_OV(t-02)	-0.0064002	0.263266
MEDFRAC(t-02) *GMM_GMS_S_OV(t-02)	-0.0052939	0.0989652
TOTALBIO(t-01) *BS_PFRAC(t-02)	0.0035345	0.0417395
LANDINGS(t-01) *GMS_BS_S_OV(t-02)	-0.0019616	0.0142333

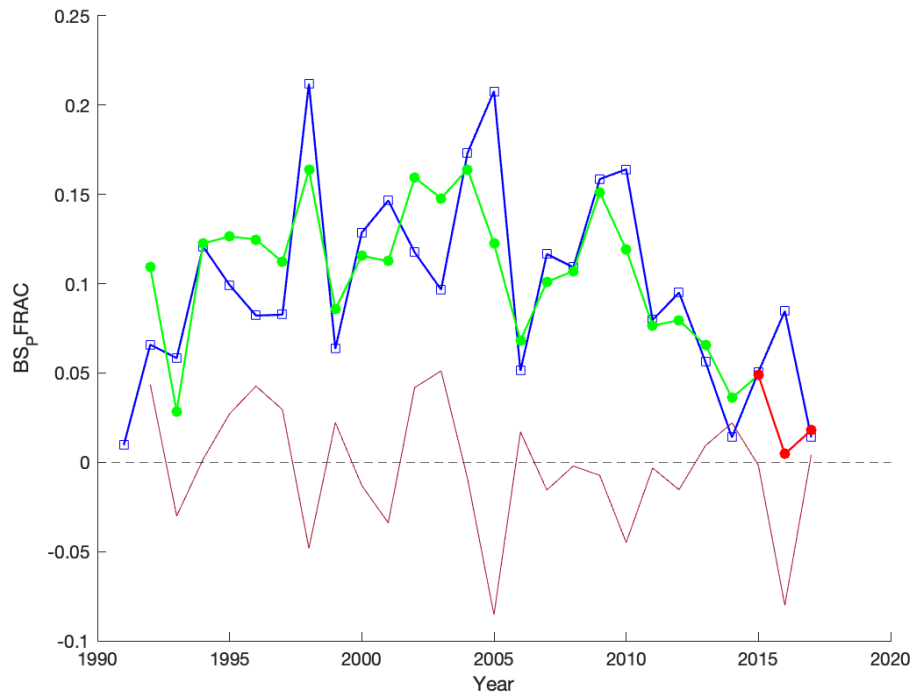
5.3.1.4. *Boreogadus saida*

Figure 5.8. NARMAX fit versus fraction of cod diet accounted for by *Boreogadus saida*. Blue: Observed data, Green: NARMAX fit to training data, Thick-Red: NARMAX fit to test data, Thin-Red: Difference between Observed and NARMAX fit.

The optimal model for BS\_PFRAC is of degree 1, a linear model, with a maximum lag of 1 year and no autoregressive terms. The model has six parameters. Model fit is shown in Figure 5.8. Model performance is quite poor, with a MAPE of 32.0% and 42.7% on training and test data respectively. Performance measures for this model are listed in Table 5.8. Visual inspection of model fit reveals a clear dissonance between modelled points and observed points in both the training and test sets. The model does a poor job of quantifying the variability of the observed data, and also of quantifying its magnitude. Overall, this is the worst performing model within the prey consumption variable group and the entire study. As with *Melanogrammus aeglefinus*, this poor performance may be a result of the small sample size and localised distribution of the species.

The model structure is linear with five variable parameters and a constant term. These parameters are listed in Table 5.9. The most significant term is the constant value of 0.1, with an ERR of 68.94. The most significant variable parameter is GML\_BS\_S\_OV(t-01), the summer overlap between large cod

and Boreogadus saida, which has an ERR of 18.9. The remaining variable parameters have ERR between 1.88-0.64. The variables chosen in the final model are drawn from species overlap, diet, and population structure groups. The structure of this model is similar to the model for MA\_PFRAC, which also underperformed compared to the models for other prey groups. This suggests that in this case too, some key data was missing which would allow NARMAX to fit a more complex model with an adequate degree of validity. In this case, a simple linear model was the best candidate.

*Table 5.8 NARMAX model performance measures for BS\_PFRAC*

	<b>COR</b>	<b>VAF</b>	<b>NRMSE</b>	<b>MAE</b>	<b>MAPE</b>
Training	<b>0.739822</b>	0.547337	0.909411	0.0267958	31.9684
Test	<b>-0.278374</b>	0	0.654181	0.0286515	42.6648

*Table 5.9 NARMAX model structure for BS\_PFRAC (Variable Explanations in Appendix E)*

<b>Parameter</b>	<b>Coefficient</b>	<b>ERR</b>
<b>GML_BS_S_OV(t-01)</b>	0.034078	18.9463
<b>constant</b>	0.096074	68.9359
<b>LARGEFRAC(t-01)</b>	-0.027673	1.87498
<b>GMS_BS_S_OV(t-01)</b>	-0.0065138	0.850353
<b>PB_PFRAC(t-01)</b>	-0.018762	0.968066
<b>MEDFRAC(t-01)</b>	-0.016733	0.642482

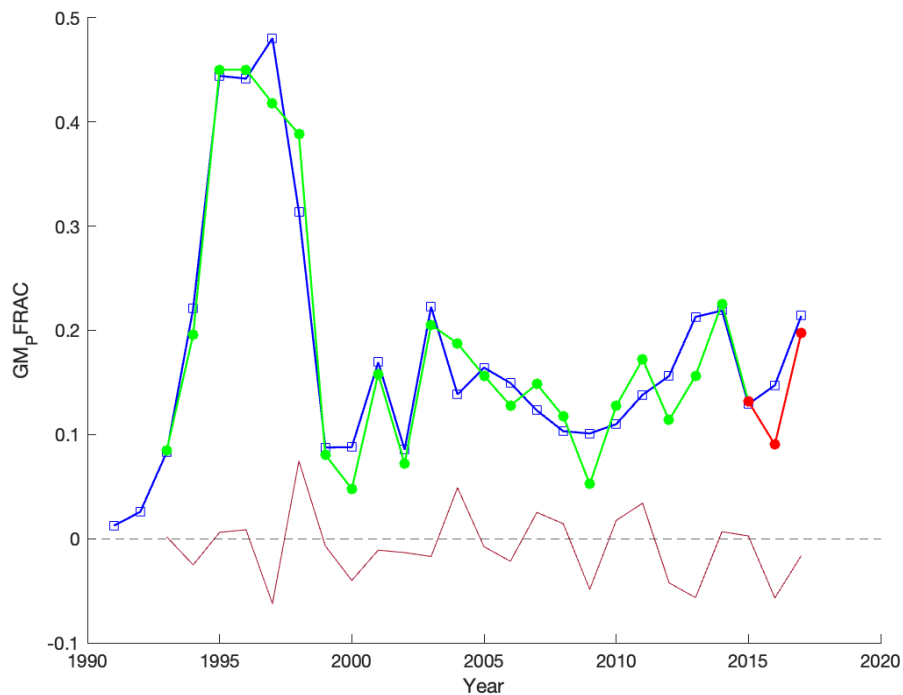
5.3.1.5. *Gadus morhua*

Figure 5.9. NARMAX fit versus fraction of cod diet accounted for by *Gadus morhua*. Blue: Observed data, Green: NARMAX fit to training data, Thick-Red: NARMAX fit to test data, Thin-Red: Difference between Observed and NARMAX fit.

The optimal model for GM\_PFRAC is of degree 1, a linear model, with a maximum lag of 2 years, an autoregressive term with 1 year of maximum delay and 11 parameters in the final model. Model fit is shown in Figure 5.9. Model performance was quite good overall, with a MAPE of 16.9% and 16.1% for training and test sets respectively. Performance measures for this model are listed in Table 5.10. Visual inspection of the model fit shows good agreement between modelled points and observed points generally in both training and test sets. The large peak from 1994 to 1996 is generally well captured, with the following period, which appears to be a step change in pattern, also reasonably well captured by the model. The model values lack the smoothness of the observed data during the period around 2005 to 2012, but remains quite close in absolute value.

The model structure is of 1st degree, a linear model, with 11 variable parameters of which one is autoregressive. These parameters are listed in Table 5.11. The most significant parameter is the autoregressive GM\_PFRAC(t-01), the proportion of diet accounted for by *Gadus morhua* during the

previous year, the only autoregressive term appearing in any of the diet variable models. This parameter is associated with an ERR of 82.9. The remaining parameters have an ERR between 5.12 - 0.67. The variables selected for the final model are drawn from a range of groups: Three parameters are diet variables, three are cod population variables and five are overlap measures. The most interesting result is that this is the only diet variable for which an autoregressive term has been included in the NARMAX model equation, and that term has the highest ERR. This indicates that previous measures of cannibalism may be useful for predicting future cannibalism.

*Table 5.10 NARMAX model performance measures for GM\_PFRAC*

	<b>COR</b>	<b>VAF</b>	<b>NRMSE</b>	<b>MAE</b>	<b>MAPE</b>
Training	0.962066	0.920954	0.276305	0.0268577	16.8912
Test	0.827092	0.535351	0.403372	0.0252508	16.0862

*Table 5.11 NARMAX model structure for GM\_PFRAC (Variable Explanations in Appendix E)*

<b>Parameter</b>	<b>Coefficient</b>	<b>ERR</b>
<b>GM_PFRAC(t-01)</b>	0.9625	82.9072
<b>MA_PFRAC(t-02)</b>	0.003992	5.12037
<b>GMM_BS_S_OV(t-02)</b>	0.023533	1.43868
<b>FBAR(t-01)</b>	0.3005	1.3287
<b>BS_PFRAC(t-02)</b>	-0.30702	1.97449
<b>GMM_GMS_S_OV(t-02)</b>	0.1037	1.17094
<b>GMS_BS_S_OV(t-01)</b>	0.033685	1.09949
<b>GML_GMM_S_OV(t-02)</b>	0.041754	0.635027
<b>GML_GMS_S_OV(t-02)</b>	0.041868	0.704681
<b>TOTALBIO(t-01)</b>	-0.025318	0.733428
<b>RECRUITS(t-02)</b>	-0.044661	0.669739

## 5.3.2 Barents Sea cod population measures

### 5.3.2.1. *Gadus morhua* Biomass

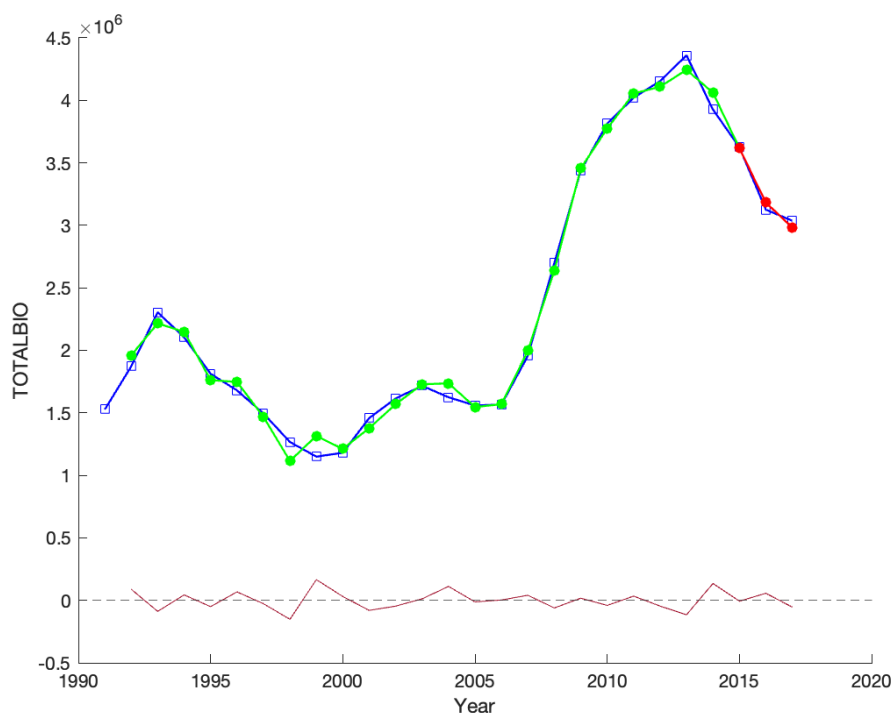


*Figure 5.10 NARMAX fit versus total mature biomass of *Gadus morhua*. Blue: Observed data, Green: NARMAX fit to training data, Thick-Red: NARMAX fit to test data, Thin-Red: Difference between Observed and NARMAX fit.*

The optimal model for TOTALBIO is of degree 1, a linear model, with one autoregressive term and a maximum input lag of 1 year. There are 11 parameters in the final model. Model fit is shown in Figure 5.10. Model performance is excellent, with a MAPE of 3.43% and 1.26% on training and test data respectively. Performance measures for this model are listed in Table 5.12. Visual inspection of the model fit shows excellent agreement between modelled points and observed points in both the training and test sets. The model accurately characterizes the full range of the data, including the large peak from 2007 to 2014.

The model structure is of 1st degree, with 11 variable parameters. These variable parameters are listed in Table 5.13. The most significant term is the autoregressive TOTALBIO(t-01), with an ERR of 98.54. The remaining parameters have ERR between 0.79-0.01. The autoregressive term clearly contains the most information in the model, but the remaining terms with very small ERR still add new information essential for capturing the shape and directionality of the observed data. Of the variables selected for inclusion in the final model, 2 are population measures, 5 are measures of diet, 3 are spatial overlap measures and 1 is a size structure measure.

*Table 5.12 NARMAX model performance measures for TOTALBIO*

	COR	VAF	NRMSE	MAE	MAPE
Training	0.99723745	0.994474428	0.0747648259	63827.0486	3.43858005
Test	0.985143356	0.968896977	0.0776888698	39300.7503	1.26446087

*Table 5.13 NARMAX model structure for TOTALBIO (Variable Explanations in Appendix E)*

Parameter	Coefficient	ERR
TOTALBIO(t-01)	1.020414324	98.5385
FBAR(t-01)	-236281.9946	0.786081
UNIQUEPREY(t-01)	11671.37649	0.294209
GML_PB_S_OV(t-01)	7229.952078	0.093094
LARGEFRAC(t-01)	151289.2097	0.039588
GM_PFRAC(t-01)	-233671.2692	0.0499637
GML_BS_S_OV(t-01)	122701.4847	0.017885
GMM_GMS_S_OV(t-01)	136298.8917	0.0276603
MV_PFRAC(t-01)	-99106.35288	0.0352997
PB_PFRAC(t-01)	-95871.67835	0.0164249
BS_PFRAC(t-01)	-79897.22299	0.00560015

### 5.3.2.2. *Gadus morhua* Spawning Biomass

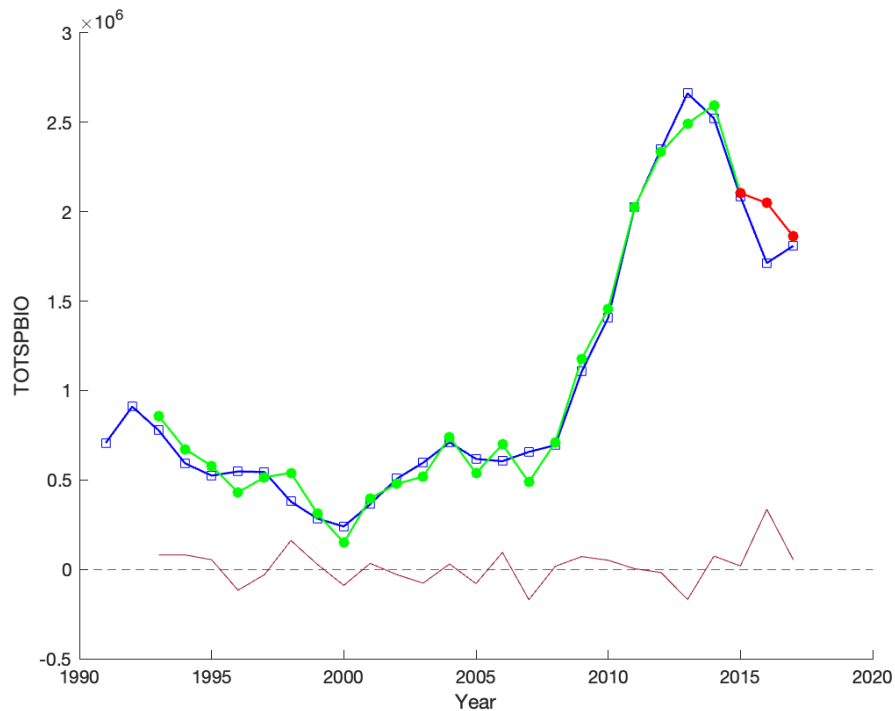


Figure 5.11 NARMAX fit versus total spawning biomass of *Gadus morhua*. Blue: Observed data, Green: NARMAX fit to training data, Thick-Red: NARMAX fit to test data, Thin-Red: Difference between Observed and NARMAX fit.

The optimal model for TOTSPBIO is of degree 1, with no autoregressive term and a maximum lag of 2 years. There are 5 terms in the final model. Model fit is shown in Figure 5.11. Model performance is good, but inferior when compared to the TOTALBIO model, a closely related variable. MAPE is 11.8% and 7.80% on training and test data respectively. Performance measures for this model are listed in Table 5.14. Visual inspection shows good agreement between modelled and observed points, though the modelled fit oscillates around the observational data between 1994 and 2007, failing to smoothly fit. Performance on test points was very good for 2 of the 3 years, and good overall.

The model structure is linear with 4 variable terms and 1 constant. The model parameters are listed in Table 5.15. The most significant variable parameter is LANDINGS(t-01) with an ERR of 22%. The constant 1,079,721 is the most significant parameter overall, with an ERR of 75.6. The remaining parameters have ERR between 1.29 - 0.32. Of variables chosen for inclusion in the final model, 2 are population measures, 1 is a diet measure and 1 is a spatial overlap measure.

*Table 5.14 NARMAX model performance measure for TOTSBIO*

	<b>COR</b>	<b>VAF</b>	<b>NRMSE</b>	<b>MAE</b>	<b>MAPE</b>
Training	0.9931615652	0.9863698946	0.1175519134	70870.61903	11.83621153
Test	0.472289164	0.1887829448	0.5285578246	135832.4136	7.80756614

*Table 5.15 NARMAX model structure for TOTSBIO (Variable Explanations in Appendix E)*

<b>Parameter</b>	<b>Coefficient</b>	<b>ERR</b>
<b>LANDINGS(t-01)</b>	404760.1114	22.0033
<b>constant</b>	1079721.3064	75.5744
<b>SMALLFRAC(t-01)</b>	362457.9703	1.29381
<b>GML_MA_S_OV(t-01)</b>	91934.264855	0.296629
<b>TOTALBIO(t-02)</b>	-79562.062082	0.318082

### 5.3.2.3. *Gadus morhua* Recruitment

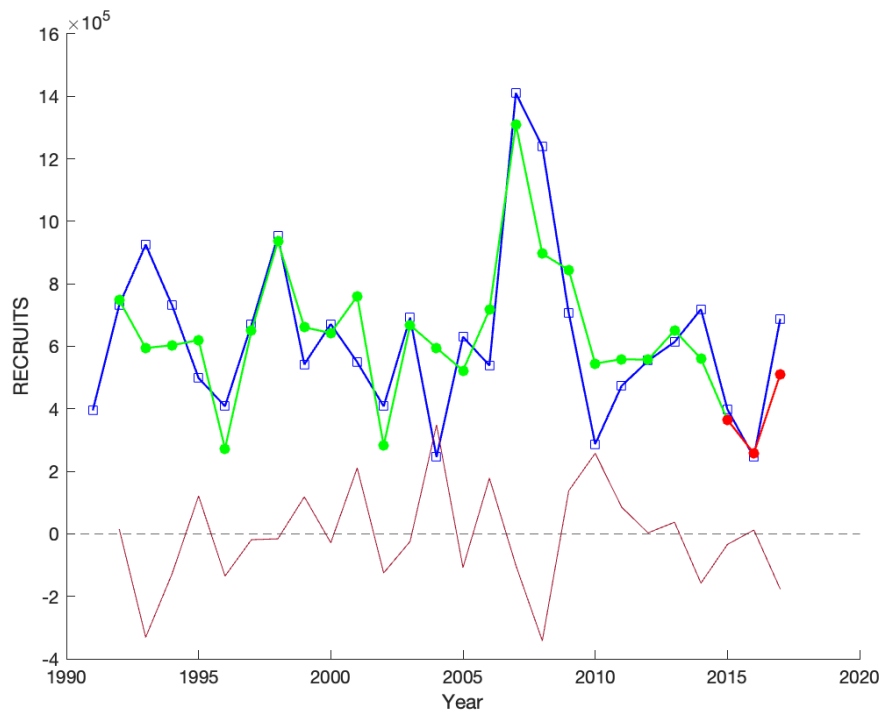


Figure 5.12 NARMAX fit versus recruitment of *Gadus morhua*. Blue: Observed data, Green: NARMAX fit to training data, Thick-Red: NARMAX fit to test data, Thin-Red: Difference between Observed and NARMAX fit.

The optimal model for RECRUITS is of degree 2, with a maximum lag of 1 year, no autoregressive terms and only three parameters in the final model. Model fit is shown in Figure 5.12. Model performance is reasonably good, but inferior to both TOTALBIO and TOTSBIO, with a MAPE of 26.02% and 13.06% on training and test data respectively. Performance measures for this model are listed in Table 5.16. Visual inspection of model fit demonstrates that the modelled points successfully capture the broad pattern of the observations, but struggle to capture the magnitude of interannual change. For example, the sudden peak in recruitment in 2007 is captured quite well, while significant drops in 2004 and 2010 are missed. The model accurately predicts the first two test points, but underestimates the final point in 2017.

The model structure is of degree 2, with two variable parameters and one constant. The model parameters are listed in Table 5.17. The most significant model term is  $\text{UNIQUEPREY}(t-01)*\text{UNIQUEPREY}(t-01)$ , with an ERR of 66.1. The next most important term is

the constant value of 432,134 with an ERR of 21.28 and the final term,  $GML\_GMM\_S\_OV(t-01) * GMM\_GMS\_S\_OV(t-01)$ , has an ERR of 7.11. It's difficult to interpret this model as the variable choices are not immediately intuitive and the inclusion of only two variable terms in the final model is interesting. There are no population measures included, such as TOTALBIO, which we might have expected to be significant. Instead, this model is effectively a combination of prey diversity and overlap between the three cod size groups, which could be a proxy for size or spatial structure of the population.

*Table 5.16 NARMAX model performance measures for RECRUITS*

	<b>COR</b>	<b>VAF</b>	<b>NRMSE</b>	<b>MAE</b>	<b>MAPE</b>
Training	0.7759858383	0.6021540212	0.8128374243	131653.3964	26.01635427
Test	0.9961852287	0.8076517997	0.2353225692	74331.86338	13.0604887

*Table 5.17 NARMAX model structure for RECRUITS (Variable Explanations in Appendix E)*

<b>Parameter</b>	<b>Coefficient</b>	<b>ERR</b>
<b>UNIQUEPREY(t-01) *UNIQUEPREY(t-01)</b>	175511.1643	66.0781
<b>constant</b>	432134.4085	21.2767
<b>GML_GMM_S_OV(t-01) *GMM_GMS_S_OV(t-01)</b>	187785.838	7.10566

### 5.3.3 Barents Sea cod Size Structure

#### 5.3.3.1. Fraction of *Gadus morhua* Population <20cm in length [*Gadus morhua* (S)]

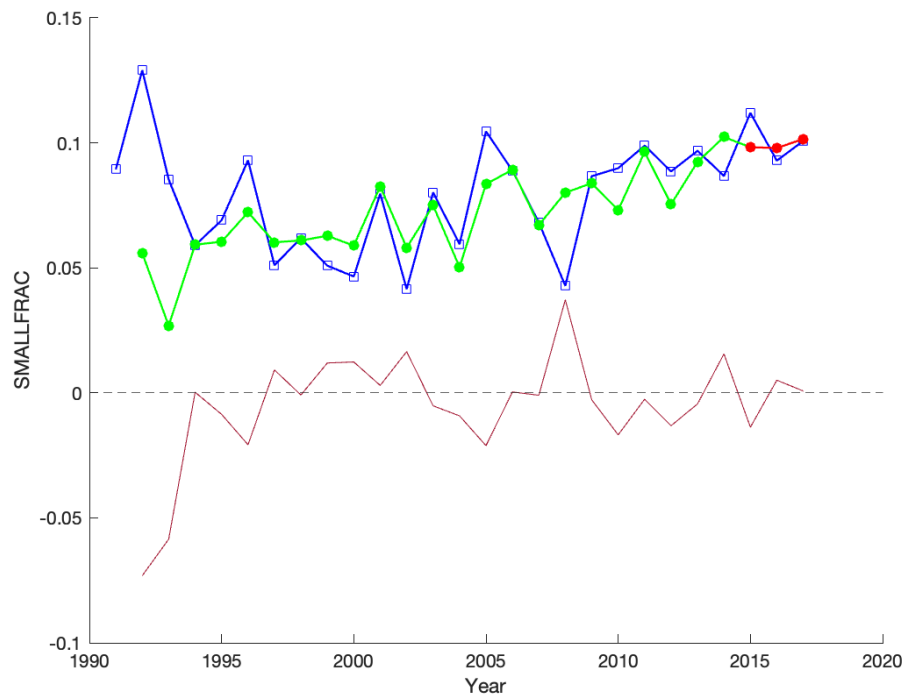


Figure 5.13 NARMAX fit versus fraction of sampled *Gadus morhua* population in IMR-PINRO database <20cm in length. Blue: Observed data, Green: NARMAX fit to training data, Thick-Red: NARMAX fit to test data, Thin-Red: Difference between Observed and NARMAX fit.

The optimal model for SMALLFRAC is of degree 1, with a maximum lag of one year, one autoregressive term and three parameters. Model fit is shown in Figure 5.13. Model performance is uneven, with a MAPE of 20.27% and 6.16% on training and test sets respectively. The full list of performance measures is shown in Table 5.18. Visual inspection of the fit shows the model successfully characterizes the general trend in the observations but struggles to capture the interannual detail. This is similar to the model for RECRUITS, which is perhaps to be expected as SMALLFRAC and RECRUITS are undoubtedly measurements of closely related aspects of the population.

The model structure has only two variable linear parameters and one constant. These parameters are listed in Table 5.19. The most significant parameter is the autoregressive SMALLFRAC(t-01) with an ERR of 89.2. The remaining terms are the constant value 0.09 with an ERR of 4.38 and LARGEFRAC(t-01) with an ERR of 3.26. The only variables chosen for inclusion in this model are size structure measurements. The structure is also similar to the model for RECRUITS, which suggests some internal consistency between the two models considering the functional proximity of the variables measured.

*Table 5.18 NARMAX model performance measures for SMALLFRAC*

	<b>COR</b>	<b>VAF</b>	<b>NRMSE</b>	<b>MAE</b>	<b>MAPE</b>
Training	0.332845	-0.0767985	1.39713	0.0149739	20.2626
Test	-0.0249575	0	0.443173	0.00651887	6.15595

*Table 5.19 NARMAX model structure for SMALLFRAC (Variable Explanations in Appendix E)*

<b>Parameter</b>	<b>Coefficient</b>	<b>ERR</b>
<b>SMALLFRAC(t-01)</b>	-0.15041	89.2016
<b>constant</b>	0.087305	4.37694
<b>LARGEFRAC(t-01)</b>	0.019936	3.25873

### 5.3.3.2. Fraction of *Gadus morhua* population between 20cm and 100cm in length [*Gadus morhua* (*M*)]

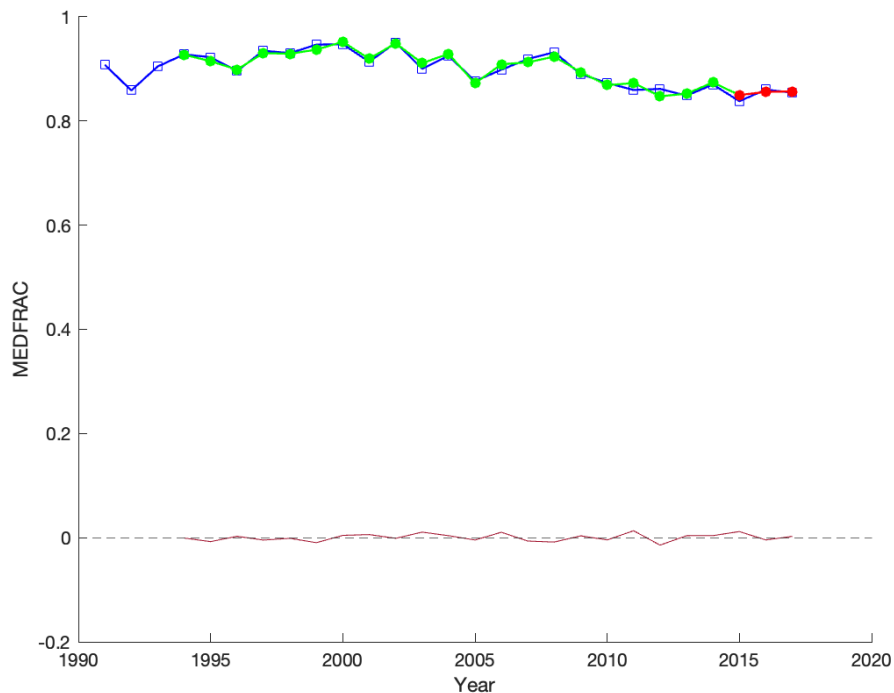


Figure 5.14 NARMAX fit versus fraction of sampled *Gadus morhua* population in IMR-PINRO database >20cm, <100cm in length. Blue: Observed data, Green: NARMAX fit to training data, Thick-Red: NARMAX fit to test data, Thin-Red: Difference between Observed and NARMAX fit.

The optimal model for MEDFRAC is of degree 2, with a maximum lag of three years, no autoregressive terms and has five parameters. Model fit is shown in Figure 5.14. Model performance is excellent, with MAPE of 0.67% and 0.74% in training and test sets respectively. Performance measures for this model are listed in Table 5.20. Visual inspection of model fit shows excellent agreement between modelled and observed data in both training and test sets. The data does not vary significantly from its mean, though there is a slight decreasing trend over time. The model appears to accurately characterize the direction of interannual change in the training data, reflected in the high COR and VAF measures.

The model structure is of degree 2, with 4 parameters constructed from six variables, and one constant value. These parameters are listed in Table 5.21. The most significant term is  $GML\_MA\_S\_OV(t-03) * GML\_MA\_S\_OV(t-03)$  with an ERR of 78.02. The remaining terms have

ERR between 21.87 - 0.01. Of the variables included in the final model, four are spatial overlap measures, one is a population measure and one is a size structure measurement.

*Table 5.20 NARMAX model performance measures for MEDFRAC*

	<b>COR</b>	<b>VAF</b>	<b>NRMSE</b>	<b>MAE</b>	<b>MAPE</b>
Training	0.97321	0.94714	0.23624	0.0059939	0.6668
Test	0.9268	0.50884	0.33102	0.0062221	0.73598

*Table 5.21 NARMAX model structure for MEDFRAC (Variable Explanations in Appendix E)*

<b>Parameter</b>	<b>Coefficient</b>	<b>ERR</b>
<b>GML_MA_S_OV(t-03) *GML_MA_S_OV(t-03)</b>	0.012159	78.0164
<b>constant</b>	0.87512	21.8686
<b>TOTSPBIO(t-02)</b>	-0.036819	0.0839765
<b>LARGEFRAC(t-01) *GMM_MA_S_OV(t-03)</b>	-0.017196	0.0187922
<b>GMM_BS_S_OV(t-03) *GMS_BS_S_OV(t-01)</b>	0.0069507	0.00612873

### 5.3.3.3 Fraction of *Gadus morhua* population > 100cm in length [*Gadus morhua* (L)]

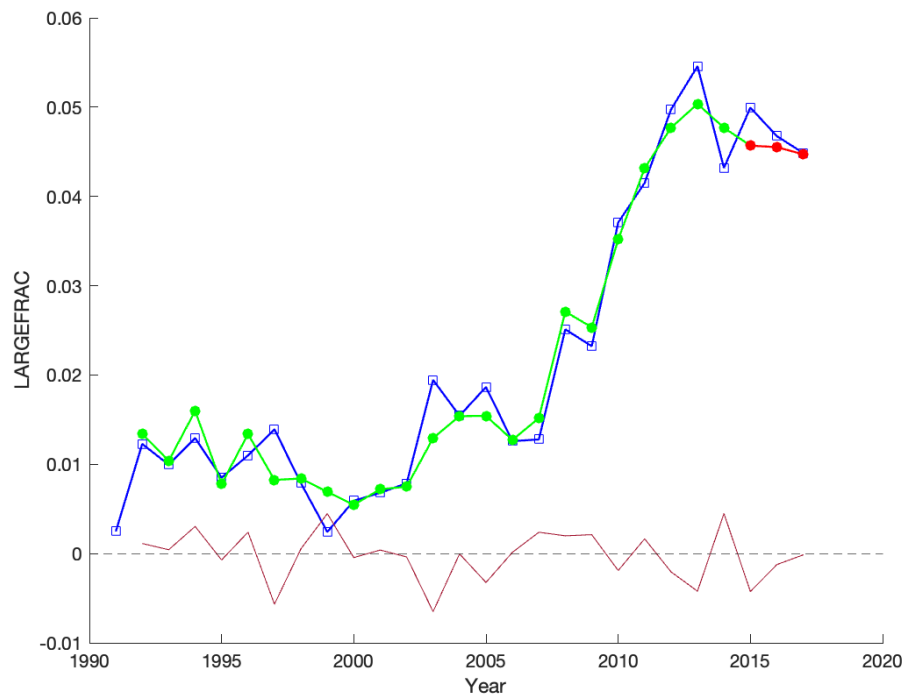


Figure 5.15 NARMAX fit versus fraction of sampled *Gadus morhua* population in IMR-PINRO database >100cm in length. Blue: Observed data, Green: NARMAX fit to training data, Thick-Red: NARMAX fit to test data, Thin-Red: Difference between Observed and NARMAX fit.

The optimal model for LARGEFRAC is of degree 1, with a maximum lag of one year, no autoregressive terms has six parameters. Model fit is shown in Figure 5.15. Model performance is reasonably good, performing better than the model for SMALLFRAC but not as well as for MEDFRAC. The MAPE on training and test data are 19.00% and 3.83% respectively. Performance measures for this model are listed in Table 5.22. Visual inspection of the model shows that the model successfully captures the broad trends in the observed data but fails to characterize the interannual detail at points. For example, the period of sudden significant increase in LARGEFRAC beginning in 2006 is generally identified by NARMAX, but in the periods 1995 - 1999 and 2002 - 2005, the model struggles to fit.

The model structure is of degree 1, with 5 variable parameters and 1 constant value. These parameters are listed in Table 5.23. The most significant variable parameter is PB\_PFRAC(t-01), which is the fraction of diet accounted for by *Pandalus borealis* during the previous year, with an

ERR of 18.82. The most significant parameter overall is the constant value of 0.024, with an ERR of 61.10. The remaining terms have ERR between 16.79 - 0.38. Of the variables selected for inclusion, one is a diet measure, two are population measures and two are spatial overlap measures.

*Table 5.22 NARMAX model performance measures for LARGEFRAC*

	<b>COR</b>	<b>VAF</b>	<b>NRMSE</b>	<b>MAE</b>	<b>MAPE</b>
Training	0.98119	0.962735	0.196743	0.00218821	18.9944
Test	0.874136	0.312716	0.503383	0.00187775	3.82669

*Table 5.23 NARMAX model structure for LARGEFRAC (Variable Explanations in Appendix E)*

<b>Parameter</b>	<b>Coefficient</b>	<b>ERR</b>
<b>PB_PFRAC(t-01)</b>	-0.0018887	18.8262
<b>constant</b>	0.02359	61.0991
<b>TOTSBIO(t-01)</b>	0.0037631	16.7581
<b>GMM_MA_S_OV(t-01)</b>	-0.011354	1.21815
<b>FBAR(t-01)</b>	-0.0030846	0.388816
<b>GMM_GMS_S_OV(t-01)</b>	-0.0023207	0.375069

## 5.4 Discussion

In this chapter we have demonstrated the success of applying a NARMAX modelling approach to many critical phenomena relevant to the trophic role of Barents Sea cod. To interpret these results, we begin by considering the absence of expected variables in the model structures, and the unintuitive interpretation of those variables which were included. The model selection process identifies orthogonal features, so highly correlated parameters will not be present in the final model. This could mean that certain variables encode similar information, and when NARMAX chooses a parameter to include which reduces error by the highest amount, it may choose a correlate of a more interpretable variable. For example, if surface temperature was highly correlated with an overlap measure, NARMAX may retain the less easily interpretable overlap measure instead because it contains marginally more information about the target variable within the parameter in which it is used. This is a correct procedure for generating the best model, and it may reveal an interesting dimension of the system, but it can make it difficult to interpret specific model structures.

Next, we consider why some models were successful while others were not. When a simple model which performs quite poorly is the optimal choice after the model selection and hyperparameter search has been carried out, this indicates that there are missing variables which are integral to the system being modelled, and no data that is available to NARMAX is capable of explaining the variability any further. Identifying those missing variables can be difficult, especially when variables which we would expect to be informative and are included end up not being used at all, for example our measure of *Mallotus villosus* biomass was not used in the optimal model for *Mallotus villosus* consumption by cod, even though we might expect that these two measures should be related (Fall, 2019) .

Consumption of *Boreogadus saida* appears as an important explanatory variable in several models, it's unclear exactly why consumption of this species recurs so frequently but there are several possible explanations. *Boreogadus saida* occupies a similar trophic niche to *Mallotus villosus* but occupies a different spatial range. As our results in Chapter 4 suggest an expansion in the distribution of *Gadus morhua* into the northeast Barents Sea, this increases the exposure between cod and polar cod. It is possible that the consumption of *Boreogadus saida* is correlated with several important ecosystem properties which drive many of the characteristics we have modelled, acting as

a sort of proxy. The relationship between *Gadus morhua* and *Boreogadus saida* is further explored in Chapter 6.

In several of the models, constant terms were found to be highly significant, particularly in the diet measures. We should be sceptical about the interpretation of these terms, as they are unlikely to describe true ecological features of the system and instead encode an approximation of some other dynamics at play. They likely indicate missing variables, or some autoregressive relationship that has not been captured within the hyperparameter bounds used in this study. Models which rely on a constant term are more likely to be overfitting to the data, and should the underlying dynamics which they obscure change significantly, these models would fail to capture the result. That is to say, these models are representing phenomena that are not currently varying significantly, and without observations of variation, NARMAX cannot identify any drivers of variation.

There are no clear differences between model structures across target groups (prey consumption vs population parameters vs size structure). While we know that prey consumption is driven by opportunity and optimal foraging theory (Townsend and Winfield, 1985), dependent on relative densities and overlap. NARMAX identifies significant correlations between consumption of species which occupy the same position (e.g. *Boreogadus saida* and *Mallotus villosus*) as high energy, high effort prey (Hop and Gjørseter, 2013). Likewise, size structure is highly related to temperature (Brander, 1995) and the availability of suitable prey to support larger individuals (Floeter and Temming, 2003). As NARMAX did not directly use any temperature measures, but instead used measures of overlap between, for example, large cod and *Mallotus villosus*, it suggests that some elements of biotic drivers are better represented than the effects of temperature, but interpretation is difficult. Finally, biomass and recruitment are functions of the environment as well as population density dependent effects, the abundance of trophically important prey species and match-mismatch of cod larvae with suitable conditions for survival (Durant et al., 2007; Endo et al., 2022).

NARMAX used autocorrelation to explain variation in total biomass, which is useful if not particularly interesting, but the most informative feature for recruitment was related to the number of unique prey in diet during the previous year, which could be a proxy for the probability of suitable prey being available at the appropriate time to support survival during the important period before recruitment. It is difficult to directly relate what we already know about the factors driving these measures and the NARMAX model structures, but they do provide a powerful tool for prediction and a starting point for refinement and ecological inquiry.

This study has several limitations. The first is that the period under study is very short, 27 data points is at the lower end of feasibility for the application of NARMAX which is often applied to engineering problems with thousands of points. This has limited our options for model validation. As mentioned previously, hierarchical partitioning methods for cross-validation of time series data were too sensitive to changes in training set size to pursue. Further, like all regression models, model performance on out of sample data is dependent on the training data being representative of the full variability of the system. For this reason, we should be careful when extrapolating insights from this model into other time periods, before or afterwards. Extending the length of our training period would help to increase the robustness of the model to a wider period of time.

Another possible limitation is that the NARMAX modelling was carried out using a desktop workstation, which due to memory and processing speed limits, required strict limits to be placed on the hyperparameter space explored. Although these limits were determined based on prior knowledge of the system, it is possible that some improvements could be made by considering long lag times or higher model degrees, but these are uncommon in other published NARMAX studies.

To improve this work, extending the data period further into the past and creating a longer time series should yield beneficial results, however, finding sufficient relevant historical data for all variables of interest is a major challenge. In our case, the study period was determined by the availability of ocean reanalysis data for physical environmental variables used in the construction of Maxent distribution models, and that data debt was carried through to this study. As investigating the spatio-temporal dynamics of cod diet and spatial overlap with key prey species was a core objective of this study, we had to accept this limitation.

## Chapter 6 - Discussion

We stated three aims in the Introduction of this thesis:

- Aim 1 - To identify the spatio-temporal and ontogenetic dimensions of variability in the diet of Barents Sea cod.
- Aim 2 - To model the distribution of Barents Sea cod and key prey species over time to reveal changes in distribution driven by environmental change.
- Aim 3 - To model key ecological measures of the Barents Sea cod stock and quantify the system of factors that drive variability, incorporating new information about temporal variability in predator-prey spatial overlap.

Through a combination of data analysis and statistical modelling, we have pursued these aims and uncovered new knowledge about the Barents Sea ecosystem and the role of *Gadus morhua* within it. In this chapter, we present our main findings pertaining to each aim and discuss our interpretation of those results, how they relate to the extant literature, and the value of our findings. We separate the discussion into three subsections corresponding to our research aims.

## 6.1. Spatio-temporal and ontogenetic patterns in the diet of Barents Sea cod

Chapter 2 analysed the spatio-temporal and ontogenetic structure of cod diet through the IMR-PINRO database. We analysed the size and age structure of *Gadus morhua* in space and time. We found spatio-temporal heterogeneity in the ontogenetic structure of the population generally in agreement with the existing literature. Spatially, we found that individuals sampled in the deep water in the north-eastern Barents Sea tend to be larger than those in the centre and south, consistent with existing studies (Ingvaldsen et al., 2017). Temporally, we also see that the average size of individuals appears to have increased over the study period, with a more significant fraction of cod sampled falling into the upper length deciles in the final years of the data than at any time previously. The latter period of the study is characterised by higher temperatures (Boitsov et al., 2012) reaching a peak in 2015-2016 (ICES, 2021) which has been positively associated with cod growth rate (Brander, 1995). Recent studies have found that length at age in closely related species *Boreogadus saida* is negatively correlated with sea-ice coverage (Dupont et al., 2020), which is also lower in the latter years of the study. We observed similar patterns in the population's age distribution, within expectations, as the two measures are closely related.

Next, we explored the spatio-temporal patterns in the diet of Barents Sea cod. We found that diet was highly variable across space and time and was ontogenetically stratified within the population, in agreement with previous studies (Eriksen et al., 2021; Holt et al., 2019; Townhill et al., 2021). While *Mallotus villosus* dominates overall diet, we found that a range of prey groups became more important when examining specific subregions of the Barents Sea. For example, the importance of *Boreogadus saida* as a prey item in the north/northeast region (Hop and Gjørseter, 2013), and when considering specific periods in time, particularly when we examined the diet of different size groups of the cod population (Holt et al., 2019). While previous studies have examined continuous ontogenetic dietary patterns or examined existing groups, our novel hierarchical clustering approach identified three groups with distinct diet profiles: 0-20cm, characterised by consumption of zooplankton and benthos consistent with previous studies of juvenile cod diet (Dalpadado and Bogstad, 2004); 20-100cm, representing the bulk of the mature cod stock with a diverse diet profile and 100cm plus, a group largely defined by the significant proportion of diet accounted for by cannibalism. Cannibalism in *Gadus morhua* has been previously correlated strongly with predator length and the abundance of juvenile cod (Bogstad et al., 1994; Yaragina et al., 2009). We found

that prey diversity differs between these groups, with the small and large groups having less diverse diets than the general population, likely due to the availability of appropriately sized prey being more restricted for the smallest or largest individuals, and the larger range of sizes in the 20-100cm group encompassing a wider range of preferable prey lengths. We also found evidence that diet diversity may be increasing over time in the small and medium cod groups, which is a new finding, but is in agreement with previous studies which have proposed increased trophic linkages between species in the Barents Sea as a result of warming (Fossheim et al., 2015).

Our analysis shares some features with the analysis by Holt et al. in 2019. We used the prey categories identified by Holt in our analysis of diet in Chapter 2, though while Holt's analysis was structured around the relationship between cod length and diet and interannual patterns, our analysis also explored the spatial dimensions of diet. Holt observed that diet diversity increases as cod size increases (up to about 90cm), which our results agree with. However, our finding that there is a significant trend of increasing diversity among cod between 0-100cm goes one step further than Holt's analysis. While we agree with Holt's assessment that the increased overlap between *Boreogadus saida* and *Gadus morhua* in the north and east of the Barents Sea does not result in an apparent increase in dietary importance for the species overall, or spatial analysis does show that polar cod is indeed an important prey item where overlap is occurring. The quantitative importance of *Boreogadus saida* consumption is one of the key outcomes of this study.

Other existing studies of the IMR-PINRO dataset have explored more focused aspects of diet, such as the rise in consumption of snow crab (*Chionoecetes opilio*) (Holt et al., 2021), which is emerging as a new major prey item for Barents Sea cod. Others have explored longer periods of diet data by incorporating quantitative and qualitative measures of Barents Sea cod diet from other data sources (Townhill et al., 2021, 2015). Extending the data period back to the 1930s shows a consistent pattern of high interannual diet variability and significant long term evolution, for example, the fall of herring as a top prey item since the mid-century and the rising importance of capelin, crustaceans and other fish species.

## 6.2. Temporal variability in the distribution and overlap of Barents Sea cod and critical prey species

Chapter 3 presented a methodological analysis of using Maxent to produce time-sensitive distribution models for cod and critical prey species. Our findings match patterns identified in the existing literature. Seasonal models have been shown to better predict the distribution of highly mobile marine species in environments with significant variability in temperature across seasons (Mannocci et al., 2017). Further, a seasonal scale is ideal for investigating the macroscale patterns in diet and overlap between species in the Barents Sea, particularly between cod and capelin (Eriksen et al., 2021a; Fall et al., 2018). Our identification of different model structures for subgroups *Gadus morhua* follows expectations, as the tolerance of more extreme environments should increase with size (Nakken and Raknes, 1987; Ottersen, 1998; Righton et al., 2010), so factors constraining distribution should be different for individuals at different life-history stages.

In Chapter 4, we applied Maxent to map the seasonal distribution of cod and key prey species across the period 1991-2017 and examined the spatial overlap between groups and the changing distribution over time. We found significant interannual variability in the modelled species' total distribution cover and the overlap between predator-prey pairs. This is consistent with the existing body of literature, where cod distribution follows suitable temperatures, which vary at seasonal scales (Fall et al., 2018; Nakken and Raknes, 1987). Generally, distribution extent and species overlap were not significantly different between summer and winter models. Though we expected a difference due to temperature, Fall et al. 2018 identified an expansion in the distribution of cod during the winter as a result of increased abundance following spawning. This highlights a potential weakness in our analysis because we have not included any measures of density or abundance, perhaps an interesting avenue for future work. Distribution is related to density by ideal free distribution theory (Kennedy and Gray, 1993) and a study of north sea *Gadus morhua* (Blanchard et al., 2005) found that during periods of low abundance, cod distribution more closely matched ideal temperature ranges. The only species to have a statistically significant variation in seasonal distribution cover was *Gadus morhua* (*L.*). We found that many modelled groups showed either multi-year periodicity in distribution area, or followed a trend of increasing distribution area across the study period. No modelled groups in either season suggested a significant trend of decreasing distribution area. Also, we found a consistent pattern of suitable habitat movement into the northeast Barents Sea. In the latter years of the study, every modelled group displayed at least some expansion

into the northeast compared to earlier model predictions. This finding supports the body of literature which suggests that borealization of the Barents Sea is taking place (Aune et al., 2018; Fossheim et al., 2015) as increasing water temperatures loosen restrictions on suitable habitats for many boreal species, increasing overlap and trophic linkages between species. As a counterpoint however, we did not find any evidence that the distribution of *Boreogadus saida*, an arctic species, was decreasing despite previous studies suggesting that increasing temperatures would lead to poorer quality habitats for the species and limit distribution (Eriksen et al., 2015). It is possible that the negative impact of higher temperatures is not currently sufficient to significantly reduce the suitable habitat area for *Boreogadus saida*.

Our results provide further evidence that increasing water temperatures are responsible for an expansion of the suitable environment available for boreal and arctic-boreal species in the Barents Sea into the north and east Barents Sea (Eriksen et al., 2017; Frainer et al., 2017; Renaud et al., 2012), and the borealization of arctic communities (Fossheim et al., 2015; Kortsch et al., 2015). The pivotal role of temperature in the Barents Sea as a primary determining factor in species distribution has long been identified (Dalpadado et al., 2009; Nakken and Raknes, 1987; Ottersen, 1998). Our results suggest that temperature is the most important factor constraining the distribution of Barents Sea cod, but the relationship between northern extent and surface or bottom temperature is not linear. In particular, we found that *Gadus morhua* (*L*) demonstrated almost none of the northern expansion in the latter years of the study that the smaller cod size classes did. We suggest that biotic factors not accounted for in our model are more important than the physical environment under the current regime for determining the environmental suitability for the largest cod individuals. As the group with the highest tolerance for lower temperature, we may have expected them to be more widely distributed than smaller cod, but they have the smallest distribution area of all cod size groups. The reason for this is likely to be related to the availability of sufficient food resources (Friman et al., 2008; Hunsicker et al., 2013; Trainor et al., 2014). As our analysis in Chapter 2 shows that the number of large individuals is increasing, understanding the factors specifically driving their distribution will become more important in the future.

### 6.3. Drivers of variability in the diet, demographics and size structure of Barents Sea cod from 1991-2017

Chapter 5 used NARMAX to quantify the relationships between key ecological measures, including population demographics, size structure, diet, and spatial overlap over time. We were able to successfully model consumption by fraction of total weight in diet for all four prey species as well as cannibalism. Two of our consumption models, for *Mallotus villosus* and *Pandalus borealis* performed significantly better than our models for consumption of *Melanogrammus aeglefinus*, *Boreogadus saida* and cannibalism. The factors driving consumption varied across species. Consumption of *Mallotus villosus*, was negatively correlated with a feature consisting of spawning biomass and the consumption of *Boreogadus saida*, with an ERR of over 75%. This matches our current understanding of the role of *Boreogadus saida* in diet; it fulfils a similar trophic niche as a prey item (Hop and Gjørseter, 2013). As *Gadus morhua* extends further into the north, we may see continued increase in overlap with *Boreogadus saida*, and therefore more consumption, and less consumption of *Mallotus villosus* (Renaud et al., 2012). We found that variability in consumption of *Boreogadus saida* was best explained by a positive correlation to overlap with *Gadus morhua* (L) with an ERR of almost 20%, and a negative correlation to the proportion of the cod population > 100cm (~2%) and overlap with *Gadus morhua* (S) (~1%). These results suggest that increased overlap between large cod subpopulations and *Boreogadus saida* may result in a prioritisation of polar cod as a prey item over *Mallotus villosus*. We see another signal that *Boreogadus saida* may be preferred as prey over existing dietary sources. Our model for consumption of *Pandalus borealis* also suggests a negative correlation with a combination of *Gadus morhua* recruitment and the consumption of *Boreogadus saida* (73% ERR). Consumption of *Melanogrammus aeglefinus* is positively correlated with total prey diversity (20% ERR), which may reflect that species role as a predator with a diverse diet (Tam et al., 2016), occupying areas with more diverse prey assemblages. A study of the interactions between *Gadus morhua* and *Melanogrammus aeglefinus* as a result of climate fluctuations found that predation between the two was greater during warmer years (Durant et al., 2020) and was related to the abundance of *Melanogrammus aeglefinus*. Additionally, higher temperatures in the arctic are associated with borealization of communities (Fossheim et al., 2015), which is likely to increase prey diversity due to an influx of invasive species and new spatial overlap boundaries (Kortsch et al., 2015). The increase in prey diversity could therefore be an indicator of higher temperatures, more food availability for *Melanogrammus aeglefinus* and therefore higher abundances and higher levels of trophic interaction. Finally, our model of cannibalism suggests

significant positive autocorrelation with previous levels of cannibalism (83% ERR). The next most informative term is a positive correlation with the consumption of *Melanogrammus aeglefinus* (5% ERR). Previous studies have investigated the causes of cod cannibalism and found that it increases with size, and is driven by the biomass of large cod, capelin and the abundance of small cod (Yaragina et al., 2018). Our model shows a slightly negative correlation with total biomass (< 1% ERR) and a slight positive correlation between cannibalism and the overlap between small and large cod (< 1% ERR). None of our models of diet use a measure of temperature or other physical environmental parameters. We suggest that the information encoded in these variables is already encoded in measures of consumption, overlap and biomass.

We found a positive correlation between total spawning biomass and the number of landings from the previous year (22% ERR). As fisheries management prohibits trawls in spawning grounds in an effort to limit catch of juvenile individuals, if there are more landings than usual in a given year, it seems reasonable that this is a response to a high abundance or density of spawning age cod. This is consistent with the fact that the Barents Sea cod stock is growing, if the population was decreasing, we might expect to see a negative correlation with landings instead. Modelling recruitment was less successful, but we were able to achieve VAF scores of 60% on training data and 80% on our three test points. The most informative feature indicates a positive correlation with the number of unique prey available squared (66% ERR) - a quadratic relationship. As discussed previously in this section, the number of unique prey is related to increasing temperatures and the borealization of the ecosystem, and actually encompasses a wide range of first order climate effects. The only other dynamic feature in the model is a positive correlation with the overlap between *Gadus morhua* (L)/*Gadus morhua* (M) and *Gadus morhua* (M)/*Gadus morhua* (S) (7% ERR). This suggests that recruitment is higher when the area suitable for the entire cod population is larger, which in turn suggests some density dependent effects. Indeed, previous studies have established that recruitment variability is highly sensitive to density effects in northeast arctic cod (Dingsør et al., 2007; Fogarty et al., 2001), with a primary mechanism being cannibalism, which operates as a regulatory factor dampening recruitment variability (Fogarty et al., 1991).

The final group of variables modelled were size structural: the fraction of the population accounted for by individuals < 20cm [*Gadus morhua* (S)], between 20 and 100cm [*Gadus morhua* (M)], and > 100cm [*Gadus morhua* (L)]. NARMAX performed best at predicting the proportion of *Gadus morhua* (M) in the population. The most informative feature in that model was a positive correlation with the overlap between *Gadus morhua* (L) and *Melanogrammus aeglefinus* (78% ERR), squared,

with a three year lag. Terms like this are particularly difficult to interpret. As discussed prior, an increase in overlap between large cod and haddock is likely related to rising temperatures, and the biotic effects of rising temperatures. This is a relationship which would be difficult to find from theory, but statistical methods may reveal. In cases like this, such complex terms may indicate complex dynamics which are heavily obscured or unintuitive, and more work needs to be done to make sense of them. The model performance is undeniable, however, with less than 1% MAPE across training and test points, we are successfully predicting the variability in this measure. Consider also how our good model performance here relates to our good performance for predicting total biomass - over 90% of the cod population falls within *Gadus morhua* (*M*) - we should expect the two measures to be closely related. Performance for models predicting the proportion of *Gadus morhua* (*L*) and *Gadus morhua* (*S*) was similar. The most informative dynamic feature for the large group was a negative correlation with the fraction of *Pandalus borealis* in diet (19% ERR), followed by a positive correlation with total spawning biomass (17% ERR). Previous studies of interaction between *Gadus morhua* and *Pandalus borealis* in the Barents Sea have suggested an inverse correlation between the abundances of the two species (Berenboim et al., 2000), which is driven by increased predation of *Pandalus borealis* when cod abundance is high. For *Gadus morhua* (*S*), our most informative feature was a negative autoregressive correlation with the previous year's fraction (89% ERR). Like recruitment, this model is difficult to interpret and the lower relative performance is likely due to missing relevant factors, such as mortality-at-age estimates. This model achieves reasonable MAPE (20.2% in training data and 6.1% in test data) but very poor VAF, at effectively 0. If the absolute proportion of the population falling below 20cm were to suddenly and dramatically change, this model would fail to capture it.

Ultimately, although our models were successful in explaining some of the variance of the target measures, they are difficult to interpret ecologically in many cases. As discussed elsewhere in this thesis, many of these results suggest that the model has identified factors which are correlated with the target measures, but not necessarily directly causative. So what is the use of this approach? We suggest that NARMAX is a powerful tool for identifying relationships between time series data, but it can only identify true relationships between two measures if the appropriate data is available. Some suggestions of data which we would have liked to include are made in Chapter 7. Powerful black box models are not a suitable replacement for expert domain knowledge, but may a) provide a quantitative structure useful for making predictions in the short term and b) suggest new directions of inquiry from the identification of obfuscated relationships between ecosystem variables.

## Chapter 7 - Conclusions

We have found that rising temperatures in the Barents Sea affect the distribution, demographics and diet of Barents Sea cod. We have identified a northward shift in a suitable environment for *Gadus morhua* and all of the prey species modelled with Maxent in both summer and winter due to increasing temperatures, sea ice loss, and possibly trophic density effects. This shifting of spatial distribution is changing the spatial overlap between species habitats, supporting existing evidence of the borealization of the arctic waters in the Barents Sea. We also found that environmental variability affects *Gadus morhua* nonuniformly, with different size groups responding differently in space and time.

We successfully modelled many key ecological measures, including population, diet and size structure measurements of *Gadus morhua*. We found strong evidence that the inclusion of variables representing the spatial overlap between cod and its prey provided novel information to our system identification model, improving model fit and predictive power. We found evidence that rising temperatures may increase the significance of *Boreogadus saida* as a prey item, while reducing the significance of *Mallotus villosus* and *Pandalus borealis* due to the increase in access to polar cod. We also found that borealization as a result of rising temperatures may increase prey diversity for cod and may lead to an increase in the consumption of *Melanogrammus aeglefinus*, possibly due to the positive effects of temperature on the abundance of both species.

Ultimately, we proved the potential of Maxent and NARMAX as tools to uncover quantitative relationships between critical parameters relating to *Gadus morhua*, its role in the Barents Sea food web and ecosystem. The results of our study add to the body of knowledge on how climate variability affects this ecosystem and demonstrate in many ways how complex and heterogeneous this response is, highlighting the difficulties of making predictions about the ecosystem state and, therefore, management decisions.

### 7.1. Limitations of this study

The IMR-PINRO database has several limitations that may affect our results. First, the sampling effort is not evenly distributed across the study period. The number of stations surveyed has been expanded since the beginning of the surveys, with most or all of the new stations being in the north/northeast Barents Sea. This introduces some spatial bias in our occurrence records for Maxent

modelling. However, the expansion of the surveys is motivated by a) the ability for vessels to access ice-free waters and b) following the limit of the distribution of *Gadus morhua*. As a result, the expanded sampling follows a real shift in the conditions of the Barents Sea cod stock and our attempts to minimise spatial bias with occurrence thinning in environmental space etc. should provide some countermeasure (Fourcade et al., 2014; Warren et al., 2014). Another limitation is that the surveys are conducted primarily with bottom trawls, meaning that individuals who tend to inhabit areas higher in the water column are less likely to be sampled (Engas and Godø, 1986). As cod is a demersal species, this is the best way to sample for them consistently, and some samples are collected by pelagic trawl (Mehl and Yaragina, 1992).

Another limitation is the lack of sufficient occurrence records for prey species. This study created prey occurrence records as proxies from their occurrence in the stomach of cod from the IMR-PINRO database. There are three possible systematic biases present using this method, one of which we have attempted to address and the other two which are difficult to reduce. The first source of systemic bias is that the species marked as an occurrence from a cod stomach may have been carried far from the site at which it was consumed. We attempted to limit the effects of this bias by filtering possible occurrences to only records with the minimum degree of digestion, which is defined as being effectively an easily identifiable organism that has yet to begin effective digestion. This limits the amount of time that the prey item may have travelled away from the consumption site to several hours or so. Even if the cod sampled had continuously travelled away from the environment in which that prey item was consumed during that time, the spatial error generated as a result should be minimal. Previous studies of cod diet attempting to relate stomach contents with foraging theory have found that the availability of prey may be a more important factor than prey preference (Floeter and Temming, 2003; Pinnegar et al., 2003), potentially suggesting that the species identified in stomachs may be more prevalent within their local environment than other prey items which are more difficult to catch. Though we do not consider prey abundance, it may provide some more evidence that the occurrence of a specific prey item in diet represents that it was consumed within a suitable environment for large numbers of its species. The second source of bias is that it selects individuals within a species that co-occupy space with *Gadus morhua* by default and does not sample any individuals from a hypothetical population area that is entirely inaccessible for Barents Sea cod. This is an extension of a fundamental problem with conducting surveys for species distributions. The amount of bias introduced by this problem is directly related to the real overlap of species niches within the region, so it is likely to be more of an issue with *Boreogadus saida* than *Mallotus villosus* records, for example. Finally, this data collection method is biased in favour of

individuals caught by the bottom trawl survey, with the same issues as we described in the previous paragraph. If specific sizes of cod are favoured in the survey as a natural result of their position in the water column, we may expect a similar bias in the length and type of prey found. This is likely to result in absences of particular species within an area that inhabit it but can avoid predation by the subgroup of cod sampled. As Maxent is a presence-only model, we may have avoided some of the methodological risks that this bias might have introduced as, as long as there are sufficient occurrence records to build a model, the principle of maximum entropy should not overzealously mark false absence sites as unsuitable.

Our layers from ocean reanalysis may introduce some systematic error. As spatially explicit data is required for Maxent and some of the environmental rasters generated are based on the extrapolation of measured data, there could be some failure to capture the high-resolution dynamics which may have existed. However, studies have shown that ocean reanalysis data is sufficient and suitable for use in species distribution modelling (Becker et al., 2016; Tyberghein et al., 2012; Xie et al., 2017).

Another limitation is the data debt incurred by connecting the outcomes of our Maxent modelling with NARMAX, which limited our scope of study to the years 1991 - 2017. The origin of this limited data is in the environmental layers used to create Maxent models at a short temporal resolution. As spatiotemporally explicit layers are required to cover any modelling period, this limits our approach to times when such data is available. In our case, the longest period for which unbroken environmental data lined up with our available diet data was 1991 - 2017, with layers extracted from a hindcasted ocean reanalysis product. This limitation meant that we could not take full advantage of the IMR-PINRO stomach database, which would have added seven more years to our NARMAX models, allowing us to model from 1984, and likely improved performance.

## 7.2. Further work

The methodology used in this study could be used to predict the future state of the Barents Sea cod population. Maxent operates independently of time and could be used to predict the distribution of cod and other species under future climate scenarios (Hijmans and Graham, 2006) and in the past e.g. (Bigg, 2014; Bigg et al., 2008). Hindcasting seasonal Maxent models to the early 20th century with extended records from the data used by (Townhill et al., 2021) would allow us to compare distribution today with recent periods of similarly high temperatures in the region, and provide a natural parallel with the extended period of diet data. One risk to projecting Maxent models to periods in the far past or future is that if conditions are present in the new scenarios which are beyond the limits of the period upon which the Maxent model was trained, the risk of error increases significantly (Fitzpatrick and Hargrove, 2009), and may be compounded by the inherent uncertainty of future climate predictions (Beaumont et al., 2008). Since NARMAX requires a sequential time series with no missing data, predicting changes in ecosystem measures in the far future or past is infeasible. However, using NARMAX to predict the next several years of a target measure is possible if the appropriate input data is available, or can be independently estimated. This could be particularly effective for measures such as biomass, which we have demonstrated can be remarkably well modelled by NARMAX and is highly dependent on the autoregressive term, which should make prediction at least 1 year ahead a feasible task.

It would also be interesting to extend this methodology to a wider range of prey species, as we discovered that changes in diet could be predicted by information about the consumption of other prey items, which each encode layers of environmental and population dynamic data. Two major candidates for this expansion would be *Clupea Harengus* (Atlantic herring) and *Chionoecetes opilio* (Snow crab), the former once being a primary prey item (Townhill et al., 2021) and the latter being an invasive species which has settled in the Barents Sea and has become a major prey item in recent years (Holt et al., 2021). Finally, this methodology could be effectively applied to study the consequences of our observed conclusions. An obvious question is: what will happen to the *Boreogadus saida* population if increasing temperatures lead to higher predation by *Gadus morhua*? *Boreogadus saida* is a clear species of concern as temperatures rise and borealization advances (Renaud et al., 2012).



## Bibliography

- Aanes, S., Alekseev, G., Anisimova, N., Arneberg, P., Baik, B., Bambulyak, A., Belikov, S., Berenboim, B., Berchenko, I., Berthinussen, I., Bjerkemo, O., Bogstad, B., Boitsov, S., Børsheim, Y., Byrkjedal, I., Cochrane, S., Dalpadado, P., Denisenko, N., Denisenko, S., Zolotariov, P., 2009. Joint Norwegian-Russian environmental status 2008. Report on the Barents Sea Ecosystem. Part I – Short version.
- Acevedo, P., Jiménez-Valverde, A., Lobo, J.M., Real, R., 2012. Delimiting the geographical background in species distribution modelling. *J. Biogeogr.* 39, 1383–1390. <https://doi.org/10.1111/j.1365-2699.2012.02713.x>
- Agnalt, Ann-Lisbeth & Jørstad, Knut & Pavlov, Valery & Olsen, Erik. (2011). Recent trends in distribution and abundance of the snow crab (*Chionoecetes opilio*) population in the Barents Sea. 10.4027/bmecipcc.2010.23.
- Aiello-Lammens, M.E., Boria, R.A., Radosavljevic, A., Vilela, B., Anderson, R.P., 2015. spThin: an R package for spatial thinning of species occurrence records for use in ecological niche models. *Ecography* 38, 541–545. <https://doi.org/10.1111/ecog.01132>
- Albouy, C., Velez, L., Coll, M., Colloca, F., Le Loc'h, F., Mouillot, D., Gravel, D., 2014. From projected species distribution to food-web structure under climate change. *Glob Chang Biol* 20, 730–741.
- Alvsvåg, J., Agnalt, A.-L., Jørstad, K.E., 2009. Evidence for a permanent establishment of the snow crab (*Chionoecetes opilio*) in the Barents Sea. *Biol. Invasions* 11, 587–595. <https://doi.org/10.1007/s10530-008-9273-7>
- Andrews, S., Leroux, S.J., Fortin, M.-J., 2020. Modelling the spatial–temporal distributions and associated determining factors of a keystone pelagic fish. *ICES J. Mar. Sci.* 77, 2776–2789. <https://doi.org/10.1093/icesjms/fsaa148>
- Andriyashev, A.P., Chernova, N., 1995. Annotated list of fishlike vertebrates and fish of the Arctic seas and adjacent waters. *J. Ichthyol.* 35, 81–123.
- Arrigo, K.R., van Dijken, G., Pabi, S., 2008. Impact of a shrinking Arctic ice cover on marine primary production. *Geophys Res Lett* 35, 529.
- Årthun, M., Eldevik, T., Smedsrud, L.H., Skagseth, Ø., Ingvaldsen, R.B., 2012. Quantifying the influence of Atlantic heat on Barents Sea ice variability and retreat. *J. Clim.* 25, 4736–4743. <https://doi.org/10.1175/JCLI-D-11-00466.1>
- Årthun, M., Schrum, C., 2010. Ocean surface heat flux variability in the Barents Sea. *J. Mar. Syst.* 83, 88–98. <https://doi.org/10.1016/j.jmarsys.2010.07.003>
- Atauchi, P.J., Peterson, A.T., Flanagan, J., 2018. Species distribution models for Peruvian plantcutter improve with consideration of biotic interactions. *J. Avian Biol.* 49, jav-01617. <https://doi.org/10.1111/jav.01617>
- Ballard, W., 2011. Predator–prey relationships, in: *Biology and Management of White-Tailed Deer*. CRC Press, pp. 264–299.
- Barton, B.I., Lenn, Y.-D., Lique, C., 2018. Observed atlantification of the Barents Sea causes the polar front to limit the expansion of winter sea ice. *J. Phys. Oceanogr.* 48, 1849–1866. <https://doi.org/10.1175/JPO-D-18-0003.1>
- Beaumont, L.J., Hughes, L., Pitman, A.J., 2008. Why is the choice of future climate scenarios for species distribution modelling important? *Ecol. Lett.* 11, 1135–1146.
- Becker, E., Forney, K., Fiedler, P., Barlow, J., Chivers, S., Edwards, C., Moore, A., Redfern, J., 2016. Moving towards dynamic ocean management: how well do modelled ocean products predict species distributions? *Remote Sens.* 8, 149. <https://doi.org/10.3390/rs8020149>

- Berenboim, B.I., Dolgov, A., Korzhev, V.A., Yaragina, N., 2000. The impact of cod on the dynamics of Barents Sea shrimp (*Pandalus borealis*) as determined by multispecies models. *J. Northw. Atl. Fish. Sci.* 27: 69-75. <https://doi.org/10.2960/J.V27.A6>
- Bigg, G.R., 2014. Environmental confirmation of multiple ice age refugia for Pacific cod, *Gadus macrocephalus*. *Evol Ecol* 28, 177–191.
- Bigg, G.R., Cunningham, C.W., Ottersen, G., Pogson, G.H., Wadley, M.R., Williamson, P., 2008. Ice-age survival of Atlantic cod: agreement between palaeoecology models and genetics. *Proc Biol Sci* 275, 163–172.
- Billings, S.A., 2013. Nonlinear system identification : NARMAX methods in the time, frequency and spatio-temporal domains. Wiley, Sheffield, UK.
- Boeuf, G., Payan, P., 2001. How should salinity influence fish growth? *Comp. Biochem. Physiol. Toxicol. Pharmacol. CBP* 130, 411–423. [https://doi.org/10.1016/s1532-0456\(01\)00268-x](https://doi.org/10.1016/s1532-0456(01)00268-x)
- Bogstad, B., Haug, T., Mehl, S., 2000. Who eats whom in the Barents Sea? *NAMMCO Sci Pub* 2, 98–119.
- Boit, A., Martinez, N.D., Williams, R.J., Gaedke, U., 2012. Mechanistic theory and modelling of complex food-web dynamics in Lake Constance. *Ecol. Lett.* 15, 594–602. <https://doi.org/10.1111/j.1461-0248.2012.01777.x>
- Boitsov, V.D., Karsakov, A.L., Trofimov, A.G., 2012. Atlantic water temperature and climate in the Barents Sea, 2000–2009. *ICES J Mar Sci* 69, 833–840.
- Bozdogan, H., 1987. Model selection and Akaike's Information Criterion (AIC): The general theory and its analytical extensions. *Psychometrika* 52, 345–370. <https://doi.org/10.1007/BF02294361>
- Brander, K.M., 1995. The effect of temperature on growth of Atlantic cod (*Gadus morhua* L.). *ICES J. Mar. Sci.* 52, 1–10. [https://doi.org/10.1016/1054-3139\(95\)80010-7](https://doi.org/10.1016/1054-3139(95)80010-7)
- Casini, M., Hjelm, J., Molinero, J.-C., Lövgren, J., Cardinale, M., Bartolino, V., Belgrano, A., Kornilovs, G., 2009. Trophic cascades promote threshold-like shifts in pelagic marine ecosystems. *Proc Natl Acad Sci U A* 106, 197–202.
- Casini, M., Lövgren, J., Hjelm, J., Cardinale, M., Molinero, J.-C., Kornilovs, G., 2008. Multi-level trophic cascades in a heavily exploited open marine ecosystem. *Proc Biol Sci* 275, 1793–1801.
- Chen, S., Billings, S.A., 1989. Representations of non-linear systems : the NARMAX model. *Int J Control* 49, 1012-1032.
- Cheung, W.W.L., Watson, R., Pauly, D., 2013. Signature of ocean warming in global fisheries catch. *Nature* 497, 365–368.
- Ciannelli, L., Dingsør, G.E., Bogstad, B., Ottersen, G., Chan, K.-S., Gjørseter, H., Stiansen, J.E., Stenseth, N.C., 2007. Spatial anatomy of species survival: effects of predation and climate-driven environmental variability. *Ecology* 88, 635–646.
- Cohen, J.E., Briand, F. and Newman, C.M. (1990) *Community food webs: data and theory*. Springer-Verlag, Berlin. <http://dx.doi.org/10.1007/978-3-642-83784-5>
- Cohen, J.E., Pimm, S.L., Yodzis, P., Saldaña, J., 1993. Body sizes of animal predators and animal prey in food webs. *J. Anim. Ecol.* 62, 67–78. <https://doi.org/10.2307/5483>
- Colwell, R.K., Futuyma, D.J., 1971. On the measurement of niche breadth and overlap. *Ecology* 52, 567–576. <https://doi.org/10.2307/1934144>
- Colwell, R.K., Rangel, T.F., 2009. Hutchinson's duality: the once and future niche. *Proc Natl Acad Sci U A* 106 Suppl 2, 19651–19658.
- Dalpadado, P., Arrigo, K.R., Hjøllø, S.S., Rey, F., Ingvaldsen, R.B., Sperfeld, E., van Dijken, G.L., Stige, L.C., Olsen, A., Ottersen, G., 2014. Productivity in the Barents sea—response to recent climate variability. *PLoS One* 9, e95273.
- Dalpadado, P., Arrigo, K.R., van Dijken, G.L., Skjoldal, H.R., Bagøien, E., Dolgov, A.V., Prokopchuk, I.P., Sperfeld, E., 2020. Climate effects on temporal and spatial dynamics of phytoplankton and zooplankton in the Barents Sea. *Prog. Oceanogr.* 185, 102320.

- <https://doi.org/10.1016/j.pocean.2020.102320>
- Dalpadado, P., Bogstad, B., Eriksen, E., Rey, L., 2009. Distribution and diet of 0-group cod (*Gadus morhua*) and haddock (*Melanogrammus aeglefinus*) in the Barents Sea in relation to food availability and temperature. *Polar Biol.* 32, 1583–1596.
- Dalpadado, P., Ingvaldsen, R.B., Stige, L.C., Bogstad, B., Knutsen, T., Ottersen, G., Ellertsen, B., 2012. Climate effects on Barents Sea ecosystem dynamics. *ICES J Mar Sci* 69, 1303–1316.
- Dolgov, A.V., Yaragina, N.A., Orlova, E.L., Bogstad, B., Johannesen, E., Mehl, S., 2007. 20th anniversary of the PINRO-IMR cooperation in the investigations of fish feeding in the Barents Sea – results and perspectives. *Proc. 12th Nor.-Russ. Symp.* 1990, 44–78.
- Dormann, C.F., Elith, J., Bacher, S., Buchmann, C., Carl, G., Carré, G., Marquéz, J.R.G., Gruber, B., Lafourcade, B., Leitão, P.J., Münkemüller, T., McClean, C., Osborne, P.E., Reineking, B., Schröder, B., Skidmore, A.K., Zurell, D., Lautenbach, S., 2013. Collinearity: a review of methods to deal with it and a simulation study evaluating their performance. *Ecography* 36, 27–46. <https://doi.org/10.1111/j.1600-0587.2012.07348.x>
- Drinkwater, K.F., 2005. The response of Atlantic cod (*Gadus morhua*) to future climate change. *ICES J. Mar. Sci.* 62, 1327–1337. <https://doi.org/10.1016/j.icesjms.2005.05.015>
- Dunne, J.A., Williams, R.J., Martinez, N.D., 2004. Network structure and robustness of marine food webs. *Mar. Ecol. Prog. Ser.* 273, 291–302.
- Durant, J.M., Ono, K., Stenseth, N.Chr., Langangen, Ø., 2020. Nonlinearity in interspecific interactions in response to climate change: Cod and haddock as an example. *Glob. Change Biol.* 26, 5554–5563. <https://doi.org/10.1111/gcb.15264>
- Elith, J., Phillips, S.J., Hastie, T., Dudík, M., Chee, Y.E., Yates, C.J., 2011. A statistical explanation of MaxEnt for ecologists. *Divers. Distrib.* 17, 43–57.
- Embling, C.B., Illian, J., Armstrong, E., van der Kooij, J., Sharples, J., Camphuysen, K.C., Scott, B.E., 2012. Investigating fine-scale spatio-temporal predator–prey patterns in dynamic marine ecosystems: a functional data analysis approach. *J. Appl. Ecol.* 49, 481–492.
- Emmerson, M.C., Raffaelli, D., 2004. Predator–prey body size, interaction strength and the stability of a real food web. *J. Anim. Ecol.* 73, 399–409. <https://doi.org/10.1111/j.0021-8790.2004.00818.x>
- Eriksen, E., Skjoldal, H.R., Dolgov, A.V., Strand, E., Keulder-Stenevik, F., Prokopchuk, I.P., Prokhorova, T.A., Prozorkevich, D., Benzik, A.N., 2021a. Diet and trophic structure of fishes in the Barents Sea: Seasonal and spatial variations. *Prog. Oceanogr.* 197, 102663. <https://doi.org/10.1016/j.pocean.2021.102663>
- Eriksen, E., Skjoldal, H.R., Dolgov, A.V., Strand, E., Keulder-Stenevik, F., Prokopchuk, I.P., Prokhorova, T.A., Prozorkevich, D., Benzik, A.N., 2021b. Diet and trophic structure of fishes in the Barents Sea: Seasonal and spatial variations. *Prog. Oceanogr.* 197, 102663. <https://doi.org/10.1016/j.pocean.2021.102663>
- Eriksen, E., Skjoldal, H.R., Gjørseter, H., Primicerio, R., 2017. Spatial and temporal changes in the Barents Sea pelagic compartment during the recent warming. *Prog Ocean.* 151, 206–226.
- Fall, J., 2019. Drivers of variation in the predator-prey interaction between cod and capelin in the Barents Sea. Doctoral thesis. University of Bergen.
- Fall, J., Ciannelli, L., Skaret, G., Johannesen, E., 2018. Seasonal dynamics of spatial distributions and overlap between Northeast Arctic cod (*Gadus morhua*) and capelin (*Mallotus villosus*) in the Barents Sea. *PLoS One* 13, e0205921.
- FAO Fisheries & Aquaculture - Cultured Aquatic Species Information Programme - *Gadus morhua* (Linnaeus, 1758) [WWW Document], n.d. URL [https://www.fao.org/fishery/culturedspecies/Gadus\\_morhua/en](https://www.fao.org/fishery/culturedspecies/Gadus_morhua/en) (accessed 12.5.21).
- Feng, X., Park, D.S., Liang, Y., Pandey, R., Papeş, M., 2019. Collinearity in ecological niche modelling: Confusions and challenges. *Ecol. Evol.* 9, 10365–10376. <https://doi.org/10.1002/ece3.5555>
- Fernandez, M., Yesson, C., Gannier, A., Miller, P.I., Azevedo, J.M., 2017. The importance of

- temporal resolution for niche modelling in dynamic marine environments. *J. Biogeogr.* 44, 2816–2827. <https://doi.org/10.1111/jbi.13080>
- Fitzpatrick, M.C., Hargrove, W.W., 2009. The projection of species distribution models and the problem of non-analog climate. *Biodivers. Conserv.* 18, 2255. <https://doi.org/10.1007/s10531-009-9584-8>
- Fossheim, M., Primicerio, R., Johannesen, E., Ingvaldsen, R.B., Aschan, M.M., Dolgov, A.V., 2015. Recent warming leads to a rapid borealization of fish communities in the Arctic. *Nat Clim Chang* 5, 673.
- Frainer, A., Primicerio, R., Kortsch, S., Aune, M., Dolgov, A.V., Fossheim, M., Aschan, M.M., 2017. Climate-driven changes in functional biogeography of Arctic marine fish communities. *Proc Natl Acad Sci U A* 114, 12202–12207.
- Francis, J.A., Hunter, E., 2006. New insight into the disappearing Arctic sea ice. *Eos Trans. Am. Geophys. Union* 87, 509–511.
- Frank, K.T., Petrie, B., Choi, J.S., Leggett, W.C., 2005. Trophic cascades in a formerly cod-dominated ecosystem. *Science* 308, 1621–1623.
- Franklin, J., Miller, J.A., 2010. Mapping species distributions: Spatial inference and prediction. Cambridge University Press. <https://doi.org/10.1017/CBO9780511810602>
- Friman, V.-P., Hiltunen, T., Laakso, J., Kaitala, V., 2008. Availability of prey resources drives evolution of predator–prey interaction. *Proc. R. Soc. B Biol. Sci.* 275, 1625–1633.
- Gherghel, I., Brischox, F., Papeş, M., 2018. Using biotic interactions in broad-scale estimates of species' distributions. *J. Biogeogr.* 45, 2216–2225. <https://doi.org/10.1111/jbi.13361>
- Gjørseter, H., Bogstad, B., Tjelmeland, S., 2009. Ecosystem effects of the three capelin stock collapses in the Barents Sea. *Mar Biol Res* 5, 40–53.
- Gjørseter, H., Loeng, H., 1987. Growth of the Barents Sea capelin, *Mallotus villosus*, in relation to climate. *Environ. Biol. Fishes* 20, 293–300.
- Gu, Y., Yang, Y., Dewald, J.P.A., van der Helm, F.C.T., Schouten, A.C., Wei, H.-L., 2021. Nonlinear modelling of cortical responses to mechanical wrist perturbations using the NARMAX method. *IEEE Trans. Biomed. Eng.* 68, 948–958. <https://doi.org/10.1109/TBME.2020.3013545>
- Hall, S.J., Gurney, W.S.C., Dobby, H., Basford, D.J., Heaney, S.D., Robertson, M.R., 1995. Inferring Feeding Patterns from Stomach Contents Data. *J. Anim. Ecol.* 64, 39–62. <https://doi.org/10.2307/5826>
- Hansen, T., Karlsen, Ø., Taranger, G.L., Hemre, G.-I., Holm, J.C., Kjesbu, O.S., 2001. Growth, gonadal development and spawning time of Atlantic cod (*Gadus morhua*) reared under different photoperiods. *Aquaculture* 203, 51–67. [https://doi.org/10.1016/S0044-8486\(01\)00610-X](https://doi.org/10.1016/S0044-8486(01)00610-X)
- Hernandez, P.A., Graham, C.H., Master, L.L., Albert, D.L., 2006. The effect of sample size and species characteristics on performance of different species distribution modelling methods. *Ecography* 29, 773–785. <https://doi.org/10.1111/j.0906-7590.2006.04700.x>
- Hijmans, R.J., Graham, C.H., 2006. The ability of climate envelope models to predict the effect of climate change on species distributions. *Glob Chang Biol.*
- Hjermann, D.Ø., Bogstad, B., Eikeset, A.M., Ottersen, G., Gjørseter, H., Stenseth, N.C., 2007. Food web dynamics affect Northeast Arctic cod recruitment. *Proc Biol Sci* 274, 661–669.
- Hodal, H., Kristiansen, S., 2008. The importance of small-celled phytoplankton in spring blooms at the marginal ice zone in the northern Barents Sea. *Deep Sea Res. Part II Top. Stud. Oceanogr.* 55, 2176–2185.
- Holland, M.M., Bitz, C.M., Tremblay, B., 2006. Future abrupt reductions in the summer Arctic sea ice. *Geophys. Res. Lett.* 33.
- Holt, R., Hvingel, C., Agnalt, A.-L., Dolgov, A., Hjelset, A., Bogstad, B., 2021. Snow crab (*Chionoecetes opilio*), a new food item for North-east Arctic cod (*Gadus morhua*) in the Barents Sea. *ICES J. Mar. Sci.* 78. <https://doi.org/10.1093/icesjms/fsaa168>

- Rebecca E Holt, Bjarte Bogstad, Joël M Durant, Andrey V Dolgov, Geir Ottersen, Barents Sea cod (*Gadus morhua*) diet composition: long-term interannual, seasonal, and ontogenetic patterns, *ICES Journal of Marine Science*, Volume 76, Issue 6, November-December 2019, Pages 1641–1652, <https://doi-org.eres.qnl.qa/10.1093/icesjms/fsz082>
- Hop, H., Gjøsæter, H., 2013. polar cod (*Boreogadus saida*) and capelin (*Mallotus villosus*) as key species in marine food webs of the Arctic and the Barents Sea. *Mar Biol Res* 9, 878–894.
- Hunsicker, M.E., Ciannelli, L., Bailey, K.M., Zador, S., Stige, L.C., 2013. Climate and demography dictate the strength of predator-prey overlap in a subarctic marine ecosystem. *PLoS One* 8, e66025.
- Huse, G., Bakketeig, I., 2018. Resource overview 2018. Report from the Norwegian Institute of Marine Research.
- Hutchings, J.A., Myers, R.A., 2011. Effect of age on the seasonality of maturation and spawning of Atlantic Cod, *Gadus morhua*, in the northwest Atlantic. *Can. J. Fish. Aquat. Sci.* <https://doi.org/10.1139/f93-271>
- ICES, 2017. Report of the Arctic Fisheries Working Group (AFWG). International Council for the Exploration of the Sea, Copenhagen, Denmark.
- Ingvaldsen, R.B., Gjøsæter, H., Ona, E., Michalsen, K., 2017. Atlantic cod (*Gadus morhua*) feeding over deep water in the high Arctic. *Polar Biol* 40, 2105–2111.
- Jakobsen, T., Ozhigin, V.K., 2011. The Barents Sea: ecosystem, resources, management : half a century of Russian-Norwegian cooperation. Tapir Academic Press.
- Jakobsson, M., Mayer, L., Coakley, B., Dowdeswell, J.A., Forbes, S., Fridman, B., Hodnesdal, H., Noormets, R., Pedersen, R., Rebecco, M., Schenke, H.W., Zarayskaya, Y., Accettella, D., Armstrong, A., Anderson, R.M., Bienhoff, P., Camerlenghi, A., Church, I., Edwards, M., Gardner, J.V., Hall, J.K., Hell, B., Hestvik, O., Kristoffersen, Y., Marcussen, C., Mohammad, R., Mosher, D., Nghiem, S.V., Pedrosa, M.T., Travaglini, P.G., Weatherall, P., 2012. The international bathymetric chart of the Arctic ocean (IBCAO) Version 3.0. *Geophys Res Lett* 39.
- Jarnevich, C.S., Talbert, M., Morissette, J., Aldridge, C., Brown, C.S., Kumar, S., Manier, D., Talbert, C., Holcombe, T., 2017. Minimising effects of methodological decisions on interpretation and prediction in species distribution studies: An example with background selection. *Ecol. Model.* 363, 48–56. <https://doi.org/10.1016/j.ecolmodel.2017.08.017>
- Jennings, S., Kaiser, M.J., 1998. The effects of fishing on marine ecosystems, in: Blaxter, J.H.S., Southward, A.J., Tyler, P.A. (Eds.), *Advances in Marine Biology*. Academic Press, pp. 201–352.
- Johannesen, E., Høines, \AAge S, Dolgov, A.V., Fossheim, M., 2012a. Demersal fish assemblages and spatial diversity patterns in the Arctic-Atlantic transition zone in the Barents Sea. *PLoS One* 7, e34924.
- Johannesen, E., Ingvaldsen, R.B., Bogstad, B., Dalpadado, P., Eriksen, E., Gjøsæter, H., Knutsen, T., Skern-Mauritzen, M., Stiansen, J.E., 2012b. Changes in Barents Sea ecosystem state, 1970–2009: climate fluctuations, human impact, and trophic interactions. *ICES J Mar Sci* 69, 880–889.
- Johnson, G.C., Lyman, J.M., 2020. Warming trends increasingly dominate global ocean. *Nat. Clim. Change* 10, 757–761. <https://doi.org/10.1038/s41558-020-0822-0>
- Johnson, S.C., 1967. Hierarchical clustering schemes. *Psychometrika* 32, 241–254. <https://doi.org/10.1007/BF02289588>
- Kearney, M., Porter, W.P., 2004. Mapping the fundamental niche: physiology, climate, and the distribution of a nocturnal lizard. *Ecology* 85, 3119–3131.
- Kjesbu, O.S., Witthames, P.R., Solemdal, P., Greer Walker, M., 1998. Temporal variations in the fecundity of Arcto-Norwegian cod (*Gadus morhua*) in response to natural changes in food and temperature. *J Sea Res* 40, 303–321.
- Kohnemann, S.H.E., Heinemann, G., Bromwich, D.H., Gutjahr, O., 2017. Extreme warming in the

- Kara Sea and Barents Sea during the winter period 2000–16. *J Clim* 30, 8913–8927.
- Kortsch, S., Primicerio, R., Fossheim, M., Dolgov, A.V., Aschan, M., 2015. Climate change alters the structure of arctic marine food webs due to poleward shifts of boreal generalists. *Proc Biol Sci* 282.
- Kotenev, B.N., Kuznetsova, E.N., Bondarenko, M.V., 2009. Investigation of age composition and growth of cod *Gadus morhua* morhua of the Barents Sea in connection with the estimation of its stocks state. *J. Ichthyol.* 49, 47–55. <https://doi.org/10.1134/S0032945209010068>
- Kurlansky, M., 1997. Cod: a biography of the fish that changed the world. Browse Work DLPP Recip. Run.-Up.
- Lindeman, R.L., 1942. The Trophic-Dynamic Aspect of Ecology. *Ecology* 23, 399–417. <https://doi.org/10.2307/1930126>
- Link, J., 2002. Does food web theory work for marine ecosystems? *Mar. Ecol. Prog. Ser.* 230, 1–9.
- Link, J.S., Bogstad, B., Sparholt, H., Lilly, G.R., 2009. Trophic role of Atlantic cod in the ecosystem. *Fish Fish* 10, 58–87.
- Liu, C., Newell, G., White, M., 2015. On the selection of thresholds for predicting species occurrence with presence-only data. *Ecol. Evol.* 6, 337–348. <https://doi.org/10.1002/ece3.1878>
- Lobo, J.M., Jiménez-Valverde, A., Real, R., 2008. AUC: a misleading measure of the performance of predictive distribution models. *Glob. Ecol. Biogeogr.* 17, 145–151. <https://doi.org/10.1111/j.1466-8238.2007.00358.x>
- Lobo, J.M., Tognelli, M.F., 2011. Exploring the effects of quantity and location of pseudo-absences and sampling biases on the performance of distribution models with limited point occurrence data. *J. Nat. Conserv.* 19, 1–7.
- Loeng, H., 1991. Features of the physical oceanographic conditions of the Barents Sea. *Polar Res* 10, 5–18.
- Mannocci, L., Boustany, A.M., Roberts, J.J., Palacios, D.M., Dunn, D.C., Halpin, P.N., Viehman, S., Moxley, J., Cleary, J., Bailey, H., Bograd, S.J., Becker, E.A., Gardner, B., Hartog, J.R., Hazen, E.L., Ferguson, M.C., Forney, K.A., Kinlan, B.P., Oliver, M.J., Perretti, C.T., Ridoux, V., Teo, S.L.H., Winship, A.J., 2017. Temporal resolutions in species distribution models of highly mobile marine animals: Recommendations for ecologists and managers. *Divers. Distrib.* 23, 1098–1109. <https://doi.org/10.1111/ddi.12609>
- Marshall, A.M., Bigg, G.R., van Leeuwen, S.M., Pinnegar, J.K., Wei, H.L., Webb, T.J., Blanchard, J.L., 2016. Quantifying heterogeneous responses of fish community size structure using novel combined statistical techniques. *Glob Chang Biol* 22, 1755–1768.
- Marshall, C.T., Kjesbu, O.S., Yaragina, N.A., Solemdal, P., Ulltang, Ø., 2011. Is spawner biomass a sensitive measure of the reproductive and recruitment potential of Northeast Arctic cod? *Can. J. Fish. Aquat. Sci.* <https://doi.org/10.1139/f98-062>
- McPherson, J.M., Jetz, W., Rogers, D.J., 2004. The effects of species' range sizes on the accuracy of distribution models: ecological phenomenon or statistical artefact? *J. Appl. Ecol.* 41, 811–823. <https://doi.org/10.1111/j.0021-8901.2004.00943.x>
- Mehl, S., Yaragina, N.A., 1992. Methods and results in the joint PINRO-IMR stomach sampling program. Interrelations between fish populations in the Barents Sea. Proceedings of the fifth PINRO-IMR Symposium Murmansk, 12-16 August 1991.
- Merow, C., Smith, M.J. and Silander, J.A., Jr (2013), A practical guide to MaxEnt for modelling species' distributions: what it does, and why inputs and settings matter. *Ecography*, 36: 1058-1069. <https://doi.org/10.1111/j.1600-0587.2013.07872.x>
- Milich, L., 1999. Resource Mismanagement Versus Sustainable Livelihoods: The collapse of the Newfoundland cod fishery. *Soc. Nat. Resour.* 12, 625–642. <https://doi.org/10.1080/089419299279353>
- Muscarella, R., Galante, P.J., Soley-Guardia, M., Boria, R.A., Kass, J.M., Uriarte, M., Anderson, R.P., 2014a. ENM eval: An R package for conducting spatially independent evaluations and

- estimating optimal model complexity for Maxent ecological niche models. *Methods Ecol. Evol.* 5, 1198–1205.
- Muscarella, R., Galante, P.J., Soley-Guardia, M., Boria, R.A., Kass, J.M., Uriarte, M., Anderson, R.P., 2014b. ENMeval: An R package for conducting spatially independent evaluations and estimating optimal model complexity for Maxent ecological niche models. *Methods Ecol. Evol.* 5, 1198–1205. <https://doi.org/10.1111/2041-210X.12261>
- Nakken, O., Raknes, A., 1987. The distribution and growth of Northeast Arctic cod in relation to bottom temperatures in the Barents Sea, 1978–1984. *Fish. Res., Comparative biology, assessment, and management of gadoids from the North Pacific and Atlantic Oceans* 5, 243–252. [https://doi.org/10.1016/0165-7836\(87\)90044-0](https://doi.org/10.1016/0165-7836(87)90044-0)
- Olsen, E., Gjøsæter, H., Røttingen, I., Dommasnes, A., Fossum, P., Sandberg, P., 2007. The Norwegian ecosystem-based management plan for the Barents Sea. *ICES J Mar Sci* 64, 599–602.
- Ottersen, G., 1998. Ambient temperature and distribution of north-east Arctic cod. *ICES J. Mar. Sci.* 55, 67–85. <https://doi.org/10.1006/jmsc.1997.0232>
- Ottersen, G., Planque, B., Belgrano, A., Post, E., Reid, P.C., Stenseth, N.C., 2001. Ecological effects of the North Atlantic oscillation. *Oecologia* 128, 1–14.
- Paine, R.T., 1980. Food webs: linkage, interaction strength and community infrastructure. *J. Anim. Ecol.* 49, 667–685.
- Phillips, S.J., Anderson, R.P., Schapire, R.E., 2006. Maximum entropy modelling of species geographic distributions. *Ecol Modell* 190, 231–259.
- Phillips, S.J., Dudík, M., 2008. Modelling of species distribution with Maxent: new extensions and a comprehensive evaluation. *Ecography* 31, 161–175.
- Phillips, S.J., Dudík, M., Elith, J., Graham, C.H., Lehmann, A., Leathwick, J., Ferrier, S., 2009. Sample selection bias and presence-only distribution models: implications for background and pseudo-absence data. *Ecol Appl* 19, 181–197.
- Puvanendran, V., Brown, J.A., 2002. Foraging, growth and survival of Atlantic cod larvae reared in different light intensities and photoperiods. *Aquaculture* 214, 131–151.
- Puvanendran, V., Brown, J.A., 1998. Effect of light intensity on the foraging and growth of Atlantic cod larvae: interpopulation difference? *Mar. Ecol. Prog. Ser.* 167, 207–214.
- Raes, N., Steege, H. ter, 2007. A null-model for significance testing of presence-only species distribution models. *Ecography* 30, 727–736. <https://doi.org/10.1111/j.2007.0906-7590.05041.x>
- Renaud, P.E., Berge, J., Varpe, Ø., Lønne, O.J., Nahrang, J., Ottesen, C., Hallanger, I., 2012. Is the poleward expansion by Atlantic cod and haddock threatening native polar cod, *Boreogadus saida*? *Polar Biol* 35, 401–412.
- Righton, D.A., Andersen, K.H., Neat, F., Thorsteinsson, V., Steingrund, P., Svedäng, H., Michalsen, K., Hinrichsen, H.-H., Bendall, V., Neuenfeldt, S., Wright, P., Jonsson, P., Huse, G., Kooij, J. van der, Mosegaard, H., Hüsey, K., Metcalfe, J., 2010. Thermal niche of Atlantic cod *Gadus morhua*: limits, tolerance and optima. *Mar. Ecol. Prog. Ser.* 420, 1–13. <https://doi.org/10.3354/meps08889>
- Robinson, N.M., Nelson, W.A., Costello, M.J., Sutherland, J.E., Lundquist, C.J., 2017. A systematic review of marine-based species distribution models (SDMs) with recommendations for best practice. *Front. Mar. Sci.* 4, 421.
- Rose, G., 2018. Atlantic Cod: A Bio-Ecology 1–5. <https://doi.org/10.1002/9781119460701.ch0>
- Sakshaug, E., 2004. Primary and secondary production in the arctic seas, in: Stein, R., MacDonald, R.W. (Eds.), *The Organic Carbon Cycle in the Arctic Ocean*. Springer Berlin Heidelberg, Berlin, Heidelberg, pp. 57–81.
- Sandø, A.B., Nilsen, J.E.Ø., Gao, Y., Lohmann, K., 2010. Importance of heat transport and local air-sea heat fluxes for Barents Sea climate variability. *J. Geophys. Res. Oceans* 115. <https://doi.org/10.1029/2009JC005884>

- Senay, S.D., Worner, S.P., Ikeda, T., 2013. Novel three-step pseudo-absence selection technique for improved species distribution modelling. PLOS ONE 8, e71218.  
<https://doi.org/10.1371/journal.pone.0071218>
- Signorini, S.R., McClain, C.R., 2009. Environmental factors controlling the Barents Sea spring-summer phytoplankton blooms. Geophys. Res. Lett. 36.
- Skagseth, Ø., Furevik, T., Ingvaldsen, R., Loeng, H., Mork, K.A., Orvik, K.A., Ozhigin, V., 2008. Volume and heat transports to the Arctic Ocean via the Norwegian and Barents Seas, in: Arctic–Subarctic ocean fluxes. Springer, pp. 45–64.
- Smedsrud, L.H., Esau, I., Ingvaldsen, R.B., Eldevik, T., Haugan, P.M., Li, C., Lien, V.S., Olsen, A., Omar, A.M., Otterå, O.H., Risebrobakken, B., Sandø, A.B., Semenov, V.A., Sorokina, S.A., 2013. The role of the Barents Sea in the Arctic climate system. Rev. Geophys. 51, 415–449.  
<https://doi.org/10.1002/rog.20017>
- Soberon, J., Nakamura, M., 2009. Niches and distributional areas: Concepts, methods, and assumptions. Proc. Natl. Acad. Sci. 106, 19644–19650.
- Stiansen, J.E., Korneev, O., Titov, O.V., Arneberg, P., Filin, A., Hansen, J.R., Høines, Å.S., Marasaev, S., 2009. Joint Norwegian-Russian environmental status 2008 : report on the Barents Sea ecosystem, part II - complete report. 378 S.
- Stockwell, D.R.B., Peterson, A.T., 2002. Effects of sample size on accuracy of species distribution models. Ecol. Model. 148, 1–13. [https://doi.org/10.1016/S0304-3800\(01\)00388-X](https://doi.org/10.1016/S0304-3800(01)00388-X)
- Suzuki, R., Shimodaira, H., 2006. Pvcust: an R package for assessing the uncertainty in hierarchical clustering. Bioinformatics 22, 1540–1542.
- Townhill, B., Holt, R., Bogstad, B., Durant, J., Pinnegar, J., Dolgov, A., Yaragina, N., Johannesen, E., Ottersen, G., 2021. Diets of the Barents Sea cod (*Gadus morhua*) from the 1930s to 2018. Earth Syst. Sci. Data 13, 1361–1370. <https://doi.org/10.5194/essd-13-1361-2021>
- Townhill, B.L., Maxwell, D., Engelhard, G.H., Simpson, S.D., Pinnegar, J.K., 2015. Historical arctic logbooks provide insights into past diets and climatic responses of cod. PLoS One 10. <https://doi.org/10.1371/journal.pone.0135418>
- Trainor, A.M., Schmitz, O.J., Ivan, J.S., Shenk, T.M., 2014. Enhancing species distribution modelling by characterising predator–prey interactions. Ecol. Appl. 24, 204–216.  
<https://doi.org/10.1890/13-0336.1>
- Traon, P.-Y., Ali, A., Alvarez Fanjul, E., Aouf, L., Axell, L., Aznar, R., Ballarotta, M., Behrens, A., Mounir, B., Bentamy, A., Bertino, L., Bowyer, P., Brando, V., Breivik, L., Buongiorno Nardelli, B., Cailleau, S., Ciliberti, S., Clementi, E., Colella, S., Zuo, H., 2017. The Copernicus Marine Environmental Monitoring Service: main scientific achievements and future prospects. Mercat. Ocean J. 56.
- Tyberghein, L., Verbruggen, H., Pauly, K., Troupin, C., Mineur, F., De Clerck, O., 2012. Bio-ORACLE: a global environmental dataset for marine species distribution modelling. Glob. Ecol. Biogeogr. 21, 272–281. <https://doi.org/10.1111/j.1365-3113.2011.04656.x>
- Vitale, F., Worsøe Clausen, L., Ní Chonchúir, G., 2019. Handbook of fish age estimation protocols and validation methods. Copenhagen.
- Walters, C.J., Maguire, J., 1996. Lessons for stock assessment from the northern cod collapse. Rev. Fish Biol. Fish 6, 125–137.
- Wassmann, P., Reigstad, M., Haug, T., Rudels, B., Carroll, M.L., Hop, H., Gabrielsen, G.W., Falk-Petersen, S., Denisenko, S.G., Arashkevich, E., Slagstad, D., Pavlova, O., 2006. Food webs and carbon flux in the Barents Sea. Prog. Ocean. 71, 232–287.
- Wei, H., Bigg, G.R., 2017. The dominance of food supply in changing demographic factors across Africa: a model using a systems identification approach. Soc. Sci. 6, 122.  
<https://doi.org/10.3390/socsci6040122>
- Wei, H.L., Balikhin, M.A., Gu, Y., Walker, S.N., Boynton, R., 2020. Quantile NARMAX model: modelling uncertainty for data based space weather forecasts 2020, SM035-09.
- Williams, R.J., Martinez, N.D., 2000. Simple rules yield complex food webs. Nature 404, 180–183.

- <https://doi.org/10.1038/35004572>
- Wilmot, C., n.d. *Gadus morhua* (Cod) [WWW Document]. Anim. Divers. Web. URL [https://animaldiversity.org/accounts/Gadus\\_morhua/](https://animaldiversity.org/accounts/Gadus_morhua/) (accessed 12.5.21).
- Wisn, M.S., Hijmans, R.J., Li, J., Peterson, A.T., Graham, C.H., Guisan, A., 2008. Effects of sample size on the performance of species distribution models. *Divers. Distrib.* 14, 763–773. <https://doi.org/10.1111/j.1472-4642.2008.00482.x>
- Wisn, M.S., Pottier, J., Kissling, W.D., Pellissier, L., Lenoir, J., Damgaard, C.F., Dormann, C.F., Forchhammer, M.C., Grytnes, J.-A., Guisan, A., 2013. The role of biotic interactions in shaping distributions and realised assemblages of species: implications for species distribution modelling. *Biol. Rev.* 88, 15–30.
- Xie, J., Bertino, L., Counillon, F., Lisæter, K.A., Sakov, P., 2017. Quality assessment of the TOPAZ4 reanalysis in the Arctic over the period 1991–2013. *Ocean Sci.* 13, 123–144.
- Yaragina, N.A., Kovalev, Y., Chetyrkin, A., 2018. Extrapolating predation mortalities back in time: an example from North-east Arctic cod cannibalism. *Mar. Biol. Res.* 14, 203–216. <https://doi.org/10.1080/17451000.2017.1396342>
- Yodzis, P., Innes, S., 1992. Body size and consumer-resource dynamics. *Am. Nat.* 139, 1151–1175. <https://doi.org/10.1086/285380>

## Appendices

### Appendix A - IMR-PINRO metadata and sampling locations

#### A.1. Table of variables recorded in the IMR-PINRO database

Variable Name	Information	Units
Ser_No_Fish	Serial number for each fish	
Country	Country code denoting either: 58: Norway 90: Soviet Union/Russia	
Ship_kode	Ship identification code	
Station_no	Station number on each vessel starts at No. 1 at the beginning of the year, the routes are numbered continuously.	
Quadrant	0: Latitude: North, Longitude: east 1: Latitude: North, Longitude: west	
Lat1	Latitude	dd
Lat2	Latitude	mm
Long1	Longitude	dd
Long2	Longitude	mm
Year		
Month		
Date		
Time_of_day		UTC
Depth	Depth at which the fish were caught	M
Gear		

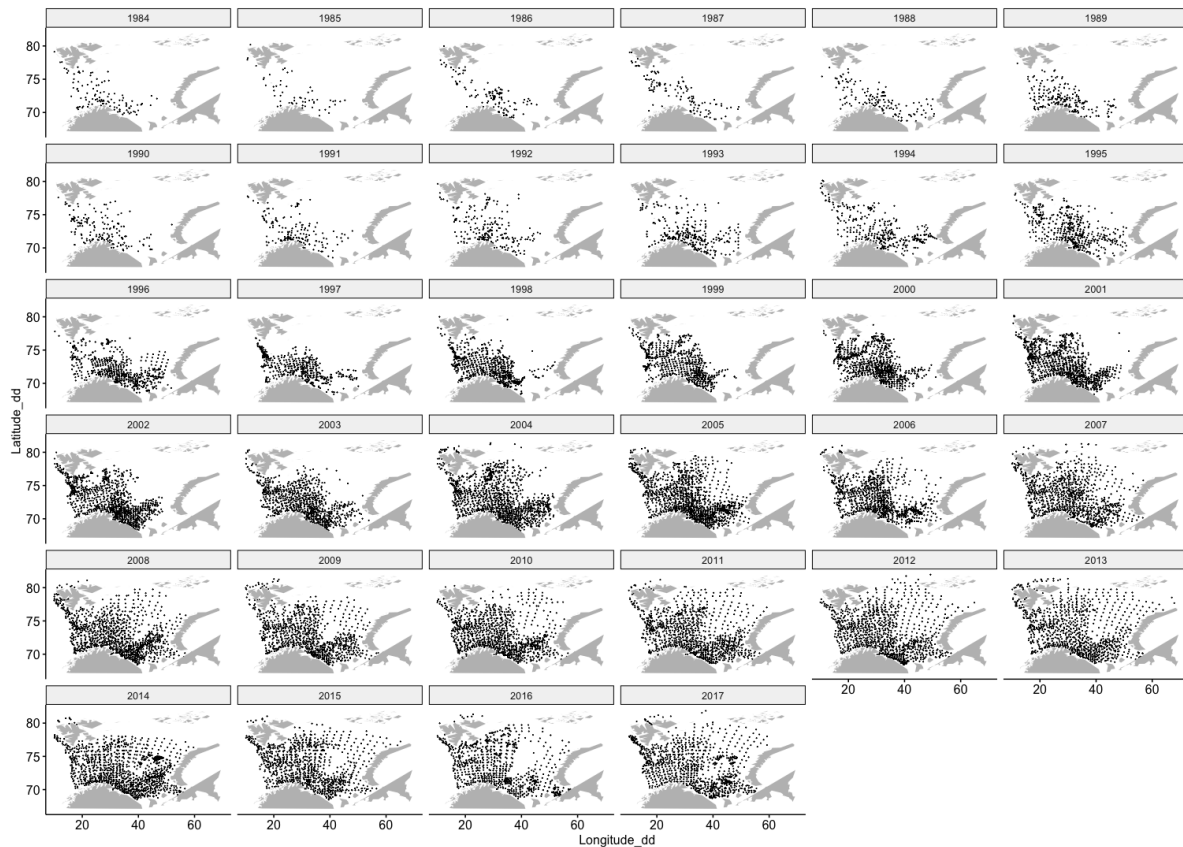
Fish_Length_cm		cm
Fish_Weight_kg		kg
Age_y		Years
Deg_stomach_fullness	Degree of stomach fullness	
No_FishLengthGroup_Haul	Number of fish of this group in the haul	
Towing_time	Time duration of each tow	hhmm
No_Regur_Stom	Number of regurgitated stomachs	
No_Empty_Stom	Number of empty stomachs	
Sex		
Maturity	Blank: not observed 1: Not mature	

1

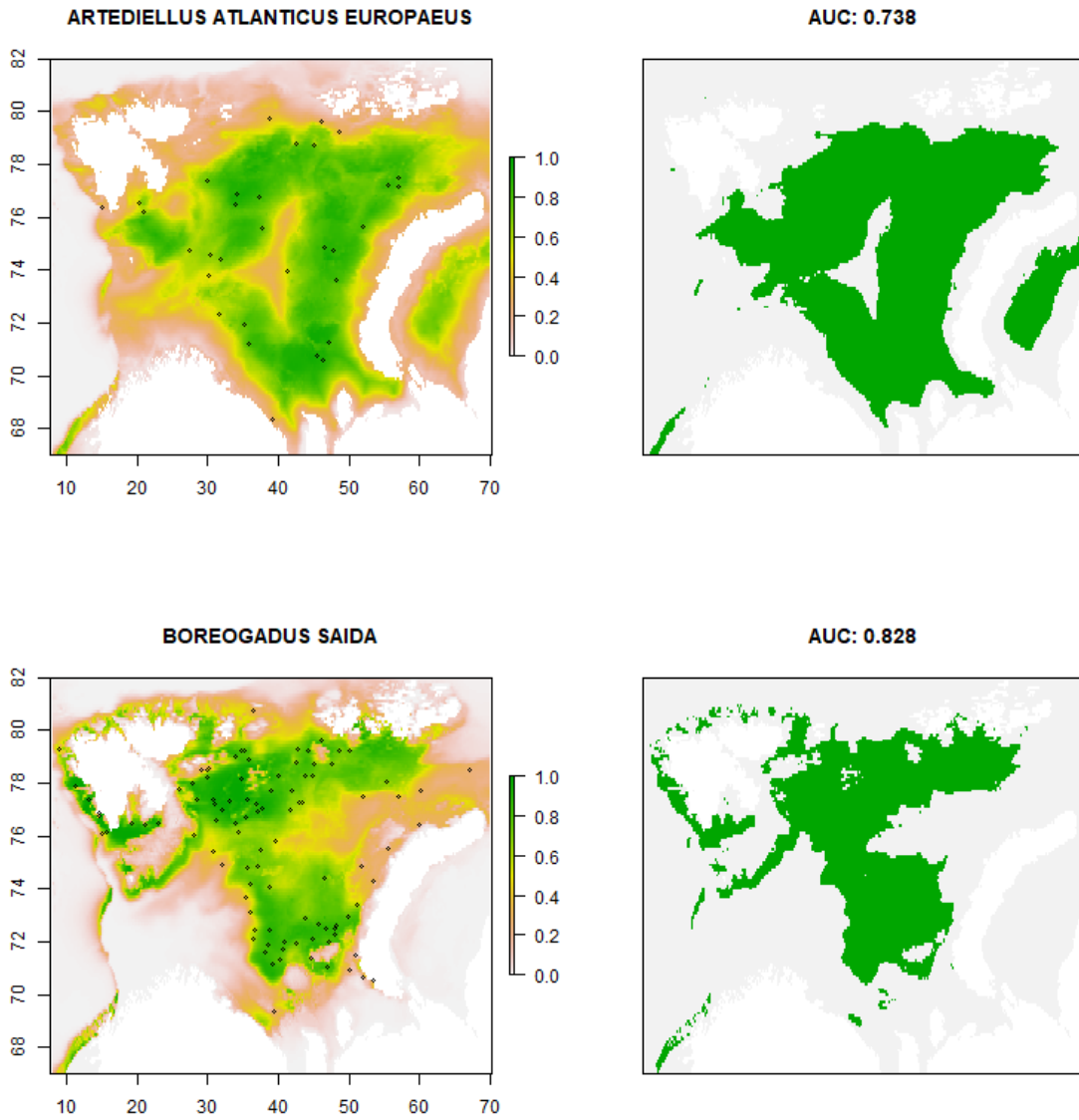
	2: Mature 3: Spawning 4: After spawning / 'resting' 5: Uncertain	
Prey_weight		g
Deg_digestion	Degree of digestion codes: Blank: Not observed 1: digestion not started, the stomach content seems fresh 2: Digestion commenced 3: Digestion progressed; the species can no longer be identified. But one can separate systematic groups 4: Digestion far advanced, one can still find eyes and bigger pieces of prey in the stomach content	

	5: Digestion almost completed, the stomach content is porous.	
No_Prey	Number of prey identified in stomach	
Prey_length_cm	Length of prey, converted using the prey weight.	cm
Prey_Category	Which prey category each prey record belongs to (Holt et al. 2019).	

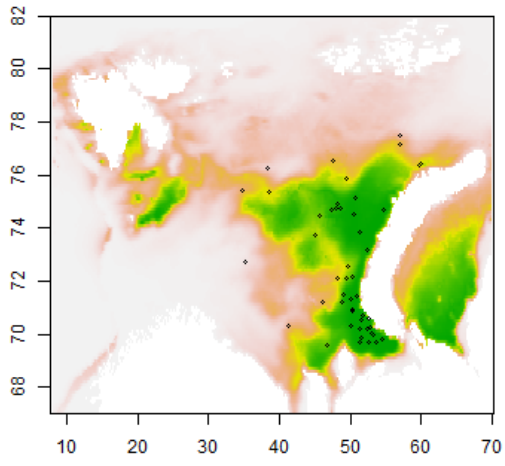
## A.2. IMR-PINRO Sampling Locations per Year.



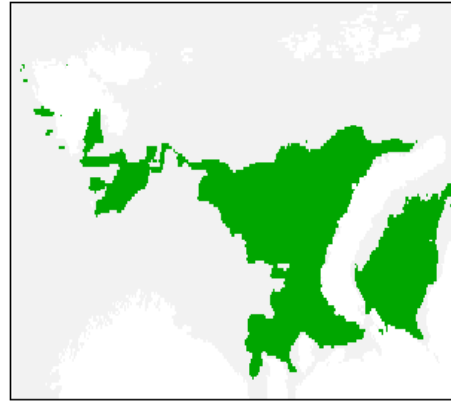
Appendix B - Prey species maxent prediction maps used in the creation of the prey availability layer



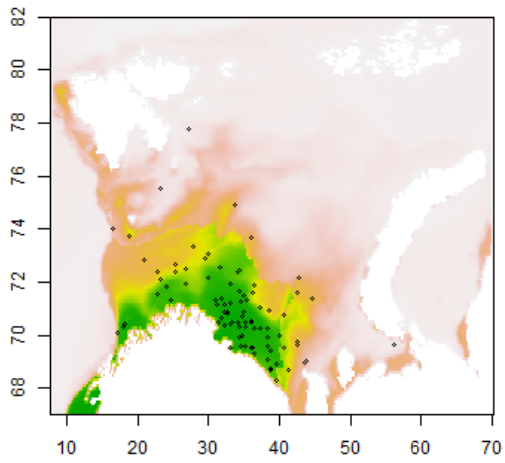
**CHIONOECETES OPILIO**



**AUC: 0.911**

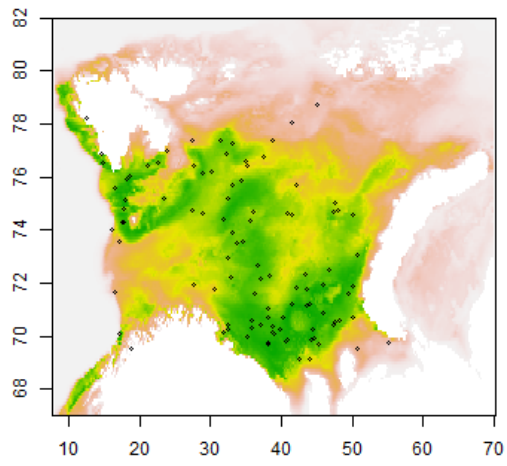
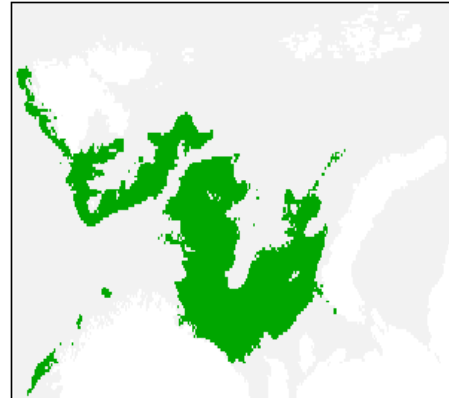
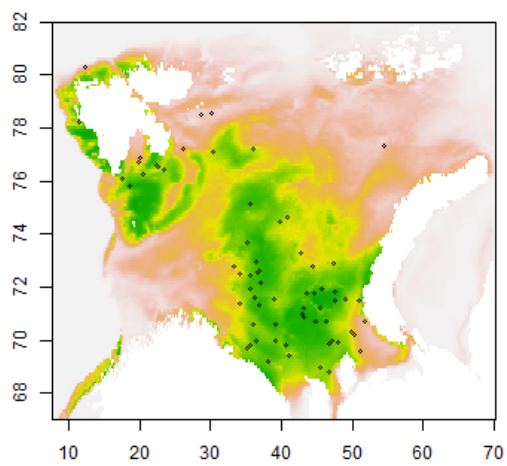
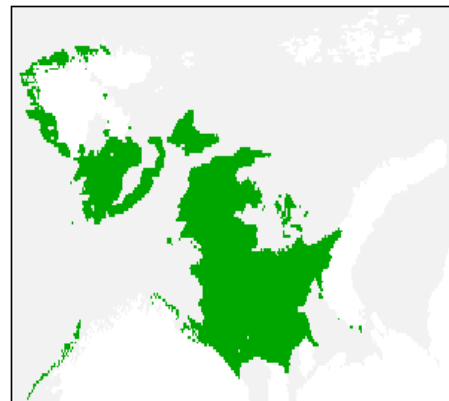


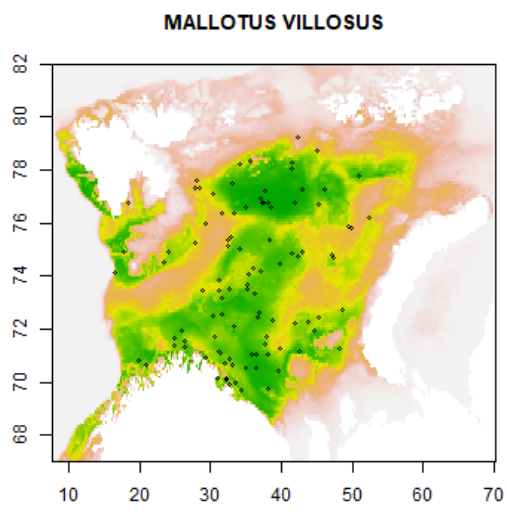
**CLUPEA HARENGUS**



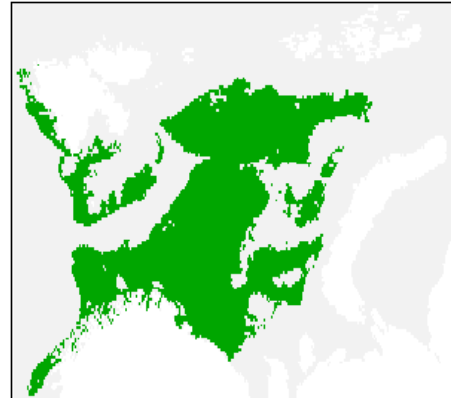
**AUC: 0.898**



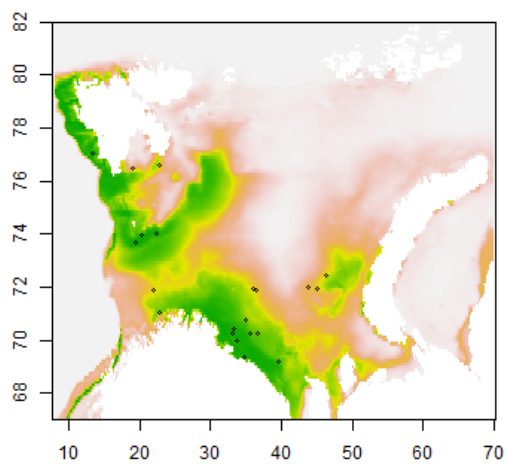
**HIPPOGLOSSOIDES PLATESSOIDES****AUC: 0.825****LEPTOCLINUS MACULATUS****AUC: 0.773**



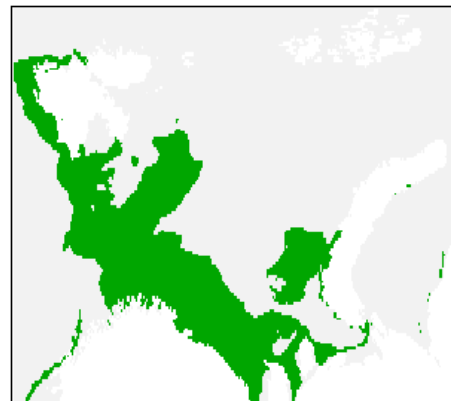
AUC: 0.778



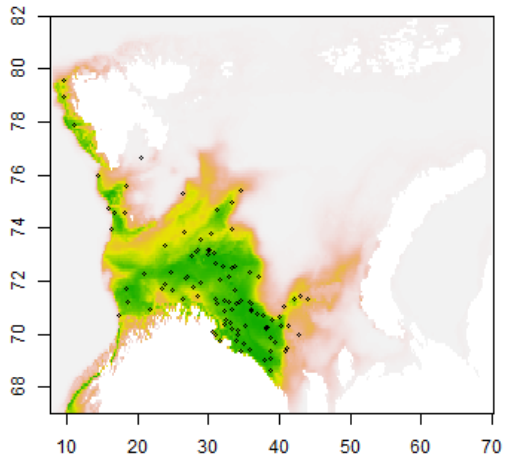
**MEGANYCTIPHANES NORVEGICA**



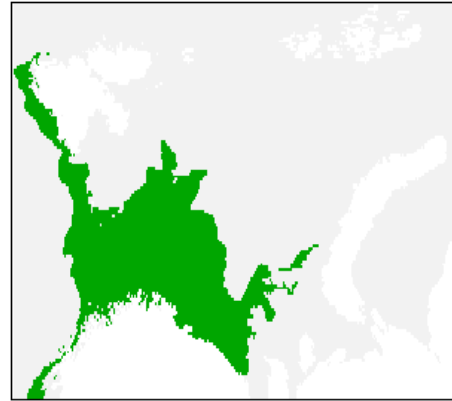
AUC: 0.874



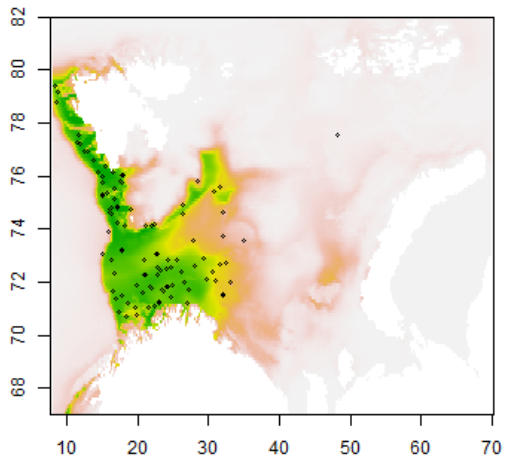
**MELANOGRAMMUS AEGLEFINUS**



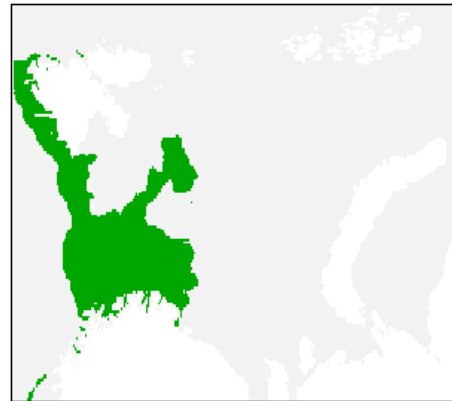
**AUC: 0.909**



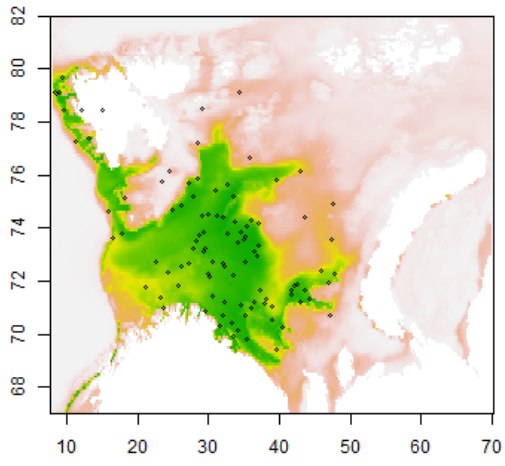
**MICROMESISTIUS POUTASSOU**



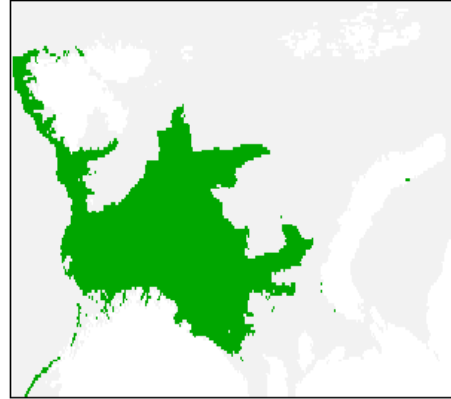
**AUC: 0.9**



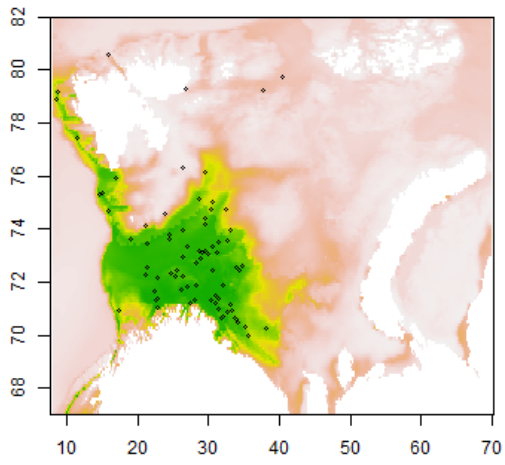
**PANDALUS BOREALIS**



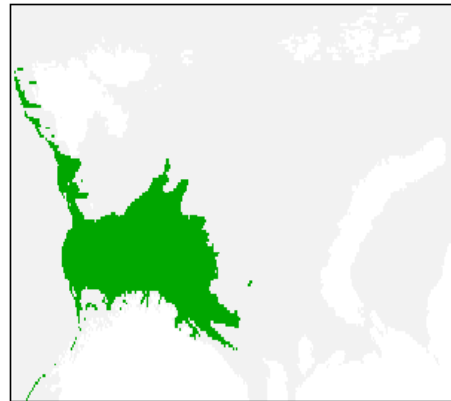
**AUC: 0.865**



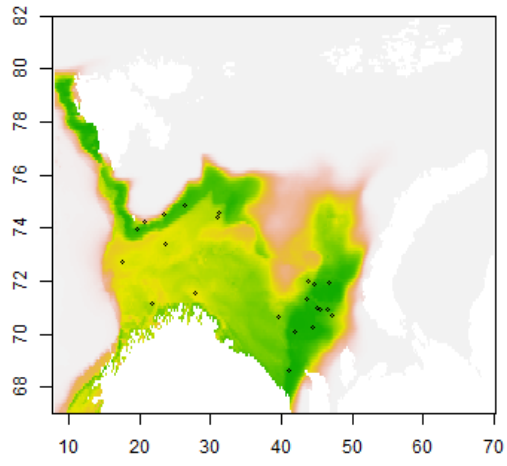
**SEBASTES MENTELLA**



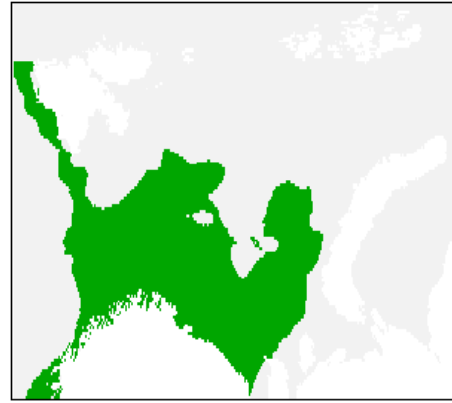
**AUC: 0.883**



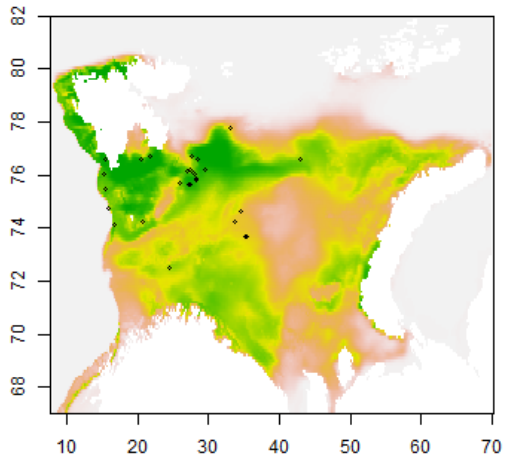
**THEMISTO ABYSSORUM**



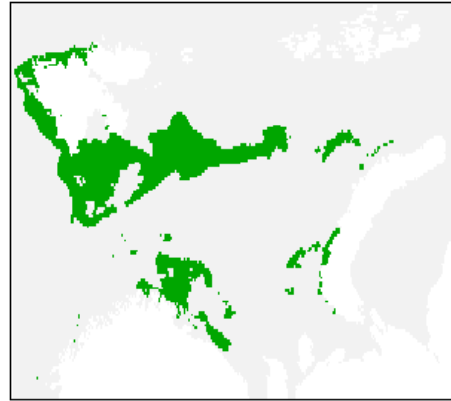
**AUC: 0.883**



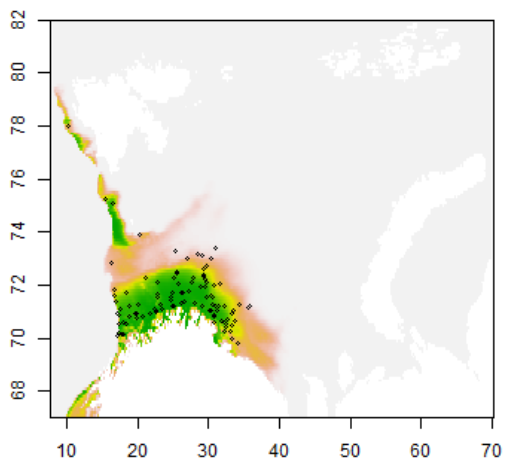
**THEMISTO LIBELLULA**



**AUC: 0.834**



**TRISOPTERUS ESMARKII**



**AUC: 0.961**



## Appendix C - Model permutation importance tables for temporal sensitivity testing

### C.1. Annual, Five and Ten-year model variable permutation importance

Permutation Importance: Annual, Five-year and Ten-year models				
Layer	Mean	S.D.	N	%
btemp_max	21.1	13.8	51	76.1
btemp_mean	24.3	11.9	16	23.9
btemp_min	NA	NA	0	0.0
fice_max	5.4	8.1	17	25.4
fice_mean	16.6	17.0	33	49.3
fice_min	0.9	2.7	26	38.8
hice_max	5.6	5.3	5	7.5
hice_mean	0.0	NA	1	1.5
hice_min	0.7	2.5	15	22.4
salinity_max	13.1	15.0	8	11.9
salinity_mean	18.0	12.8	15	22.4
salinity_min	22.2	11.8	44	65.7
temperature_max	9.4	4.7	4	6.0
temperature_mean	10.3	9.3	8	11.9

temperature_min	15.8	16.9	2	3.0
bathymetry	29.9	8.8	67	100.0
distance	15.4	9.4	67	100.0

## C.2. Annual models variable permutation importance

Permutation Importance: 1 Year Period				
Layer	Mean	S.D.	N	%
btemp_max	25.9	16.7	20.0	76.9
btemp_mean	25.5	11.8	6.0	23.1
btemp_min	NA	NA	0.0	0.0
fice_max	7.0	10.2	10.0	38.5
fice_mean	15.0	10.0	9.0	34.6
fice_min	0.6	1.5	20.0	76.9
hice_max	1.7	NA	1.0	3.8
hice_mean	NA	NA	0.0	0.0
hice_min	0.0	0.0	5.0	19.2
salinity_max	9.3	10.2	4.0	15.4
salinity_mean	19.8	11.8	4.0	15.4
salinity_min	25.6	12.7	18.0	69.2
temperature_max	11.1	4.0	3.0	11.5
temperature_mean	6.9	7.5	6.0	23.1
temperature_min	NA	NA	0.0	0.0
bathymetry	31.0	8.8	27.0	100.0
distance	9.7	6.9	27.0	100.0



## C.3. Five-year period model variable permutation importance

Permutation Importance: 5 Year Period				
Layer	Mean	S.D.	N	%
btemp_max	17.4	11.9	16.0	69.6
btemp_mean	26.4	14.0	7.0	30.4
btemp_min	NA	NA	0.0	0.0
fice_max	4.7	3.2	4.0	17.4
fice_mean	18.5	22.0	14.0	60.9
fice_min	0.0	0.0	2.0	8.7
hice_max	8.7	4.3	3.0	13.0
hice_mean	NA	NA	0.0	0.0
hice_min	1.1	3.3	9.0	39.1
salinity_max	22.4	19.7	3.0	13.0
salinity_mean	12.4	12.6	7.0	30.4
salinity_min	17.4	8.1	13.0	56.5
temperature_max	NA	NA	0.0	0.0
temperature_mean	24.9	NA	1.0	4.3
temperature_min	3.8	NA	1.0	4.3
bathymetry	30.5	9.8	23.0	100.0
distance	18.0	10.4	23.0	100.0



## C.4. Ten-year period model variable permutation importance

Permutation Importance: 10 Year Period				
Layer	Mean	S.D.	N	%
btemp_max	18.6	10.0	15.0	83.3
btemp_mean	17.0	4.5	3.0	16.7
btemp_min	NA	NA	0.0	0.0
fice_max	1.2	2.0	3.0	16.7
fice_mean	15.5	15.1	10.0	55.6
fice_min	3.2	6.4	4.0	22.2
hice_max	0.0	NA	1.0	5.6
hice_mean	0.0	NA	1.0	5.6
hice_min	0.0	NA	1.0	5.6
salinity_max	0.0	NA	1.0	5.6
salinity_mean	25.9	11.9	4.0	22.2
salinity_min	22.4	12.6	13.0	72.2
temperature_max	4.2	NA	1.0	5.6
temperature_mean	16.0	NA	1.0	5.6
temperature_min	27.8	NA	1.0	5.6
bathymetry	27.5	7.5	18.0	100.0
distance	20.1	7.4	18.0	100.0

## C.5. Summer model variable permutation importance

Permutation Importance: Summer Period				
Layer	Mean	S.D.	N	%
BTemp.Aug	20.4	14.7	16	59.3
BTemp.Jul	11.7	0.0	1	3.7
BTemp.Jun	20.0	12.4	10	37.0
FIce.Aug	1.7	5.4	10	37.0
FIce.Jul	6.5	6.8	5	18.5
FIce.Jun	7.2	7.9	12	44.4
HIce.Aug	0.1	0.2	3	11.1
HIce.Jul	3.8	2.2	4	14.8
HIce.Jun	8.1	3.1	3	11.1

Sal.Aug	18.9	13.2	11	40.7
Sal.Jul	17.6	16.9	5	18.5
Sal.Jun	20.8	12.2	11	40.7
SST.Aug	22.3	16.7	13	48.1
SST.Jul	20.1	13.9	7	25.9
SST.Jun	15.5	13.6	5	18.5
bathymetry	27.2	10.2	27	100.0
distance	8.1	8.7	27	100.0

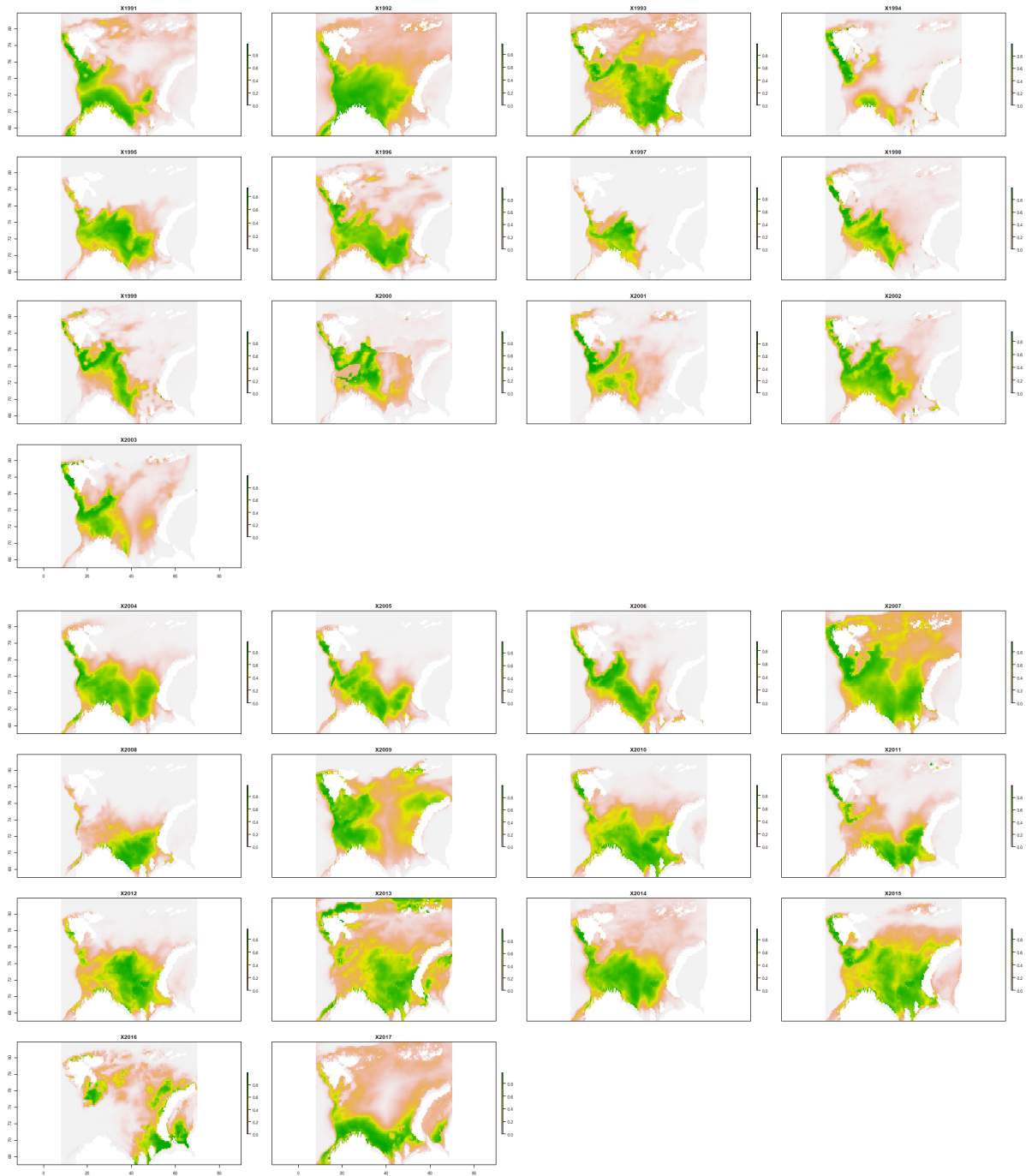
## C.6. Winter model variable permutation importance

Permutation Importance: Winter Period				
Layer	Mean	S.D.	N	%
BTemp.Dec	22.5	17.0	10.0	37.0
BTemp.Feb	22.7	16.5	11.0	40.7
BTemp.Jan	19.9	13.7	7.0	25.9
FIce.Dec	21.4	22.1	3.0	11.1
FIce.Feb	31.1	28.2	3.0	11.1
FIce.Jan	24.2	19.0	15.0	55.6
HIce.Dec	0.0	0.0	2.0	7.4
HIce.Feb	0.0	0.0	3.0	11.1
HIce.Jan	0.0	0.0	4.0	14.8
Sal.Dec	3.7	5.3	2.0	7.4
Sal.Feb	13.7	15.1	12.0	44.4
Sal.Jan	4.9	5.3	13.0	48.1
SST.Dec	46.1	25.8	4.0	14.8
SST.Feb	47.2	21.9	9.0	33.3
SST.Jan	23.2	23.1	6.0	22.2

bathymetry	17.8	9.5	27.0	100.0
distance	3.8	2.9	27.0	100.0

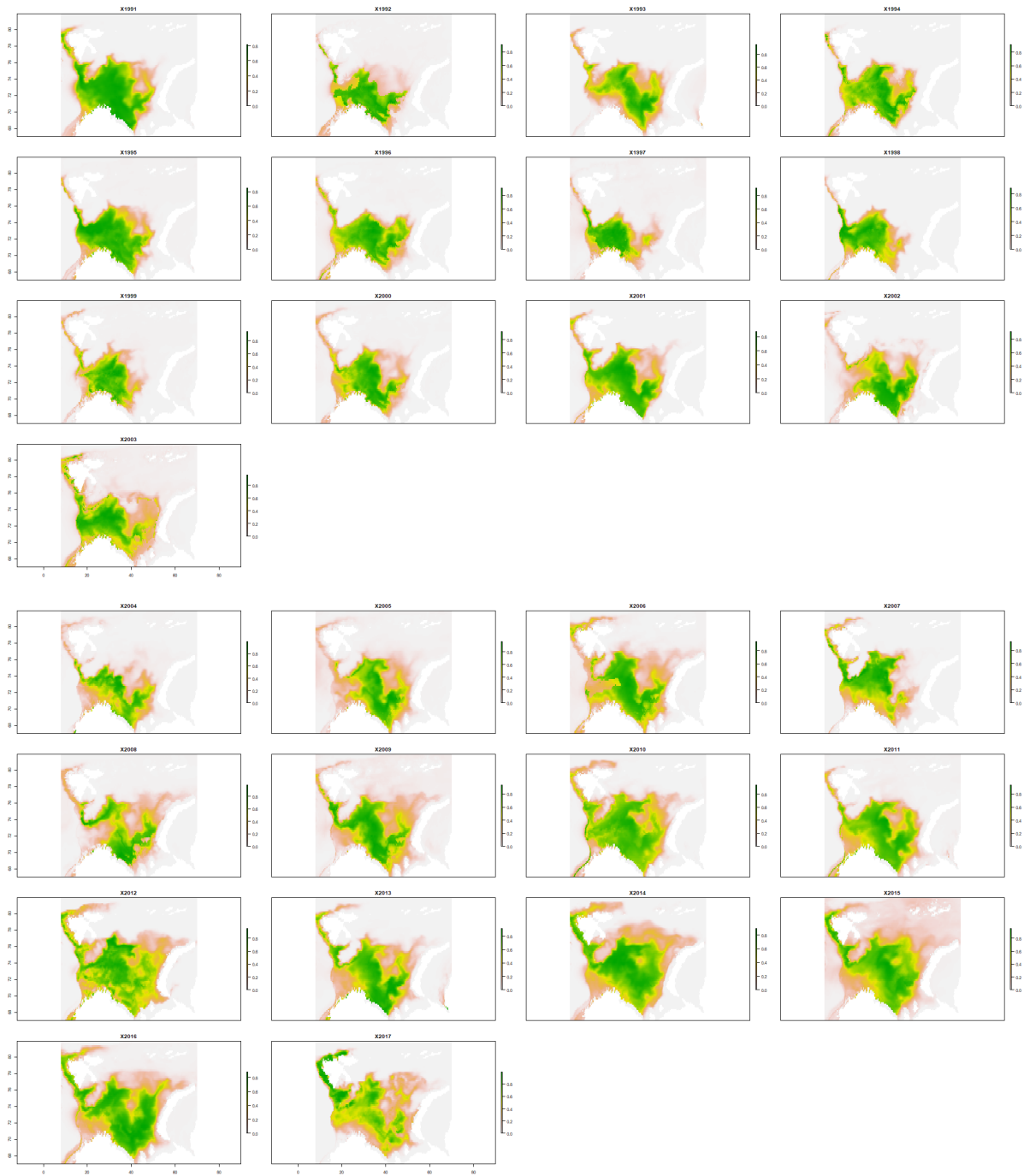
## Appendix D - Seasonal prediction maps and binary maps for each species group modelled in Chapter 4.

### *Gadus morhua* (S) - Summer

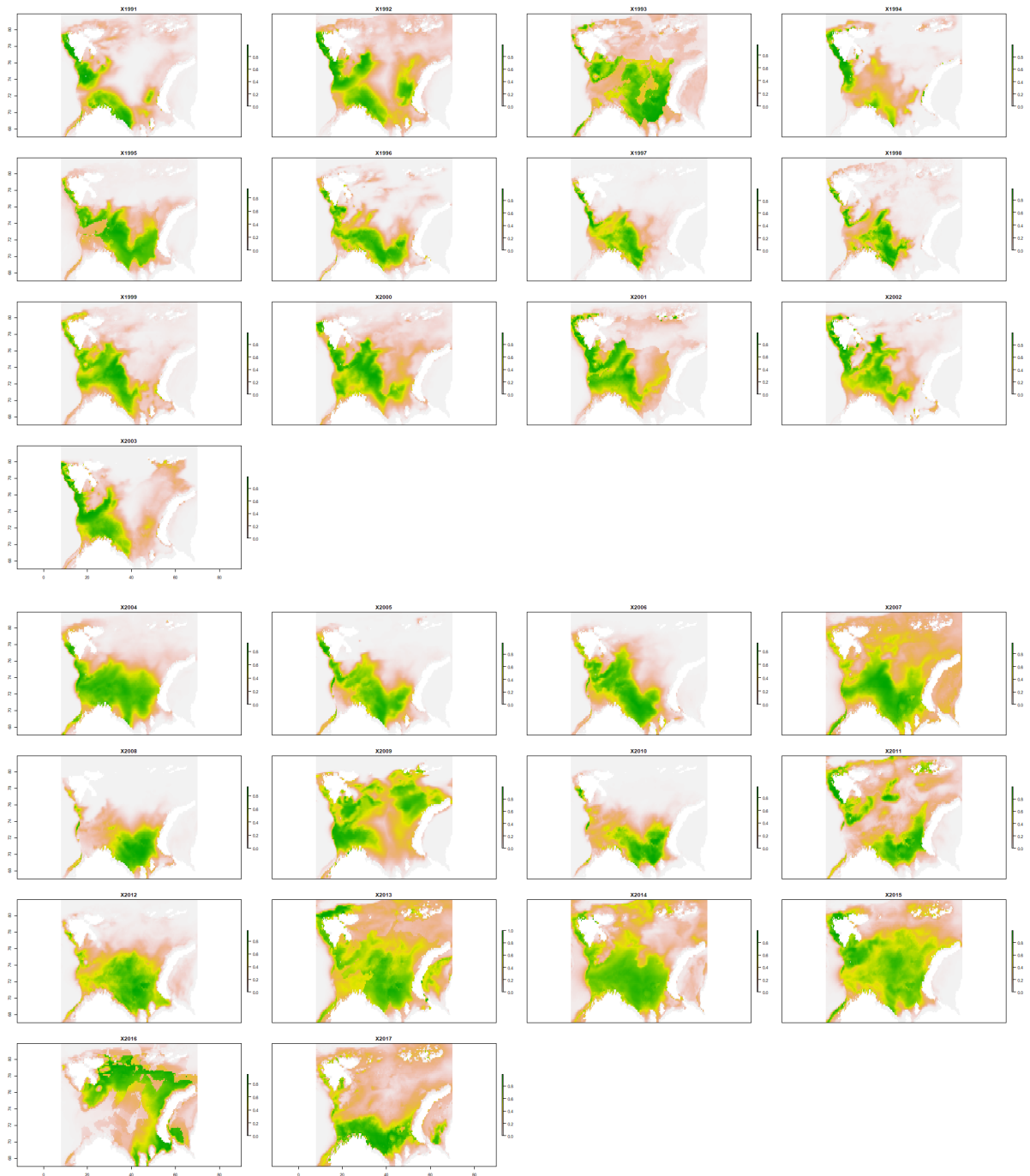


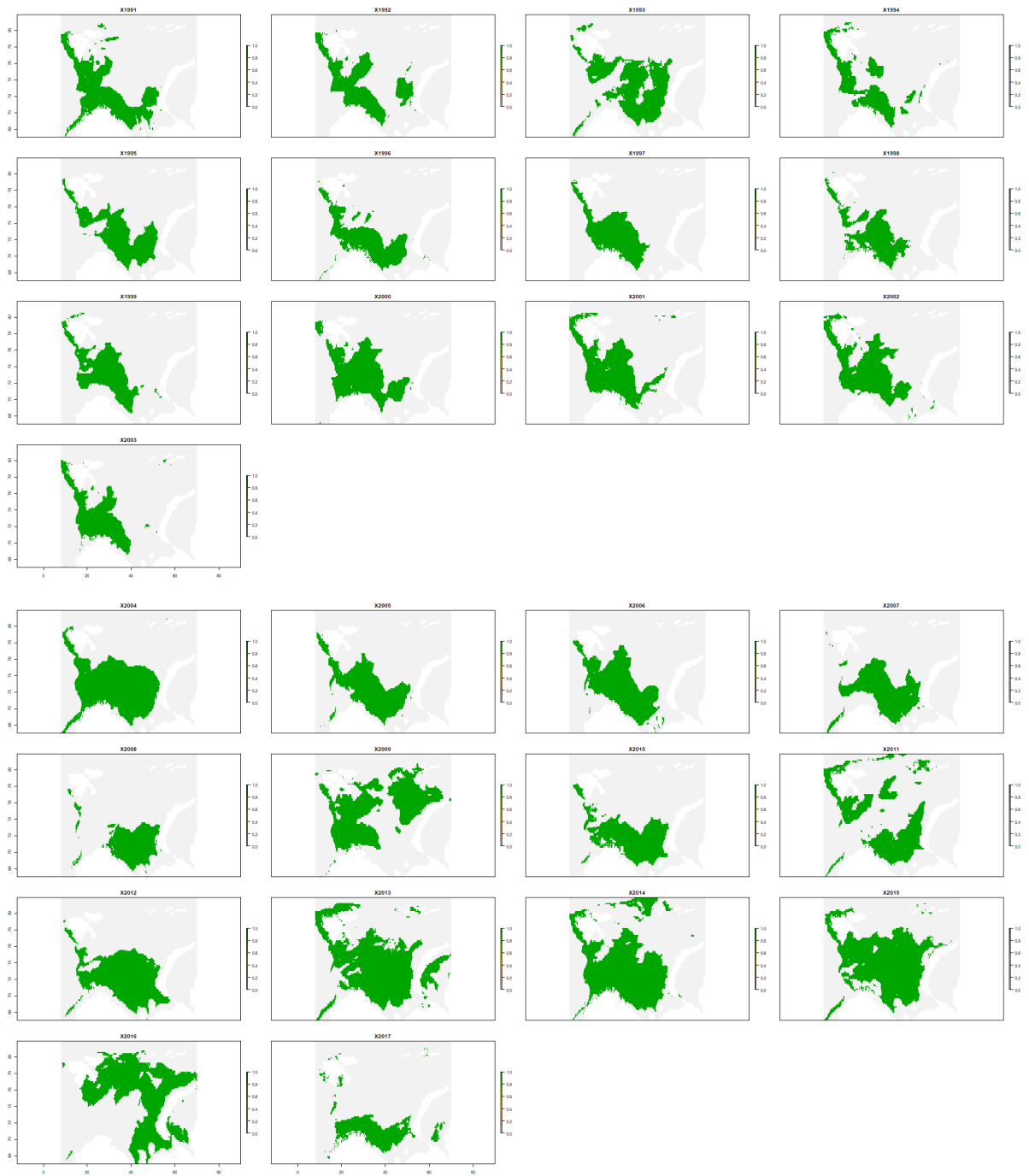


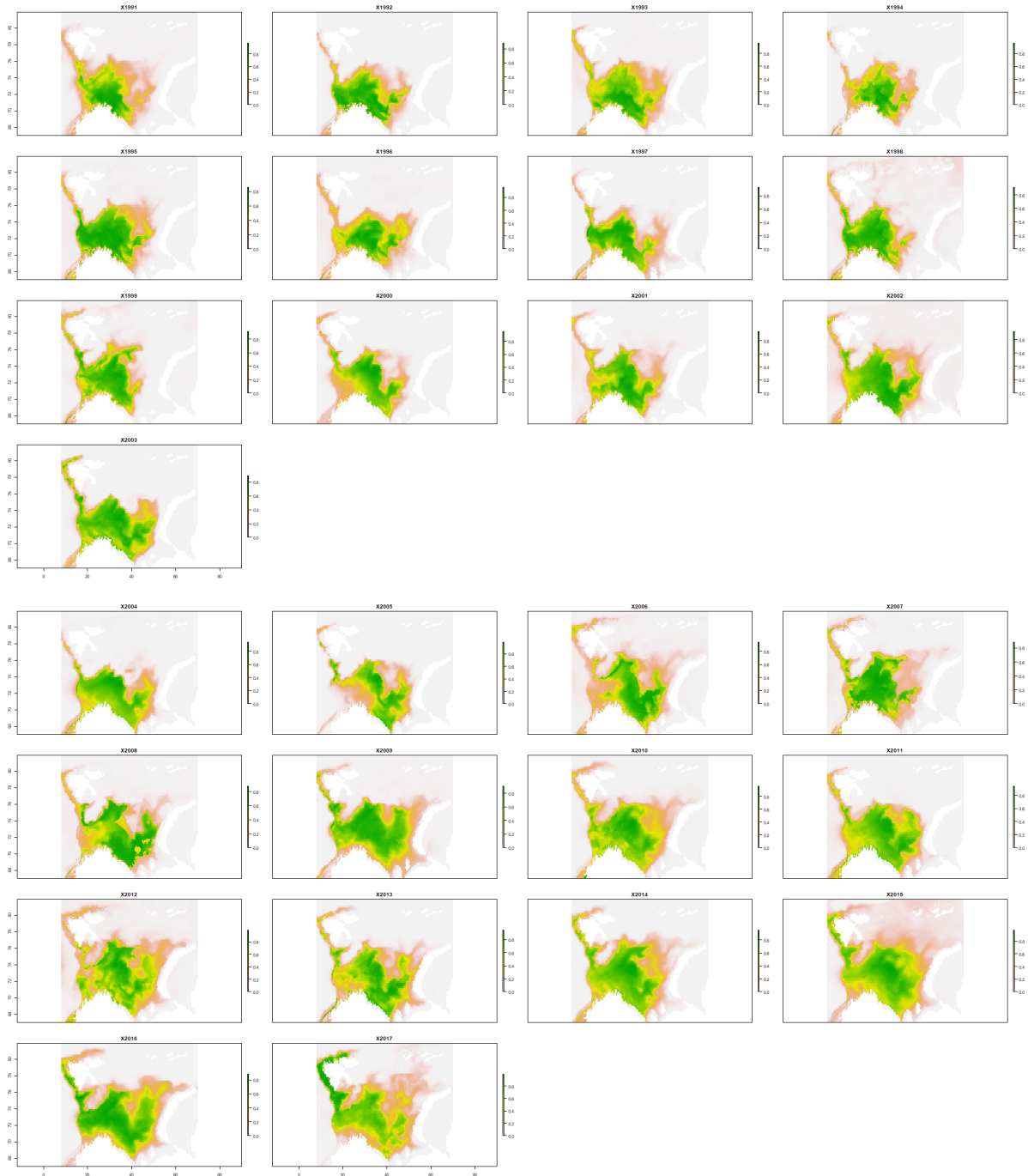
*Gadus morhua* (S) - Winter





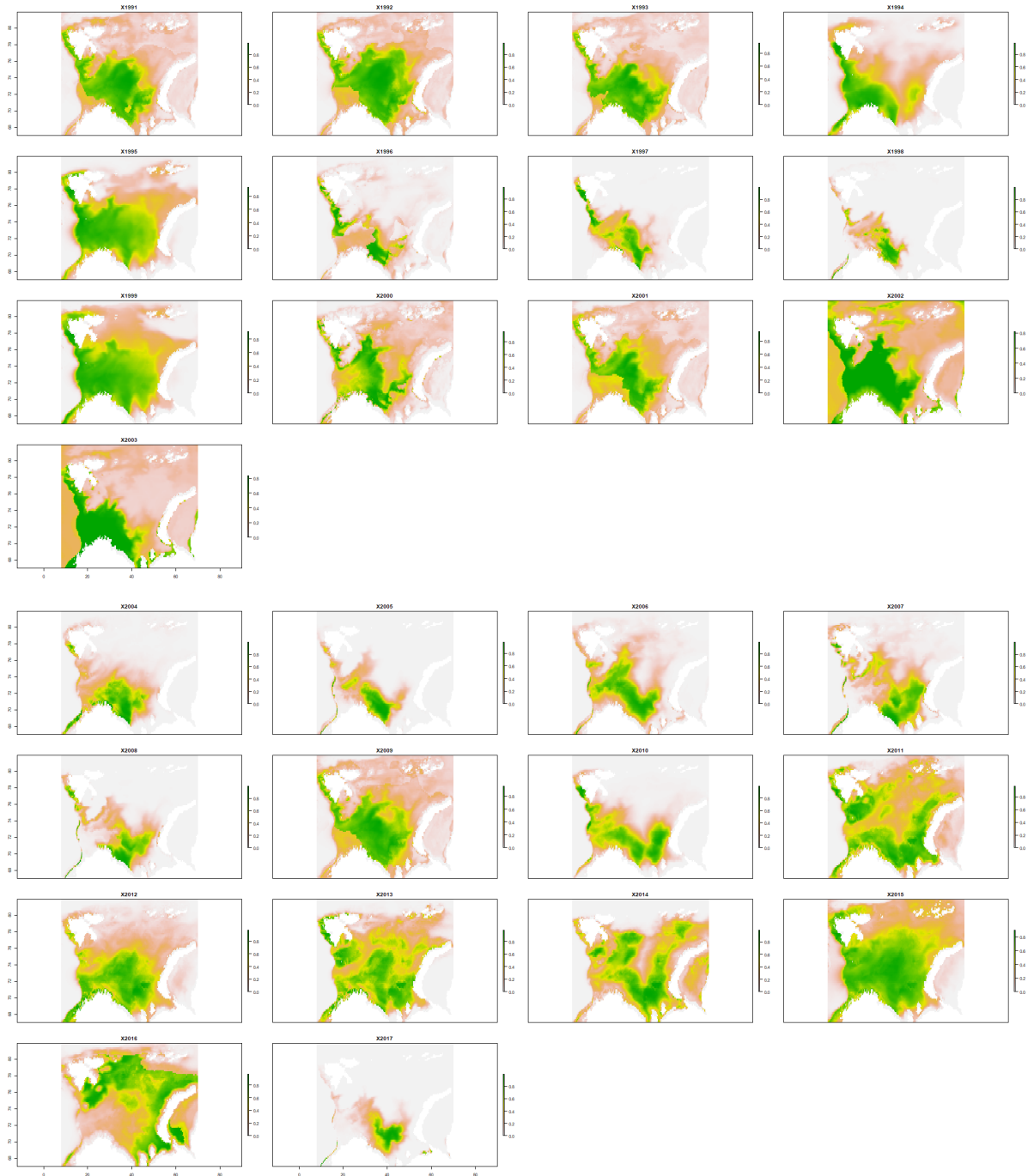
***Gadus morhua* (M) - Summer**

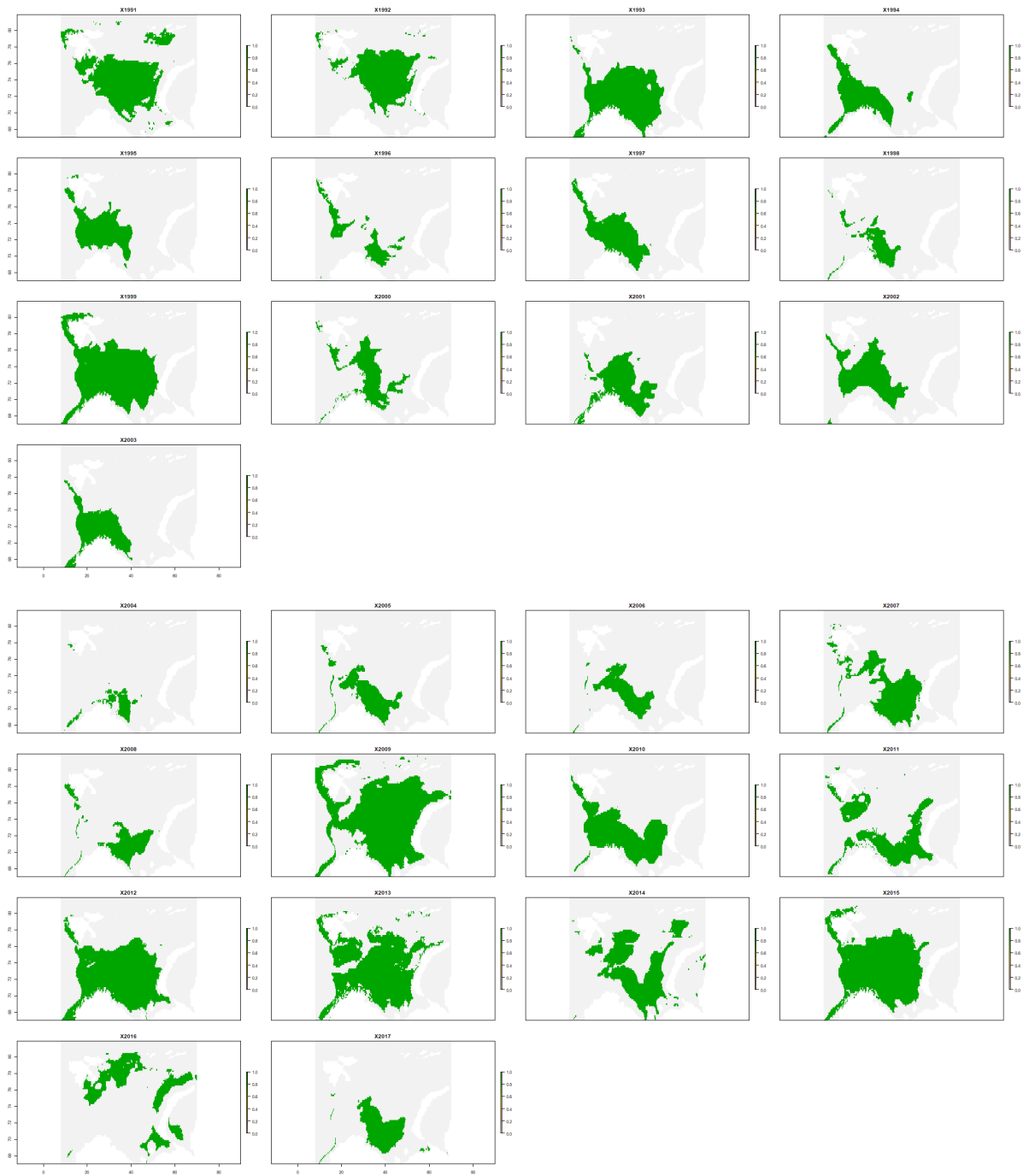


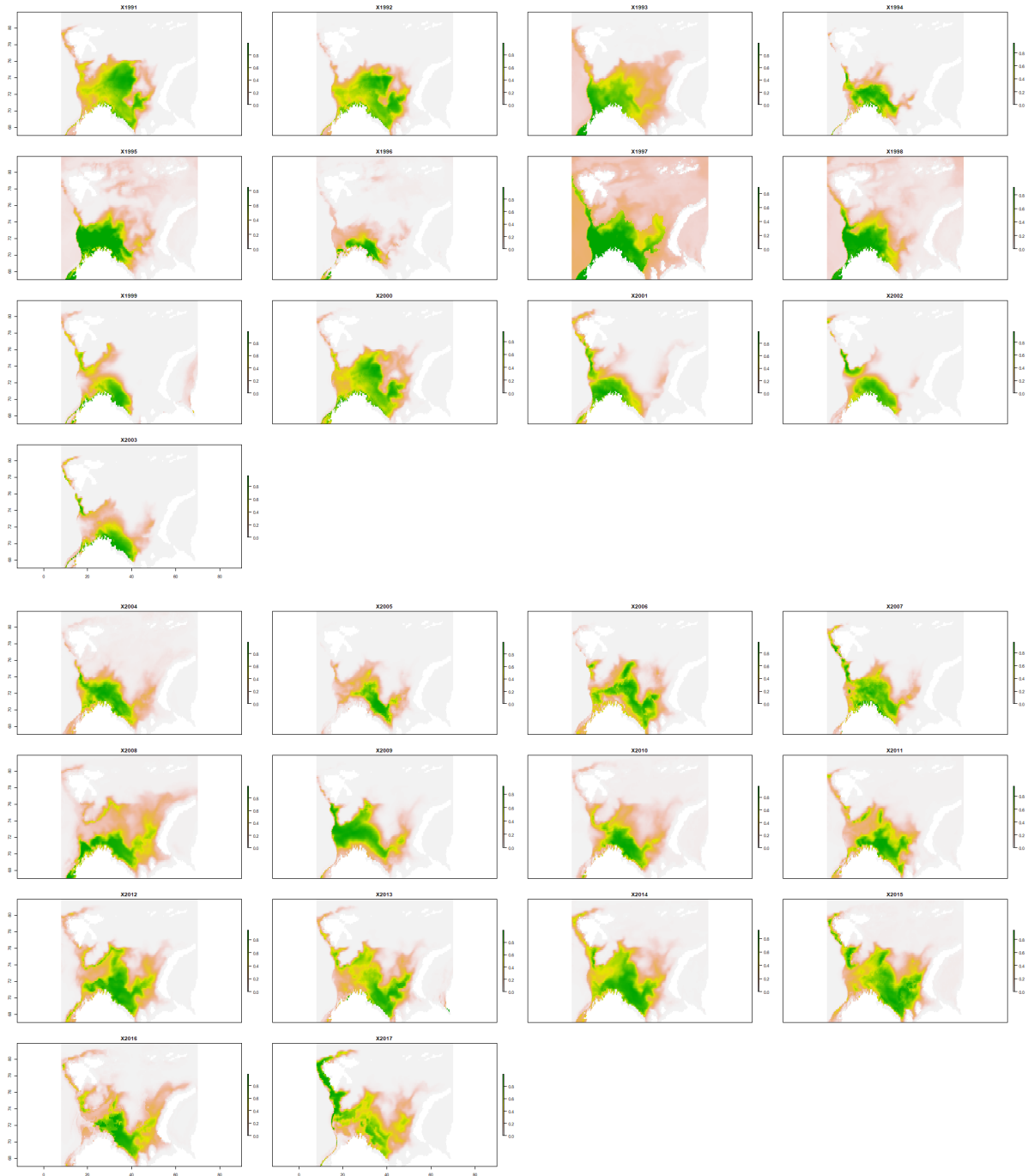
***Gadus morhua* (M) - Winter**

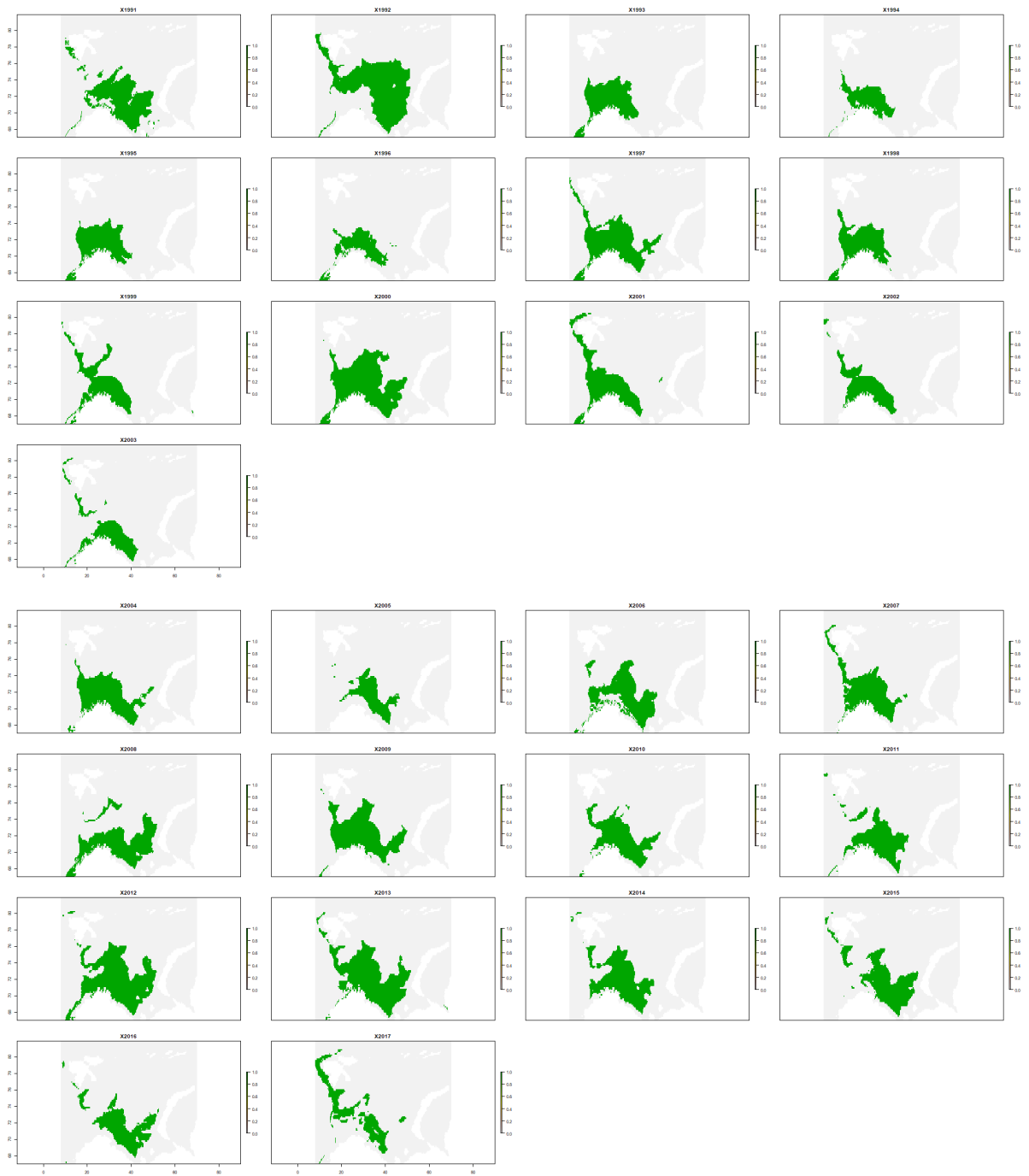


*Gadus morhua* (L) - Summer

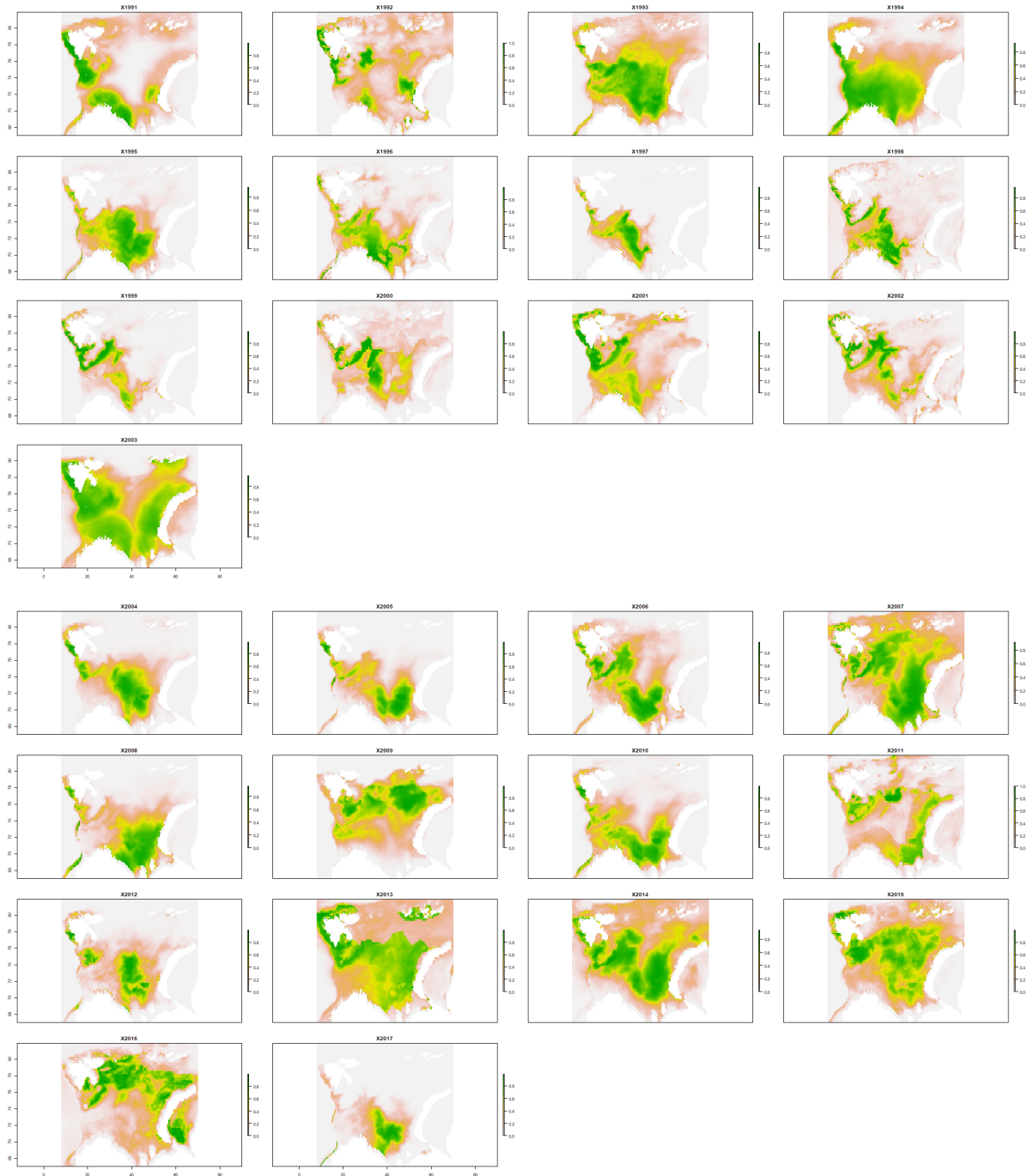


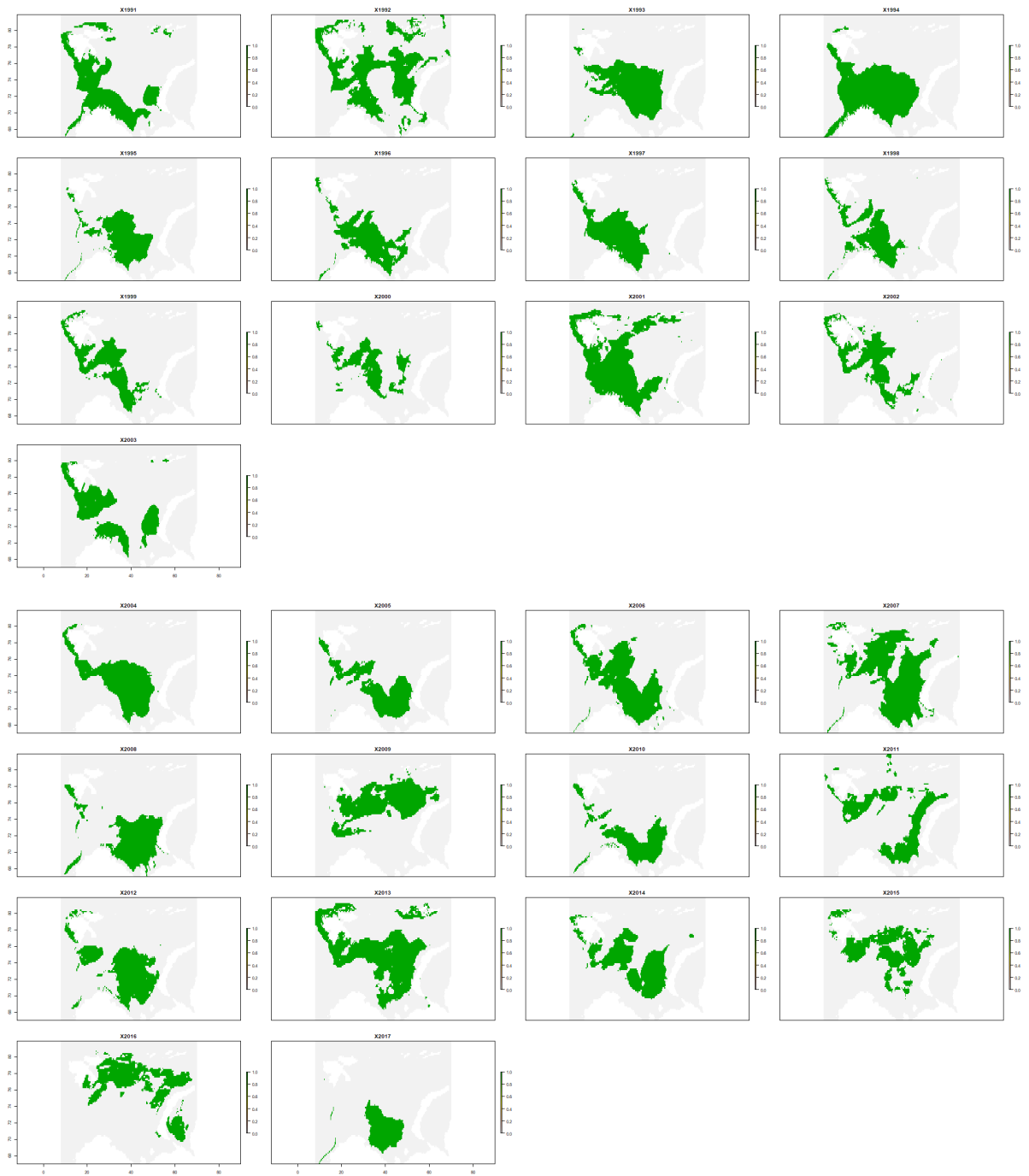


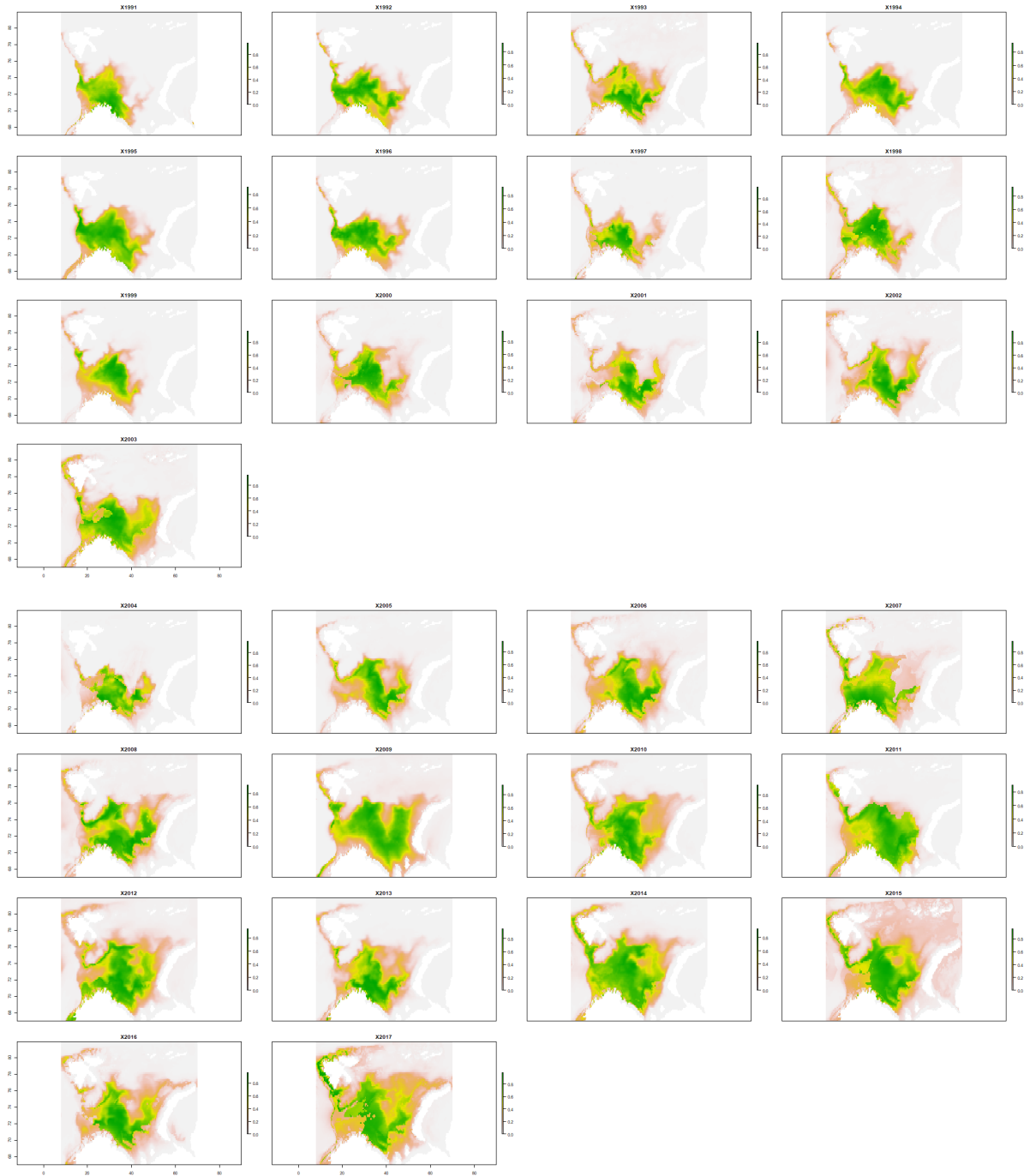
*Gadus morhua* (L) - Winter



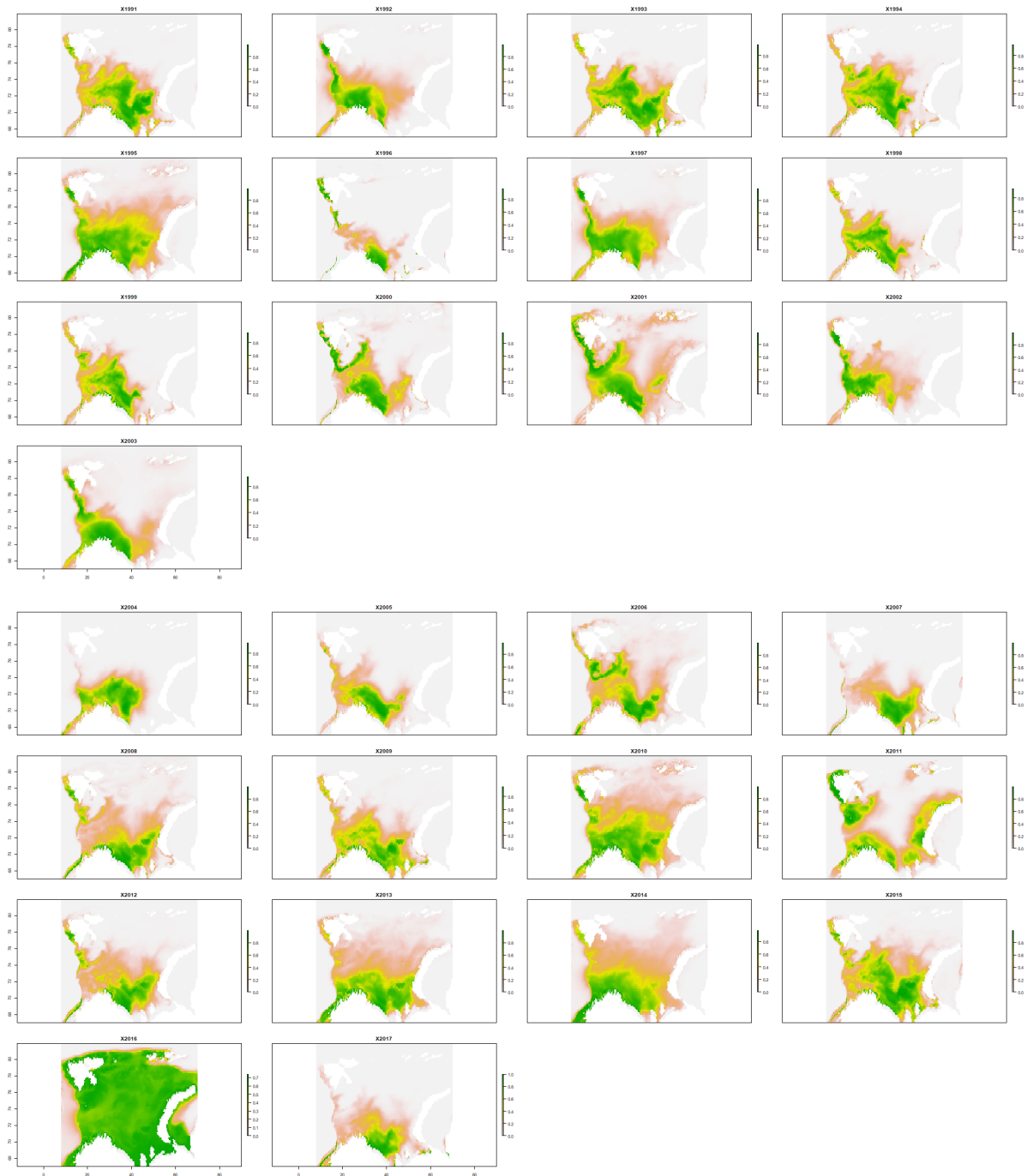
*Mallotus villosus* - Summer

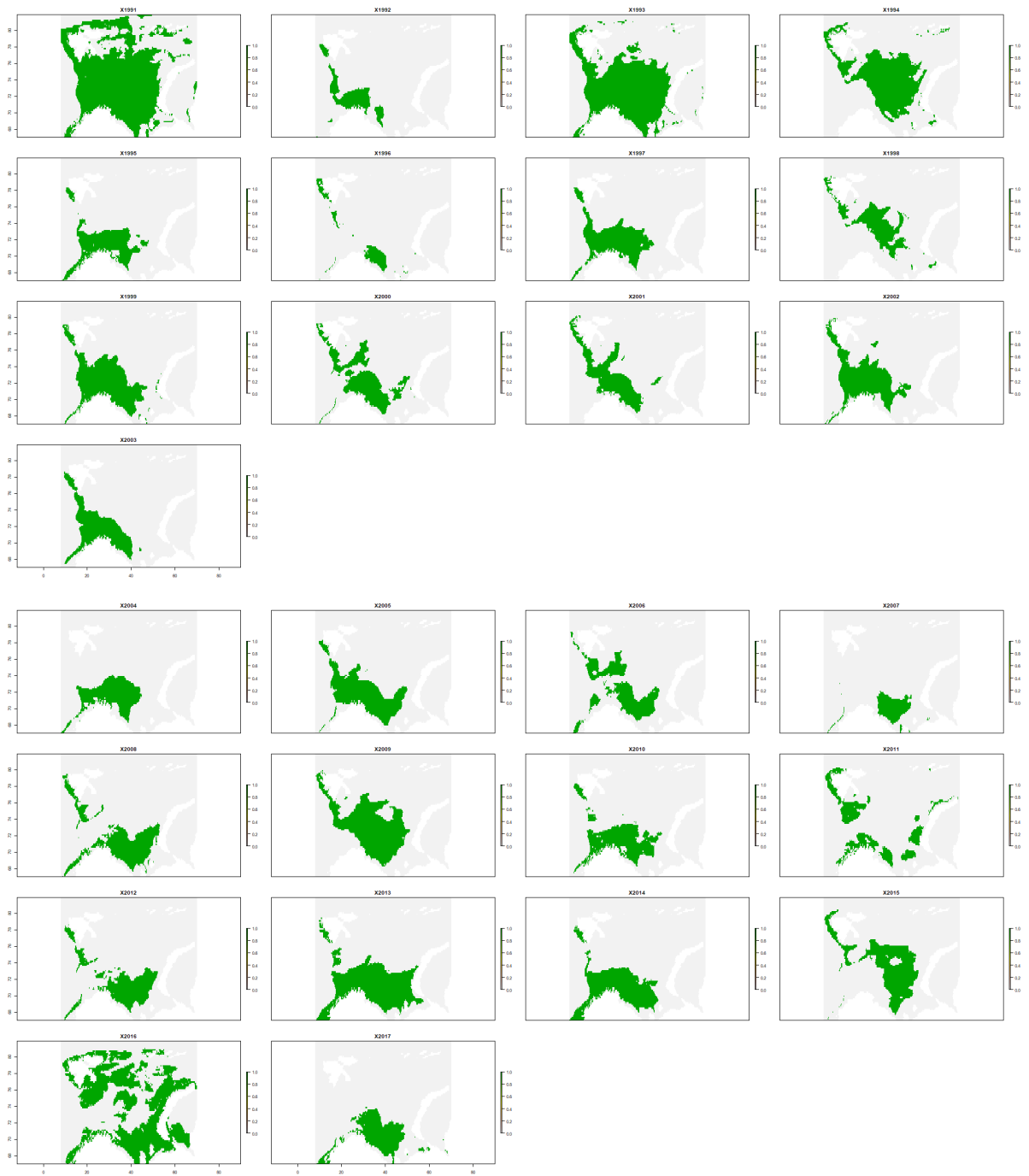




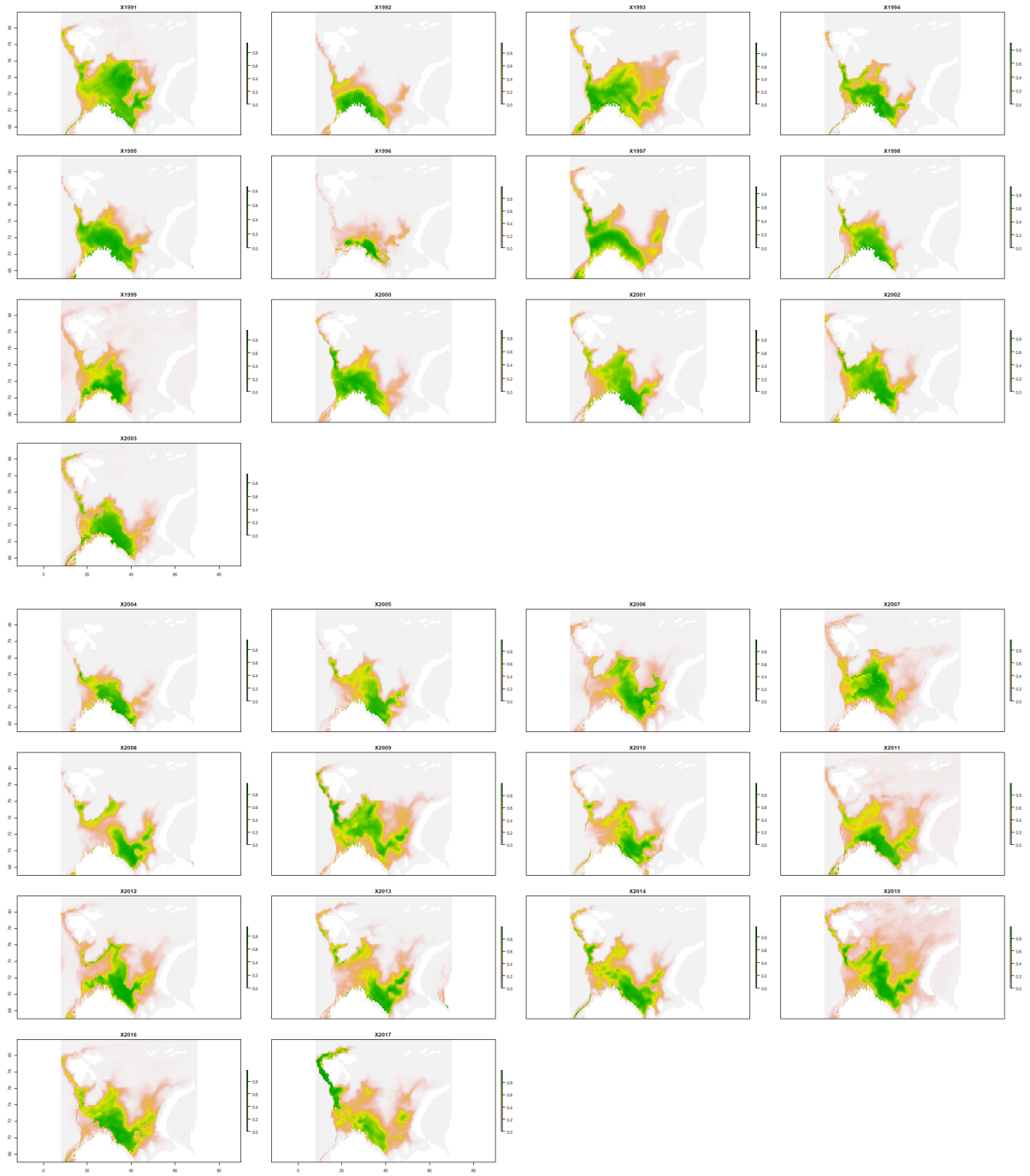
*Mallotus villosus* - Winter

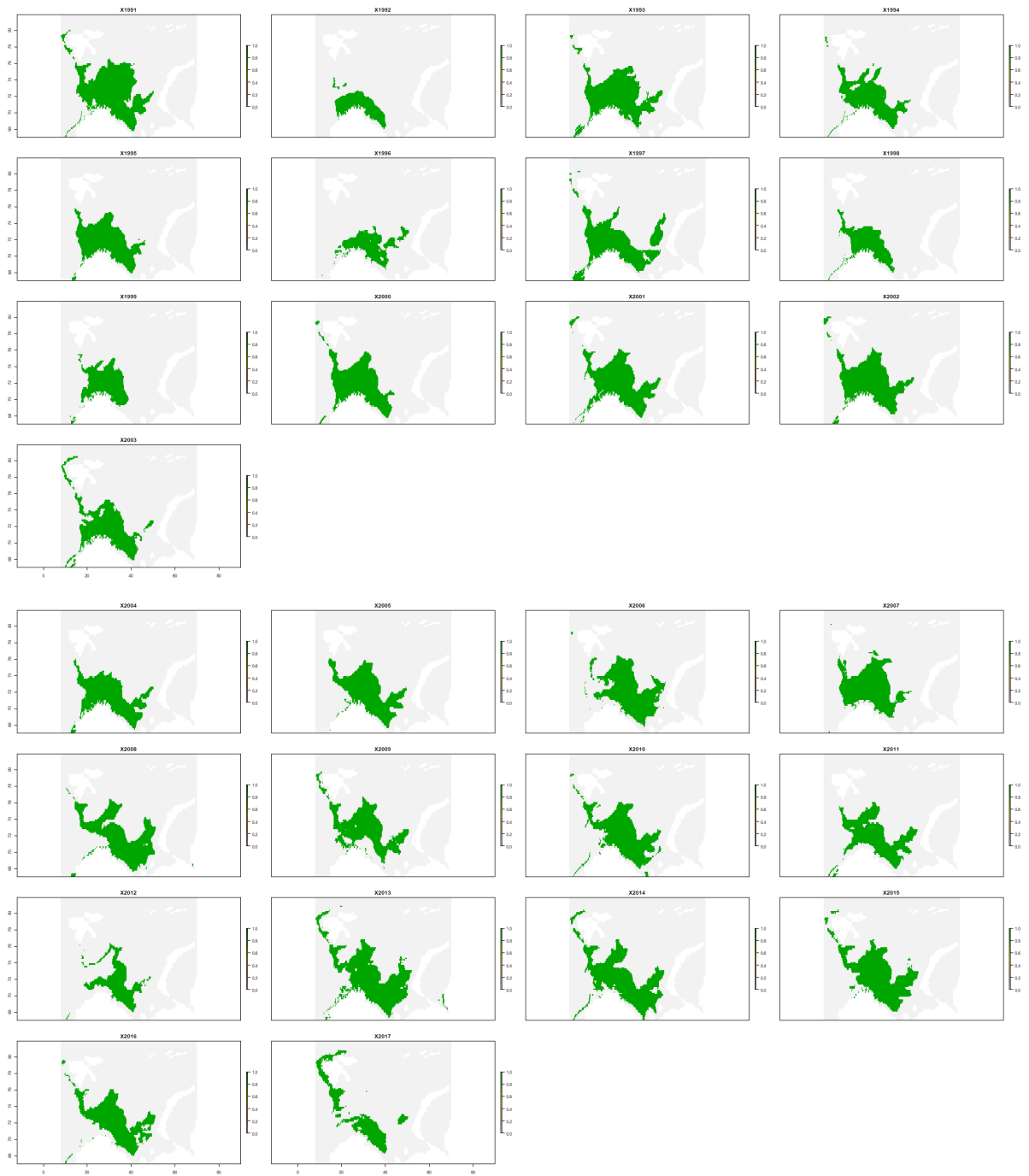


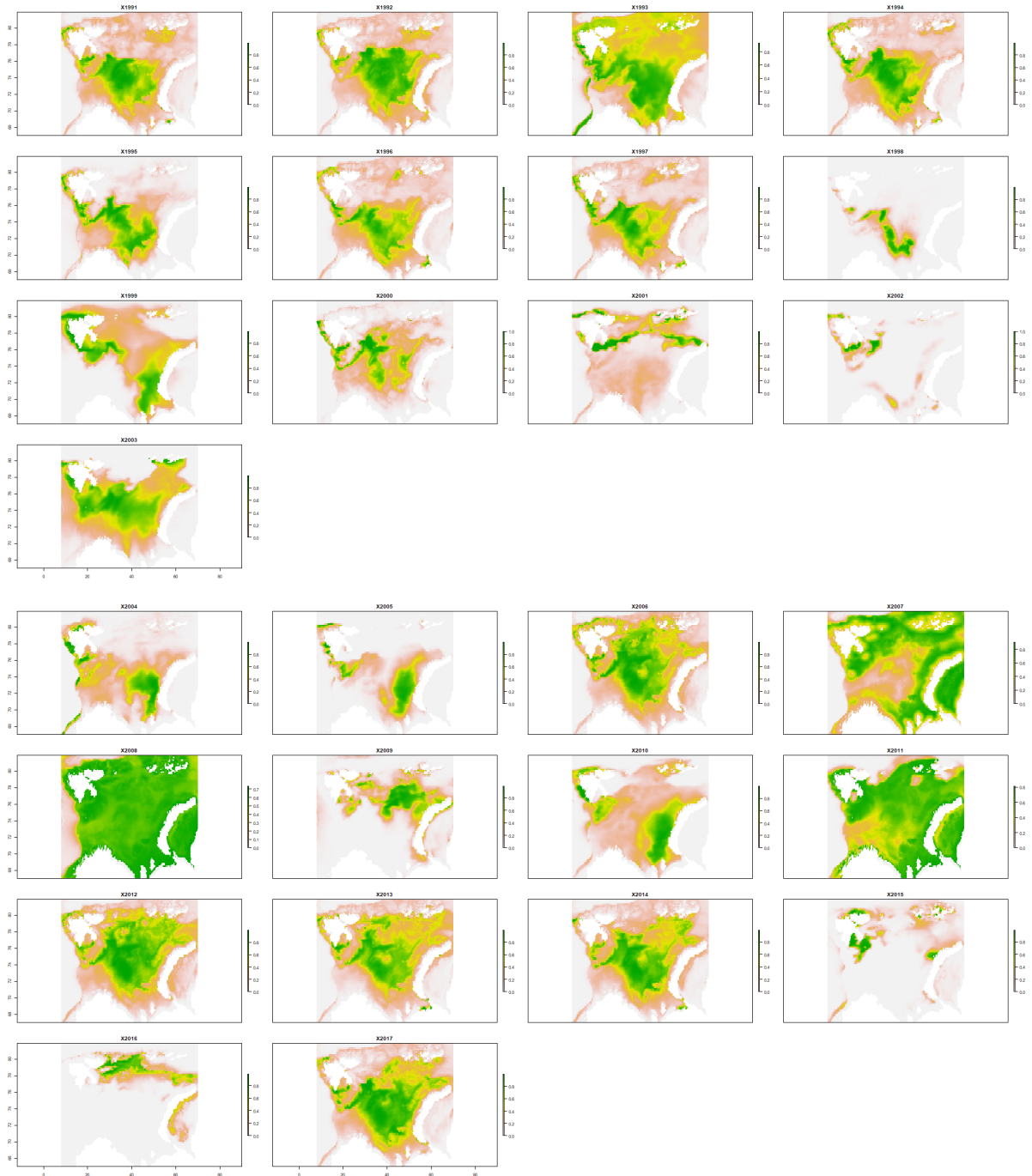
*Melanogrammus aeglefinus* - Summer



*Melanogrammus aeglefinus* - Winter

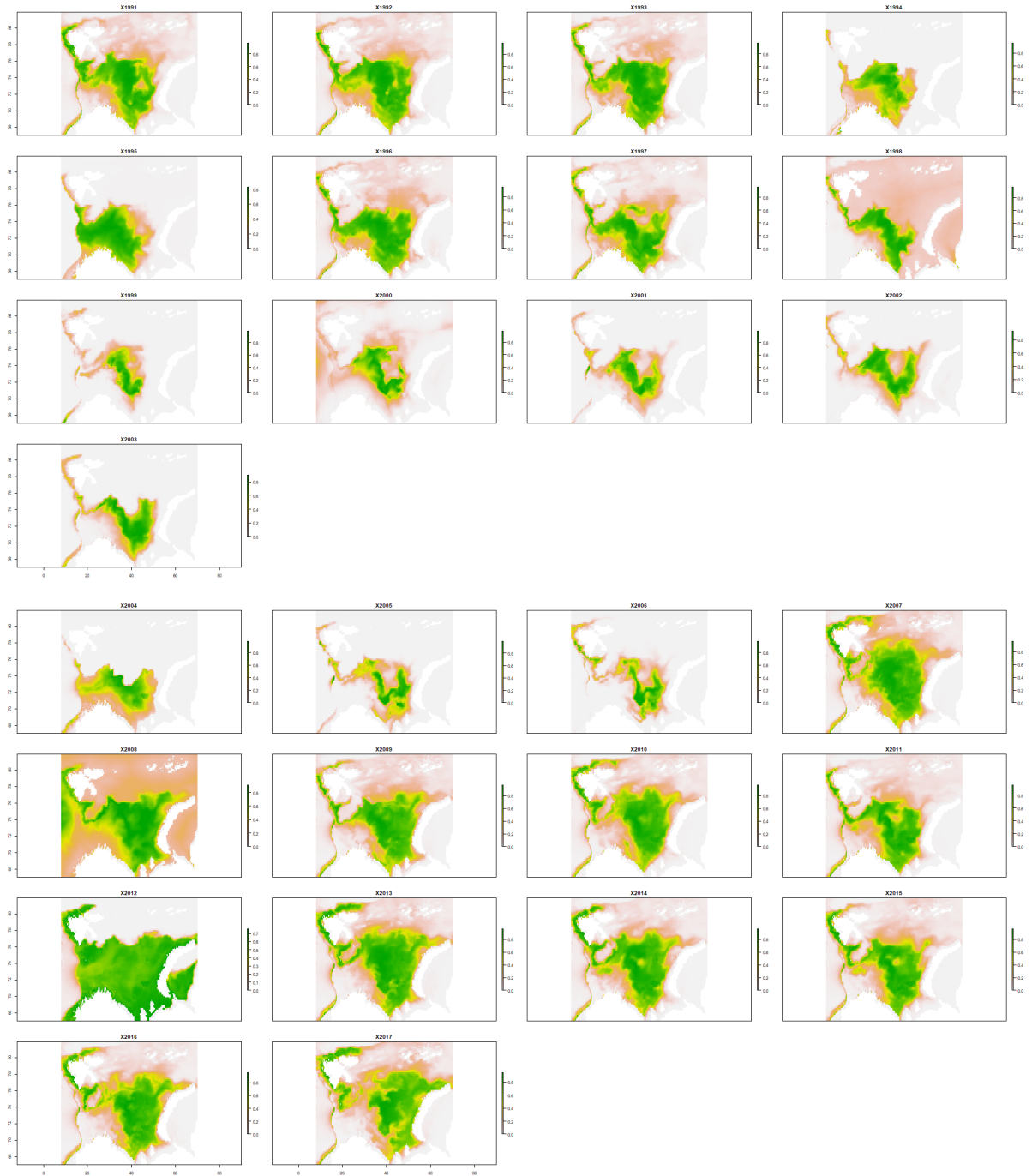


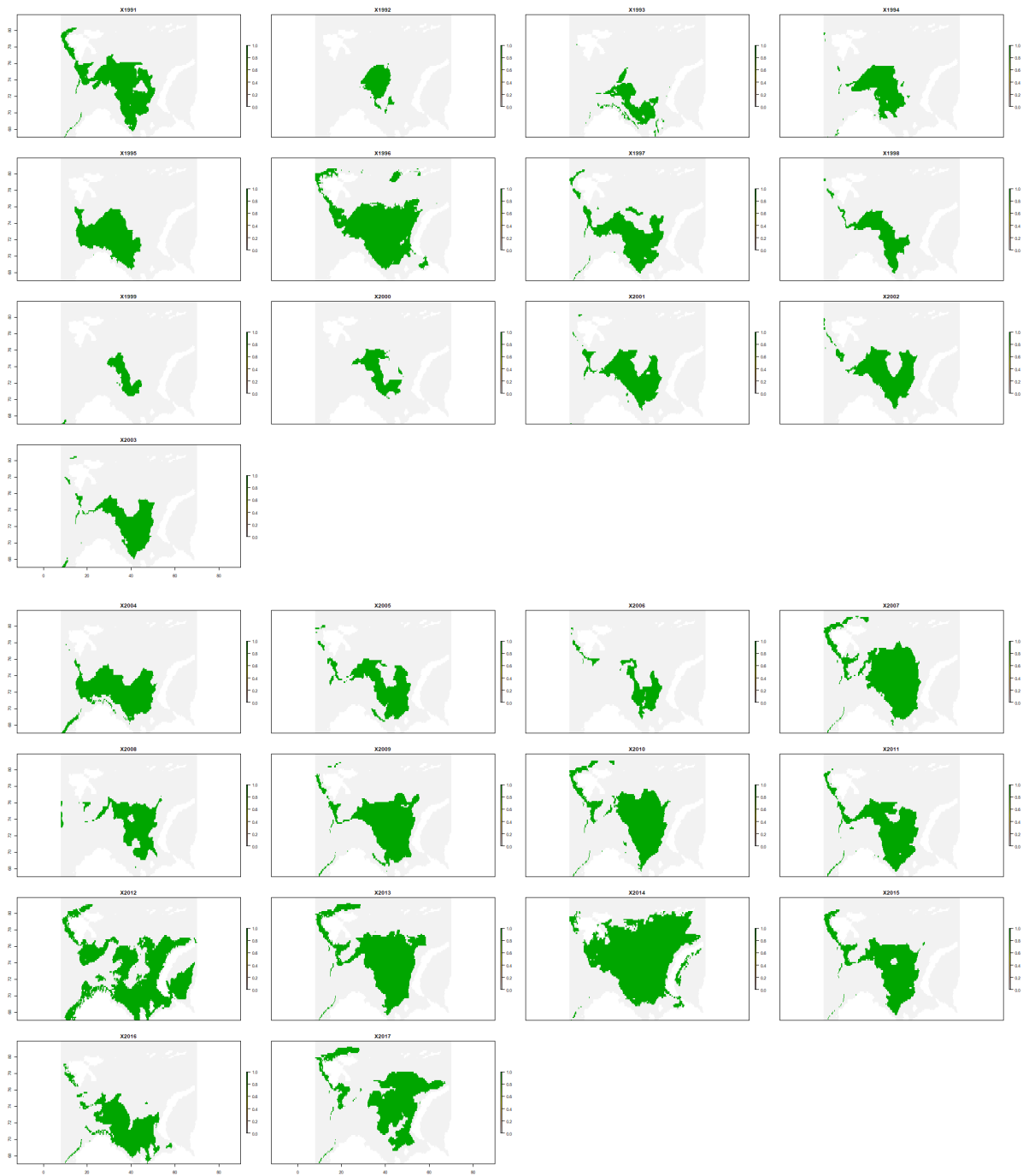


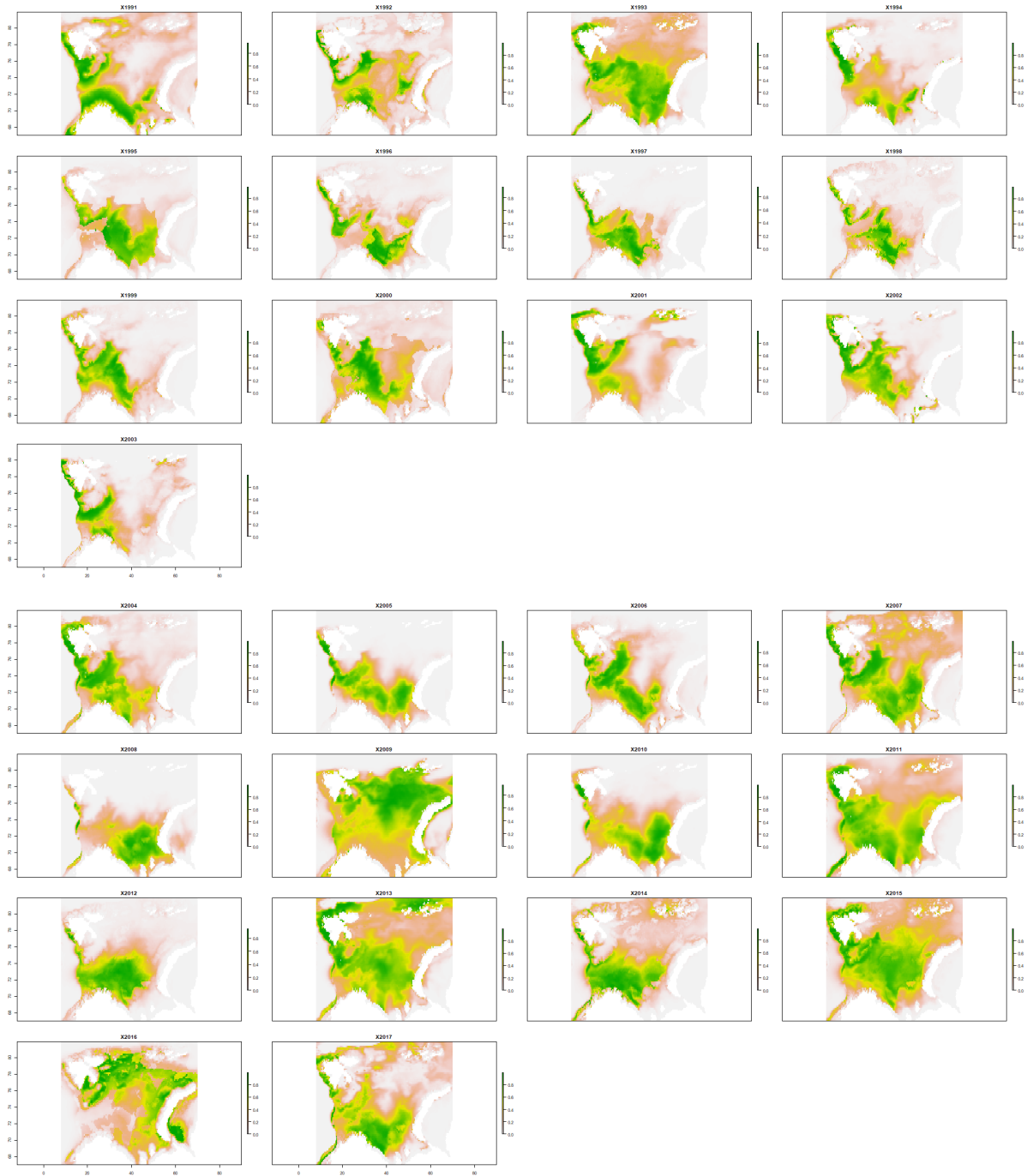
*Boreogadus saida* - Summer



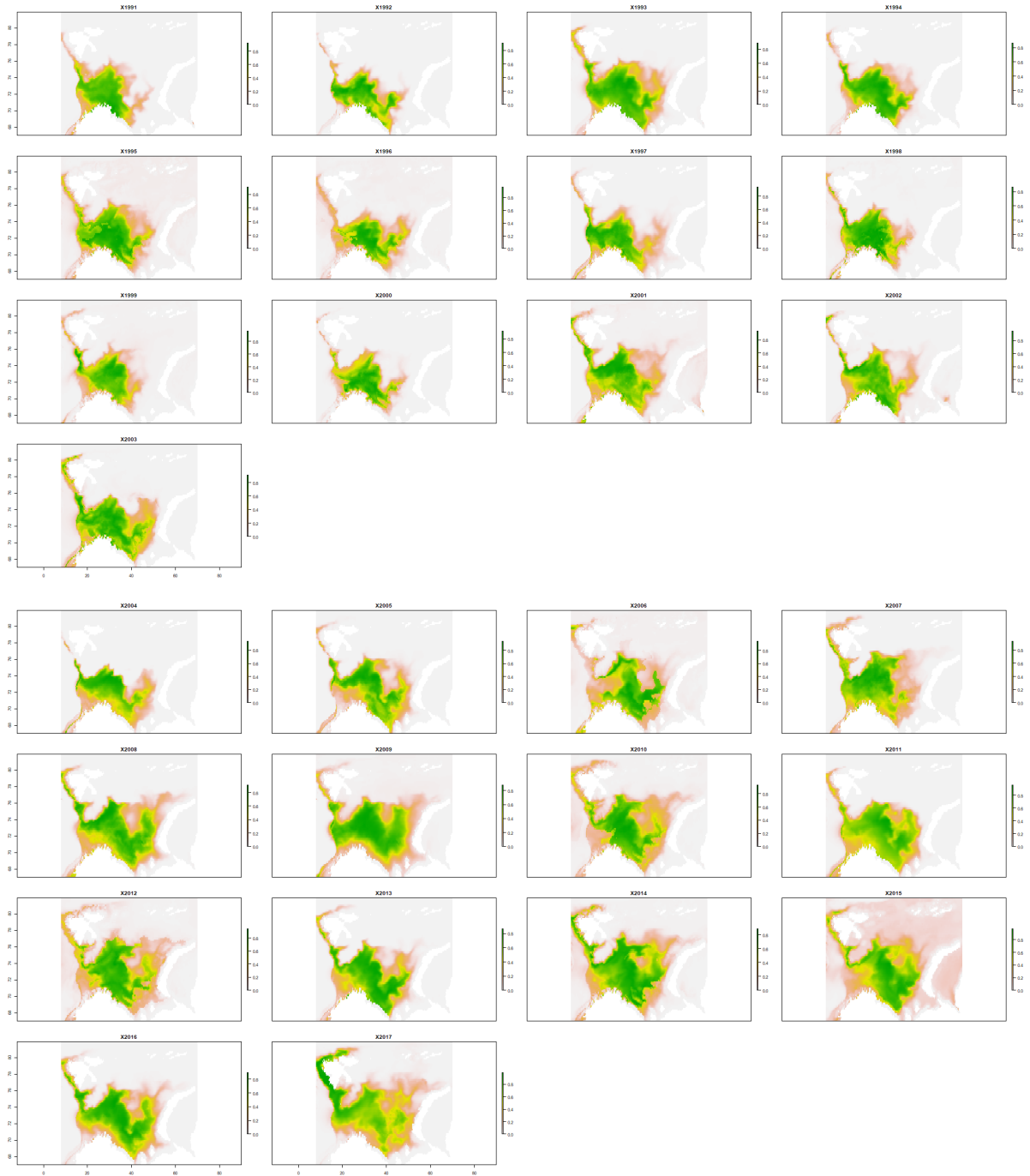
*Boreogadus saida* - Winter





*Pandalus borealis* - Summer



*Pandalus borealis* - Summer



## Appendix E - NARMAX input data table

Number	Variable	Description	Unit
1	Year		
2	RECRUITS	Recruitment	Thousands
3	TOTALBIO	Total biomass	Tonnes
4	TOTSPBIO	Total spawning biomass	Tonnes
5	LANDINGS	Total landings	Tonnes
6	YIELD/SSB	Yield per spawning biomass	
7	FBAR 5-10	Exploitation rate	
8	BS_PFRAC	Boreogadus saida prey fraction	
9	GM_PFRAC	Gadus morhua prey fraction	
10	MV_PFRAC	Mallotus villosus prey fraction	
11	MA_PFRAC	Melanogrammus aeglefinus prey fraction	
12	PB_PFRAC	Pandalus borealis prey fraction	
13	UNIQUEPREY	Number of unique prey in diet	
14	LARGEFRAC	Fraction of population < 100cm	
15	MEDFRAC	Fraction of population 20-100cm	
16	SMALLFRAC	Fraction of population < 20cm	
17	BOREOGADUS_SAIDA_SUMMER_AREA	Area covered during summer	km2
18	GADUS_MORHUA_L_SUMMER_AREA	Area covered during summer	km2
19	GADUS_MORHUA_M_SUMMER_AREA	Area covered during summer	km2
20	GADUS_MORHUA_S_SUMMER_AREA	Area covered during summer	km2
21	MALLOTUS_VILLOSUS_SUMMER_AREA	Area covered during summer	km2

22	MELANOGRAMMUS AEGLEFINUS_SUMMER_AREA	Area covered during summer	km2
23	PANDALUS BOREALIS_SUMMER_AREA	Area covered during summer	km2
24	BOREOGADUS_SAIDA_WINTER_AREA	Area covered during winter	km2
25	GADUS_MORHUA_L_WINTER_AREA	Area covered during winter	km2
26	GADUS_MORHUA_M_WINTER_AREA	Area covered during winter	km2
27	GADUS_MORHUA_S_WINTER_AREA	Area covered during winter	km2
28	MALLOTUS_VILLOSUS_WINTER_AREA	Area covered during winter	km2
29	MELANOGRAMMUS AEGLEFINUS_WINTER_AREA	Area covered during winter	km2
30	PANDALUS BOREALIS_WINTER_AREA	Area covered during winter	km2
31	GML_BS_S_OV	Overlap area during summer	km2
32	GMM_BS_S_OV	Overlap area during summer	km2
33	GMS_BS_S_OV	Overlap area during summer	km2
34	GML_GMM_S_OV	Overlap area during summer	km2
35	GML_GMS_S_OV	Overlap area during summer	km2
36	GML_MV_S_OV	Overlap area during summer	km2
37	GML_MA_S_OV	Overlap area during summer	km2
38	GML_PB_S_OV	Overlap area during summer	km2
39	GMM_GMS_S_OV	Overlap area during summer	km2
40	GMM_MV_S_OV	Overlap area during summer	km2
41	GMM_MA_S_OV	Overlap area during summer	km2
42	GMM_PB_S_OV	Overlap area during summer	km2
43	GMS_MV_S_OV	Overlap area during summer	km2
44	GMS_MA_S_OV	Overlap area during summer	km2
45	GMS_PB_S_OV	Overlap area during summer	km2

46	GML_BS_W_OV	Overlap area during winter	km2
47	GMM_BS_W_OV	Overlap area during winter	km2
48	GMS_BS_W_OV	Overlap area during winter	km2
49	GML_GMM_W_OV	Overlap area during winter	km2
50	GML_GMS_W_OV	Overlap area during winter	km2
51	GML_MV_W_OV	Overlap area during winter	km2
52	GML_MA_W_OV	Overlap area during winter	km2
53	GML_PB_W_OV	Overlap area during winter	km2
54	GMM_GMS_W_OV	Overlap area during winter	km2
55	GMM_MV_W_OV	Overlap area during winter	km2
56	GMM_MA_W_OV	Overlap area during winter	km2
57	GMM_PB_W_OV	Overlap area during winter	km2
58	GMS_MV_W_OV	Overlap area during winter	km2
59	GMS_MA_W_OV	Overlap area during winter	km2
60	GMS_PB_W_OV	Overlap area during winter	km2
61	TKOLA_SURF	Kola section surface temperature	°C
62	TKOLA_BOT	Kola section bottom temperature	°C
63	NAO_INDEX	North Atlantic Oscillation index	
64	CAPELIN_IMM_BIOMASS_T	Immature capelin biomass	Tonnes
65	CAPELIN_M_BIOMASS_T	Mature capelin biomass	Tonnes
66	CAPELIN_RECRUITMENT	Capelin recruitment	Thousands
67	POLARCOD_BIOMASS_000T	Polar cod biomass	Kilotonnes
68	ICEVOLUME_WINTER	Winter sea ice volume	km3
69	ICEVOLUME_SUMMER	Summer sea ice volume	km3

